LEVEL 2

ALEX(01)-TR-78-01

A050316

CONTINUATION OF THE SEISMIC RESEARCH OBSERVATORIES EVALUATION

TECHNICAL REPORT NO. 13
VELA NETWORK EVALUATION AND AUTOMATIC PROCESSING RESEARCH

Prepared by
Leonard C. Weltman and Robert R. Oliver

TEXAS INSTRUMENTS INCORPORATED
Equipment Group
Post Office Box 6015
Dallas, Texas 75222

D D C
RECEIVED
AUG 16 1979
C

Prepared for

AIR FORCE TECHNICAL APPLICATIONS CENTER
Alexandria, Virginia 22314

Sponsored by

ADVANCED RESEARCH PROJECTS AGENCY
Nuclear Monitoring Research Office
ARPA Program Code No. 7F10
ARPA Order No. 2551

20 November 1978

INFO SCTY BR., IQ
AFTAC   7 FEB 1979

8705-79-011

79 08 16 015   Equipment Group

REPORT DOCUMENTATION PAGE		READ INSTRUCTIONS BEFORE COMPLETING FORM
1. REPORT NUMBER	2. GOVT ACCESSION NO.	3. RECIPIENT'S CATALOG NUMBER
4. TITLE (and Subtitle) CONTINUATION OF THE SEISMIC RESEARCH OBSERVATORIES EVALUATION.		5. TYPE OF REPORT & PERIOD COVERED Technical rept. no. 13,
		6. PERFORMING ORG. REPORT NUMBER TI-ALEX(01)-TR-78-01
7. AUTHOR(s) Leonard C. Weltman and Robert R. Oliver		8. CONTRACT OR GRANT NUMBER(s) F08606-77-C-0004, ARPA Order-2551
9. PERFORMING ORGANIZATION NAME AND ADDRESS Texas Instruments Incorporated Equipment Group Dallas, Texas 75222		10. PROGRAM ELEMENT, PROJECT, TASK AREA & WORK UNIT NUMBERS VELA T/8705/B/PMP
11. CONTROLLING OFFICE NAME AND ADDRESS Advanced Research Projects Agency Nuclear Monitoring Research Office Arlington, Virginia 22209		12. REPORT DATE 20 November 1978
		13. NUMBER OF PAGES 243
14. MONITORING AGENCY NAME & ADDRESS(if different from Controlling Office) Air Force Technical Applications Center VELA Seismological Center Alexandria, Virginia 22314		15. SECURITY CLASS. (of this report) UNCLASSIFIED
		15a. DECLASSIFICATION/DOWNGRADING SCHEDULE

16. DISTRIBUTION STATEMENT (of this Report)

244 p

This document has been approved for public release and sale; its distribution is unlimited.

17. DISTRIBUTION STATEMENT (of the abstract entered in Block 20, if different from Report)

18. SUPPLEMENTARY NOTES

ARPA Order No. 2551

19. KEY WORDS (Continue on reverse side if necessary and identify by block number)

Seismic Research Observatories   Detection Capability
Data Quality   Discrimination Capability
RMS Noise Levels M_s-m_b Relationships
Noise Spectral Content

20. ABSTRACT (Continue on reverse side if necessary and identify by block number)

This report presents the results of an ongoing evaluation of the Seismic Research Observatories performed by Texas Instruments Incorporated at the Seismic Data Analysis Center in Alexandria, Virginia. Seven stations of the types noted are evaluated:

SRO :   Albuquerque, New Mexico (ANMO)
          Mashhad, Iran (MAIO)
          Chiang Mai, Thailand (CHTO)

DD FORM 1 JAN 73 1473   EDITION OF 1 NOV 65 IS OBSOLETE

20. continued

ASRO: Charters Towers, Australia (CTAO)
La Paz (Zongo), Bolivia (ZOBO)
Kabul, Afghanistan (KAAO)
Matsushiro, Japan (MAJO).

The major area of investigation in the evaluation were:

- Analysis of RMS noise levels, RMS noise trends, and noise spectral content;

- Estimation of the detection capability of the individual stations on a regionalized basis;

- Estimation of the discrimination capability of the individual stations;

- Estimation of the detection capability of the stations functioning as a network, and

- Evaluation of the performance of the short-period detector.

Estimates were also made of data quality, station reliability, and probability of mixed events. Conclusions regarding the above areas of interest and plans for further work are also presented in this report.

Accession For

NTIS GRA&I

DDC TAB

Unannounced

Justification

By

Distribution/

Availability Codes

Dist   Avail and/or special

A

ABSTRACT

This report presents the results of an ongoing evaluation of the
Seismic Research Observatories performed by Texas Instruments Incorporated
at the Seismic Data Analysis Center in Alexandria, Virginia. Seven stations
of the types noted are evaluated:

SRO :   Albuquerque, New Mexico (ANMO)

            Mashhad, Iran (MAIO)

            Chiang Mai, Thailand (CHTO)

ASRO: Charters Towers, Australia (CTAO)

            La Paz (Zongo), Bolivia (ZOBO)

            Kabul, Afghanistan (KAAO)

            Matsushiro, Japan (MAJO).

The major areas of investigation in the evaluation were:

● Analysis of RMS noise levels, RMS noise trends, and noise
spectral content.

● Estimation of the detection capability of the individual stations
on a regionalized basis.

● Estimation of the discrimination capability of the individual
stations.

● Estimation of the detection capability of the stations function-
ing as a network.

● Evaluation of the performance of the short-period detector.

Estimates were also made of data quality, station reliability, and probability of mixed events. Conclusions regarding the above areas of interest and plans for further work are also presented in this report.

iv

ACKNOWLEDGMENTS

v

TABLE OF CONTENTS

TABLE OF CONTENTS
(continued)

LIST OF FIGURES

viii

LIST OF FIGURES
(continued)

LIST OF FIGURES
(continued)

LIST OF FIGURES
(continued)

LIST OF FIGURES
(continued)

LIST OF FIGURES
(continued)

LIST OF FIGURES
(continued)

LIST OF TABLES

LIST OF TABLES
(continued)

LIST OF TABLES
(continued)

SECTION I
INTRODUCTION

A. THE SEISMIC RESEARCH OBSERVATORY SYSTEM

It has been noted (Robinson, 1967) that seismic data recorded by surface-sited instruments are degraded or obscured to a significant degree by wind-induced earth tilts. Theoretical data and tests indicated that this wind-induced noise component decreases rapidly with depth. Therefore, it is possible to enhance the seismic data quality by locating the seismic sensor at a depth of approximately 100 meters. The Seismic Research Observatories form the first network of single sites to implement this observation.

The Seismic Research Observatories data acquisition and recording system has been described in detail previously by Strauss (1976). Therefore, only a brief description of the system is presented here.

Broadband seismic energy is recorded by force-balance type seismometers which produce an output proportional to earth acceleration over the frequency range of 0.02 to 1.0 Hz. Both long-period and short-period data are produced from each sensor by selectively filtering the broadband output. The long-period data are digitized and recorded continuously on an 800 bit per inch magnetic tape. The vertical component of short-period motion is input to an automatic detector, which permits recording of vertical-component short-period motion only when certain operator-specified conditions are satisfied. Each magnetic tape can hold up to fourteen days of digital seismic data. When full, these magnetic tapes are shipped to the Albuquerque Seismological Laboratory at Kirtland Air Force Base in New Mexico. Copies of these tapes are sent to the Seismic Data Analysis Center at Alexandria, Virginia.

I-1

Long-period data are sampled once per second. The instrument response peaks at a period of 25 seconds with a quantization factor of 5 computer counts per millimicron of ground motion.

Short-period data are sampled 20 times per second. The instrument response peaks at a period of 1 second. The 1 second quantization factor is 2000 computer counts per millimicron of ground motion with the following exceptions. Beginning 1 May 1976 at Guam, 14 April 1976 at Wellington, New Zealand, and 13 May 1976 at Taipei, Taiwan, short-period data were quantized at 2 computer counts per millimicron of ground motion to prevent data clipping.

Also evaluated in this report are the Abbreviated Seismic Research Observatories (ASRO). These stations feature surface-vault seismometers rather than the borehole type. Data sampling rates are identical and response characteristics are very similar to those of the SRO sites. Normalized response characteristics for ASRO and SRO instruments are shown in Figure I-1. Quantization factors at 1 and 25 second periods are 10 and 1000 computer counts per millimicron, respectively.

B.   THE EVALUATION TASK

This report presents the results of a continued evaluation of the Seismic Research Observatories. The specific goals of this evaluation are:

- To estimate the data quality and reliability of each station
- To investigate the short-period and long-period noise field characteristics of each station
- To evaluate the performance of the short-period automatic detector
- To estimate the detection capability of each station

Long-Period
Normalized at 25 Seconds

Short-Period
Normalized at 1 Second

Period (seconds)

Relative Response
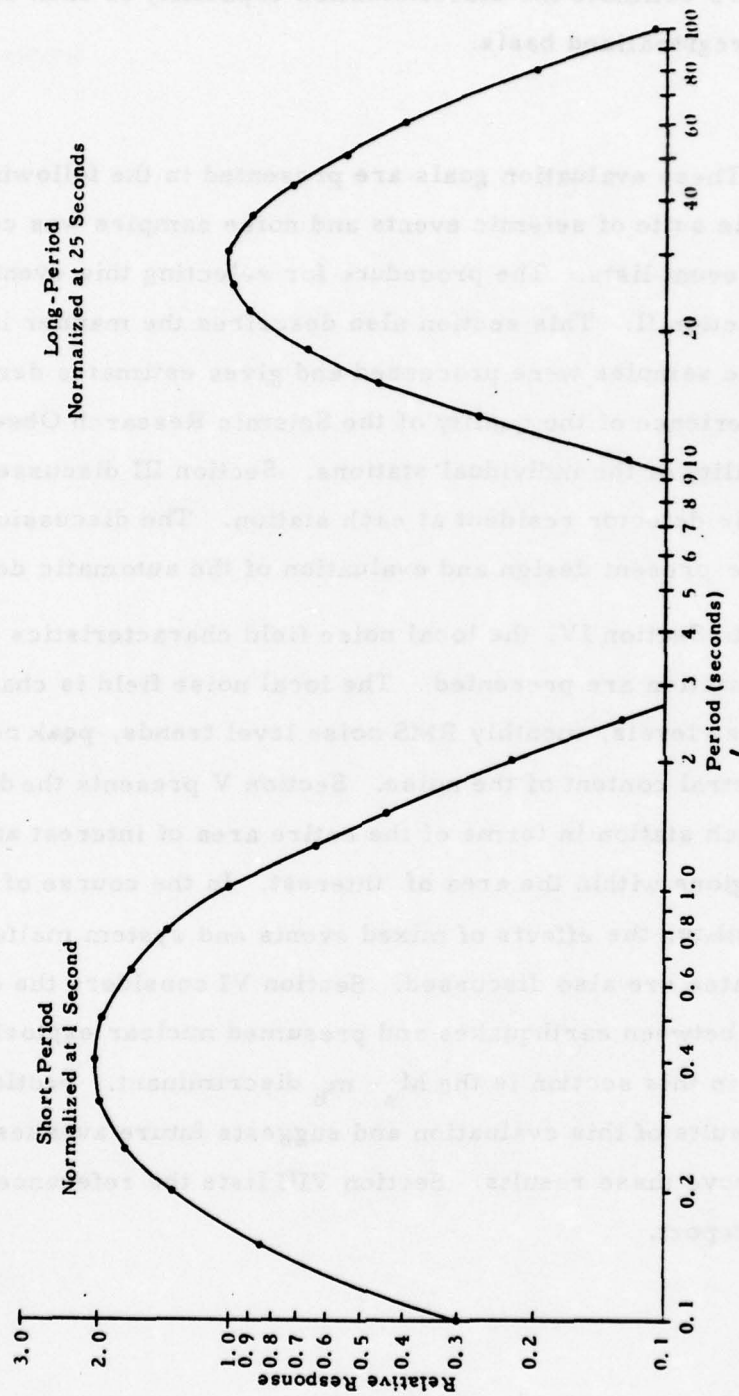
FIGURE I-1

NORMALIZED INSTRUMENT RESPONSE CURVES

- To estimate the discrimination capability of each station on a regionalized basis.

These evaluation goals are presented in the following manner. First, a suitable suite of seismic events and noise samples was constructed from available event lists. The procedure for selecting this event suite is described in Section II. This section also describes the manner in which the events and noise samples were processed and gives estimates derived from processing experience of the quality of the Seismic Research Observatory data and reliability of the individual stations. Section III discusses the short-period automatic detector resident at each station. The discussion of this topic covers the present design and evaluation of the automatic detector.

In Section IV, the local noise field characteristics at each evaluated SRO station are presented. The local noise field is characterized by the RMS noise levels, monthly RMS noise level trends, peak noise amplitudes, and spectral content of the noise. Section V presents the detection capability of each station in terms of the entire area of interest and in terms of specified regions within the area of interest. In the course of estimating detection capability, the effects of mixed events and system malfunctions on these estimates are also discussed. Section VI considers the question of discriminating between earthquakes and presumed nuclear explosions. The technique used in this section is the $M_s - m_b$ discriminant. Section VII summarizes the results of this evaluation and suggests future avenues of investigation to improve these results. Section VIII lists the references cited in the text of the report.

I-4

SECTION II
THE DATA BASE

A.   DATA AVAILABILITY

The Seismic Research Observatory network, when fully operational, will consist of at least the eighteen stations listed in Table II-1 and shown in Figure II-1. (The shaded area of Figure II-1 shows the area in which events used in this evaluation occurred.) During the contract period covered by this report, data were available from twelve of these stations: Albuquerque, New Mexico (ANMO); Mashhad, Iran (MAIO); Guam, Marianas Islands (GUMO); Narrogin, Western Australia (NWAO); Taipei, Taiwan (TATO); Wellington (South Karori), New Zealand (SNZO); Chiang Mai, Thailand (CHTO); Charters Towers, Australia (CTAO); Kabul, Afghanistan (KAAO); Matsushiro, Japan (MAJO); Zongo, Bolivia (ZOBO); and Bogota, Columbia (BOCO). Stations included in this evaluation are: ANMO, MAIO, CHTO, CTAO, ZOBO, KAAO, and MAJO.

Figure II-2 shows diagrammatically the availability of data for each evaluated station from the start-up date through March 1978. The vertical dashed lines in Figure II-2 enclose the time frame of the event detection capability studies. Data availability is nearly continuous for all stations within their evaluation time frames with the exception of MAJO, which was down for extended periods of time due to equipment failure.

B.   FORMATION OF THE EVENT DATA BASE

This report presents detection and discrimination studies for five new stations: CHTO, CTAO, ZOBO, KAAO, and MAJO.

TABLE II-1

SEISMIC RESEARCH OBSERVATORIES

Station Number	Location	Designator	Type	Coordinates	
				Latitude	Longitude
30	Albuquerque, New Mexico	ANMO	SRO	34°56'30"N	106°27'30"W
Unknown	Ankara, Turkey	ANTO	SRO	39°54' N	32°47' E
Unknown	Bangui, Central African Republic	BCAO	SRO	Unknown	Unknown
32	Bogota, Columbia	BOCO	SRO	4°35'46"N	74° 2'57"W
33	Chiang Mai, Thailand	CHTO	SRO	18°47'24"N	98°58'37"E
50	Charters Towers, Australia	CTAO	ASRO	20° 5'18"S	146°15'16"E
Unknown	Grafenburg, Germany	GFRO	SRO	Unknown	Unknown
35	Guam, Marianas Islands	GUMO	SRO	13°35'16"N	144°51'59"E
52	Kabul, Afghanistan	KAAO	ASRO	34°32'27"N	69° 2'34"E
Unknown	Kongsberg, Norway	KONO	ASRO	Unknown	Unknown
36	Mashhad, Iran	MAIO	SRO	36°18'00"N	59°29'40"E
53	Matsushiro, Japan	MAJO	ASRO	36°32'30"N	138°12'32"E
38	Narrogin, Western Australia	NWAO	SRO	32°55'42"S	117°14' 9"E
Unknown	Quetta, Pakistan	QUPO	SRO	Unknown	Unknown
Unknown	Shillong, India	SHIO	SRO	25°34' N	91°53' E
42	Wellington (South Karori), New Zealand	SNZO	SRO	41°18'37"N	174°42'17"E
41	Taipei, Taiwan	TATO	SRO	24°58'34"N	121°29'20"E
51	Zongo, Bolivia	ZOBO	ASRO	16°16'12"S	68° 7'30"W

MILLER MODIFIED MERCATOR PROJECTION
MAP SCALE: 0.02000 INCHES/DEGREE LONGITUDE
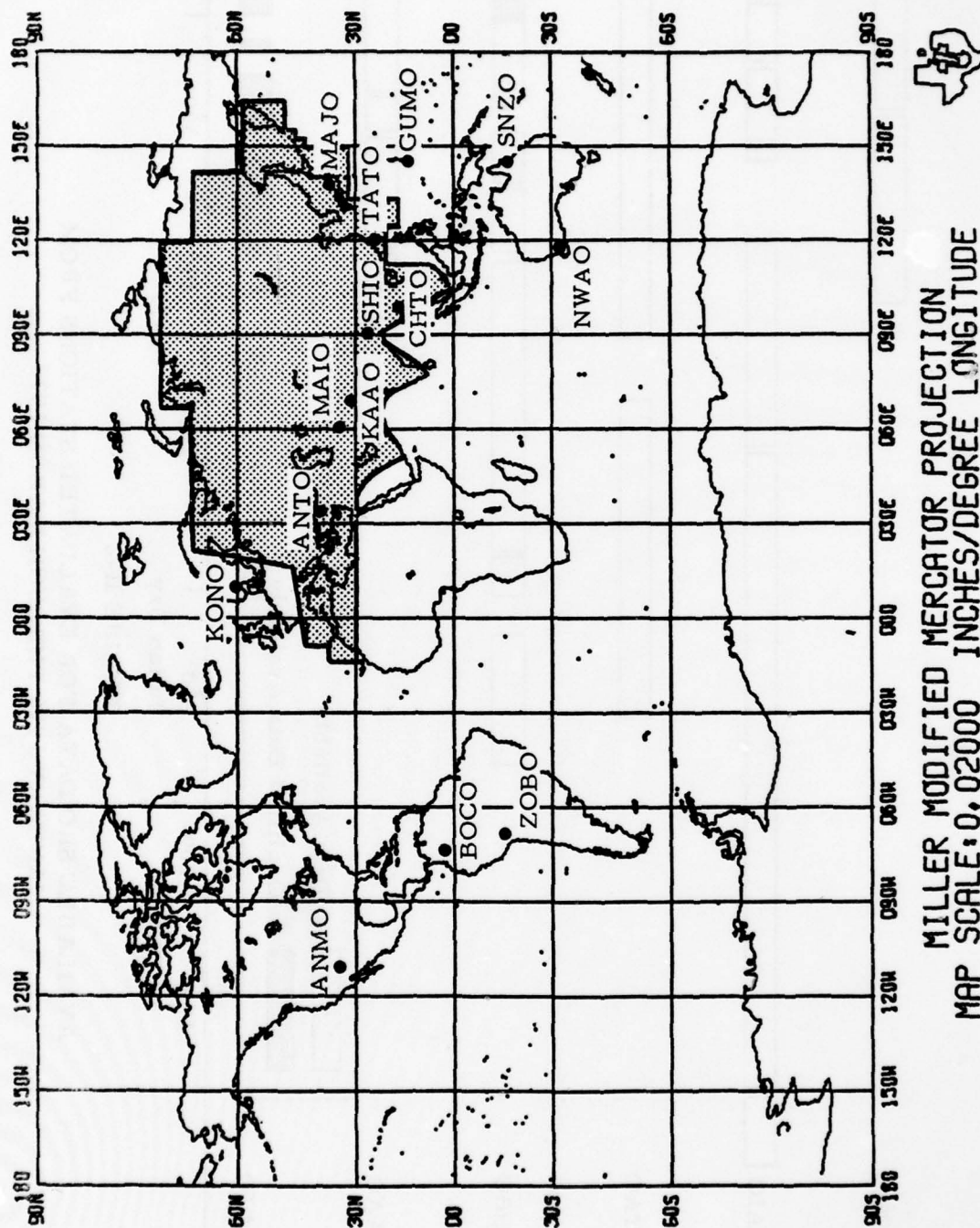
FIGURE II-1

LOCATIONS OF SRO STATIONS
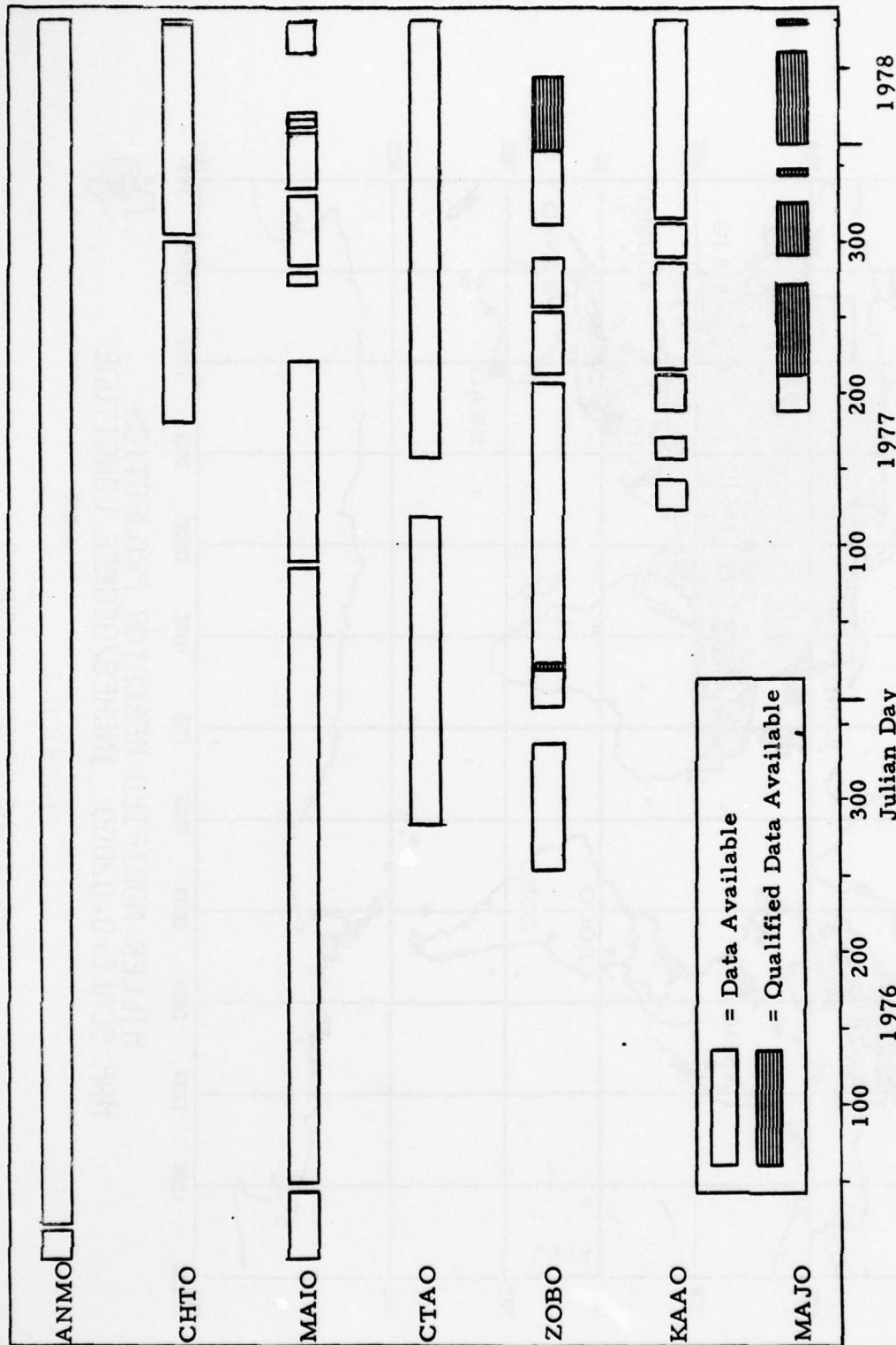
FIGURE II-2

AVAILABLE SRO DATA FOR EVALUATED STATIONS FROM
JANUARY 1976 THROUGH MARCH 1978

Evaluation of these stations begins on station date 1 September 1977. This is the approximate two month operational anniversary of MAJO, which is the Matsushiro, Japan ASRO station, and the newest site evaluated. This two month waiting period was initiated in order to allow personnel time to correct any malfunctions which may occur early in the operational life of a seismic station. As of the middle of August 1978, microfiche records for the stations of interest were unavailable past station date 31 November 1977. This date marks the end of the new station evaluation time frame.

Events within this time frame were edited from the NORSAR and NEIS lists. Those events satisfying the previously imposed geographic restraints formed a final Eurasian data base of 247 events.

The short-period data base used in this evaluation is simply a subset of the above-described data base. All members of this subset have station-epicenter separations of less than 103 degrees. This restriction was placed on the short-period data base since detection of the P wave beyond 103° from the event epicenter is limited by a shadow zone. At ZOBO this restriction severely limited the size of the data base, since these stations are located far from the general area of interest. Table II-2 presents the mean earthquake epicentral distance to each station. (These values are derived from the station-epicenter separation of the events.)

The description of the noise sample data base is given in detail in Section IV of this report. In brief, the short-period noise samples were selected from time gates immediately preceding the observed signal which triggered the automatic detector. Long-period noise samples were arbitrarily processed at noon of each day. Short-period and long-period noise samples were edited every fourth field tape day. Noise samples were quality checked by visual examination of paper plots and/or microfiche and samples containing signals were rejected.

TABLE II-2

MEAN EARTHQUAKE EPICENTRAL DISTANCES (DEGREES)

Station	Mean Distance	Standard Deviation
CHTO	45.8	19.8
CTAO	86.0	25.7
ZOBO	131.2	21.9
KAAO	39.4	24.1
MAJO	42.1	29.3

C.   DATA PROCESSING

    Long-period signal and noise data and short-period noise data were processed in two stages; a pre-analysis processing and an analysis processing stage involves the use of the multi-purpose program TISSPROG (Schmidt, 1978). A description of this program, as it processes SRO data, follows (Figure II-3).

    Given input data consisting of epicentral locations and origin times, TISSPROG will estimate short- or long-period arrival times and edit events or noise samples from a field tape. Short-period data are resampled to a one-tenth of a second time interval, and long-period data are resampled from a one-second to a two-second time interval. Long-period edit gates are automatically set at 4096 seconds, and short-period edit gates are determined by the 'on time' of the short-period detector (see Section III). Short-period edit gates are limited to 204.8 seconds. Trace means are next removed, and long-period data are rotated from their vertical, north, east configuration to a vertical, transverse, radial configuration. At this stage, samples are saved on an event tape for further analysis. Finally, TISSPROG produces 0.5-4.0 Hz bandpass filtered short-period or 0.023-0.059 bandpass filtered long-period plots.

    Noise and signal analyses follow. Since procedures are detailed in later sections, only brief descriptions will be included here.

    All data samples were visually quality checked. Long-period events were analyzed for detection and 25 second M_s - m_b discrimination capability. Long-period noise samples yielded 512 point noise analysis gates. These noise gates were further processed to produce peak 20, 25, and 30 second noise amplitudes, RMS noise amplitudes in the 10-25, 17-41, and 40-64 second spectral bandwidths, and power spectra. Values were later grouped as averages and/or functions of time.

800
BPI
Field
Tape

Create
Data Base

NEIS and
NORSAR
Event
Lists

TISSPROG

Compute
Arrival
Times

Calculate
Edit Length
(Short-Period
Only)

Edit
Field
Tape

Bandpass
Filter
Data

Rotate
V, N, E, to
V, T, R
(Long-Period
Only)

Remove
Trace
Means

1600
BPI
Plot
Tape

1600
BPI
Event
Tape
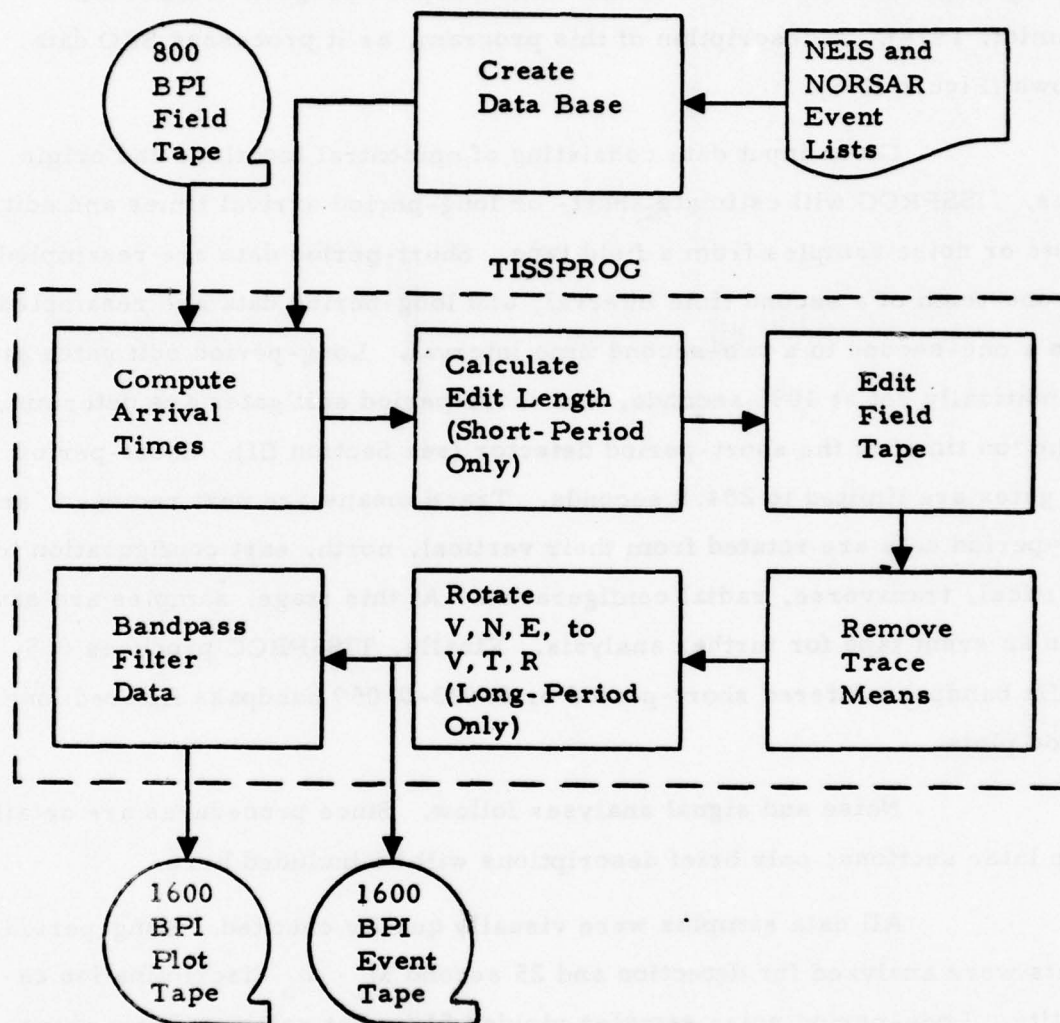
FIGURE II-3
DATA PROCESSING FLOW CHART

Since short-period data are recorded only when the SRO detector is signal activated (Section III), acceptable extended noise gates are non-existant. However, each time the detector triggers, the preceding 20 seconds of data are recorded as a lead-in buffer. Therefore, the first 12.8 seconds of short-period detections were used for noise analysis. Following visual inspection, an analysis processing routine was employed to produce a peak one second amplitude, 0.5-4.0 Hz RMS amplitude, and power spectrum. These values were also grouped as averages and/or time functions.

Short-period detection capability was estimated with the aid of microfiche analyses. Computer processing proved necessary only for those few events satisfying the following criteria:

- No signal could be identified visually on microfiche records.

- Estimated signal arrival time occurred more than 30 seconds after the start time of the first record of an automatic detection.

D. PROCESSING SUMMARY

Table II-3 summarizes the processing results of the work performed during the current contract period on the Seismic Research Observatories evaluation task. In this table, the 'SP' and 'LP' under the heading 'DATA TYPE' refer to short-period data and long-period data, respectively. The heading 'DETECTED' refers to the number of events which were visually detected (Calcomp plot for LP, microfiche or Calcomp plot for SP) under the detection criteria of Section V. The heading 'NOT DETECTED' refers to the number of events for which only seismic noise was observed in the signal gate. The heading 'MIXED' refers to the number of events which were not detectable due to the presence of some other signal in the signal gate. The heading 'MICROFICHE DETECTED ONLY' refers to the number of events not detected

TABLE II-3

SUMMARY OF SRO EVENT PROCESSING

Station	Data Type	Detected	Not Detected	Mixed	Microfiche Detected Only	No Data Recorded	Mal-function	Δ > 103°	Total
CHTO	SP	87	88	9	20	34	3	6	247
	LP	95	72	40	--	34	6	--	247
CTAO	SP	14	156	3	3	3	0	66	245
	LP	53	121	68	--	3	0	--	245
ZOBO	SP	2	32	0	0	69	0	144	247
	LP	20	64	72	--	73	18	--	247
KAAO	SP	139	62	14	8	18	0	6	247
	LP	133	35	51	--	21	6	--	246
MAJO	SP	58	102	3	13	71	0	0	247
	LP	88	44	30	--	79	6	--	247

II-10

by the short-period automatic detector. The heading 'SYSTEM FAILURE -
NO DATA RECORDED' refers to the number of events for which no data were
recorded since the system had gone down (failed). The heading 'MALFUNC-
TION' refers to the number of events for which the detection status could not
be determined due to malfunctions (spikes, glitches, and the like) in the sig-
nal gate. The heading '$\Delta < 103^{\circ}$' refers to the number of events for which
short-period data were not processed due to their epicentral distances being
greater than 103°.

The quality of the data recorded at the Seismic Research Ob-
servatories was very good in most cases. The types of malfunctions which
degrade the data quality were described in detail in the preliminary evalua-
tion of the Seismic Research Observatories (Strauss, 1976). The overall fre-
quency of occurrence of these malfunctions can be estimated from Table II-3.

Long-period malfunctions which occurred at ZOBO and MAJO
were hardware related, and these stations have since been repaired.

Estimates of station reliability were made using the following
argument. If a station is perfect in that it always produces seismic record-
ings which the analyst can check for detections, it is considered to have a
reliability factor of 1.0. If on the other hand, the station is never producing
seismic recordings due to instrument problems (instruments recording im-
properly or not at all), it is considered to have a reliability factor of 0.0.
In practice, of course, the reliability factor lies somewhere between these
extremes. Since station down time and station malfunction time are the two
factors which render the station reliability less than 1.0, the reliability fac-
tor is defined as

Reliability Factor = 1.0 - (Percentage of time station is down
+ Percentage of time station is mal-
functioning)

II-11

where the two percentages are estimated empirically from the data of Table II-3. Thus, the percentage of time the station is down is estimated from the number of events for which no data were recorded divided by the total number of events for which processing was attempted and the percentage of time the station is malfunctioning is the number of events for which malfunctions (spikes, glitches, and data drop-outs) overrode the seismic data divided by the total number of events for which processing was attempted. When computing the short-period reliability factors, those events for which no data were recorded due to the automatic detector were excluded, since it is not possible to determine how many would contain malfunctions.

The reliability estimates are presented in Table II-4. The relatively low reliabilities of MAJO and ZOBO are due primarily to station down time, when no data were recorded (see Figure II-2).

From the data base processed in this evaluation, it was possible to form estimates of the probability than an event of interest will be masked by some other event (a 'mixed' event). From the data of Table II-3, one can see that the probability that any short-period event will be mixed is very small. This low probability of mixing for short-period data is due to the length of the signal coda, which is quite short relative to the average time between signals.

The long-period data presents quite a different picture. Due to their relatively long signal coda, there is a significant probability of mixing for long-period data. Table II-5 presents estimates of the probability of mixing derived from the processed data base. The high frequency of mixed events evident at ZOBO is most probably due to the distance from that station to Eurasia. The signal arrives over a large gate consequently, there is more opportunity for mixing to occur.

II-12

TABLE II-4

STATION RELIABILITY ESTIMATES

Station	Short-Period	Long-Period
CHTO	0.85	0.84
CTAO	0.99	0.99
ZOBO	0.72	0.63
KAAO	0.93	0.89
MAJO	0.71	0.66

TABLE II-5

LONG-PERIOD MIXED EVENT OCCURRENCE FREQUENCIES

Station	Frequency
CHTO	0.19
CTAO	0.28
ZOBO	0.46
KAAO	0.23
MAJO	0.19

SECTION III
THE SHORT-PERIOD AUTOMATIC DETECTOR

For convenience in the SRO short-period automatic detector performance evaluation, the detector performance criteria (Subsection A) and the detector design description (Subsection B) from last year's SRO evaluation report (Strauss and Weltman, 1977) are repeated. These subsections are followed by the current evaluation of the detector performance.

A.   DISCUSSION

This section reviews the design of the short-period automatic detector currently in operation at the Seismic Research Observatory stations and discusses the problems of this detector discovered during the course of this evaluation.

The prime reason for incorporating a short-period automatic detector at the Seismic Research Observatory stations was to minimize the amount of short-period data recorded during which no short-period seismic events could be observed and thus maximize the recording life of each magnetic tape. This would minimize expenditures for the purchasing and transportation of magnetic tapes and the amount of data lost during tape changes without seriously decreasing the number of short-period seismic events recorded. Since the single component of short-period motion is sampled twenty times per second while the three components of long-period motion are each sampled once per second, the bulk of each tape (87%) would be filled with short-period data if short-period data were recorded continuously. In this continuous recording mode, the recording life of a 2400 foot, 800 BPI magnetic tape would be approximately four days. With the automatic detector in operation, this has been extended to up to sixteen days.

III-1

The design of any automatic detector should take into account the following points:

- Maximum detection probability consistent with the largest tolerable false alarm rate

- Stable false alarm rate over a wide range of ambient noise levels

- Minimum number of detections declared from the same event while retaining the ability to detect possible secondary phase arrivals within the coda

- Minimum time necessary to re-establish equilibrium after parameter value changes

- Low sensitivity to degraded data quality (Swindell and Snell, 1977).

In this evaluation of the automatic detector design, data output by the automatic detector will be assessed in terms of the above points.

B.   DESIGN OF THE PRESENT SHORT-PERIOD AUTOMATIC DETECTOR

Each Seismic Research Observatory station is equipped with a short-period automatic event detector (hereafter referred to as the SRO automatic detector) which is intended to discriminate between seismic noise and short-period seismic events. The design of the SRO automatic detector is based on a study carried out by the Charles Stark Draper Laboratory (Eterno, et al., 1974).

The design concept of the SRO automatic detector is illustrated by Figure III-1. The short-period analog data from the sensor unit is first digitized at a rate of twenty samples per second. At the SRO automatic detector input, each datum is converted to a twelve bit integer quantity. The digitized

Input Digital Data

Bandpass Filter
(3 dB down at 0.5 and 2.0 Hz)

Rectify

Short Term Average
(STA)

Reset
Window

Scale

Long Term Average
(10, 20, 30, 40 sec) (A)

STA

Scale (threshold value)

no   STA ≥ A   A

yes

Freeze LTA
Decrement Window

Window
≤ 0   no   Process Next Sample

yes

Declare Detection
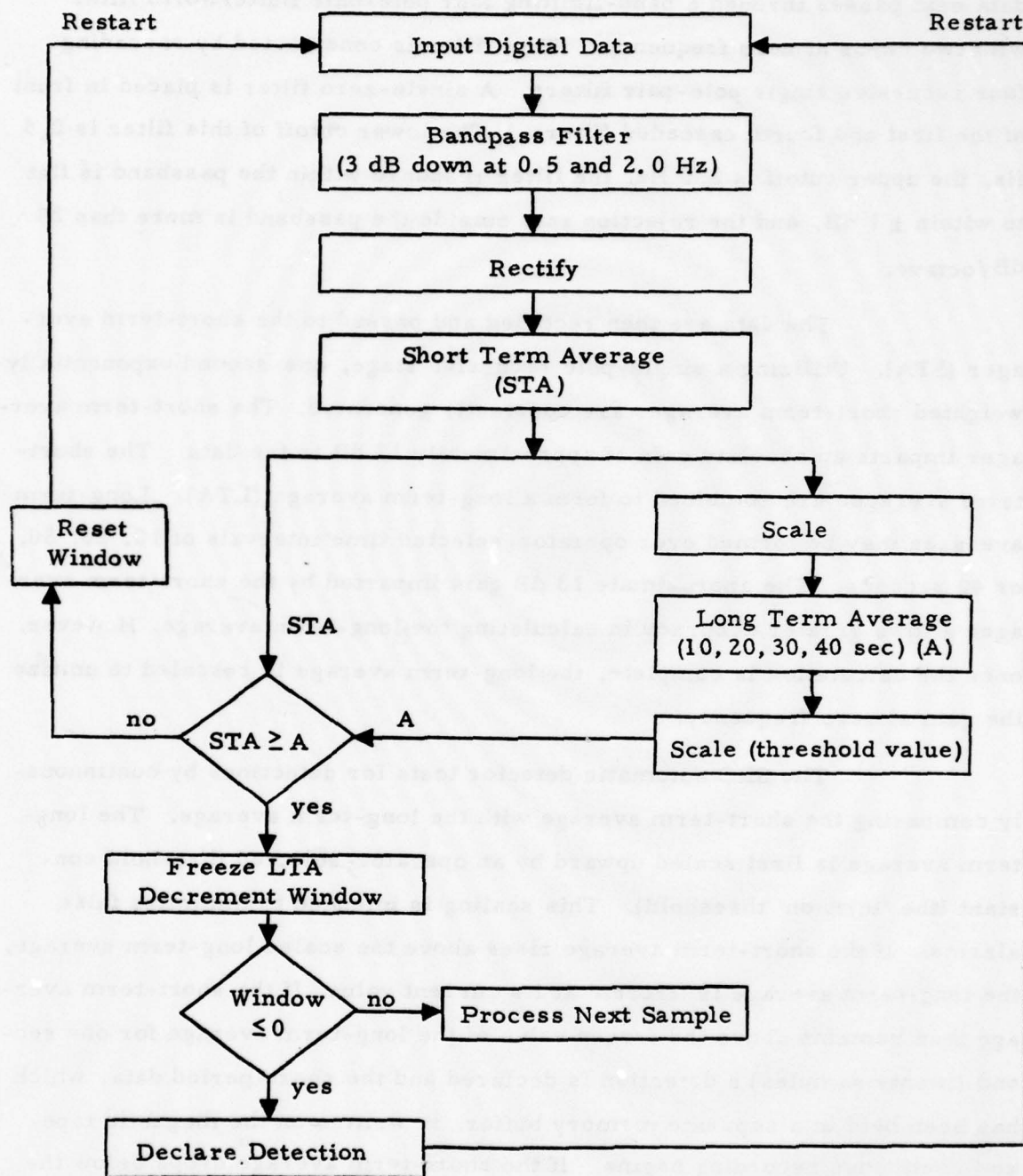
FIGURE III-1

SHORT-PERIOD DETECTOR CONCEPT

III-3

data next passes through a band-limiting four pole-pair Butterworth filter with two zeros at zero frequency. (This filter is constructed by cascading four recursive single pole-pair filters. A single-zero filter is placed in front of the first and fourth cascaded filters.) The lower cutoff of this filter is 0.5 Hz, the upper cutoff is 2.0 Hz, the filter response within the passband is flat to within ± 1 dB, and the rejection rate outside the passband is more than 25 dB/octave.

The data are then rectified and passed to the short-term averager (STA). Utilizing a single-pole recursive stage, one-second exponentially-weighted short-term averages are constantly generated. The short-term averager imparts an absolute gain of approximately 13 dB to the data. The short-term averages are combined to form a long-term average (LTA). Long-term averages may be formed over operator-selected time intervals of 10, 20, 30, or 40 seconds. The approximate 13 dB gain imparted by the short-term averager allows greater accuracy in calculating the long-term average. However, once the calculation is complete, the long-term average is rescaled to unitize the gain at zero frequency.

The SRO automatic detector tests for detections by continuously comparing the short-term average with the long-term average. The long-term average is first scaled upward by an operator-selected threshold constant (the 'turn-on' threshold). This scaling is intended to minimize false alarms. If the short-term average rises above the scaled long-term average, the long-term average is 'frozen' at its current value. If the short-term average then remains above the frozen value of the long-term average for one second (twenty samples) a detection is declared and the short-period data, which has been held in a separate memory buffer, is written on the magnetic tape, and continuous recording begins. If the short-term average drops below the frozen long-term average before the one second gate is over, no detection is declared, the long-term average is 'unfrozen' and updated.

III-4

Once a detection has been declared, the frozen long-term average is scaled upward by a second operator-selected threshold constant (the 'turn-off' threshold). When the short-term average drops below the rescaled long-term average, the event is considered to be over and the current buffer of short-period data completes the magnetic tape record. Scaling the frozen long-term average by the turn-off threshold is intended to minimize the recording of the sometimes persistent coda that can follow the initial arrival of a short-period event.

Thus, the operator can 'tune' the SRO automatic detector via four adjustable constants: the long-term averager time constant, the detection turn-on threshold, the detection turn-off threshold, and the digital gain factor. In addition, the operator can override the SRO automatic detector and record short-period continuously.

Set procedures exist for setting the proper digital gain factor. However, selection of the other constants is largely a matter of trial-and-error. The operator zeros in on optimum values after selecting initial values within experimentally determined ranges.

C. EVALUATION OF THE AUTOMATIC DETECTOR

Microfiches, covering the time period 1 September 1977 through 30 November 1977, were obtained for SRO station CHTO (Chiang Mai, Thailand). Every third day was visually examined and analyst detection logs were compiled. Detection criteria were a 3 dB peak-signal-to-peak noise ratio and an apparent signal character as determined by the analyst. These logs were compared to automatic detector logs which were generated from CHTO field tapes.

The automatic detector logs are based on the conformity of record times rather than on the detection status bit included in each field

tape short-period record. This method was preferred since detections of less than one record duration (49 seconds) may not be flagged by the status bit.

Comparison of the analyst-generated and automatic detector log yielded detection statistics which may be used to gauge detector performance. Semi-monthly sums over every third day (a total of 5 days or 120 hours per period) of automatic detector 'misses', 'false alarms', and 'confirmed detections' are given in Table III-1. An item in the column labeled 'Number Detected by Analyst Only' is called a 'miss' and refers to the condition: signal in the appropriate time gate, no detection declared. The column labeled 'Number Detected by Automatic Detector' reflects the false alarm rate and refers to the condition: no signal in the time gate, detection declared. The column labeled 'Number Detected by Both' shows the number of automatic detections confirmed by the analyst. The total number of valid detections then is found by adding the numbers of missed and confirmed detections. The numbers in Table III-1 translate into the detector operating characteristics, Figure III-2.

We observe that the probability of detection, P_D, ranges approximately from 50% to 80% at false alarm rates (FAR) varying between 0.2 and 2.1 false alarms per hour (FA/H). While the averaging periods (5 days in a half-month interval) should be sufficiently long to give solid statistics, the probability of detection seems rather independent of the FAR. This probability reflects the FAR instability inherent in a straight STA/LTA detector which does not account for changes in the STA variance for noise (Lacoss, 1972; Swindell and Snell, 1977; Unger, 1978).

Several points should be considered with regard to the validity of the analyst-detector comparisons. The analyst was not concerned with source-to-station distances when picking signals. Since the automatic detector is not tuned for local events (Personal Communication, John Hoffman,

III-6

TABLE III-1

ANALYST VERSUS AUTOMATIC DETECTION, STATION CHTO

| Period (1977) | Automatic Detector Only (False Alarms) | Number of Detections | | Total Detections (Missed and Confirmed) |
		Analyst Only (Missed Detections)	Both (Confirmed Detections)	
09/01 - 09/15	10	32	46	78
09/16 - 09/30	2	21	39	60
10/01 - 10/15	13	18	56	74
10/16 - 10/30	16	13	53	66
11/01 - 11/07		Detector Malfunction		
11/08 - 11/15	10	16	18	34
11/16 - 11/30	25	24	52	76

III-7
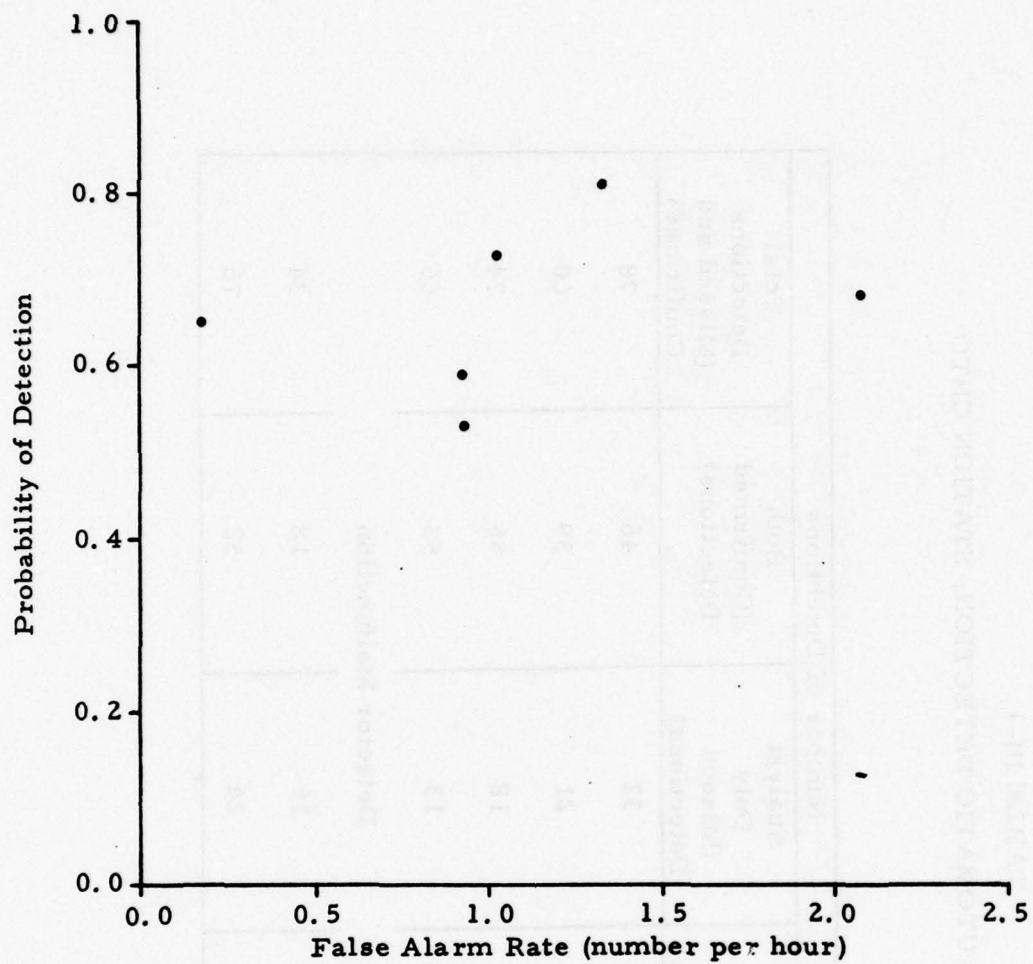
FIGURE III-2

SRO SP DETECTOR OPERATING CHARACTERISTICS,
STATION CHTO, 09/01/77 - 11/30/77

III-8

1978), the number of missed events may be higher than what would be expected for teleseismic data only. Also, as illustrated in Figure III-1, a bandpass filter precedes the automatic detection process. The microfiche viewed was not bandpass filtered, and the large number of analyst picks, along with limited computer availability, prohibited such processing. Thus, the estimated operating characteristics may be biased. Finally, as can be seen in Table III-1, the CHTO automatic detector malfunctioned for eight days. Data were recorded almost continuously and no attempt was made at automatic detector evaluation for that time period.

Another problem causing FAR instability, encountered in last year's evaluation (Strauss and Weltman, 1977) is illustrated in Table III-2. In many instances, there was no relation between the number of detections and the amount of recording time, which indicated possible difficulties in the setting and freezing of detector parameters (Strauss and Weltman, 1977).

An identical study was conducted this year on the five new stations under evaluation. The percentage time recorded and the number of detections were charted for a nine-day period and are shown in Table III-3. The data seem much more constant with time for a given station. This suggests that an improvement has been made in the parameter setting and freezing problem.

TABLE III-2

PERFORMANCE OF AUTOMATIC DETECTOR FOR AN ARBITRARY
TEN-DAY PERIOD IN 1976
(Strauss and Weltman, 1977)

Date	Number of Detections					
	ANMO	GUMO	MAIO	NWAO	TATO	SNZO
06/21/76	6	36	11	23	9	7
06/22/76	19	53	9	0	1	1
06/23/76	14	11	9	3	4	1
06/24/76	16	0	6	1	2	2
06/25/76	16	4	20	6	0	2
06/26/76	4	8	15	3	0	0
06/27/76	8	18	11	4	2	3
06/28/76	15	64	12	3	1	2
06/29/76	13	62	6	4	2	6
06/30/76	15	22	5	3	7	4

Date	Percentage of Time Recorded					
	ANMO	GUMO	MAIO	NWAO	TATO	SNZO
06/21/76	59	10	12	1	2	67
06/22/76	6	33	9	0	9	>1
06/23/76	3	42	23	>1	1	>1
06/24/76	4	0	7	>1	>1	>1
06/25/76	6	3	14	20	0	89
06/26/76	1	1	32	3	0	100
06/27/76	2	2	26	2	>1	64
06/28/76	3	9	22	1	96	>1
06/29/76	3	49	11	>1	5	42
06/30/76	3	2	54	>1	1	41

TABLE III-3

PERFORMANCE OF AUTOMATIC DETECTOR FOR
AN ARBITRARY NINE-DAY PERIOD IN 1977

Date	Number of Detections				
	CHTO	CTAO	KAAO	MAJO	ZOBO
11/14/77	13	20	28	8	26
11/15/77	4	29	30	6	22
11/16/77	19	24	41	10	37
11/17/77	12	22	24	2	33
11/18/77	15	20	33	11	29
11/19/77	13	18	31	4	33
11/20/77	7	56	29	7	35
11/21/77	10	42	32	14	50
11/22/77	10	28	38	4	26

Date	Percentage of Time Recorded				
	CHTO	CTAO	KAAO	MAJO	ZOBO
11/14/77	1	3	10	2	6
11/15/77	1	3	7	3	2
11/16/77	11	4	7	5	6
11/17/77	3	3	4	2	5
11/18/77	8	3	11	2	5
11/19/77	1	2	7	>1	7
11/20/77	1	5	6	1	4
11/21/77	4	4	11	4	9
11/22/77	4	7	11	1	4

SECTION IV

NOISE ANALYSIS

A.   DISCUSSION

The goal of this section is to characterize the noise field at each site under evaluation.   Presented in this section are peak 1, 20, 25, and 30 second noise values, RMS trends and average RMS values in the 0.5-1.25, 10-25, 17-41, and 40-64 second passbands, and average short- and long-period RMS spectra.

All noise values in this section are presented without instrument response correction, since it is recognized that the analyst is primarily concerned with the noise as he will see it, i.e., after it has passed through the sensing, filtering, and recording instrumentation.   Instrument response corrected noise values are presented in Appendix B.

B.   VERTICAL COMPONENT SHORT-PERIOD NOISE

The short-period noise analysis for the five new stations currently being evaluated (CHTO, CTAO, KAAO, MAJO, and ZOBO) extended from 1 July 1977 to 31 December 1977.   Subject to data availability, three samples were taken from every fourth day, and from these three samples, one was chosen to represent that day.   All samples were picked in one of two ways.   First, on days that contained events from the data base, samples were taken from the portion of the automatic detector edit preceeding a detected event.   On days that contained no events from the data base, samples were picked randomly from automatic detector logs (see Section III) with the only requirement being that the time separating consecutive automatic detections exceed one hour.   This was done to prevent selecting a sample inside

IV-1

a series of multiple detections. The standardized length of each noise sample was 12.8 seconds, starting on the first point of the detector edit.

After all unacceptable samples were screened out, each sample was filtered by a 0.5-4.0 Hz bandpass filter. RMS noise was then computed by the equation

$$RMS \ NOISE = \left[\frac{\sum_{i=1}^{n} (x_i)^2}{n} \right]^{\frac{1}{2}}$$

where

n = number of data points

x_i = the ith data point.

The calculated RMS values (in millimicrons) were then plotted against Julian day in Figures IV-1 to IV-3 and the monthly RMS noise trends derived from these values were plotted in Figures IV-4 to IV-6.

The RMS noise trends for stations CHTO and ZOBO showed little change with time. Of these two, ZOBO had the lowest and the most consistent noise level. CHTO, on the other hand, showed several small peaks between days 200 and 270. These are possibly due to periods of storm activity.

Station KAAO showed very good day-to-day consistency, but the trend plot showed a peak through August and September. Stations CTAO and MAJO showed the most variability in both daily and trend RMS noise, with MAJO increasing slowly with time and CTAO decreasing with time.

Table IV-1 contains the mean short-period RMS noise values. A correlation between mean RMS noise level at a station and the distance between that station and the nearest coast is evident. This correlation was previously noted by Strauss and Weltman (1977). The stations with the lowest noise levels are located farthest from the nearest coast,

IV-2
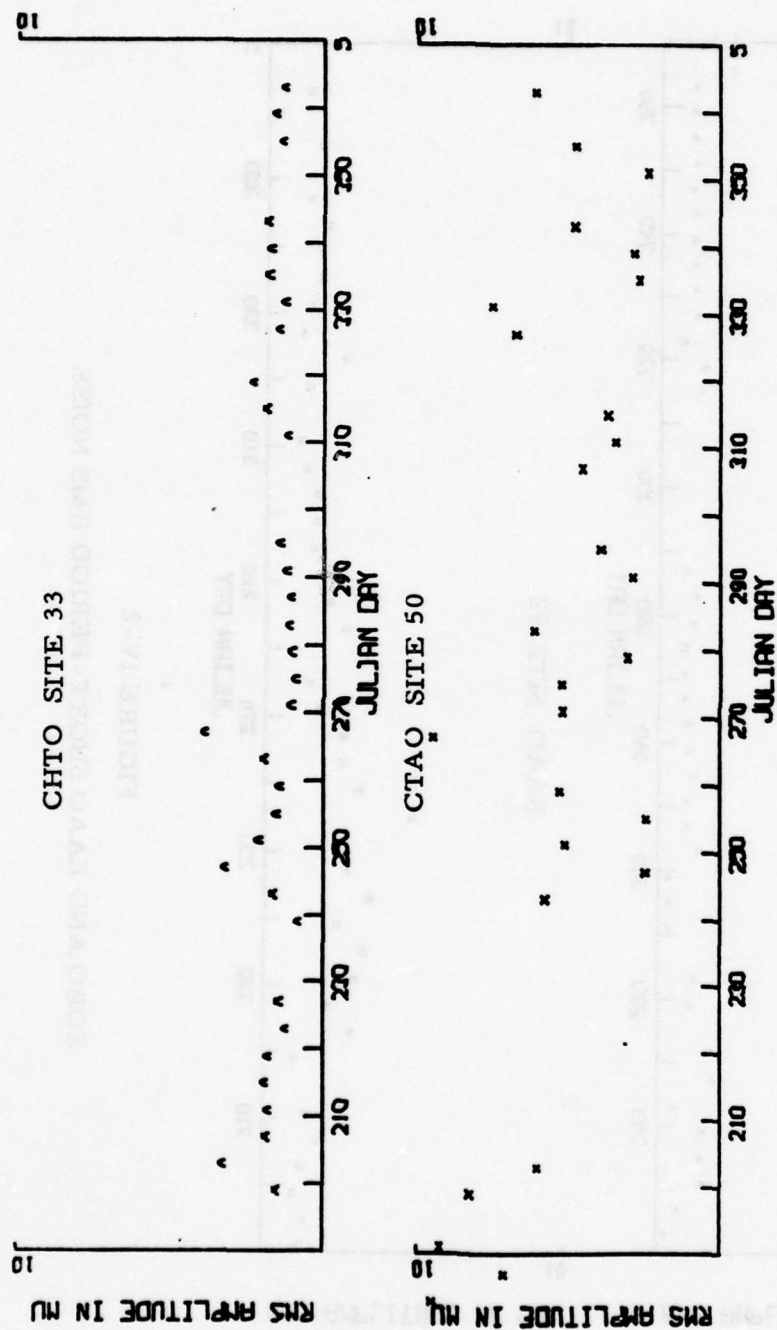
FIGURE IV-1

CHTO AND CTAO SHORT-PERIOD RMS NOISE
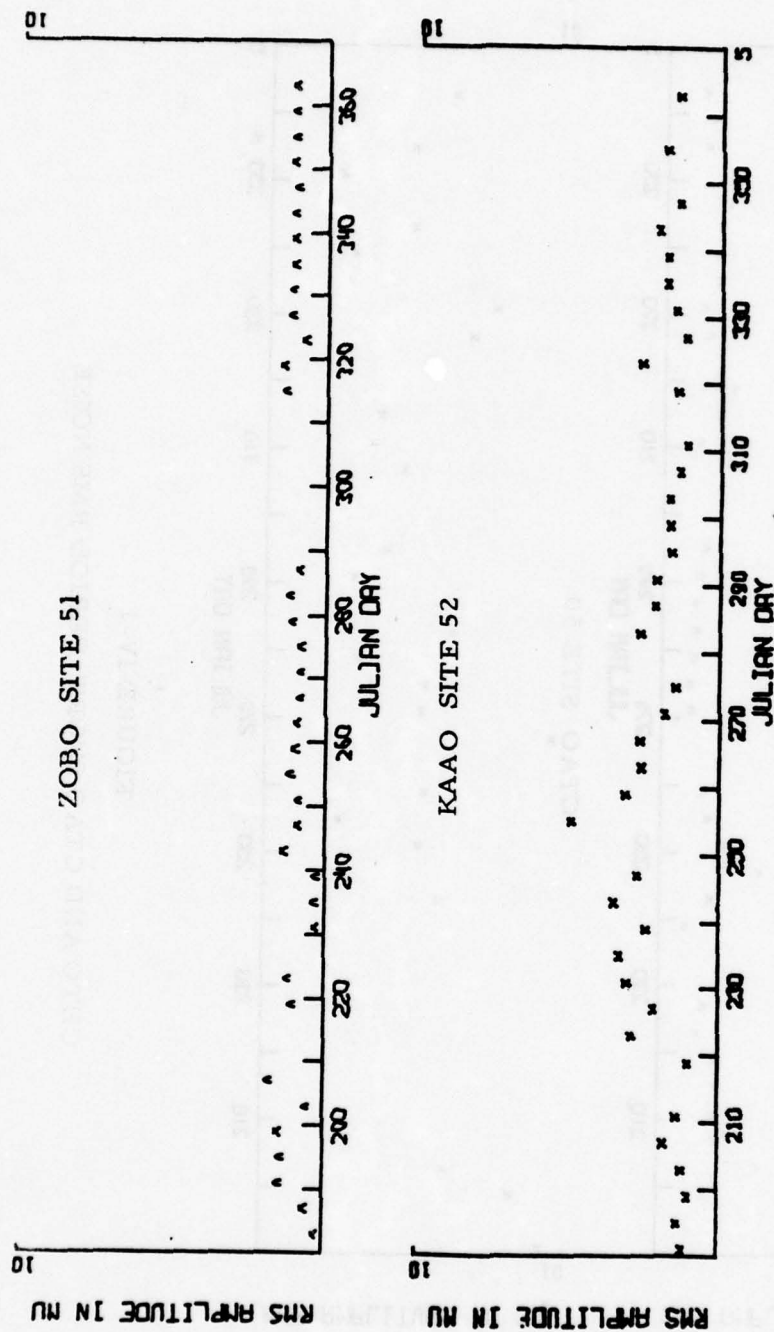
FIGURE IV-2

ZOBO AND KAAO SHORT-PERIOD RMS NOISE
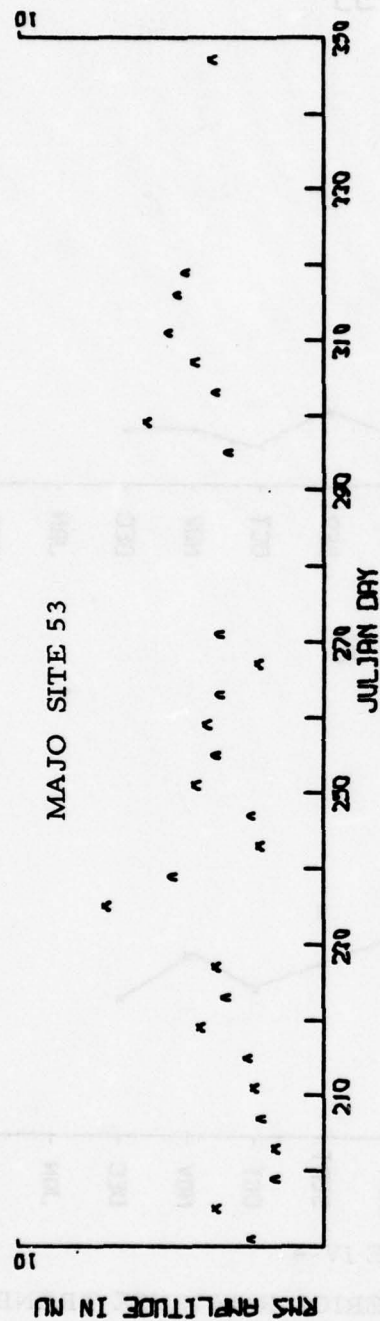
MAJO SITE 53

FIGURE IV-3

MAJO SHORT-PERIOD RMS NOISE

IV-5

SITE 33
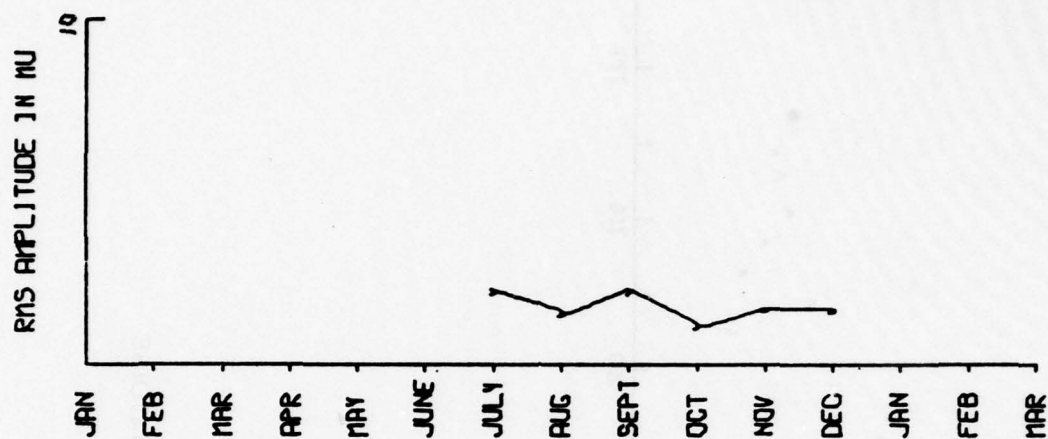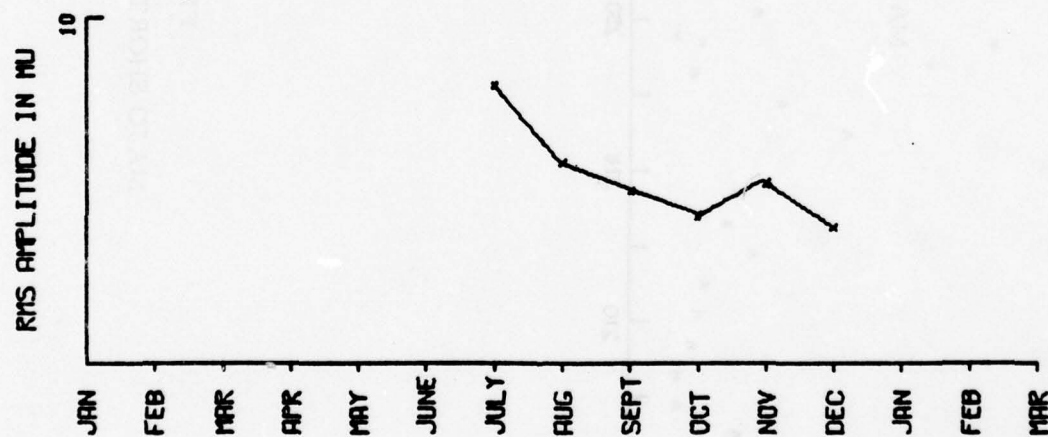
SITE 50

FIGURE IV-4

CHTO AND CTAO SHORT-PERIOD RMS NOISE TRENDS

IV-6
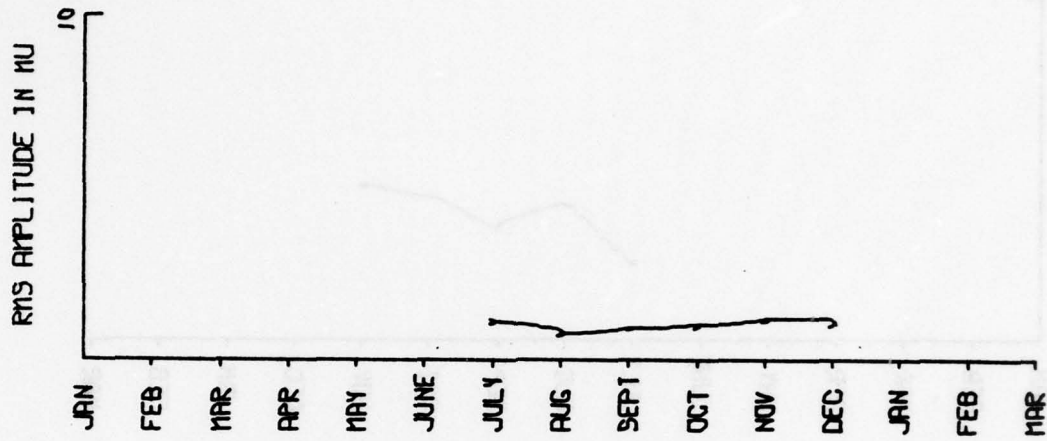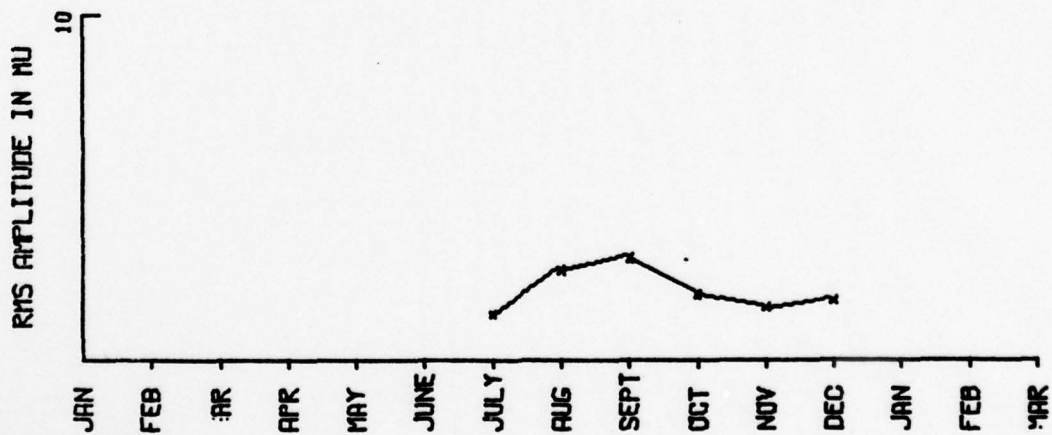
SITE 51

SITE 52

FIGURE IV-5

ZOBO AND KAAO SHORT-PERIOD RMS NOISE TRENDS

SITE 53
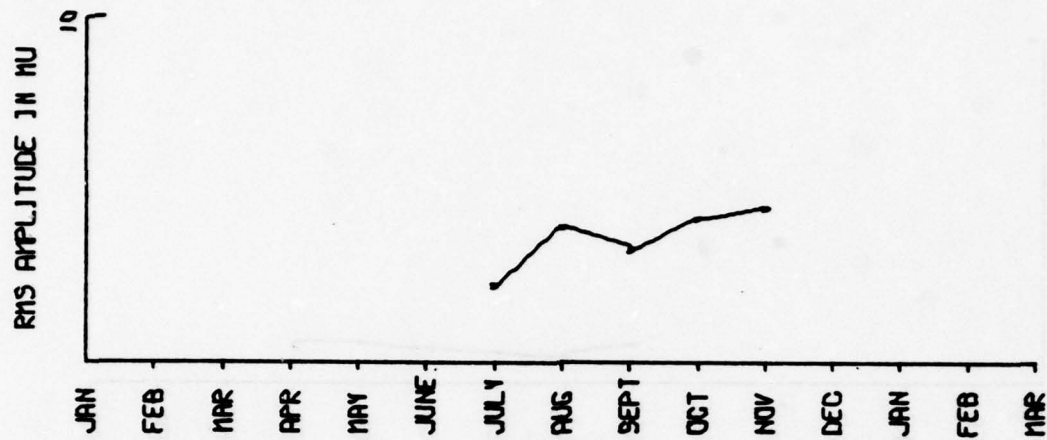
FIGURE IV-6

MAJO SHORT-PERIOD RMS NOISE TRENDS

IV-8

TABLE IV-1
MEAN SHORT-PERIOD RMS NOISE (VERTICAL COMPONENT)

Station	Approximate Distance to Nearest Coast (km)	Mean RMS Noise (mμ)	Standard Deviation	Number of Samples
CHTO	290	1.67	0.67	34
CTAO	120	5.55	2.27	28
KAAO	1100	1.94	0.69	37
MAJO	110	3.53	1.31	28
ZOBO	300	1.02	0.36	37

i. e. , ZOBO, CHTO, and KAAO. MAJO and CTAO are much closer to the coast than the other three stations and their noise levels are significantly higher. As can be seen from Table IV-1, however, the correlation is not exact. For this reason, the 'baseline RMS', the level above which short-period noise is caused by sea wave energy, cannot be accurately defined. These data place the baseline between 1.0 mμ and 2.0 mμ .

Maximum zero-to-peak one-second period noise was also measured for each sample. The statistics of these measurements are presented in Table IV-2 in terms of the mean and standard deviation of the logarithm of the measured values.

Short-period noise analysis was expanded this year to include spectral analysis. Each sample was filtered with a 0.5-4.0 Hz bandpass filter and the mean and standard deviation of the amplitude spectrum was calculated for each frequency increment. The mean spectral density and the logarithm of the mean spectral density with standard deviations are plotted in Figures IV-7 to IV-11.

In a study of ambient earth motion, Fix (1972) observed peaks in the spectral density at periods of 0.3 and 0.5 seconds, with the 0.5 second peak being slightly less prominent. These were proved to be primarily fundamental mode Rayleigh waves (Douze, 1967). The results of our analyses compare fairly well with those findings. MAJO and CHTO show peaks at approximately 0.3 seconds, and ZOBO and CHTO show clear peaks at 0.5 and 0.55 seconds, respectively. Stations CTAO and KAAO, however, show neither of these peaks clearly. KAAO shows a peak at approximately 0.75 seconds, but at shorter periods the spectrum contains no clear peaks. There is a concentration of energy between periods of 0.3 to 0.6 seconds, but there is no 'structure' to the spectrum like those at the other stations mentioned. This concentration is probably caused by cultural noise. The CTAO spectrum is even more unlike the spectra of the other stations. Not only are the

TABLE IV-2

SHORT-PERIOD NOISE
LOG_{10} (PEAK ONE-SECOND NOISE AMPLITUDE) STATISTICS

Station	Mean Log_{10} Peak 1-Second	Standard Deviation Log_{10} Peak 1-Second	Number of Samples
CHTO	0.369	0.182	29
CTAO	0.614	0.260	21
KAAO	0.463	0.207	33
MAJO	0.556	0.213	26
ZOBO	0.098	0.199	33

PERIOD (SECONDS)

SITE 33

Log RMS Amplitude

2.20   1.20   0.20

Station	Mean Log Peak 1-Second	Standard Deviation Peak 1-Second	Number of Samples
CHTO		0.185	49
	0.14	0.260	21
	0.403	0.202	73
	0.550	0.219	26
	0.068	0.139	37

PERIOD
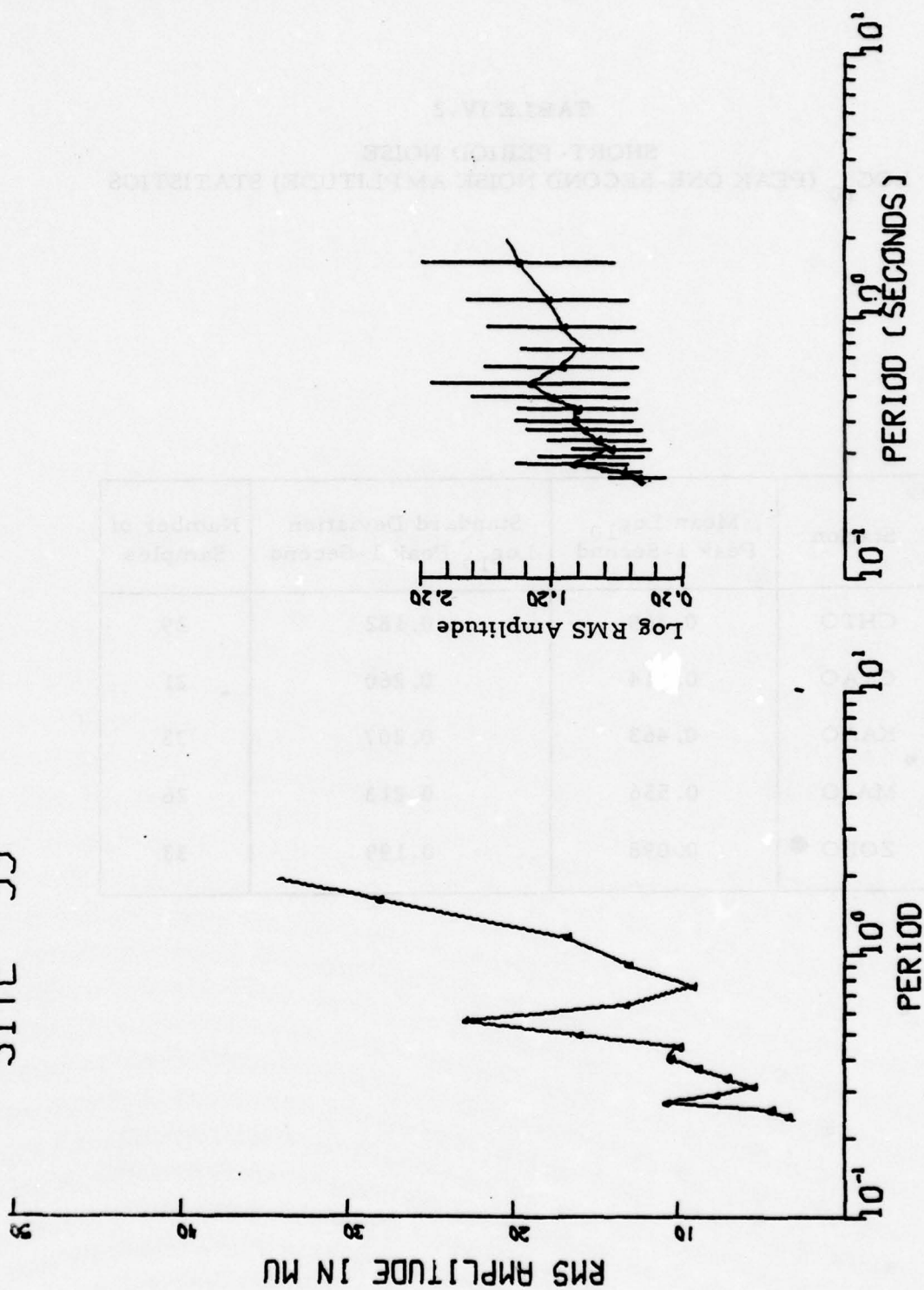
RMS AMPLITUDE IN MU

FIGURE IV-7

AVERAGE RMS AMPLITUDE SPECTRA CHTO SHORT-PERIOD NOISE

SITE 50

RMS AMPLITUDE IN MU

PERIOD

Log RMS Amplitude

PERIOD (SECONDS)
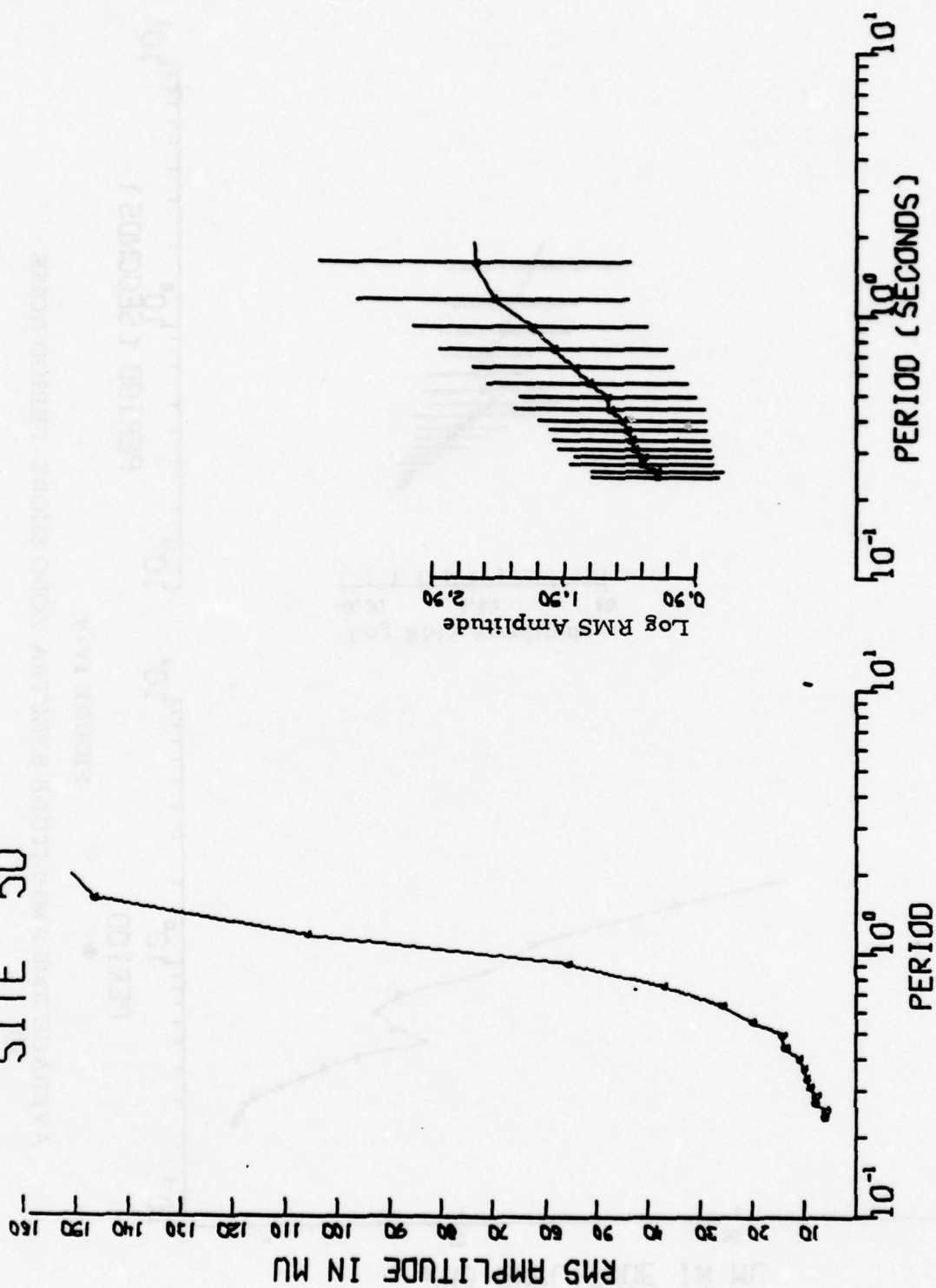
FIGURE IV-8

AVERAGE RMS AMPLITUDE SPECTRA CTAO SHORT-PERIOD NOISE

IV-13

SITE 51

RMS AMPLITUDE IN MU

PERIOD

PERIOD (SECONDS)
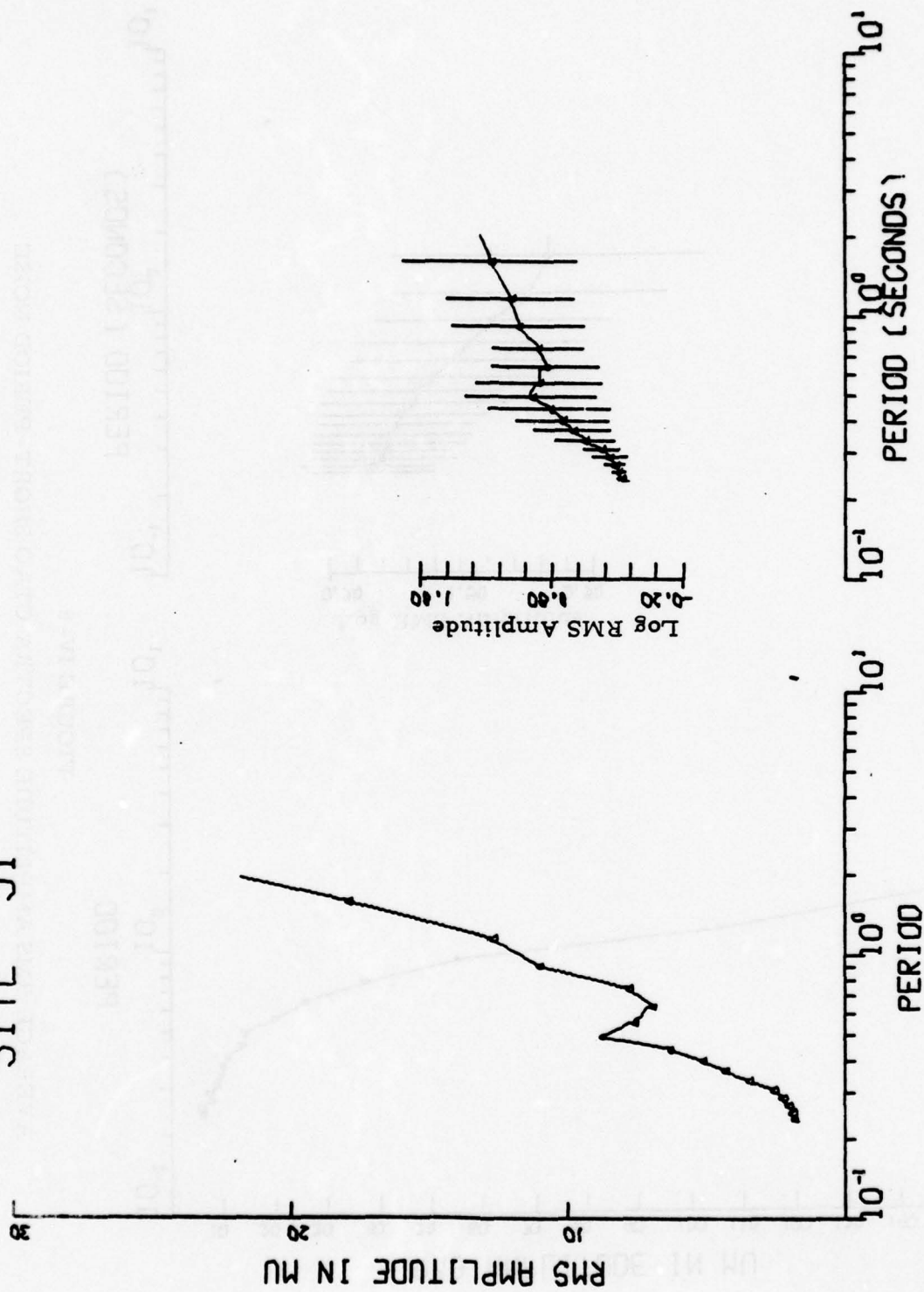
Log RMS Amplitude

FIGURE IV-9

AVERAGE RMS AMPLITUDE SPECTRA ZOBO SHORT-PERIOD NOISE

IV-14
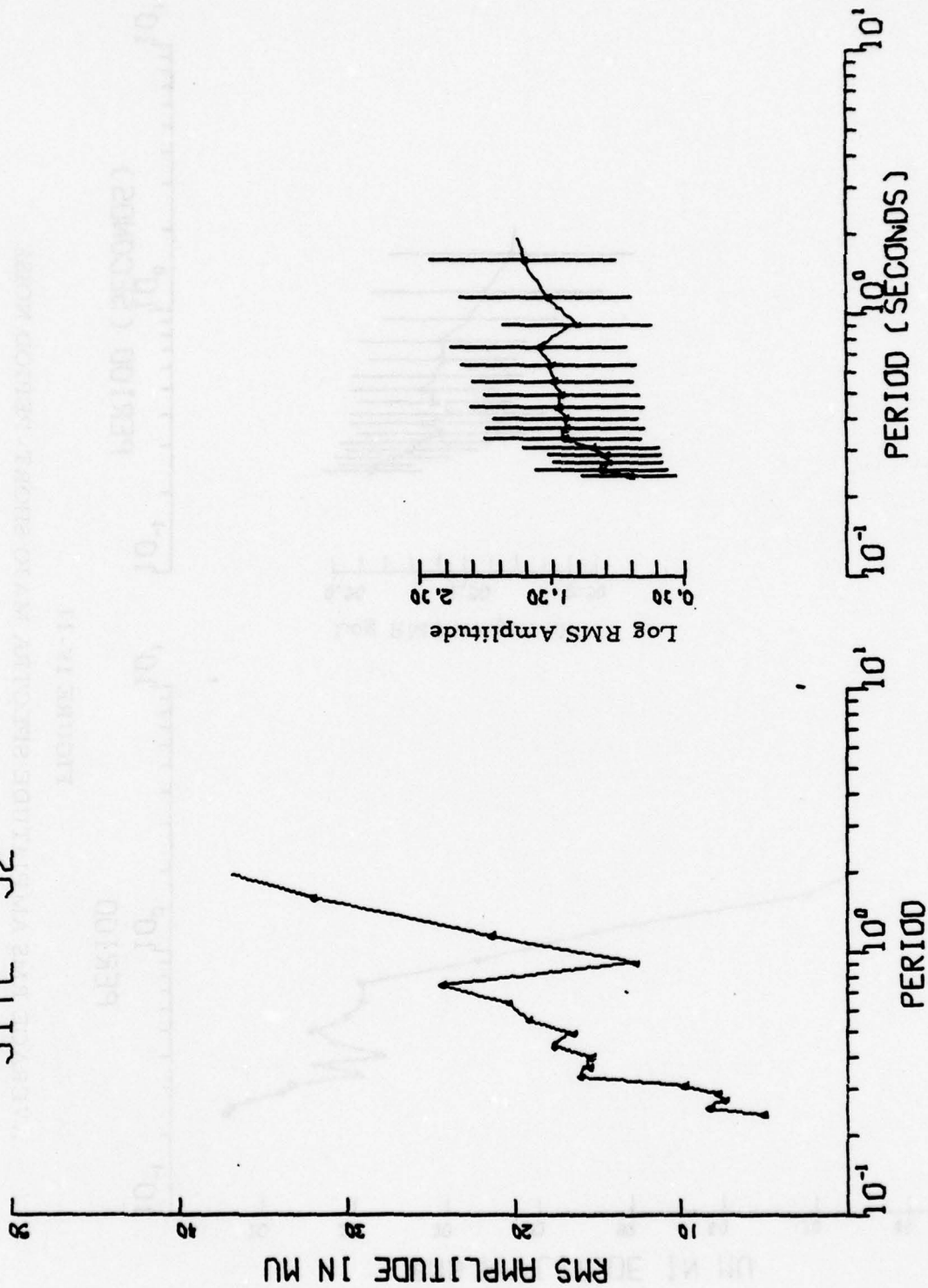
SITE 52

FIGURE IV-10

AVERAGE RMS AMPLITUDE SPECTRA KAAO SHORT-PERIOD NOISE

IV-15
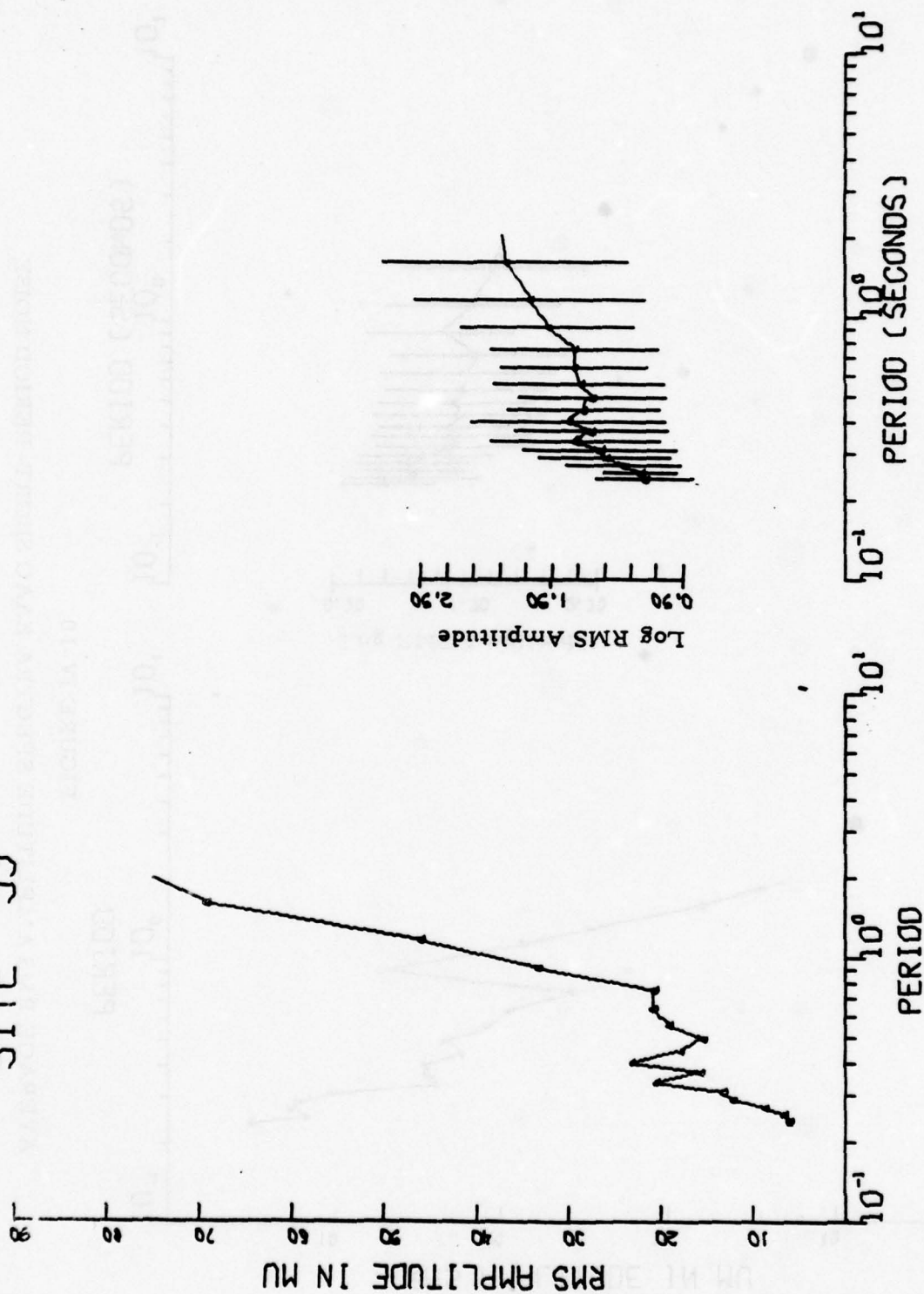
FIGURE IV-11

AVERAGE RMS AMPLITUDE SPECTRA MAJO SHORT - PERIOD NOISE

amplitudes inflated, but there are no apparent concentrations of energy at any frequency. No ready explanation can be given for this peculiarity. Perhaps the site is contaminated by some strong source of cultural noise.

C. THREE COMPONENT LONG-PERIOD NOISE

The goals of the long-period noise analysis were to estimate long-period RMS noise levels, peak noise amplitudes, and the spectral content of the noise field for each of the three components (V, N, E) at each station under evaluation.

Long-period noise processing usually began two months after each station's declared operational date and continued as long as time and computer availability permitted. The time periods covered are shown in Table IV-3. The two-months delay was instituted to ensure that each station was functioning properly prior to evaluation. Noise analysis time frames were limited to one data year and periods of known hardware malfunction were deleted from the noise data base.

The 4096-second noise samples were processed as described in Section II. The V, N, E configuration was maintained. Samples were processed at 1200 hours every fourth day, where possible. Samples were visually screened for signals and unreported system malfunctions and 1024-second noise analysis gates were selected. If an entire sample proved unacceptable, a second attempt followed, and an acceptable noise sample was usually found at an edit time within two hours of the first. Noise samples and analysis gates were then input into a primary analysis program which performed the following functions:

- Computed RMS noise values with and without instrument response in the following passbands: 10-25, 17-41, and 40-64 seconds.

- Measured zero-to-peak 20, 25, and 30-second noise amplitudes.

TABLE IV-3
LONG-PERIOD NOISE DATA BASE

Station	Start Date (Year-Julian Day)	End Date (Year-Julian Day)	Number of Samples
ANMO	77009	76362	88
CHTO	77251	78022	31
MAIO	76001	76365	82
CTAO	77003	77363	83
ZOBO	77153	77341	39
KAAO	77191	78050	53
MAJO	78090	78177	20

• Computed power spectra.

The variety of RMS and peak amplitude measurements were made for the following reasons. The 17-41 second passband encompasses the signal band traditionally of interest from a detection and discrimination capability viewpoint; the 10-25 second passband is centered upon the 17-second microseismic peak evident at most stations, and the 40-64 second passband provides a look at lower frequency noise present at SRO sites. The variety of peak amplitude measurements further describes the noise field at each site.

All RMS and peak noise values, and the first half of each power spectrum (128 points) were recorded on magnetic tape. This tape served as input to the final analysis and plotting routines.

Long-period RMS noise values (uncorrected for instrument response) for the vertical, north, and east components are plotted versus Julian day in Figures IV-12a through IV-17c for stations ANMO, MAIO, CHTO, CTAO, ZOBO, and KAAO. Data gaps of up to eight days usually reflect an inability to find uncontaminated noise samples. Larger gaps usually imply station down-time.

Figures IV-12a, IV-12b, and IV-12c show ANMO RMS noise versus Julian day within the three passbands. For both ANMO and MAIO, which are represented by Figures IV-14a, IV-14b, and IV-14c, the greater variances in daily noise values appear in days 1 to 90 and again in days 300 to 360, implying winter storm activity at these stations (Strauss and Weltman, 1977). The most stable noise passband for ANMO and MAIO is the 40-64 second passband, a fact common to most stations. MAIO exhibits another common property; vertical component noise is significantly lower in amplitude than horizontal component noise in the 40-64 second passband. CHTO, Figures IV-13a, IV-13b, and IV-13c, shows no real pattern; its daily variance remains rather constant. RMS values seem most stable in the 40-64

IV-19

SITE 30

Vertical

North

East

RMS AMPLITUDE IN MU
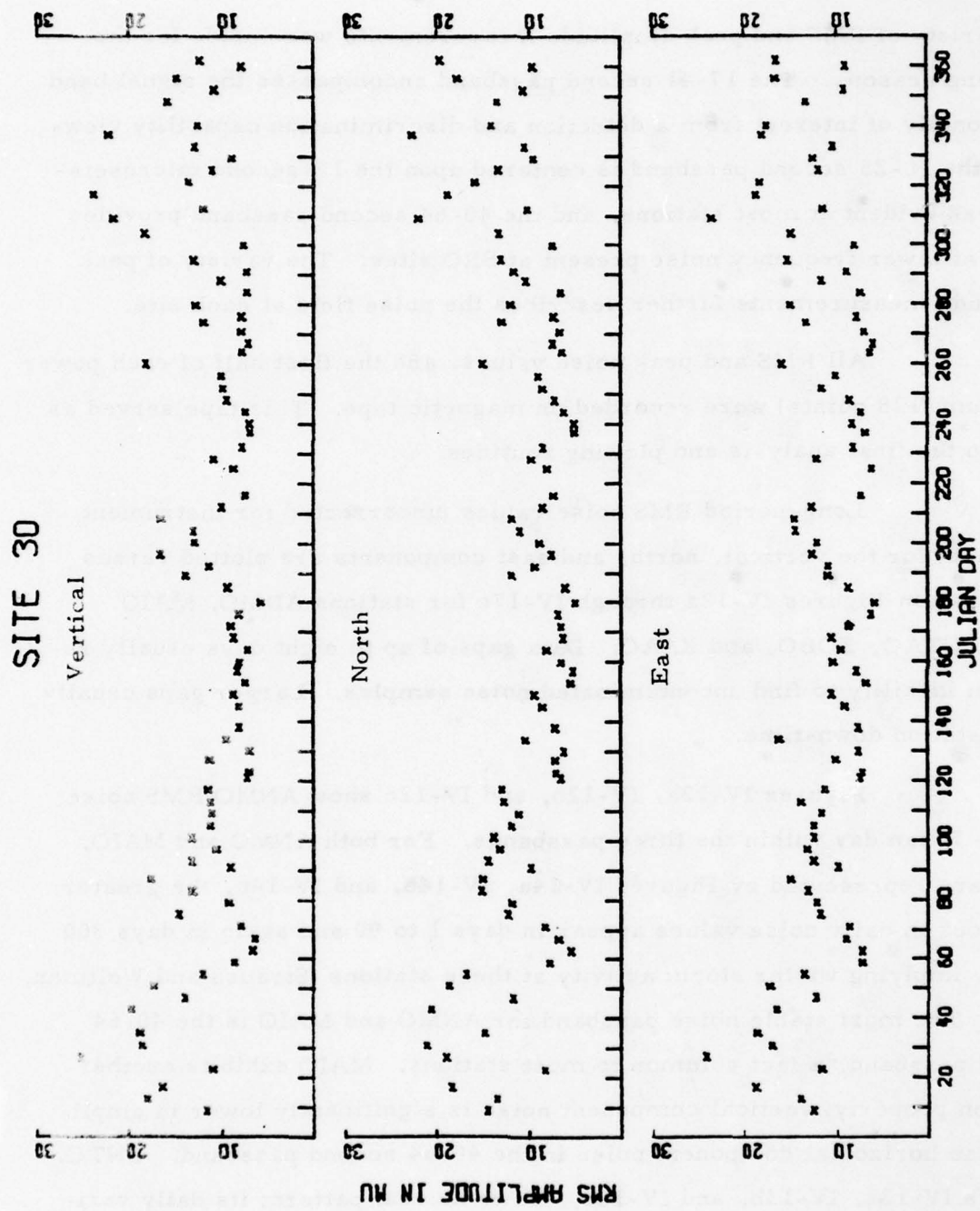
JULIAN DAY

FIGURE IV-12a

ANMO 10-25 SECOND RMS NOISE
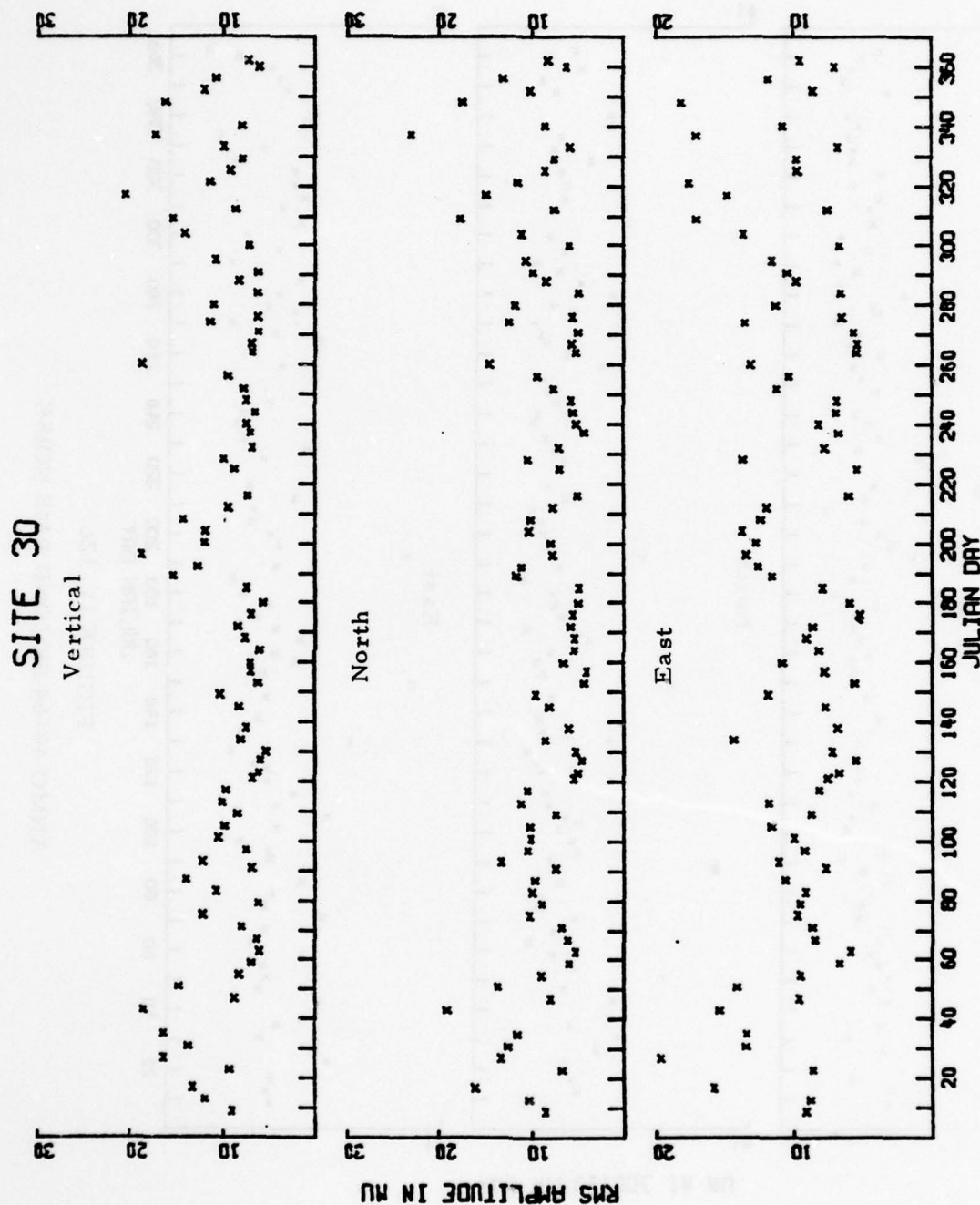
FIGURE IV-12b

ANMO 17-41 SECOND RMS NOISE

SITE 30

Vertical

North

East
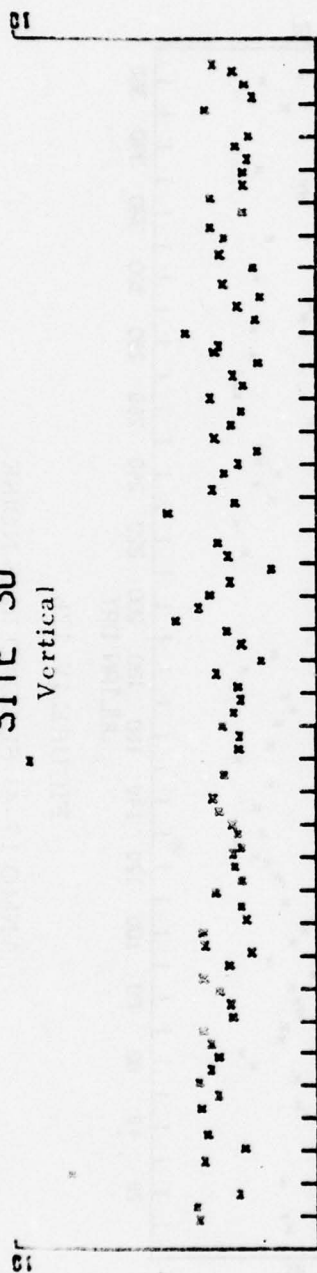
RMS AMPLITUDE IN MU
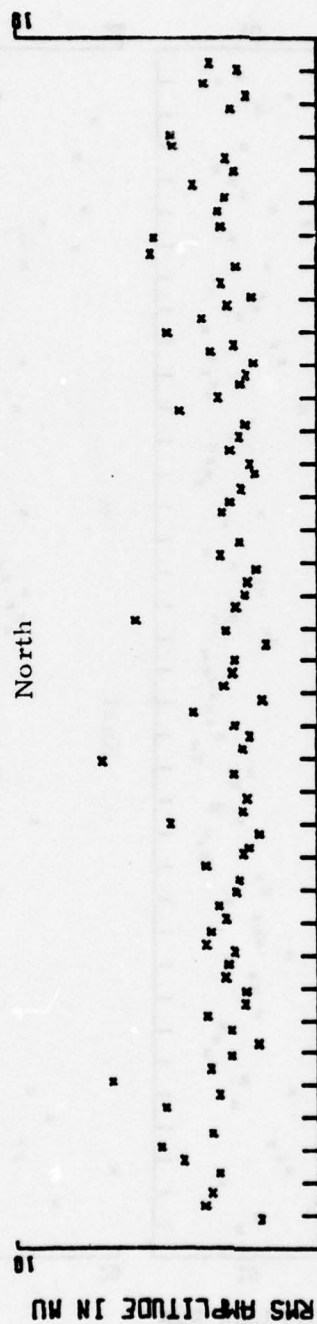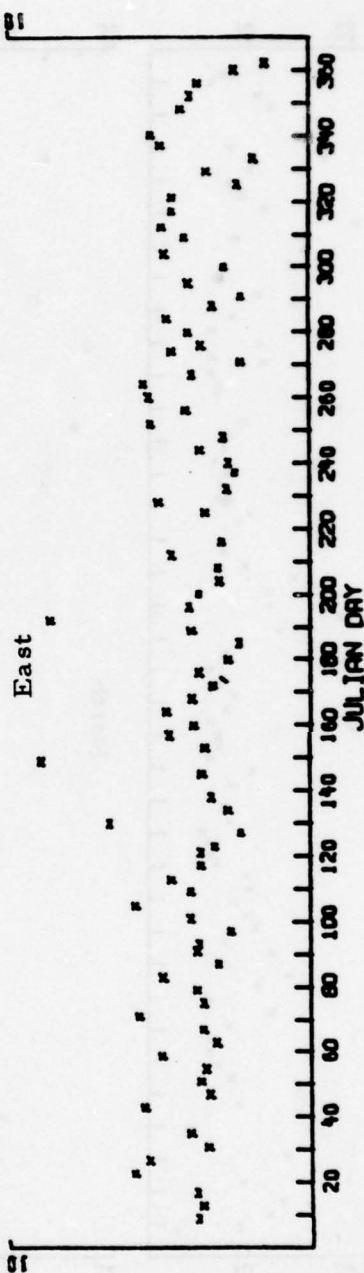
JULIAN DAY

FIGURE IV-12c

ANMO 40-64 SECOND RMS NOISE

IV-22
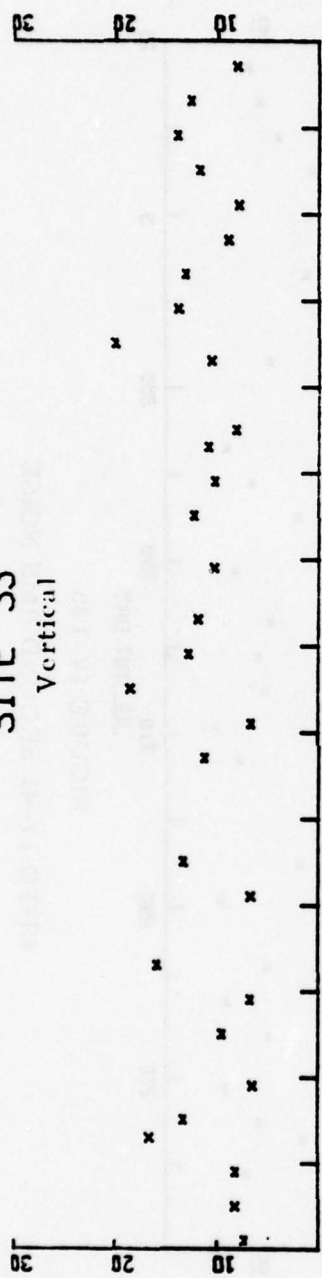
SITE 33
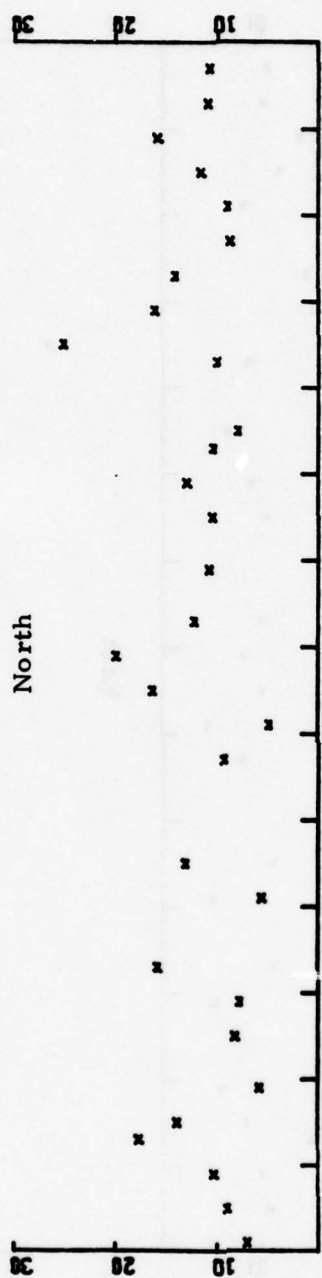
Vertical
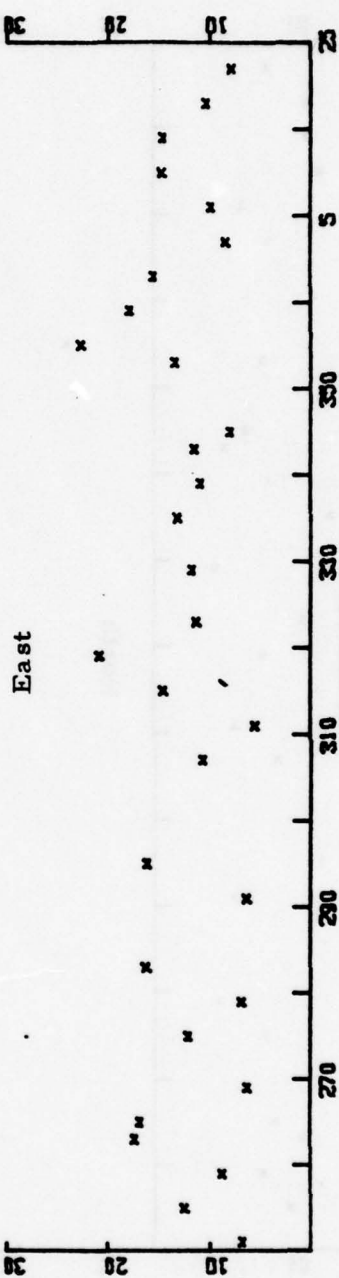
North

East

RMS AMPLITUDE IN MU

JULIAN DAY

FIGURE IV-13a

CHTO 10-25 SECOND RMS NOISE

IV-23

SITE 33

Vertical

North

East

RMS AMPLITUDE IN MU
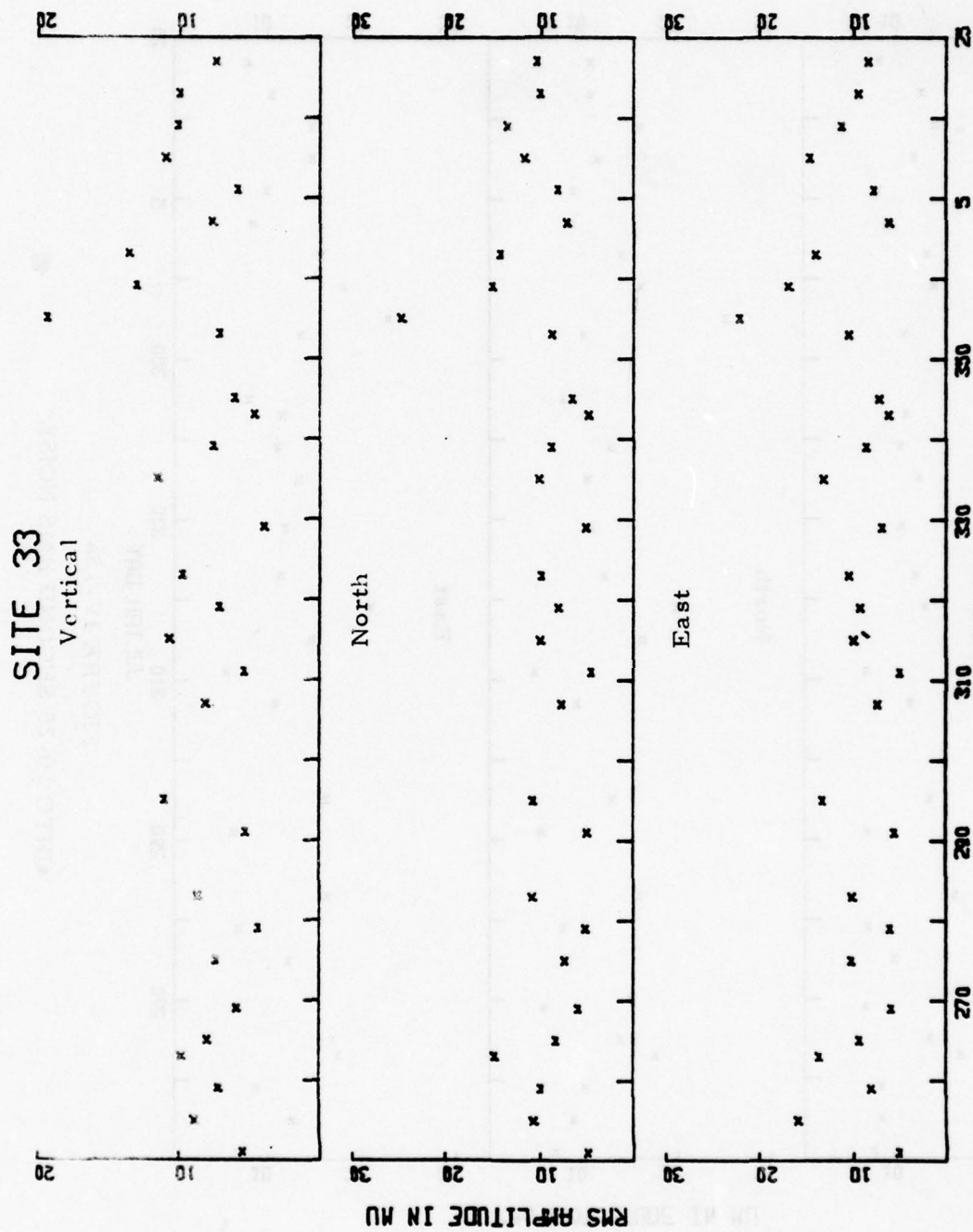
JULIAN DAY

FIGURE IV-13b

CHTO 17-41 SECOND RMS NOISE

SITE 33
Vertical

North

East

RMS AMPLITUDE IN MU
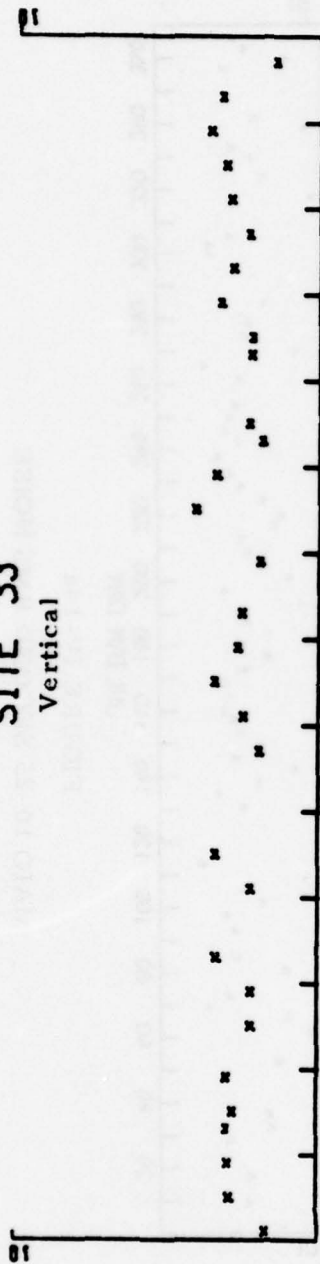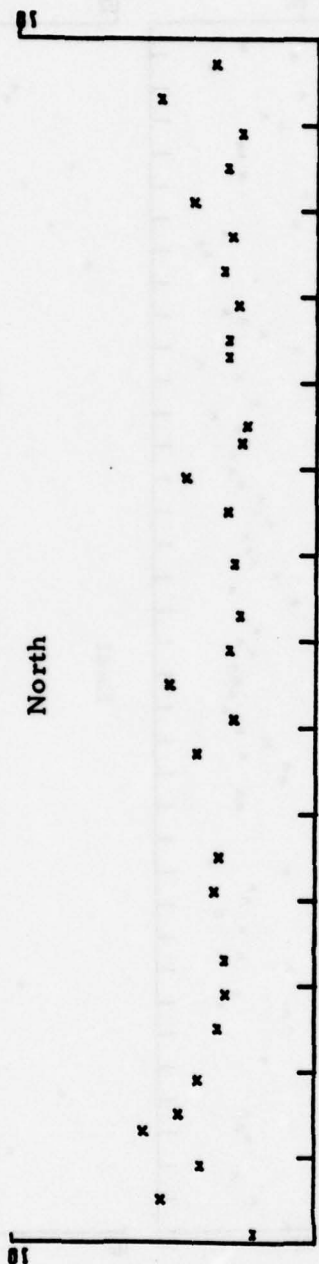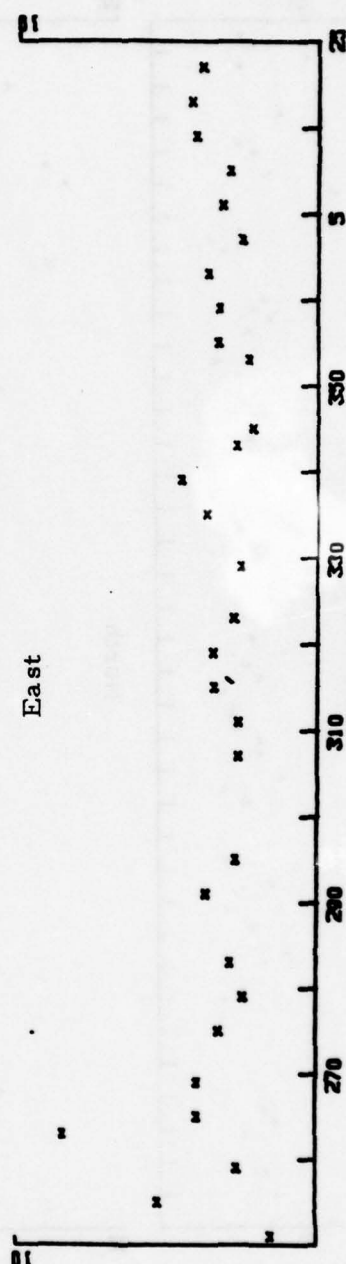
JULIAN DAY

FIGURE IV-13c

CHTO 40-64 SECOND RMS NOISE

IV-25

SITE 36

Vertical

North

East

RMS AMPLITUDE IN MU

JULIAN DAY
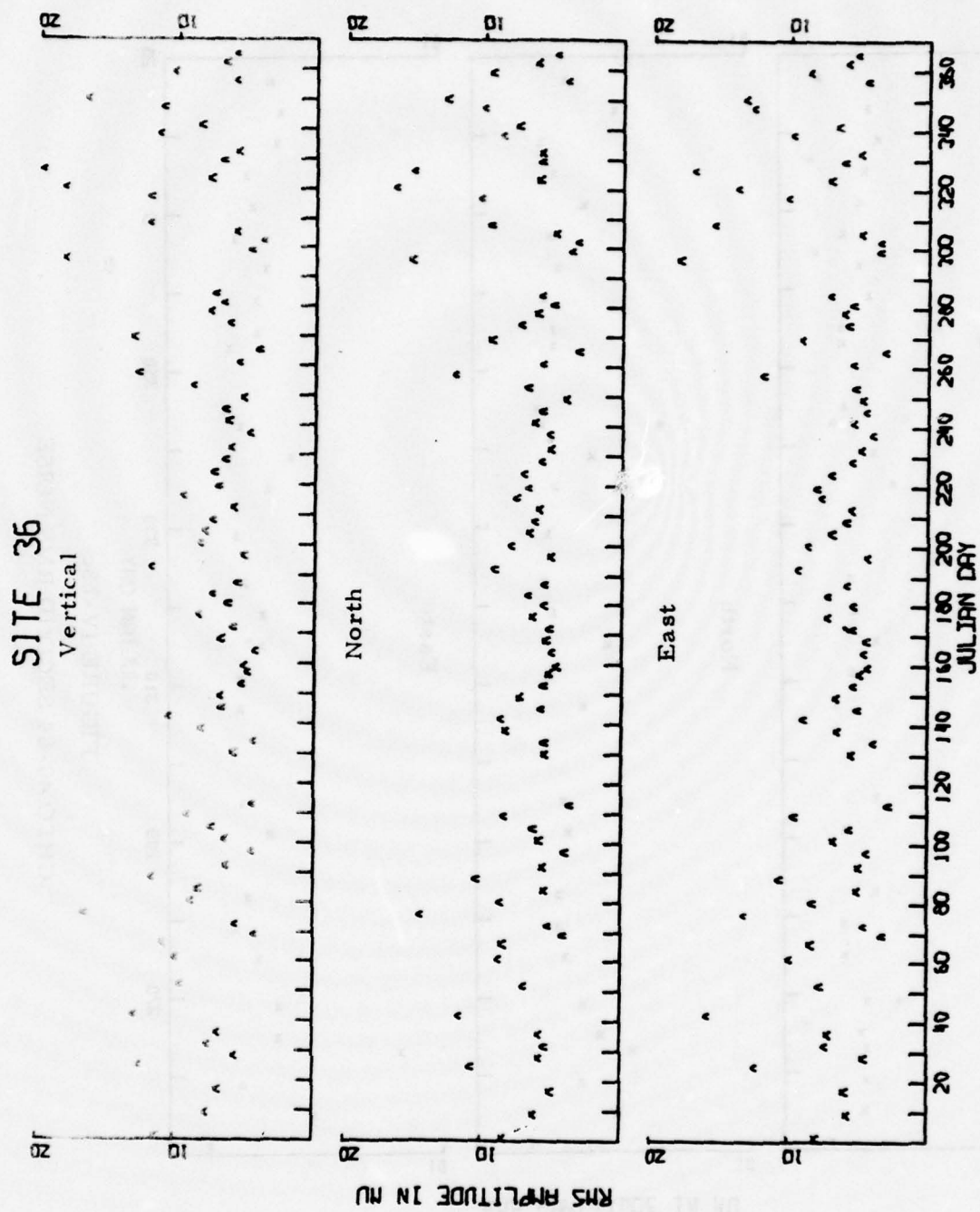
FIGURE IV-14a

MAIO 10-25 SECOND RMS NOISE

IV-26

SITE 36
Vertical

North

East

RMS AMPLITUDE IN NU

JULIAN DAY
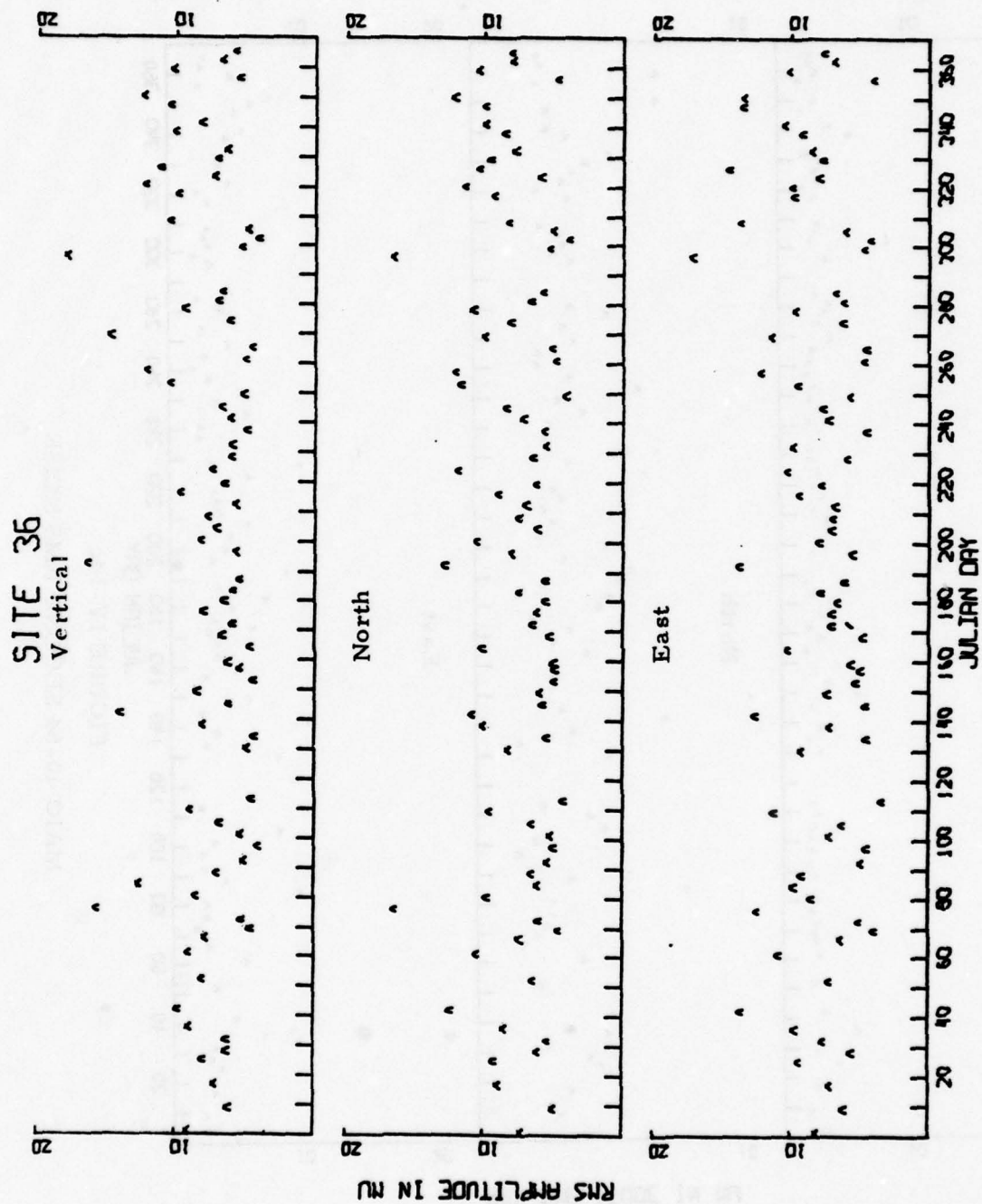
FIGURE IV-14b

MAIO 17-41 SECOND RMS NOISE

IV-27

SITE 36
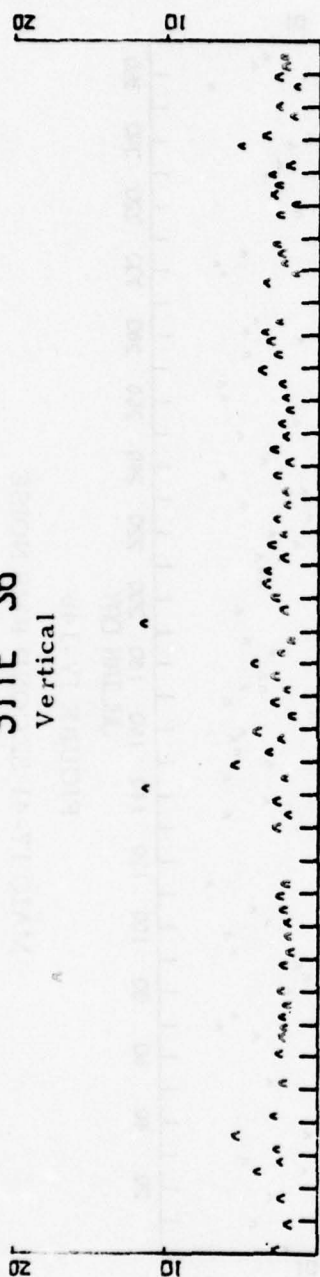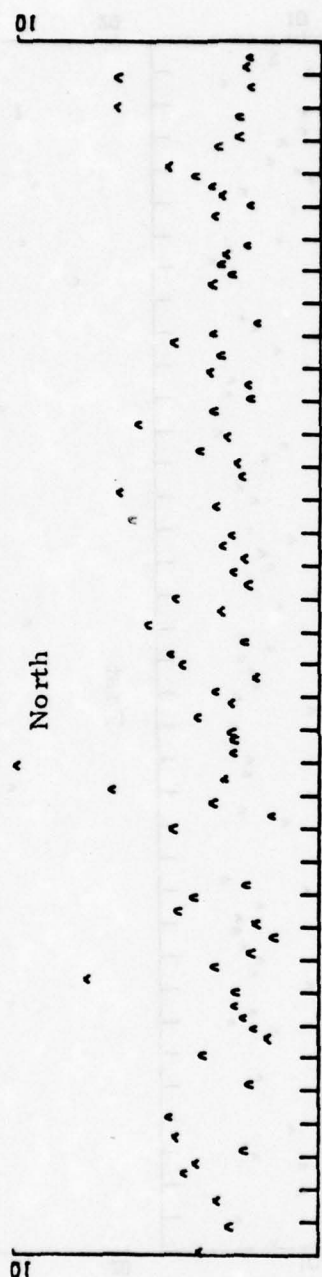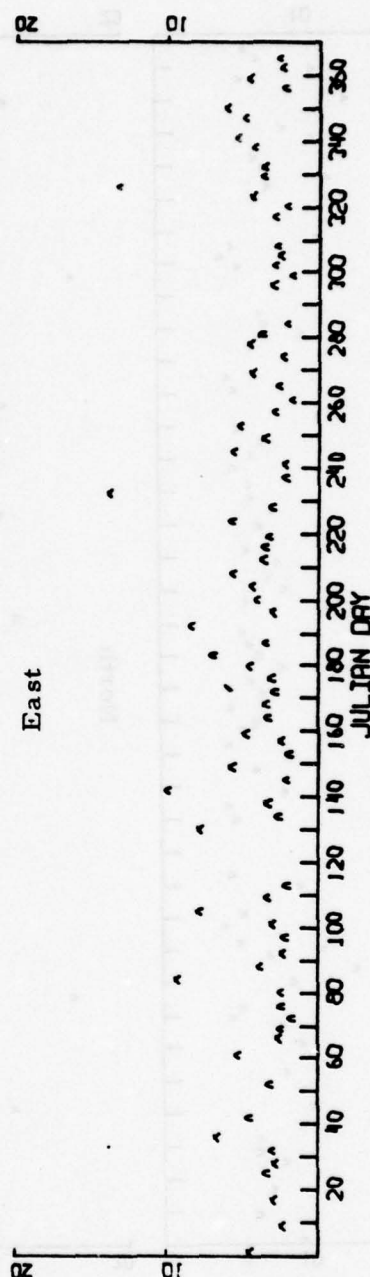
FIGURE IV-14c

MAIO 40-64 SECOND RMS NOISE
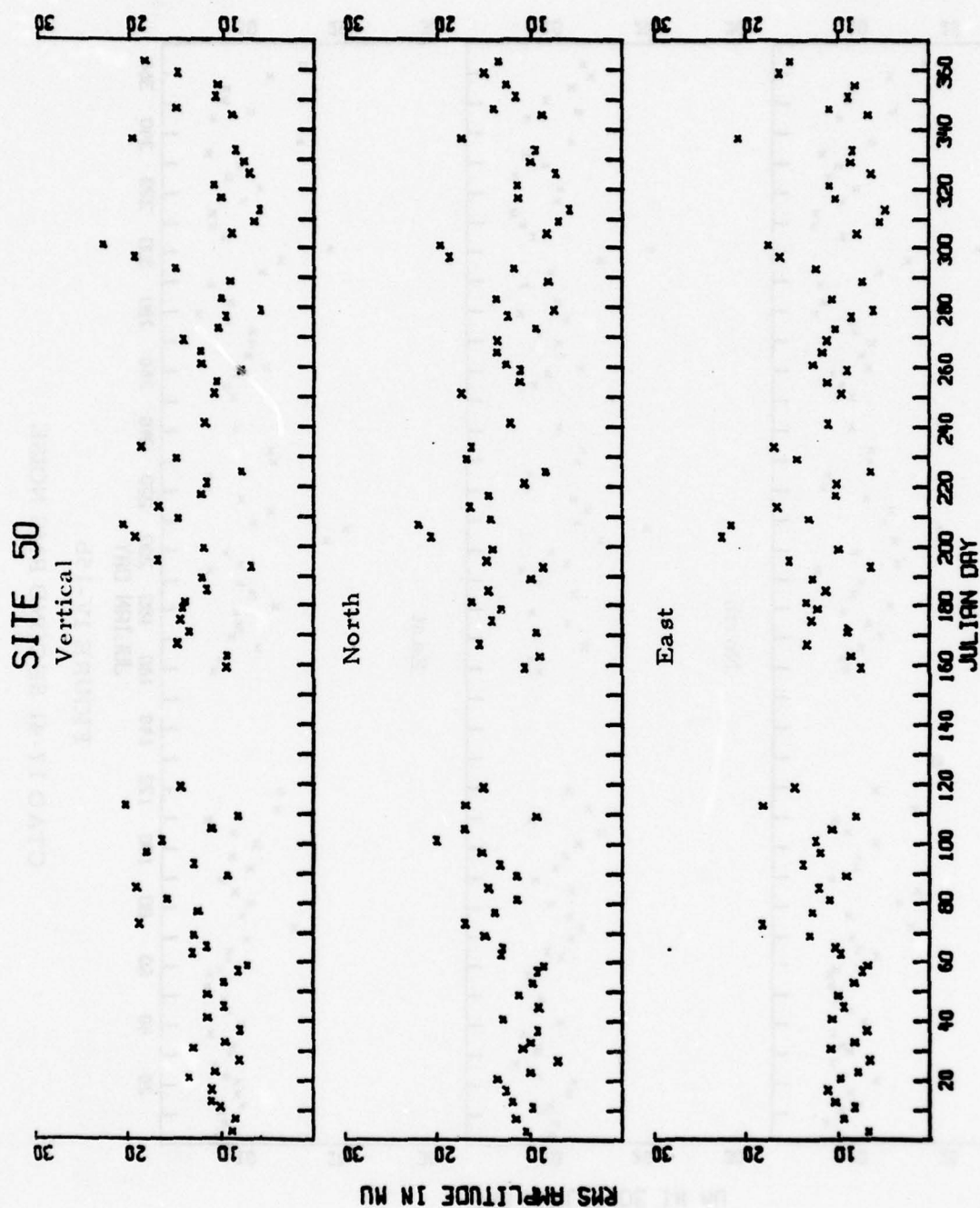
SITE 50

FIGURE IV-15a

CTAO 10-25 SECOND RMS NOISE

IV-29

SITE 50

Vertical

North

East

RMS AMPLITUDE IN MU
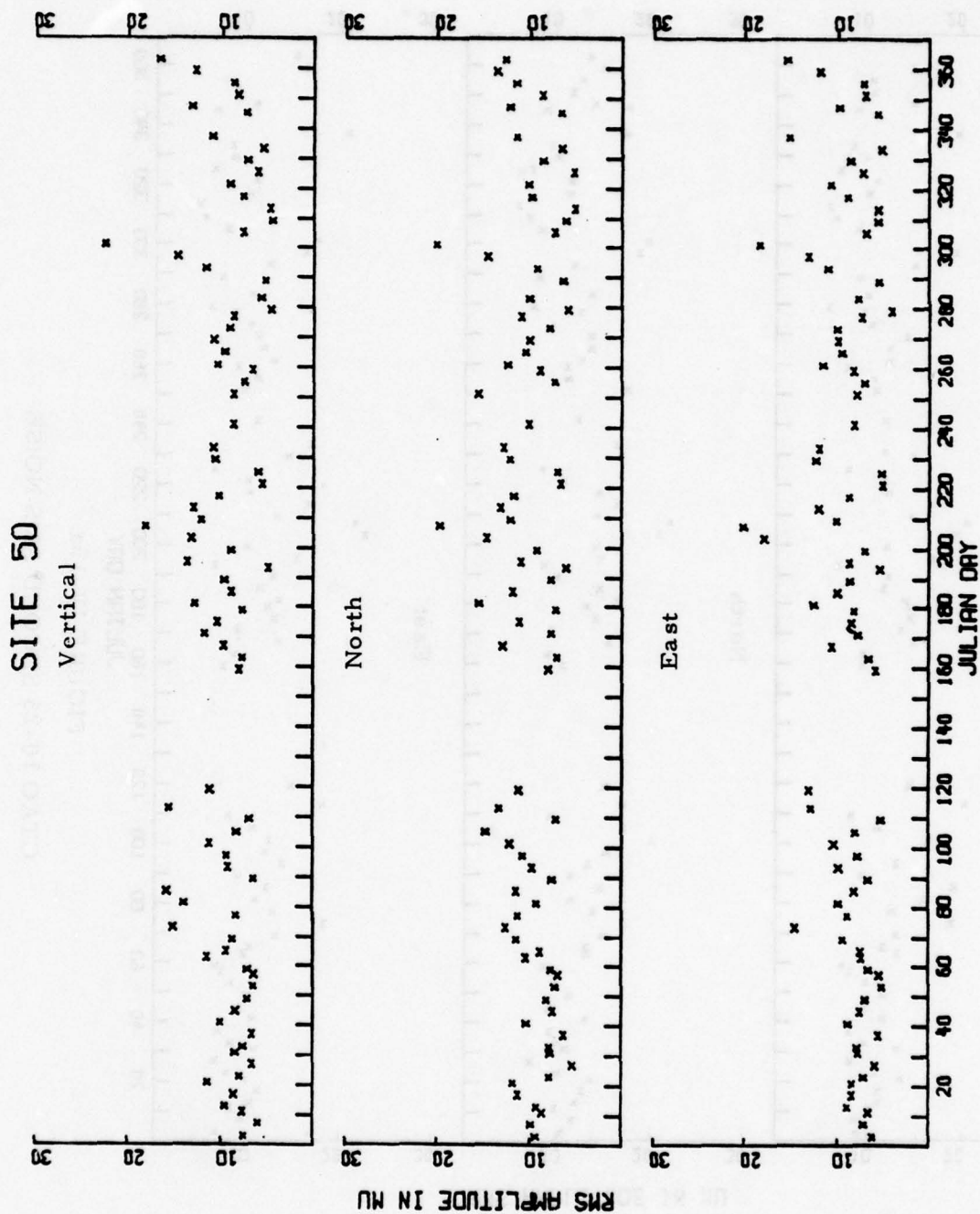
JULIAN DAY

FIGURE IV-15b

CTAO 17-41 SECOND RMS NOISE

IV-30

SITE 50

Vertical

North

East

RMS AMPLITUDE IN MU
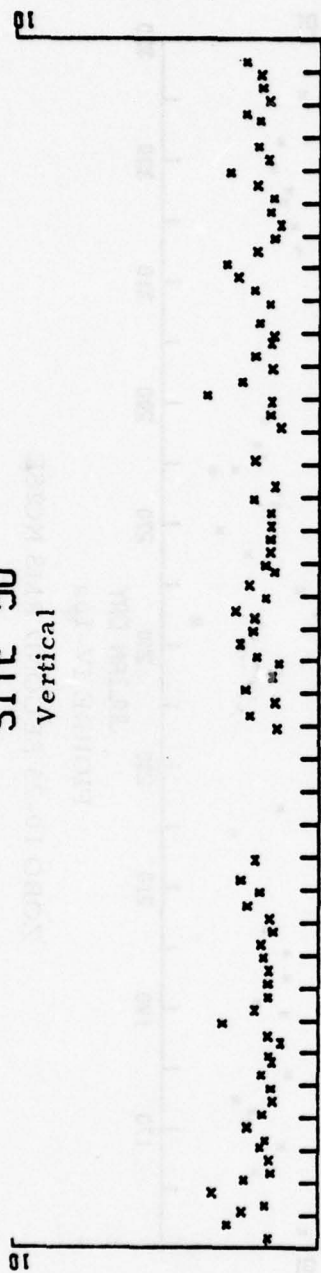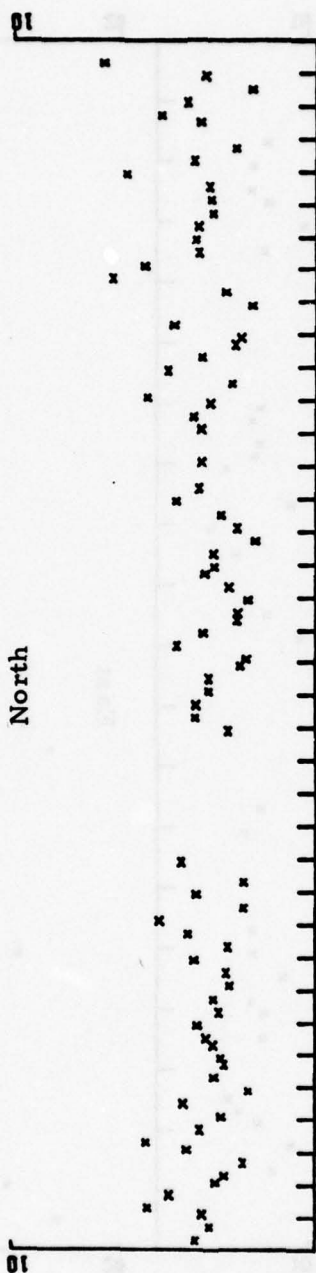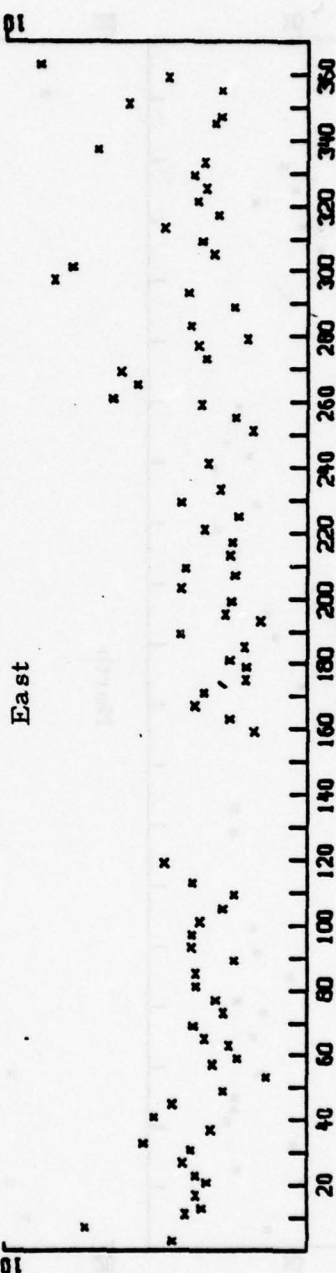
JULIAN DAY

FIGURE IV-15c

CTAO 40-64 SECOND RMS NOISE

SITE 51

Vertical

North

East

RMS AMPLITUDE IN MU
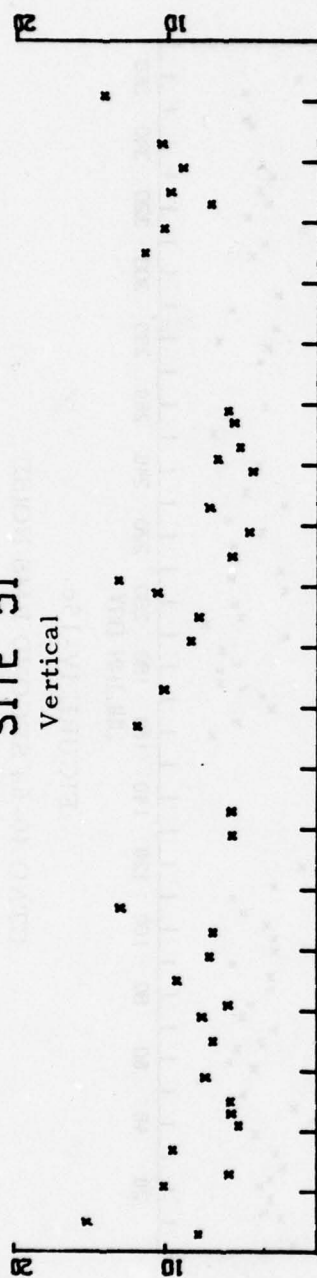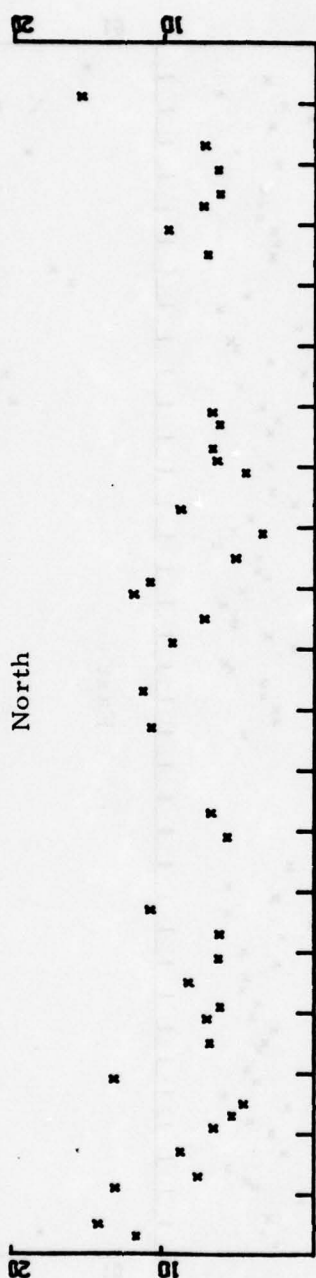
JULIAN DAY

FIGURE IV-16a

ZOBO 10-25 SECOND RMS NOISE

IV-32

SITE 51

Vertical

North

East

JULIAN DAY

RMS AMPLITUDE IN MU

ZOBO 17-41 SECOND RMS NOISE

FIGURE IV-16b

IV-33

SITE 51
Vertical

North

East

RMS AMPLITUDE IN MU

JULIAN DAY
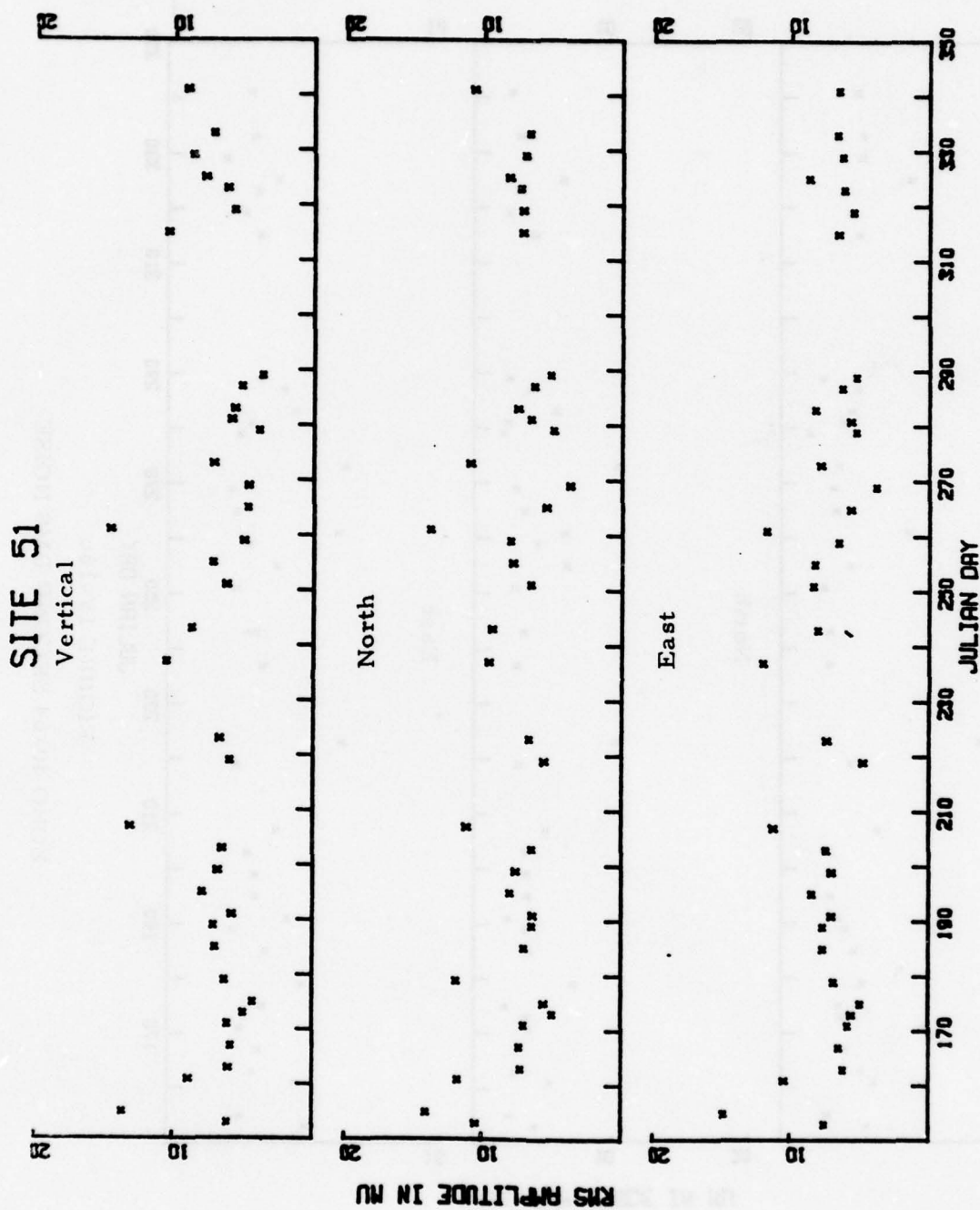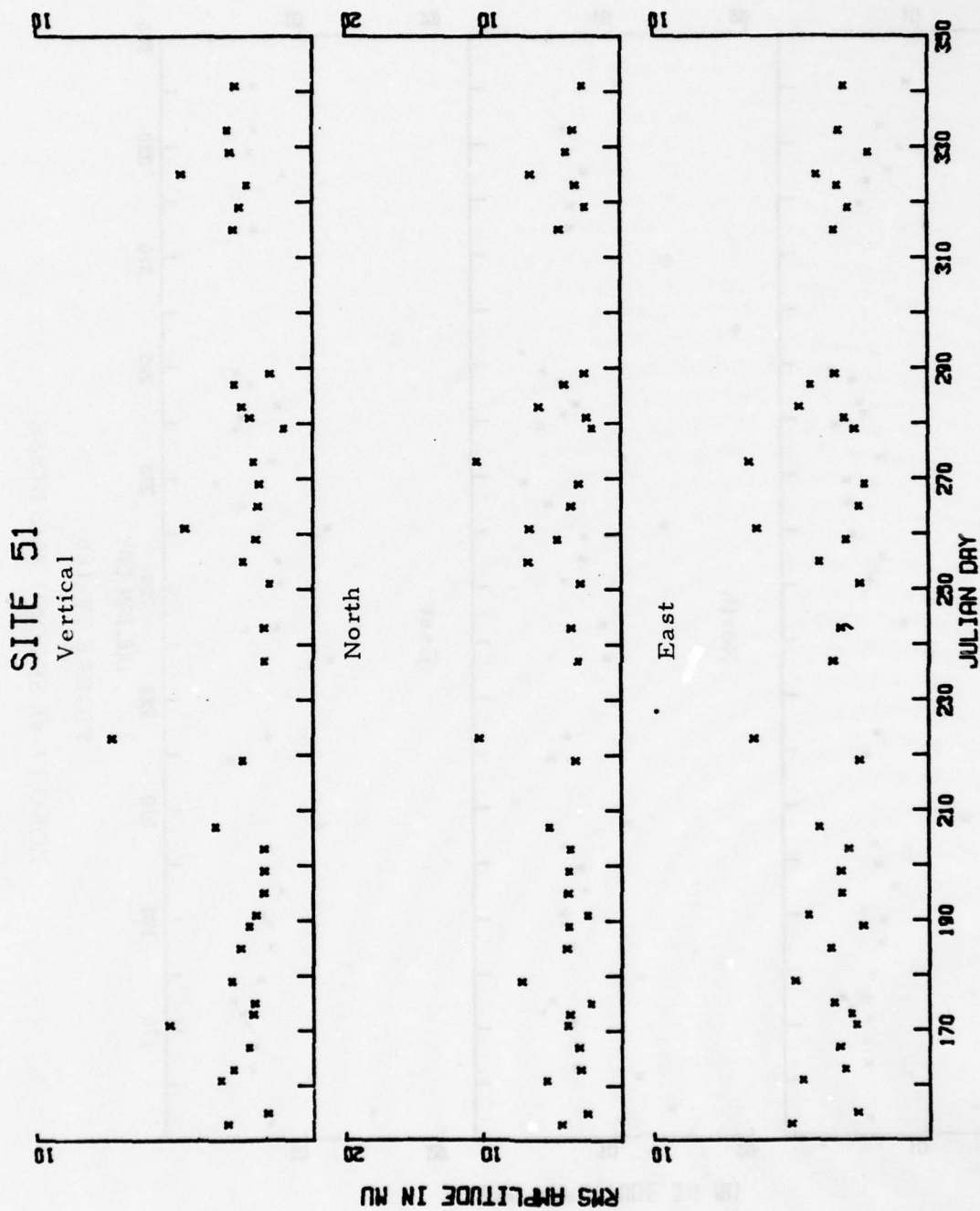
FIGURE IV-16c

ZOBO 40-64 SECOND RMS NOISE

IV-34

SITE 52

Vertical

North

East

RMS AMPLITUDE IN MU

JULIAN DAY
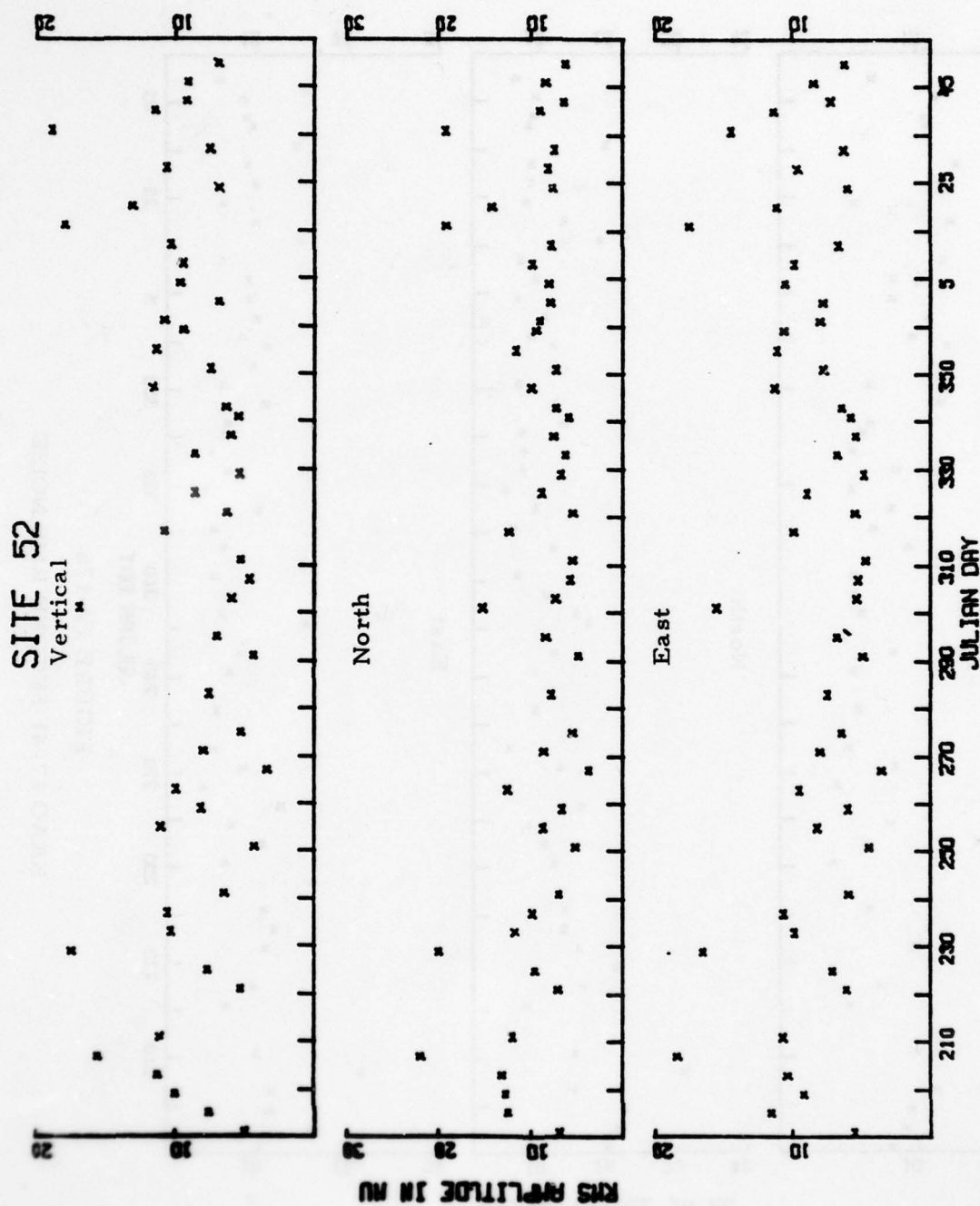
FIGURE IV-17a

KAAO 10-25 SECOND RMS NOISE

SITE 52
Vertical

North

East

RMS AMPLITUDE IN MU

JULIAN DAY
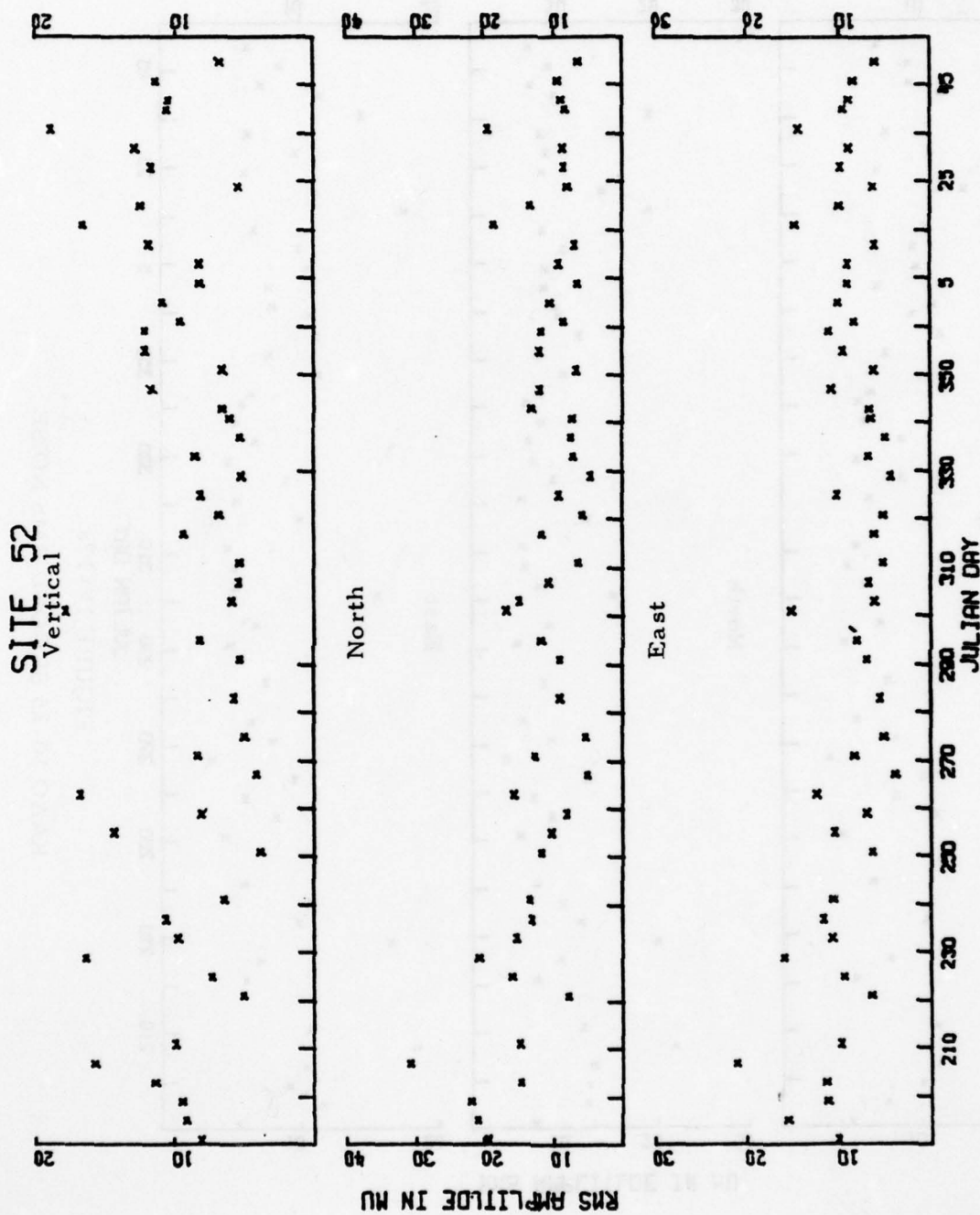
FIGURE IV-17b

KAAO 17-41 SECOND RMS NOISE

IV-36

SITE 52

Vertical

North

East

RMS AMPLITUDE IN MU

JULIAN DAY
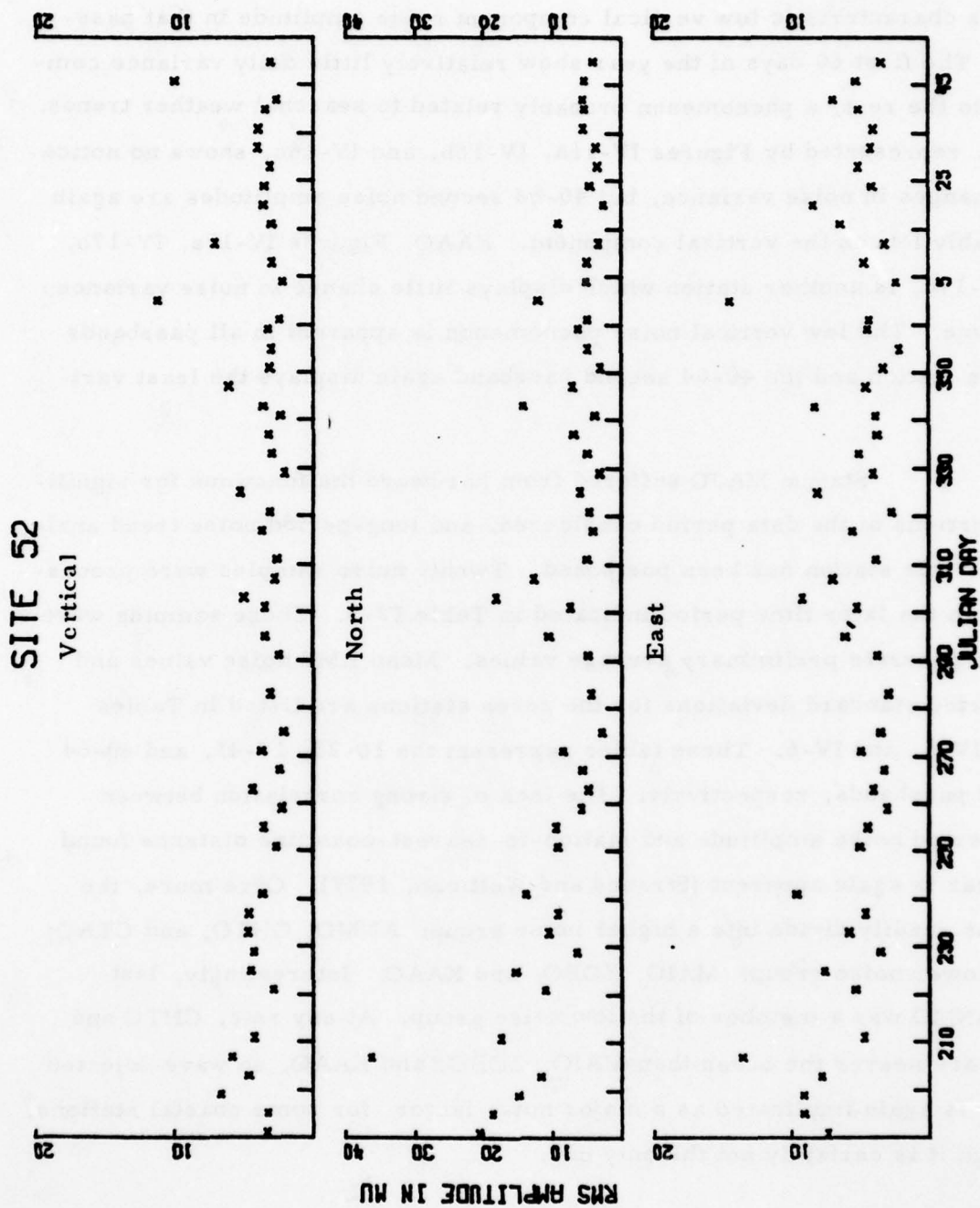
FIGURE IV-17c

KAAO 40-64 SECOND RMS NOISE

second passband, as they did for ANMO and MAIO. CTAO (Figures IV-15a, IV-15b, and IV-15c) is almost stable in the 40-64 second passband and shares MAIO's characteristic low vertical component noise amplitude in that pass-band. The first 60 days of the year show relatively little daily variance compared to the rest, a phenomenon probably related to seasonal weather trends. ZOBO, represented by Figures IV-16a, IV-16b, and IV-16c, shows no noticeable changes in noise variance, but 40-64 second noise amplitudes are again noticeably low on the vertical component. KAAO, Figures IV-17a, IV-17b, and IV-17c, is another station which displays little change in noise variance with time. The low vertical noise phenomenon is apparent in all passbands for this station and the 40-64 second passband again displays the least variance.

Station MAJO suffered from hardware malfunctions for significant portions of the data period considered, and long-period noise trend analysis for this station has been postponed. Twenty noise samples were processed from the later time period indicated in Table IV-3. These samples were used to generate preliminary average values. Mean RMS noise values and associated standard deviations for the seven stations are listed in Tables IV-4, IV-5, and IV-6. These tables represent the 10-25, 17-41, and 40-64 second passbands, respectively. The lack of strong correlation between long-period noise amplitude and station-to-nearest-coastline distance found last year is again apparent (Strauss and Weltman, 1977). Once more, the stations readily divide into a higher noise group: ANMO, CHTO, and CTAO; and a lower noise group: MAIO, ZOBO, and KAAO. Interestingly, last year ANMO was a member of the low noise group. At any rate, CHTO and CTAO are nearer the ocean than MAIO, ZOBO, and KAAO, so wave-injected energy is again implicated as a major noise factor for some coastal stations, although it is certainly not the only one.

TABLE IV-4

MEAN 10-25 SECOND RMS NOISE AMPLITUDES IN $m\mu$

Station	Vertical		North		East	
	Mean	S. D.	Mean	S. D.	Mean	S. D.
ANMO	11.56	4.33	10.96	4.41	11.67	4.00
CHTO	11.16	3.54	11.70	4.47	12.27	4.42
MAIO	8.14	3.46	7.11	2.78	7.19	3.30
CTAO	12.22	3.89	12.53	3.47	11.00	3.74
ZOBO	8.23	2.79	8.23	2.86	8.15	2.46
KAAO	8.96	3.62	9.55	4.06	8.65	3.38
MAJO	6.64	2.04	7.68	2.01	7.79	2.40

S. D. = Standard Deviation

TABLE IV-5

MEAN 17-41 SECOND RMS NOISE AMPLITUDES IN $m\mu$

Station	Vertical		North		East	
	Mean	S. D.	Mean	S. D.	Mean	S. D.
ANMO	9.73	3.61	8.80	3.67	10.01	3.32
CHTO	8.46	3.21	9.45	4.14	9.96	3.98
MAIO	7.70	2.96	7.80	2.73	8.07	2.91
CTAO	9.41	3.29	9.90	3.02	8.78	3.18
ZOBO	7.15	2.53	7.87	2.43	7.40	2.21
KAAO	9.40	3.78	12.53	7.59	9.61	4.96
MAJO	6.42	1.56	7.26	1.90	7.75	2.05

S. D. = Standard Deviation

TABLE IV-6
MEAN 40-64 SECOND RMS NOISE AMPLITUDES IN $m\mu$

Station	Vertical		North		East	
	Mean	S. D.	Mean	S. D.	Mean	S. D.
ANMO	3.12	1.08	3.23	1.08	3.95	1.24
CHTO	2.73	0.62	3.40	0.92	3.39	1.22
MAIO	3.08	2.22	3.57	1.50	4.03	2.32
CTAO	1.95	0.52	3.65	1.04	3.66	1.48
ZOBO	2.65	1.15	4.24	1.94	3.56	1.09
KAAO	4.03	1.93	9.46	9.28	6.06	4.66
MAJO	3.92	1.57	6.00	1.70	4.74	2.05

S. D. = Standard Deviation

Figures IV-18a through IV-23c show monthly noise level trends which are derived from the Julian day plots. ANMO 10-25, 17-41, and 40-64 second RMS noise trends are shown in Figures IV-18a, IV-18b, and IV-18c, respectively. The noise level for ANMO shows a clear pattern as it drops from January through June and rises again through November. A significant rise in the noise level in July is possibly explained by thunderstorm activity (Personal Communication, John Hoffman, 1978). While trends are evident in the 10-25 second passband, they become less pronounced in the 17-41 second passband. In the 40-64 second passband no noise trend can be discerned.

Station CTAO, represented in Figures IV-21a, IV-21b, and IV-21c, shows a similar phenomenon between passbands, though some small trend is discernable in the horizontal components in the 40-64 second passband. This trend points to a noise peak in September and October. Other passbands show a clear peak in July, which may be due to winter storm activity in the southern hemisphere.

MAIO, in Figures IV-20a, and IV-20b, representing the 10-25 and 17-41 second passbands, follows a trend similar to that of ANMO. However, the 40-64 second passband shows a trend which does not appear to relate to the traditional seasons.

KAAO shows noise values decreasing from July through September in Figures IV-23a, IV-23b, and IV-23c. Values rise after November in the 10-25 and 17-41 second passbands, but continue to decline in the 40-64 second passband. Unlike stations ANMO and CTAO, KAAO noise trends appear most pronounced in the 40-64 second passband, at least for the horizontal components.

CHTO, represented in Figures IV-19a, IV-19b, and IV-19c, shows a December peak in the 10-25 and 17-41 second trends. This peak is absent in the 40-64 second passband.

SITE 30
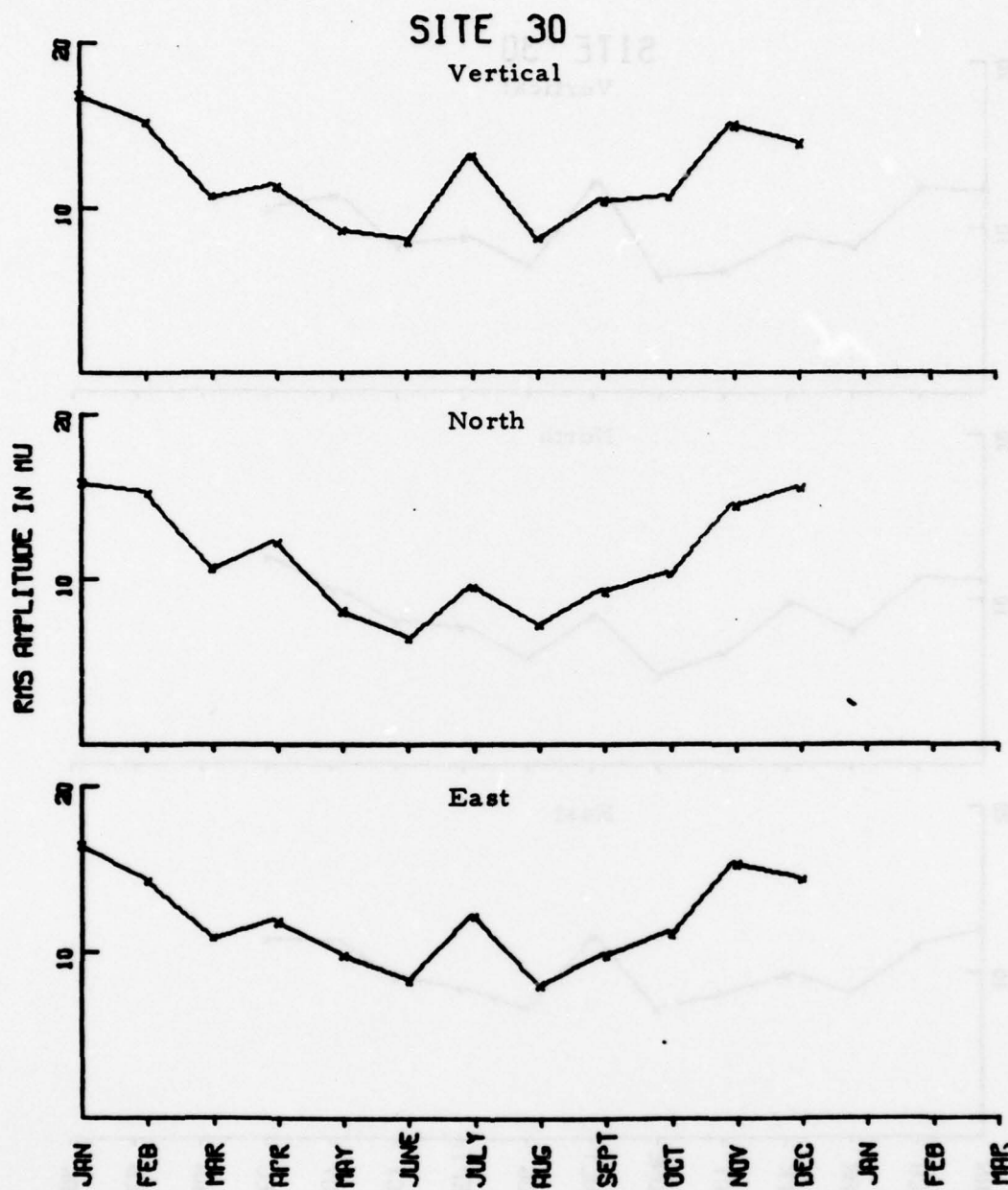
FIGURE IV-18a

ANMO 10-25 SECOND RMS NOISE TRENDS

IV-43
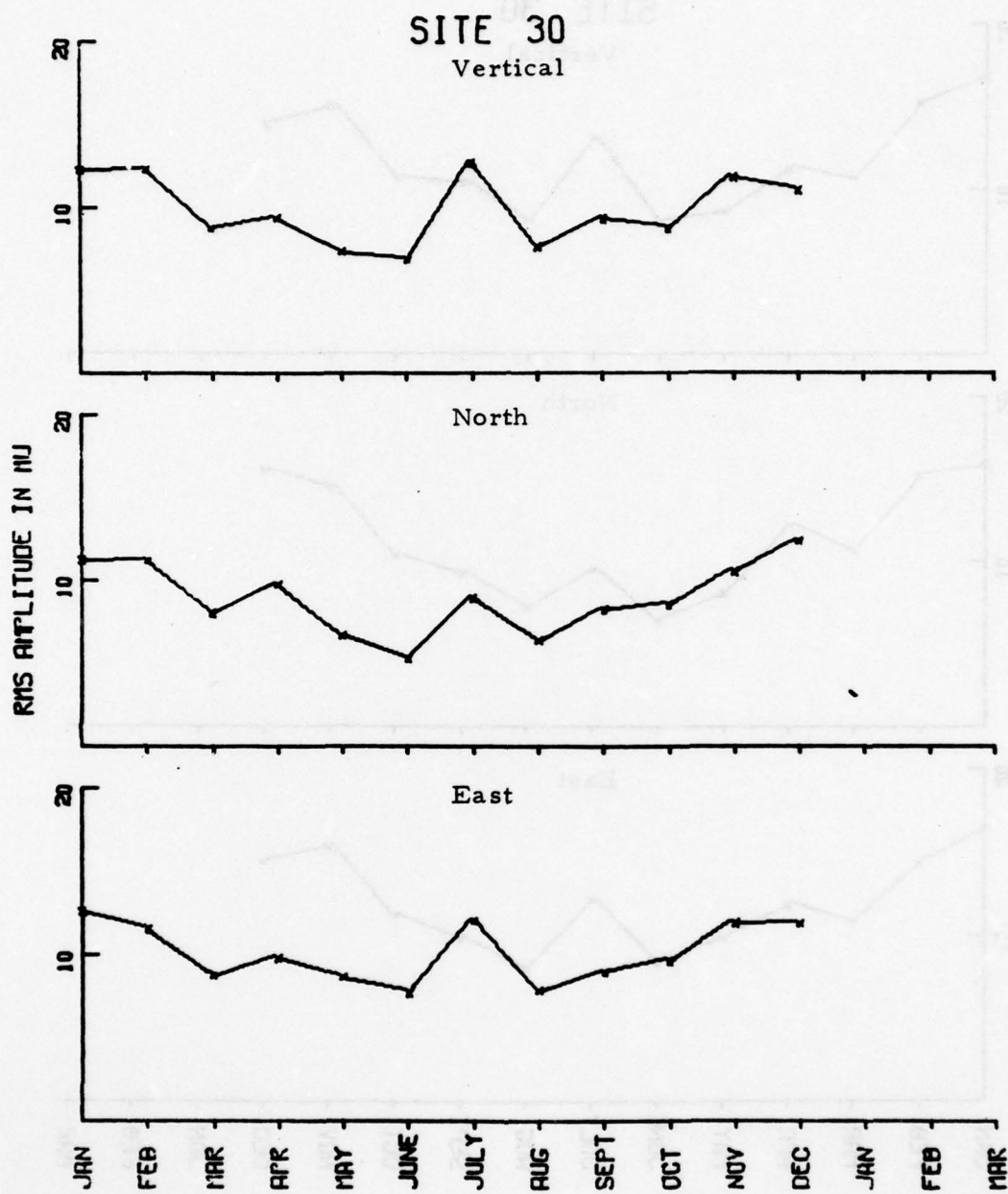
FIGURE IV-18b

ANMO 17-41 SECOND RMS NOISE TRENDS
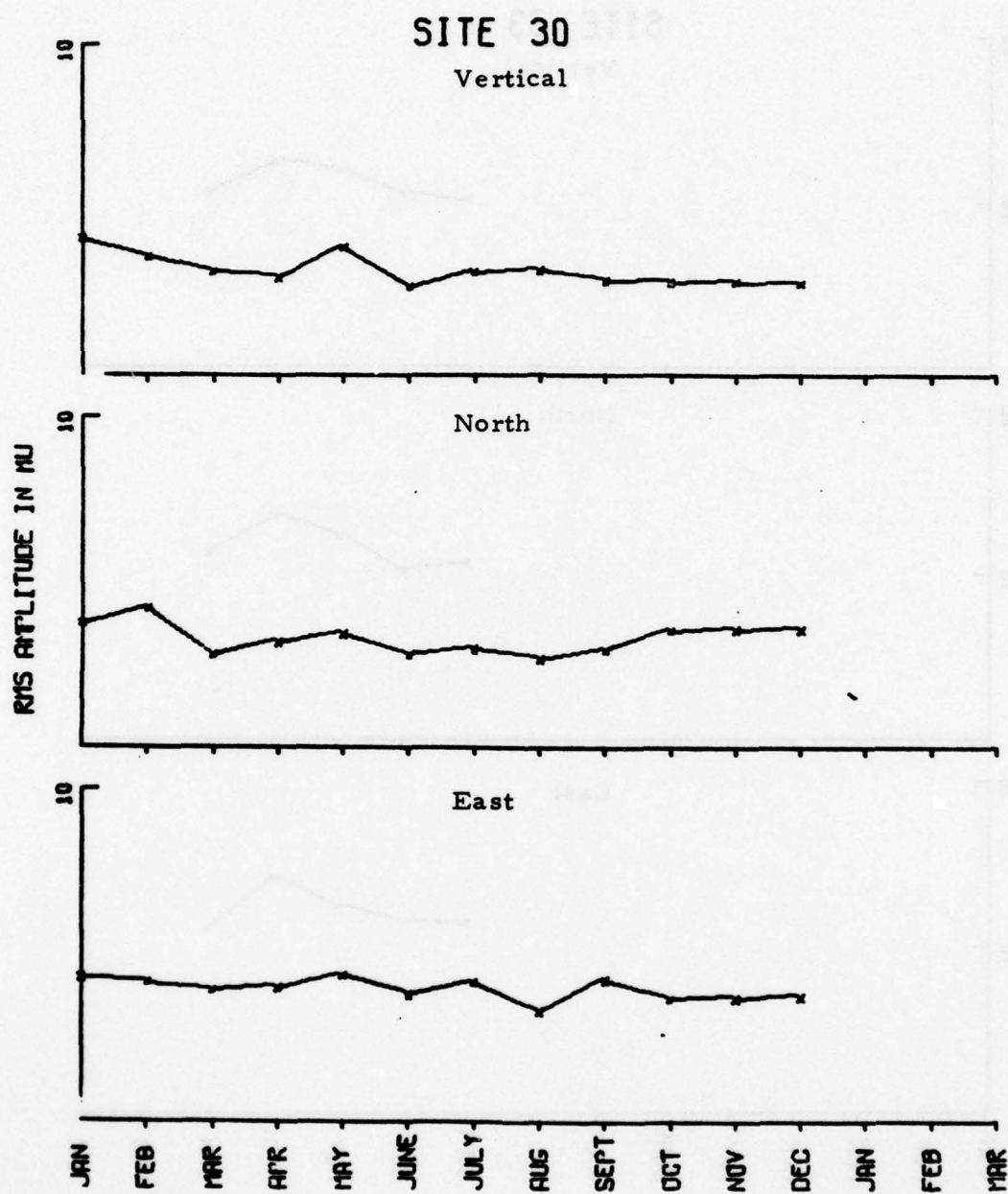
FIGURE IV-18c

ANMO 40-64 SECOND RMS NOISE TRENDS

IV-45
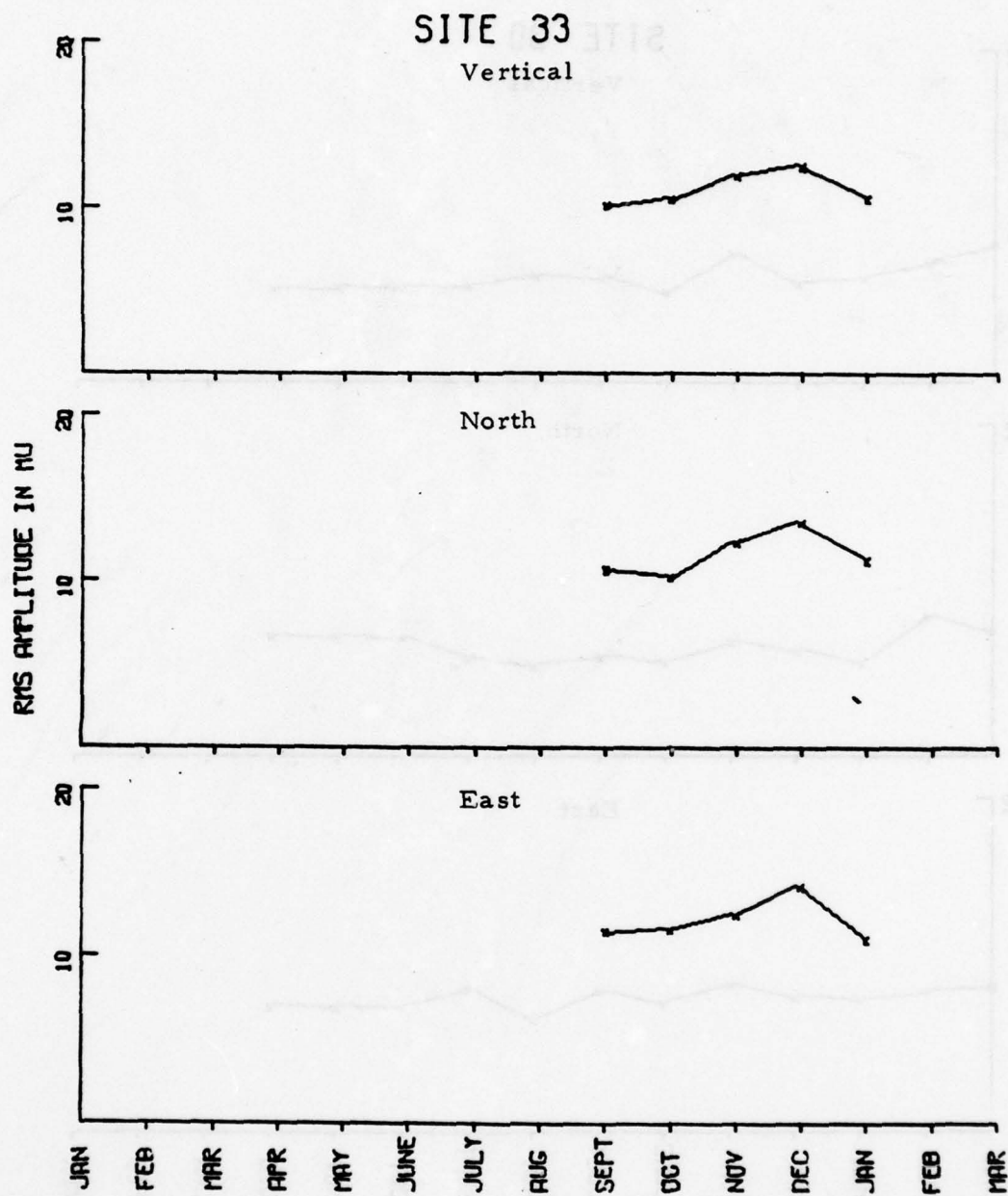
FIGURE IV-19a

CHTO 10-25 SECOND RMS NOISE TRENDS

IV-46

SITE 33
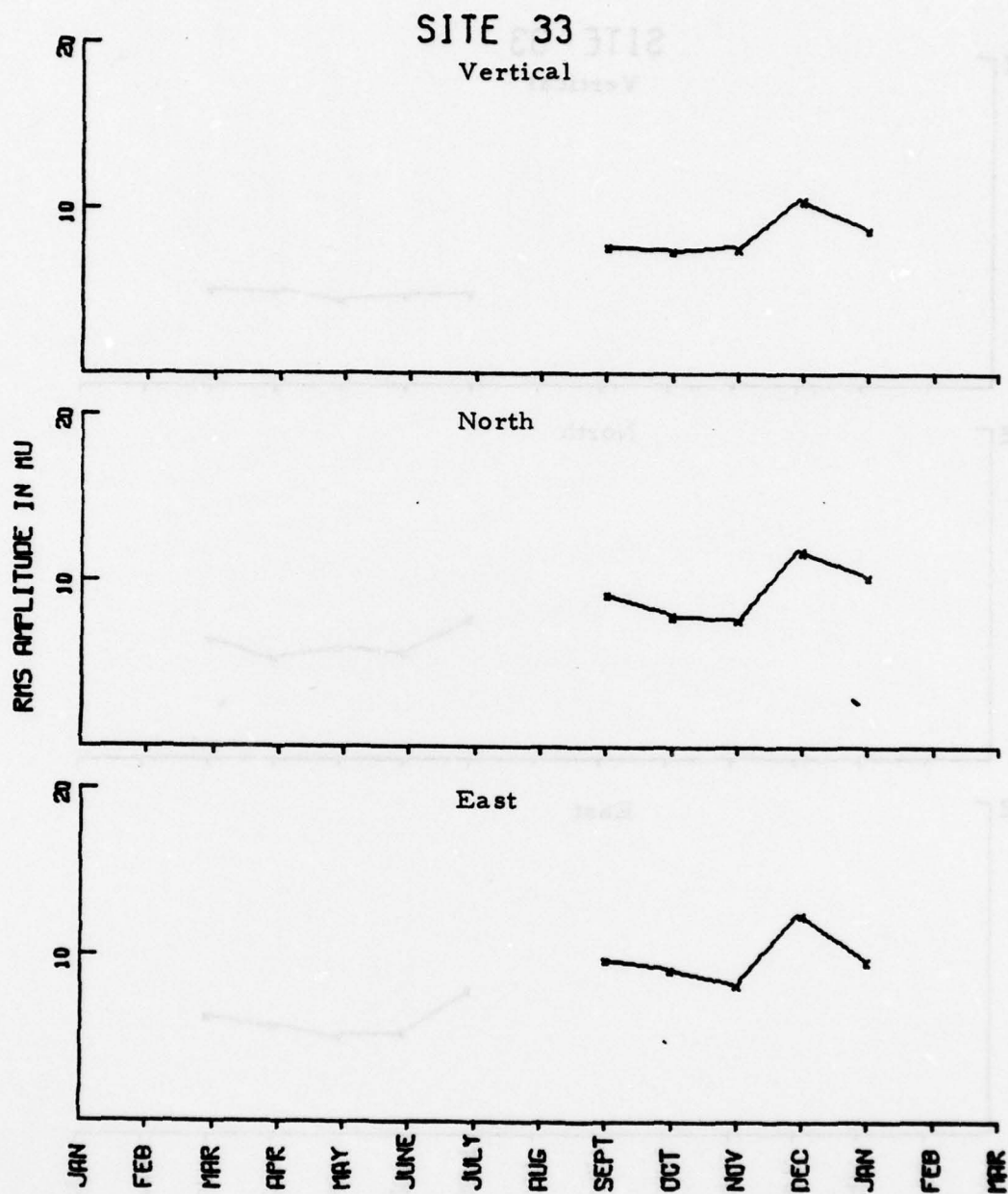
FIGURE IV-19b

CHTO 17-41 SECOND RMS NOISE TRENDS

IV-47

SITE 33

Vertical

North

East
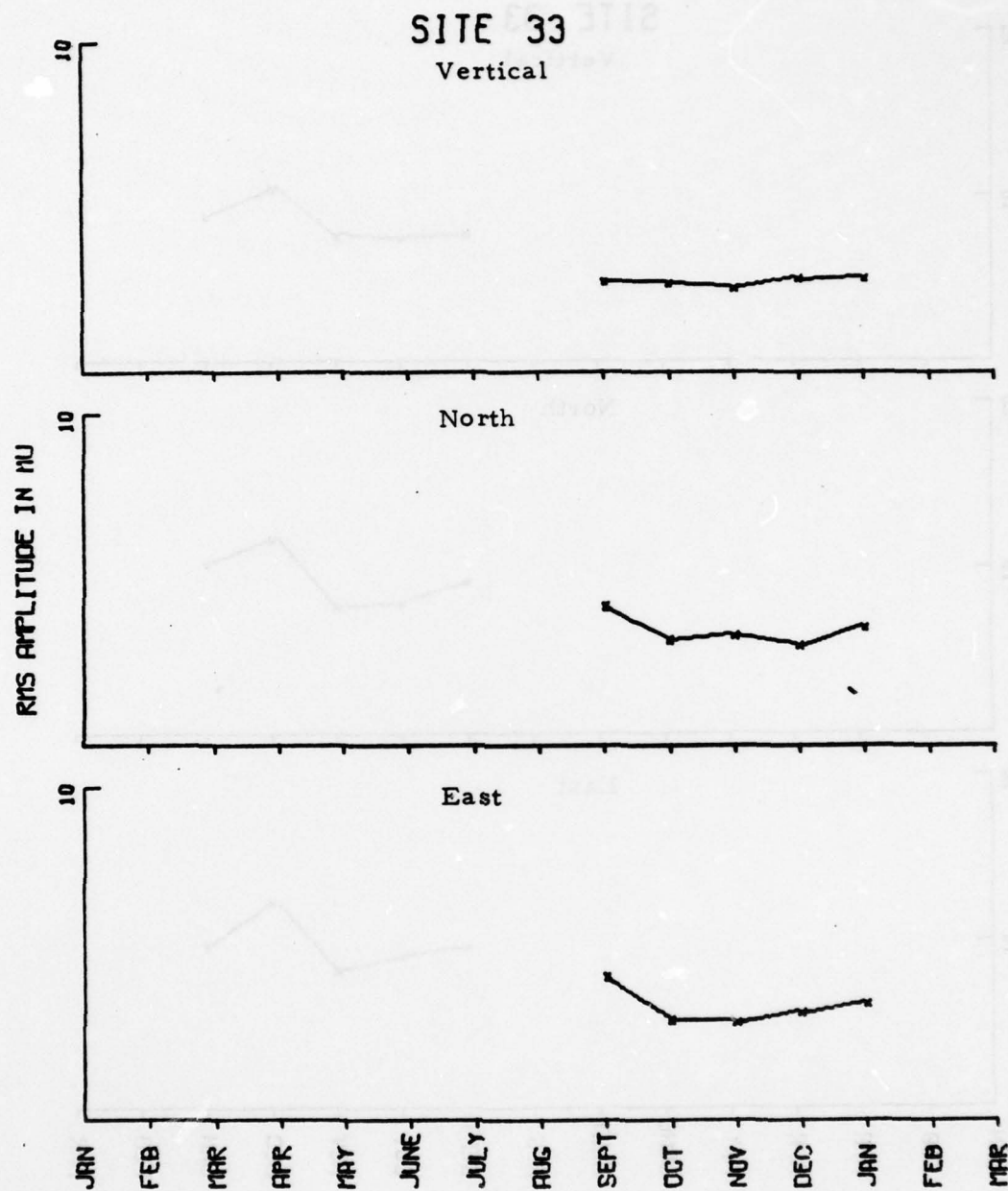
FIGURE IV-19c

CHTO 40-64 SECOND RMS NOISE TRENDS
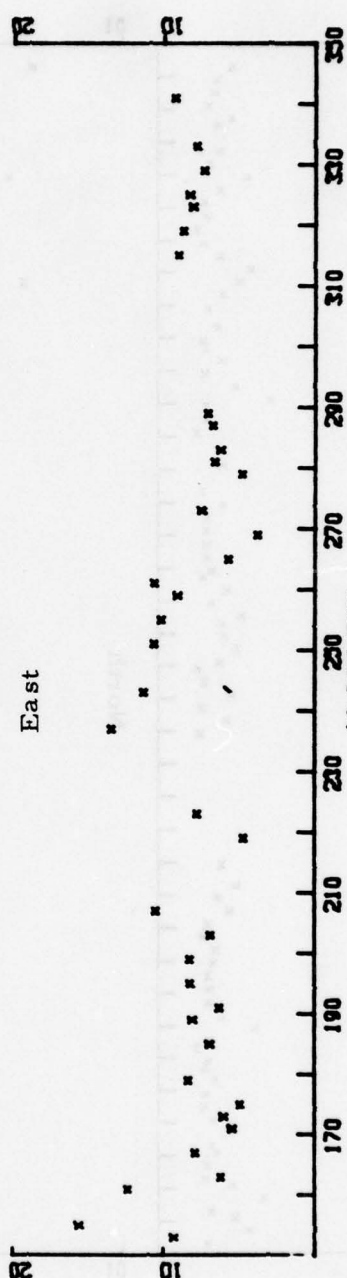
IV-48
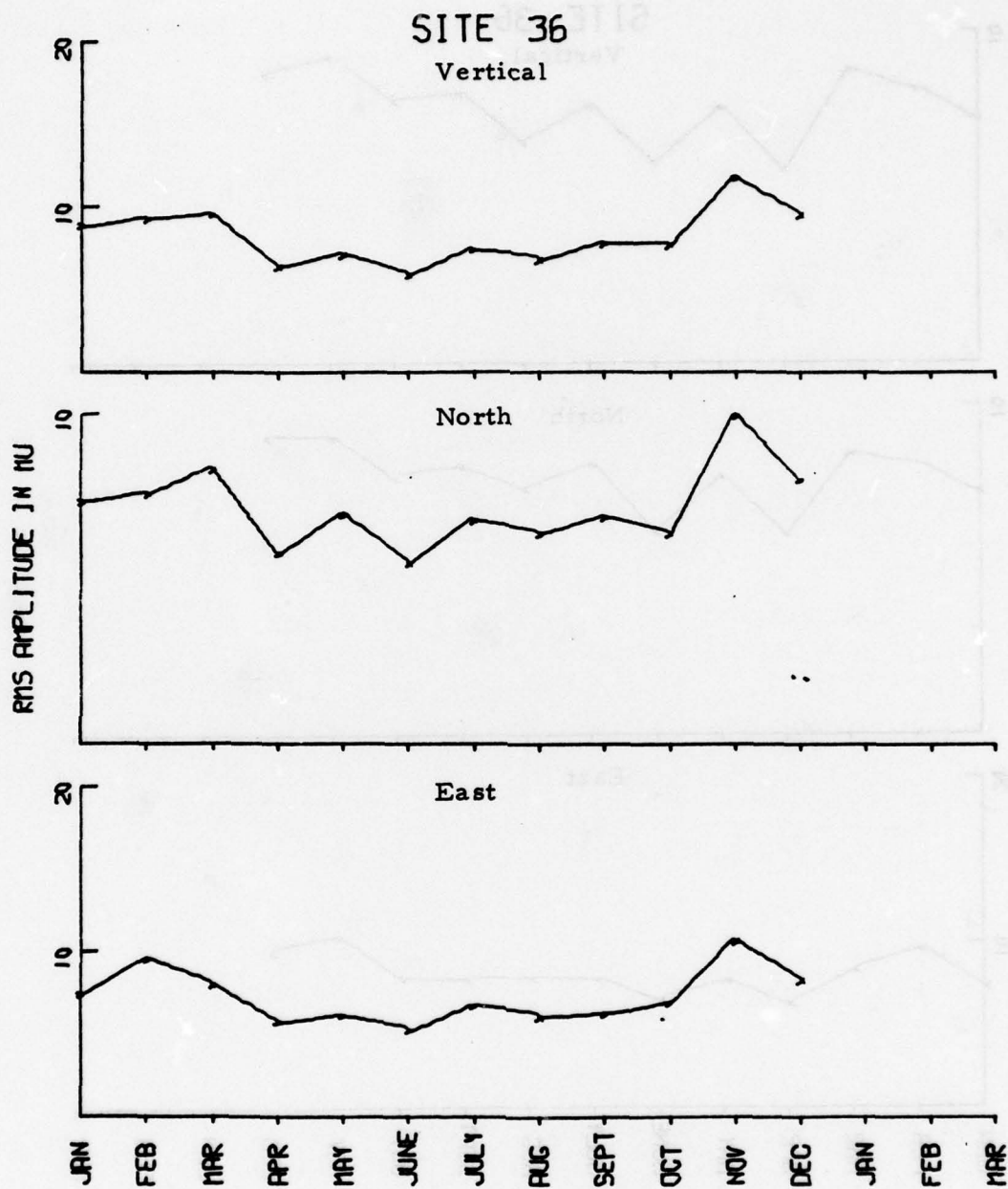
FIGURE IV-20a

MAIO 10-25 SECOND RMS NOISE TRENDS

IV-49

SITE 36

Vertical

North

East

RMS AMPLITUDE IN MU

JAN FEB MAR APR MAY JUNE JULY AUG SEPT OCT NOV DEC JAN FEB MAR
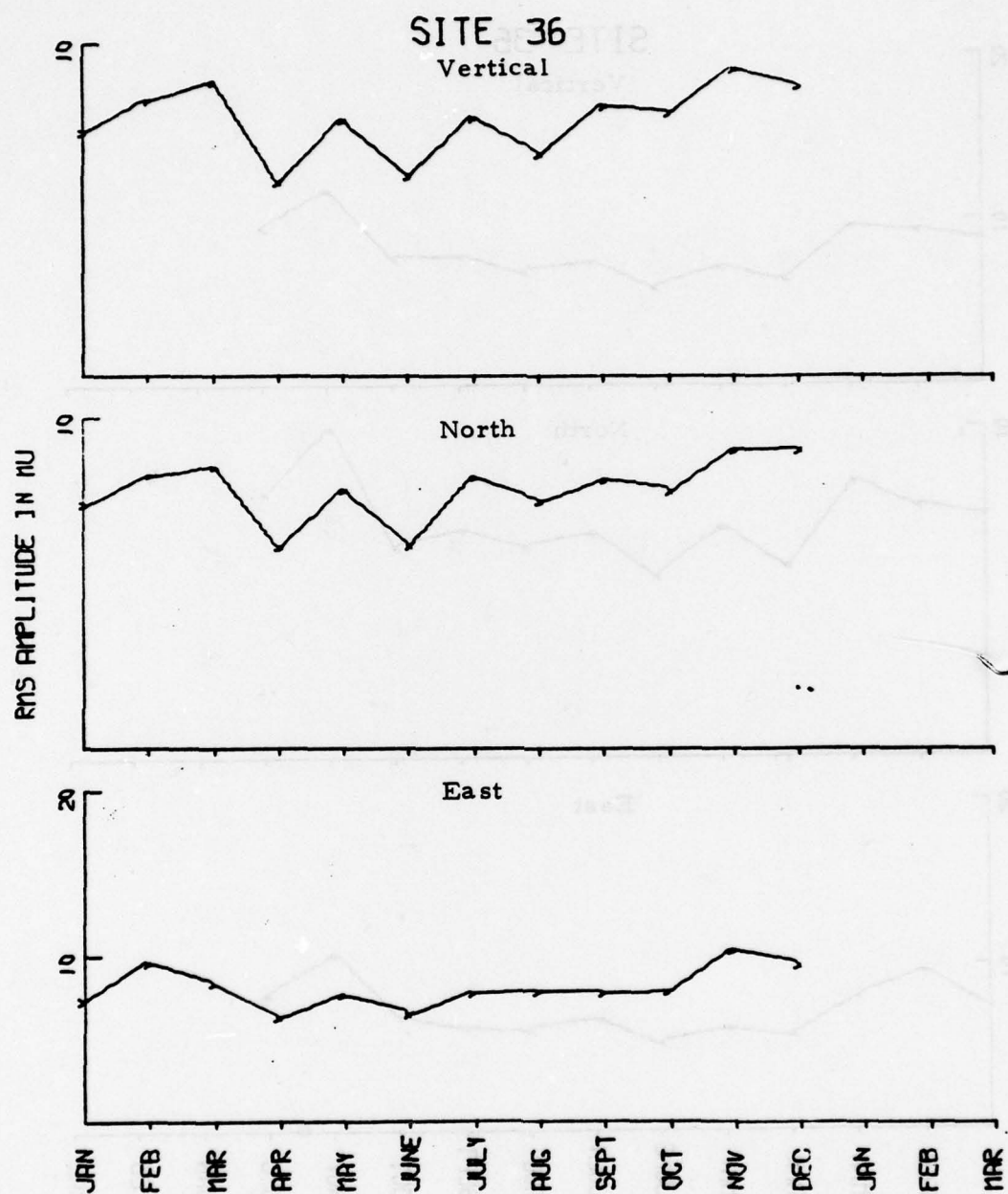
FIGURE IV-20b

MAIO 17-41 SECOND RMS NOISE TRENDS

IV-50

SITE 36

Vertical

North

RMS AMPLITUDE IN MU

East

JAN FEB MAR APR MAY JUNE JULY AUG SEPT OCT NOV DEC JAN FEB MAR
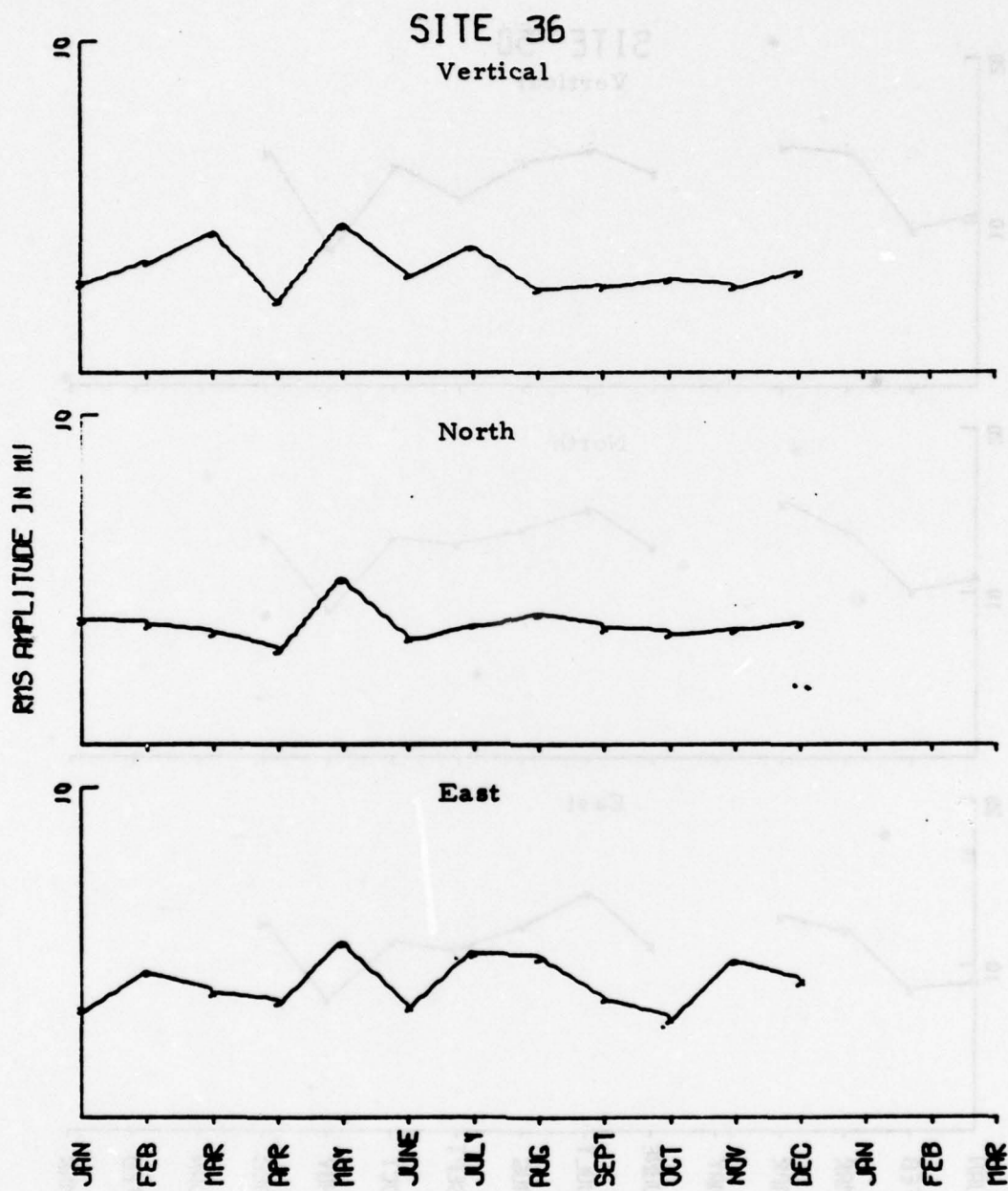
FIGURE IV-20c

MAIO 40-64 SECOND RMS NOISE TRENDS

IV-51
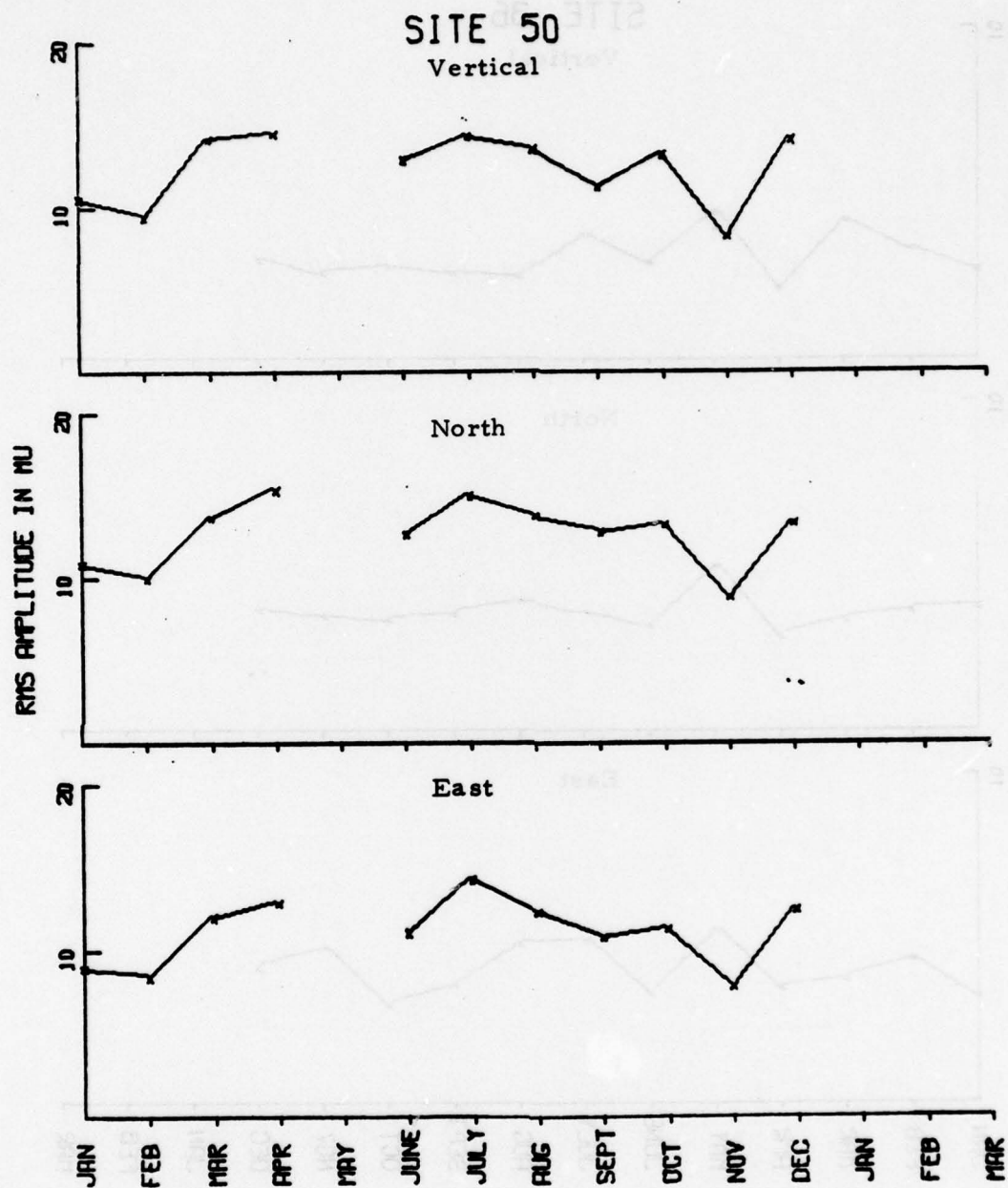
FIGURE IV-21a

CTAO 10-25 SECOND RMS NOISE TRENDS
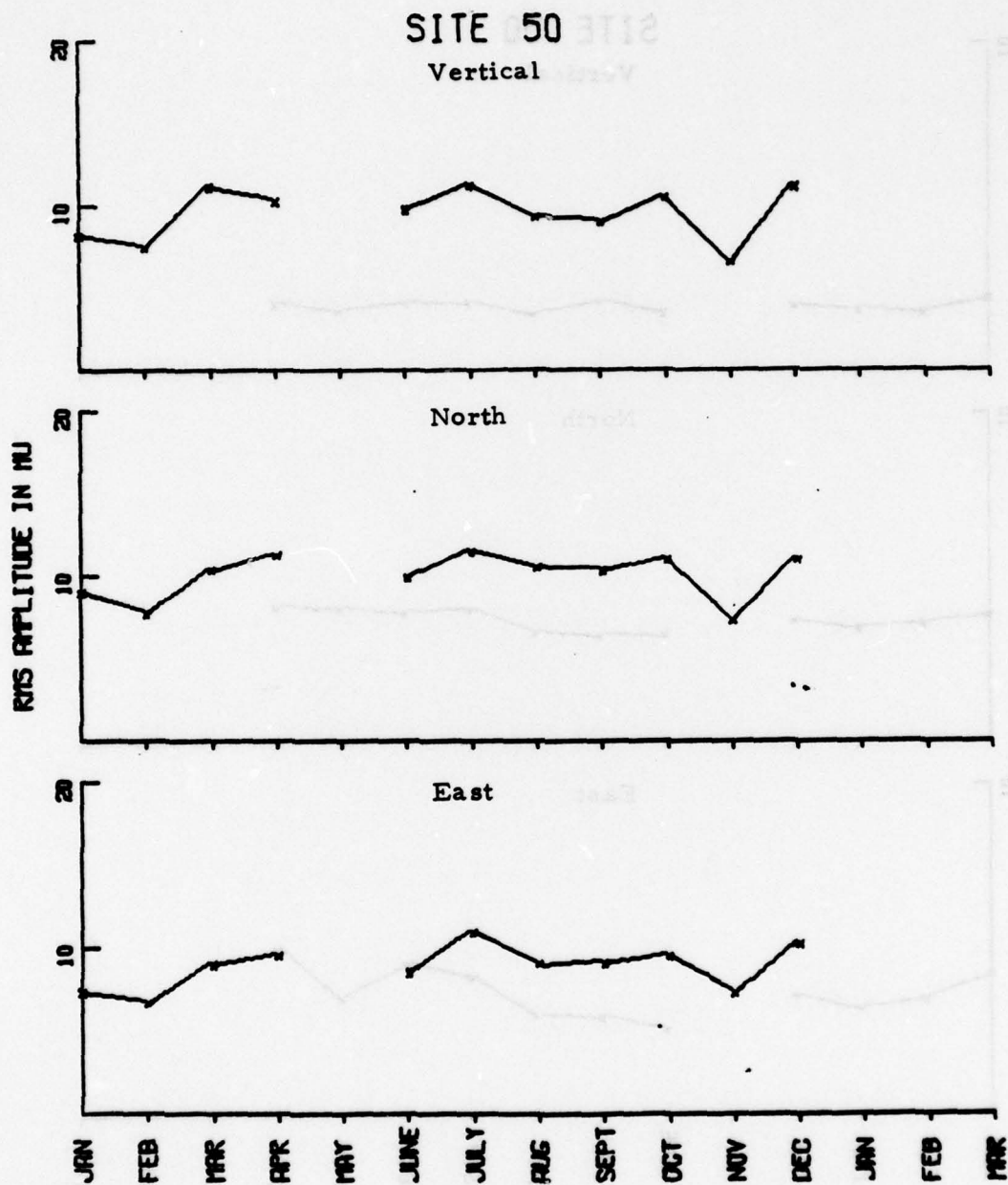
FIGURE IV-21b

CTAO 17-41 SECOND RMS NOISE TRENDS

SITE 50

Vertical

North

RMS AMPLITUDE IN MU

East

JAN FEB MAR APR MAY JUNE JULY AUG SEPT OCT NOV DEC JAN FEB MAR
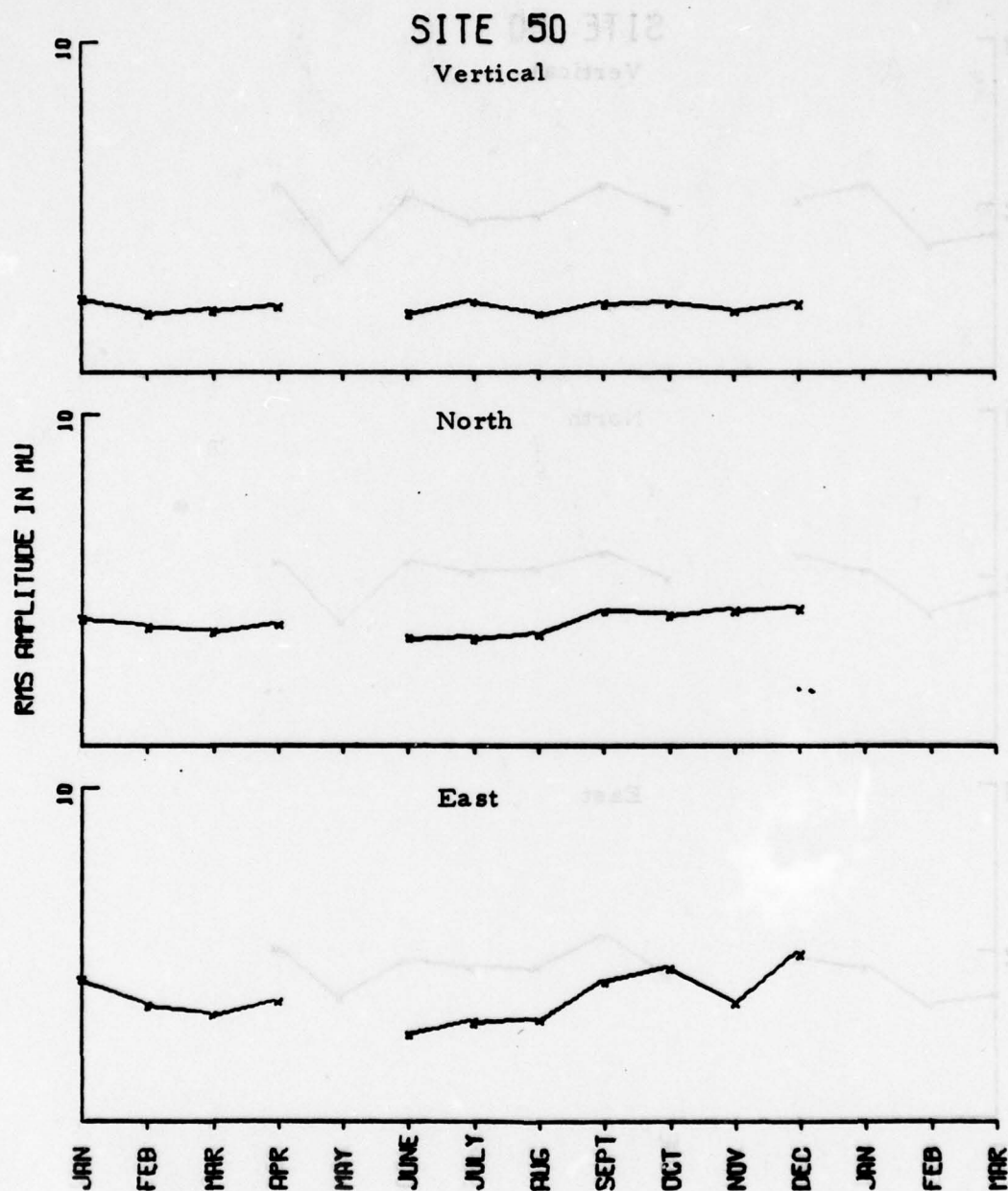
FIGURE IV-21c

CTAO 40-64 SECOND RMS NOISE TRENDS

IV-54
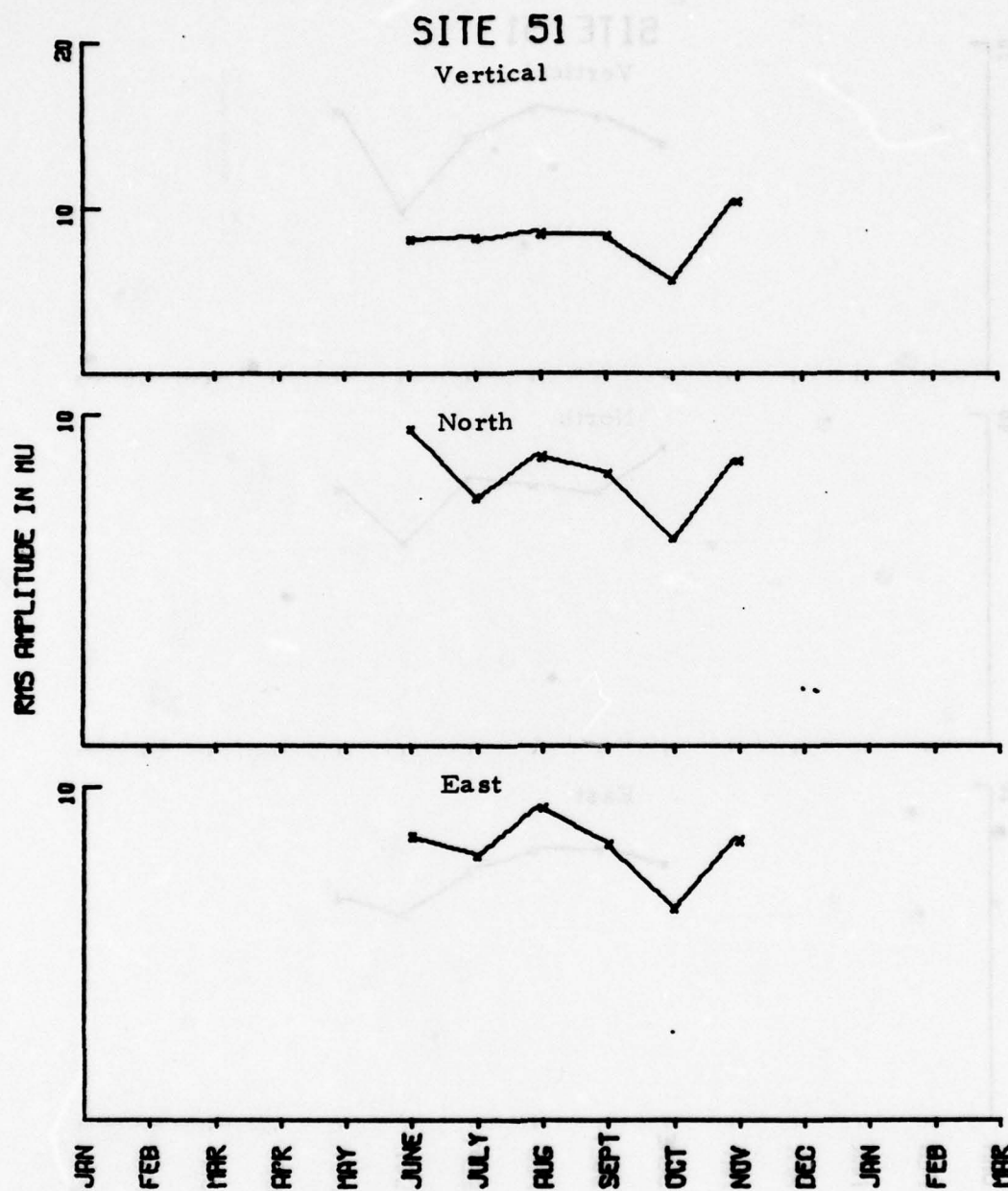
FIGURE IV-22a

ZOBO 10-25 SECOND RMS NOISE TRENDS

IV-55
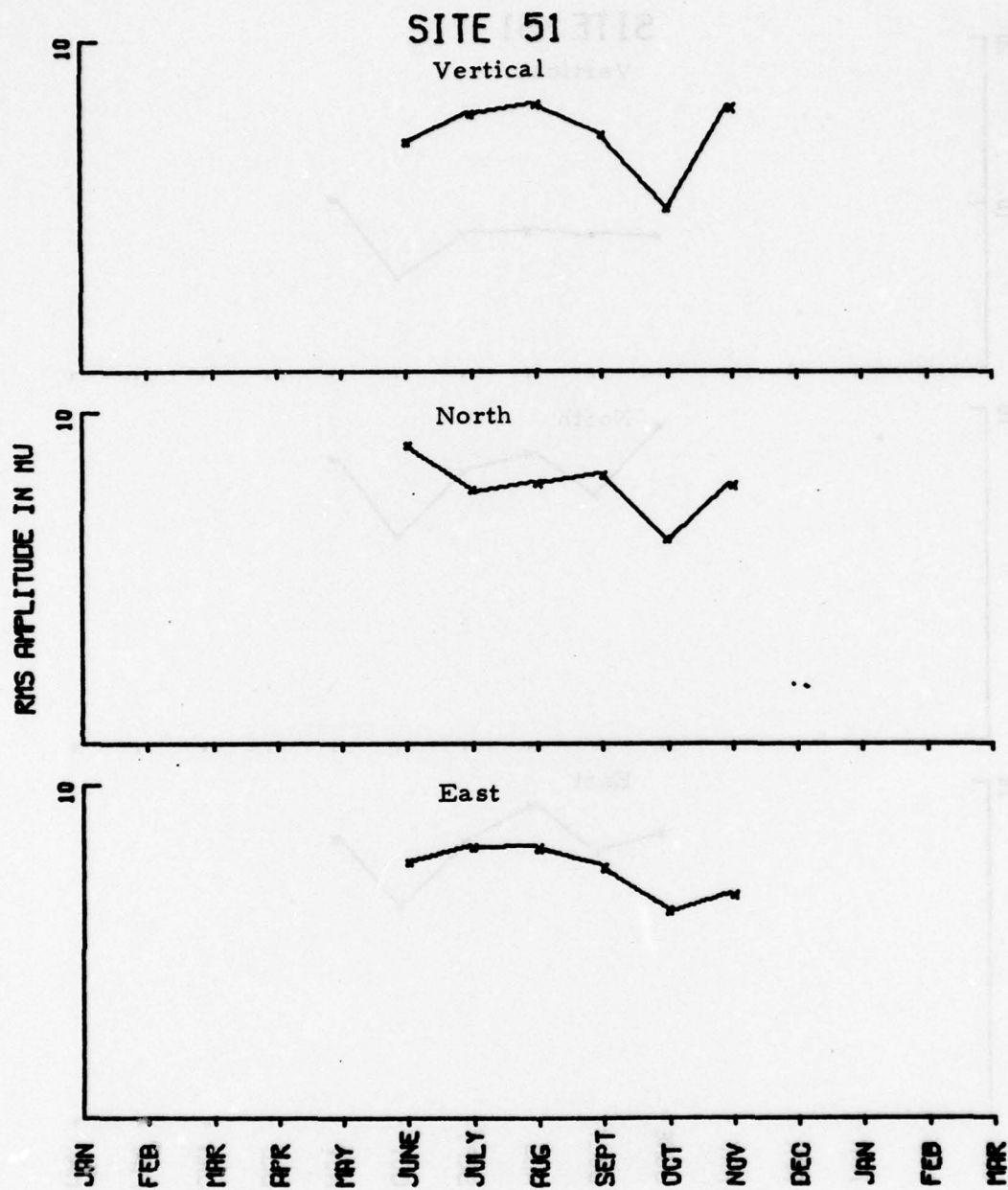
FIGURE IV-22b

ZOBO 17-41 SECOND RMS NOISE TRENDS

SITE 51

Vertical

North

East
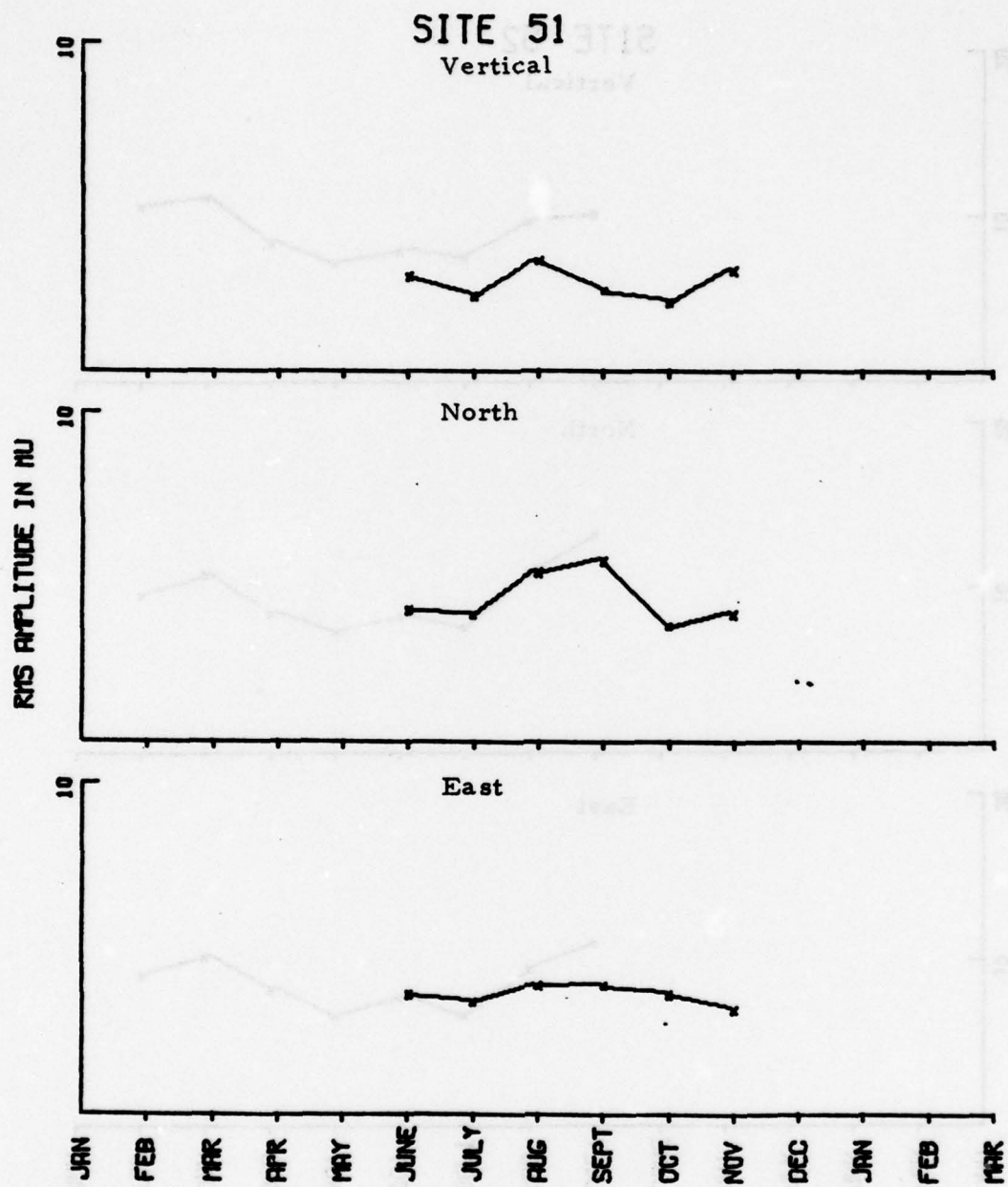
FIGURE IV-22c

ZOBO 40-64 SECOND RMS NOISE TRENDS

IV-57

SITE 52

Vertical

North

East

RMS AMPLITUDE IN MU

JAN FEB MAR APR MAY JUNE JULY AUG SEPT OCT NOV DEC JAN FEB MAR
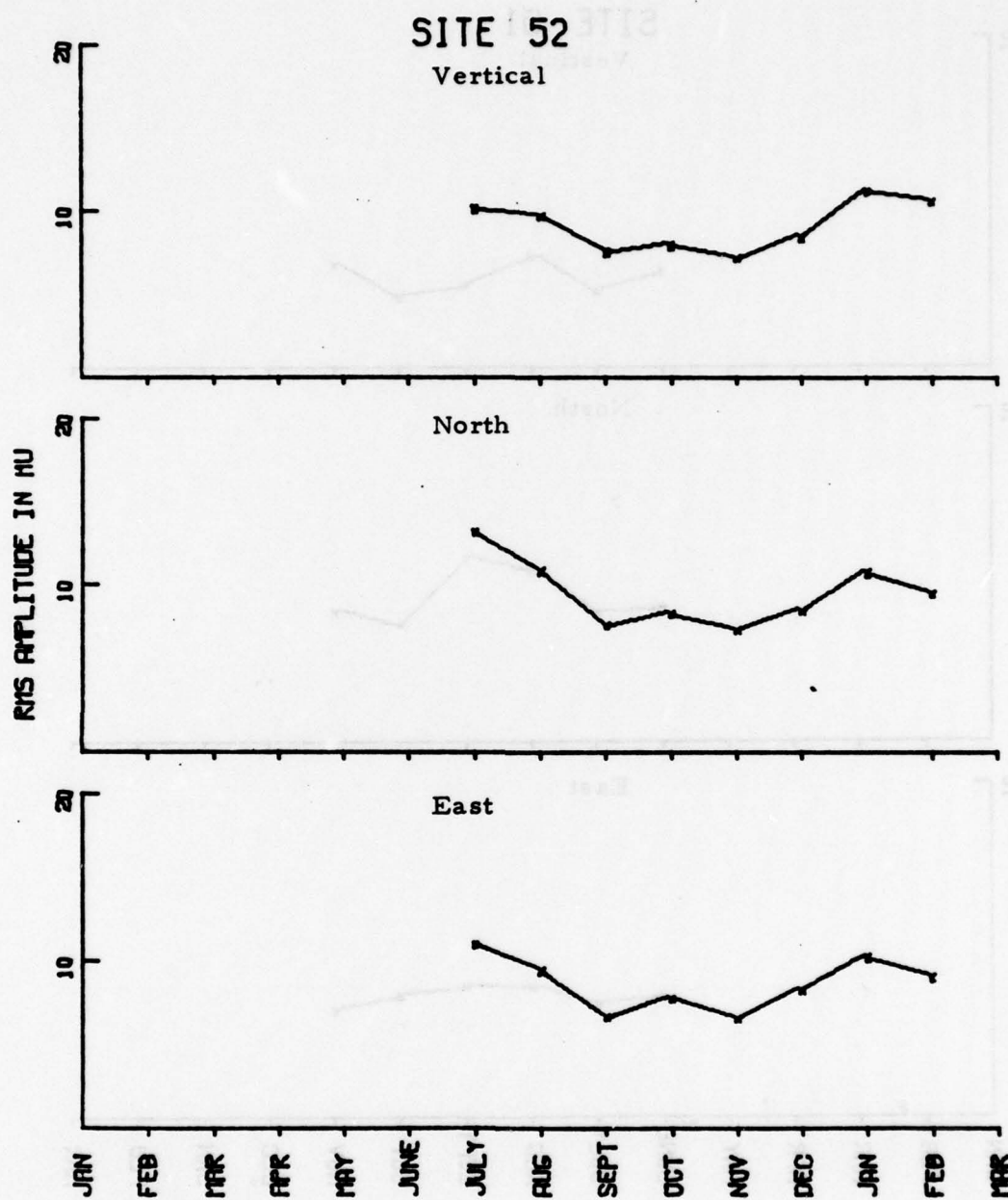
FIGURE IV-23a

KAAO 10-25 SECOND RMS NOISE TRENDS

SITE 52

Vertical

North

RMS AMPLITUDE IN MU

East

JAN FEB MAR APR MAY JUNE JULY AUG SEPT OCT NOV DEC JAN FEB MAR
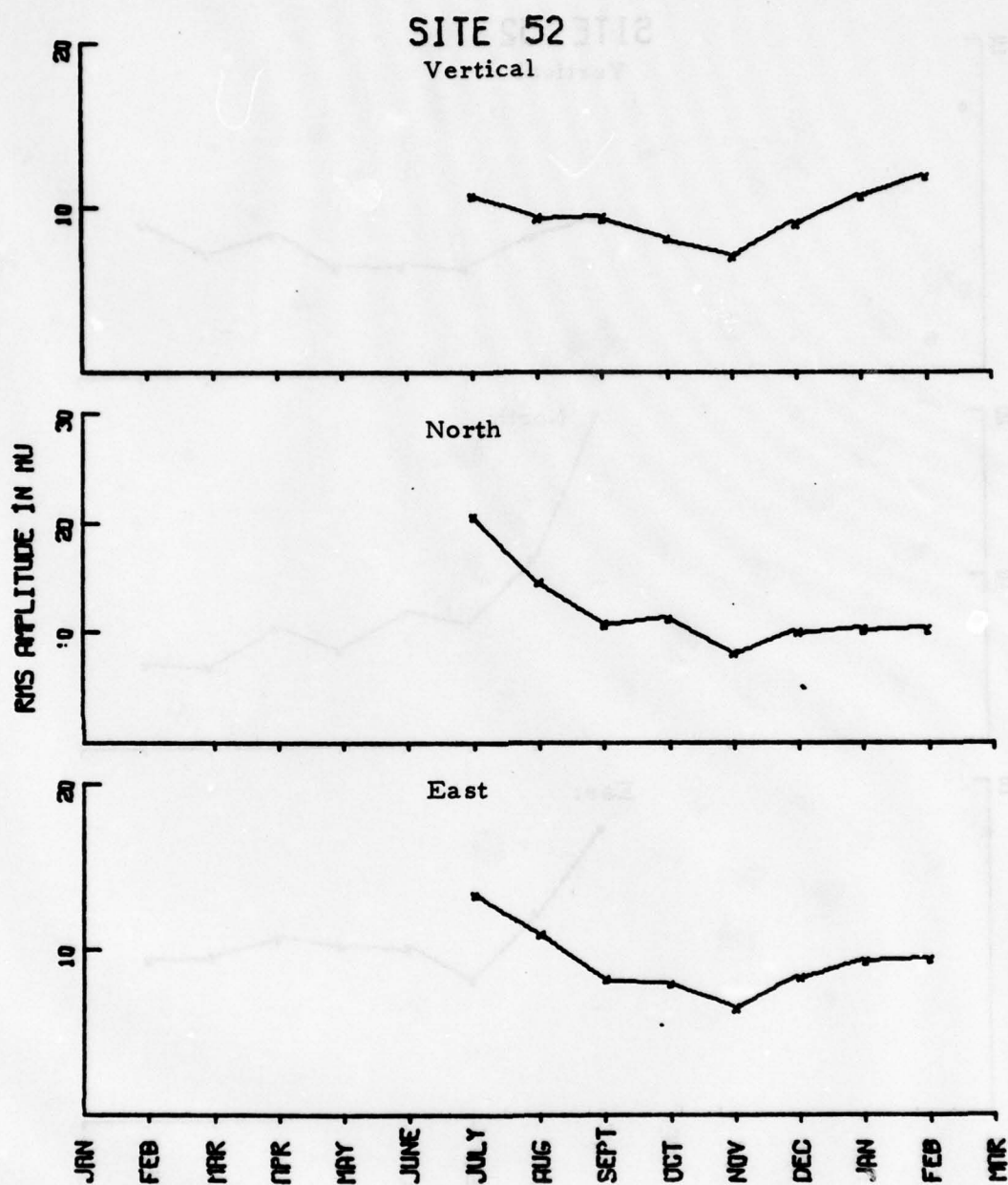
FIGURE IV-23b

KAAO 17-41 SECOND RMS NOISE TRENDS

SITE 52

Vertical

RMS AMPLITUDE IN MU

North

East

JAN FEB MAR APR MAY JUNE JULY AUG SEPT OCT NOV DEC JAN FEB MAR
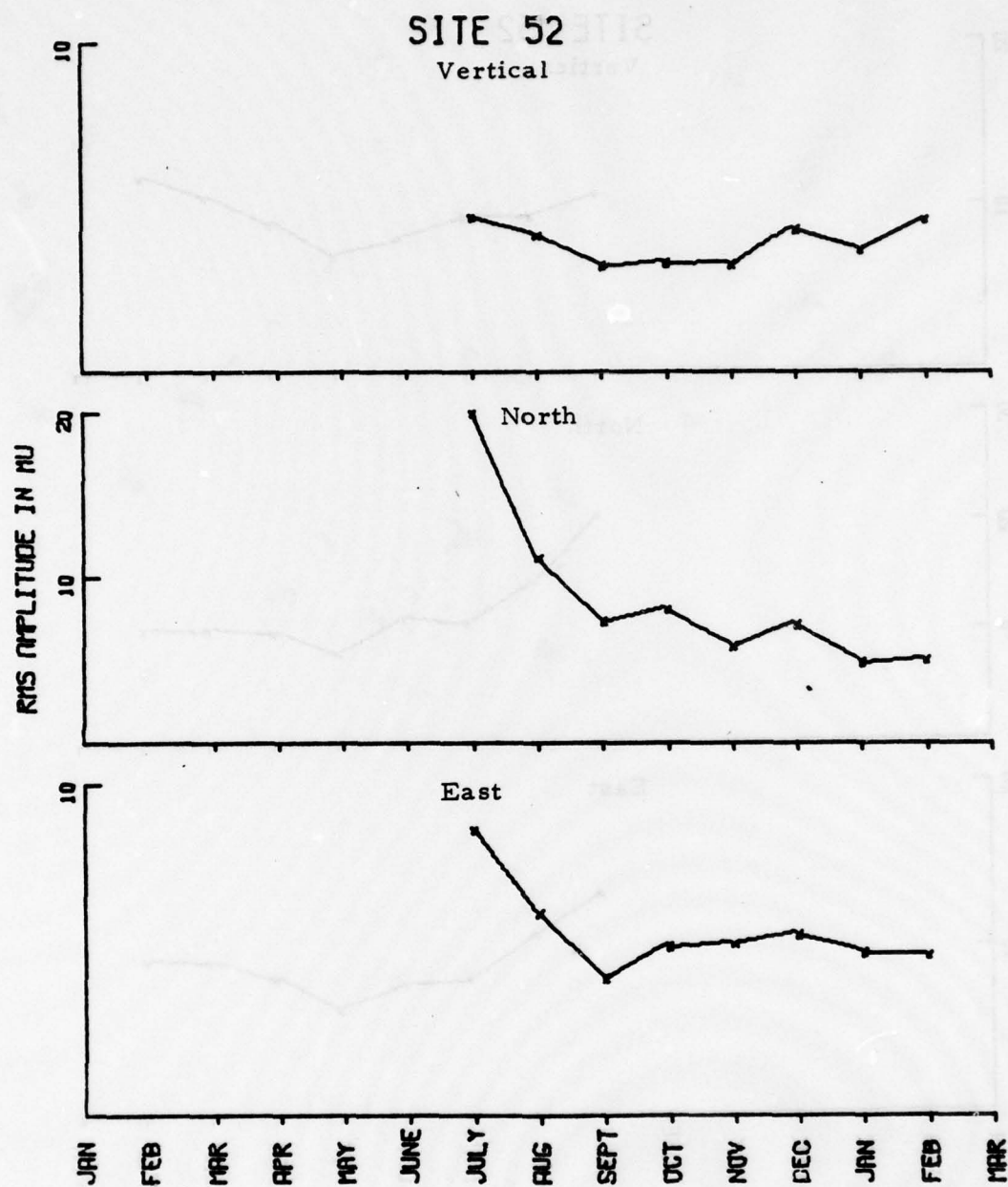
FIGURE IV-23c

KAAO 40-64 SECOND RMS NOISE TRENDS

IV-60

Figures IV-24 through IV-30 show the average RMS amplitude spectra for the noise at each station under evaluation. These spectra are uncorrected for instrument response. They were determined by averaging the individual spectra computed from the noise samples and converting them to RMS amplitudes using Parseval's formula:

$$RMS_a^b = \sqrt{f \sum_{i=a}^{b} \left|A(f_i)\right|^2 * C(f_i)^2}$$

where

Δf = the elemental frequency interval ($\Delta f = 0.001953$ Hz),

$\left|A(f_i)\right|^2$ = the discrete Fourier transform spectral density estimate at frequency f_i,

$C(f_i)$ = the instrument response correction at frequency f_i,

a = the initial frequency index, and

b = the final frequency index.

Since the RMS amplitude at each discrete frequency was desired, in this case $a = b$. Also, since no instrument response corrections were made, $C(f_i) = 1$ for all frequencies.

The left-hand side of each figure shows the average RMS noise amplitude spectra for each component of motion. These spectra were computed for the period range of 11.6 to 85.3 seconds so that the analyst can inspect the noise levels in and around the signal periods. The right-hand side of each figure shows the log mean spectra with vertical bars representing plus and minus one standard deviation. These are presented to give a qualitative idea of the day-to-day variability of the noise from period-to-period.

The following comments can be made about the individual figures:

IV-61
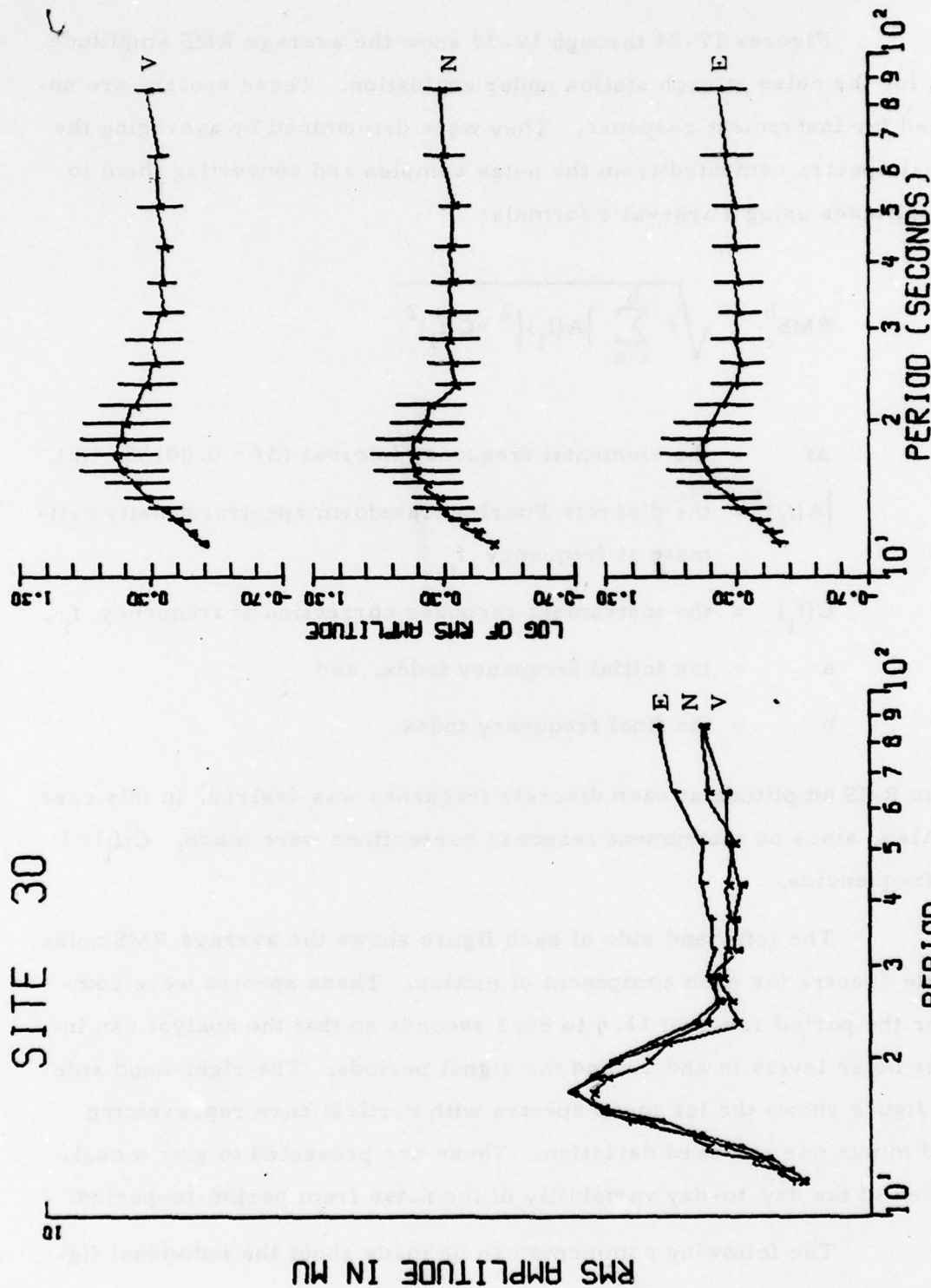
FIGURE IV-24

AVERAGE RMS AMPLITUDE SPECTRA ANMO LONG-PERIOD NOISE
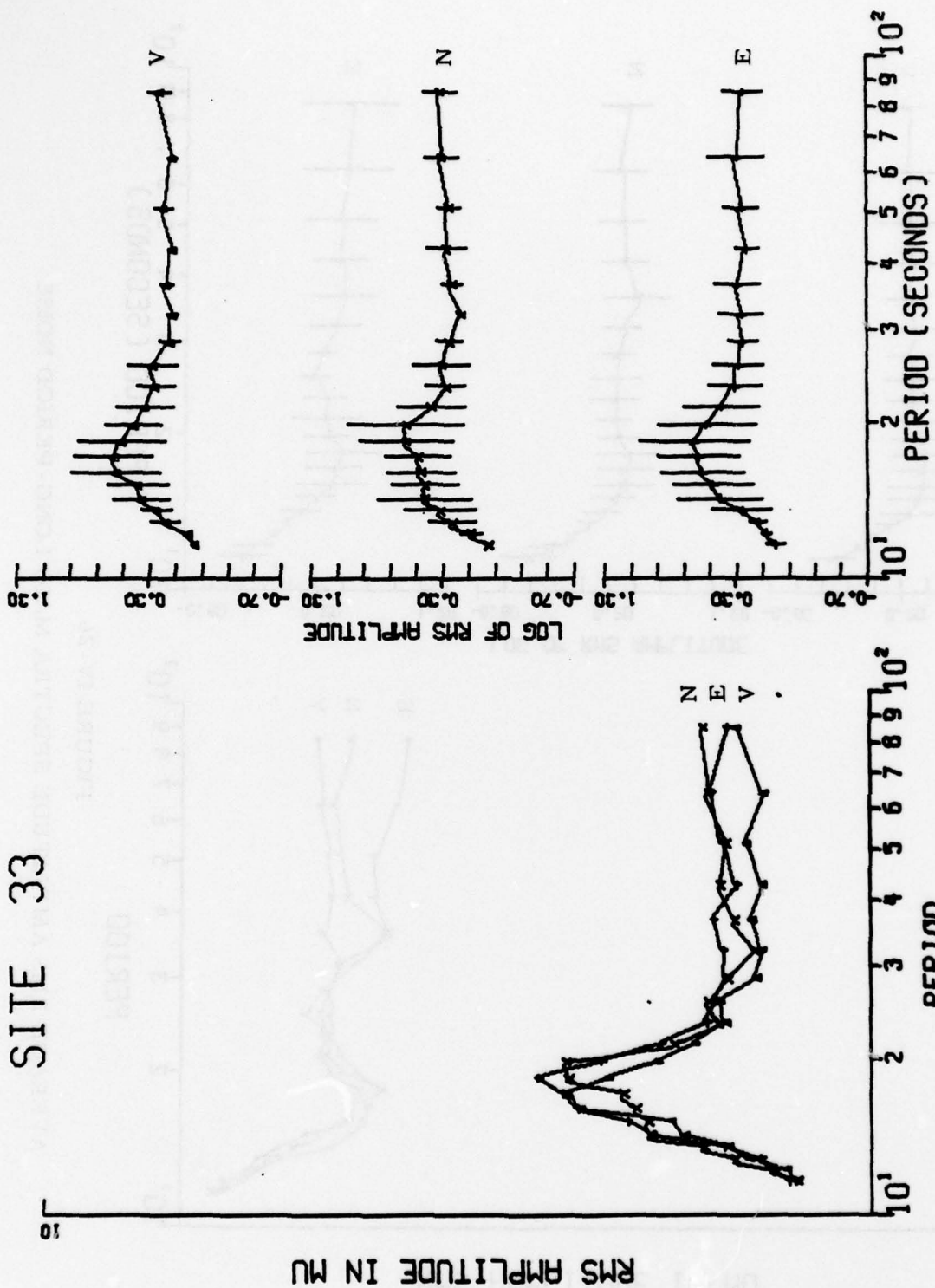
FIGURE IV-25

AVERAGE RMS AMPLITUDE SPECTRA CHTO LONG-PERIOD NOISE

SITE 36
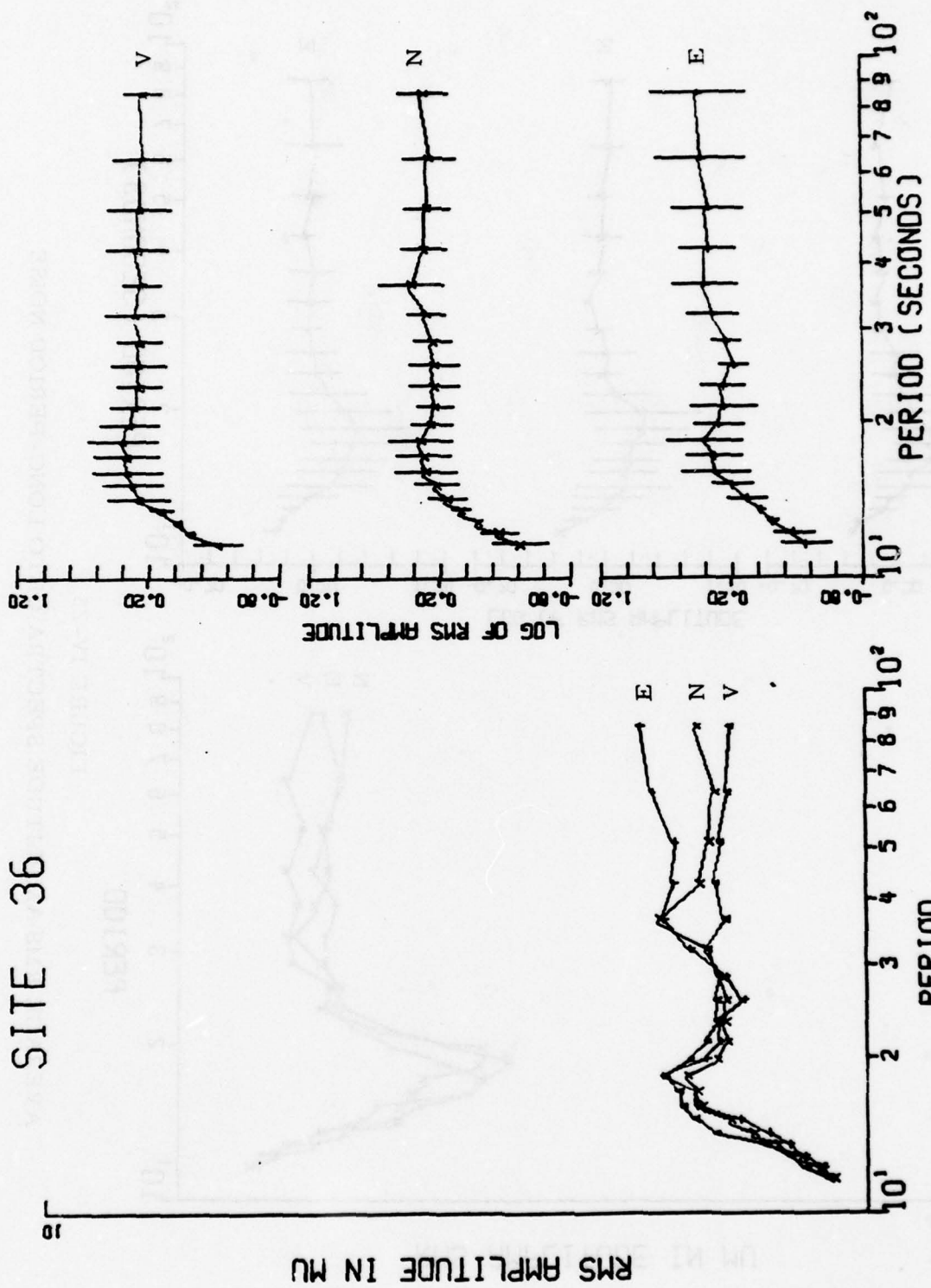
FIGURE IV-26

AVERAGE RMS AMPLITUDE SPECTRA MAIO LONG- PERIOD NOISE
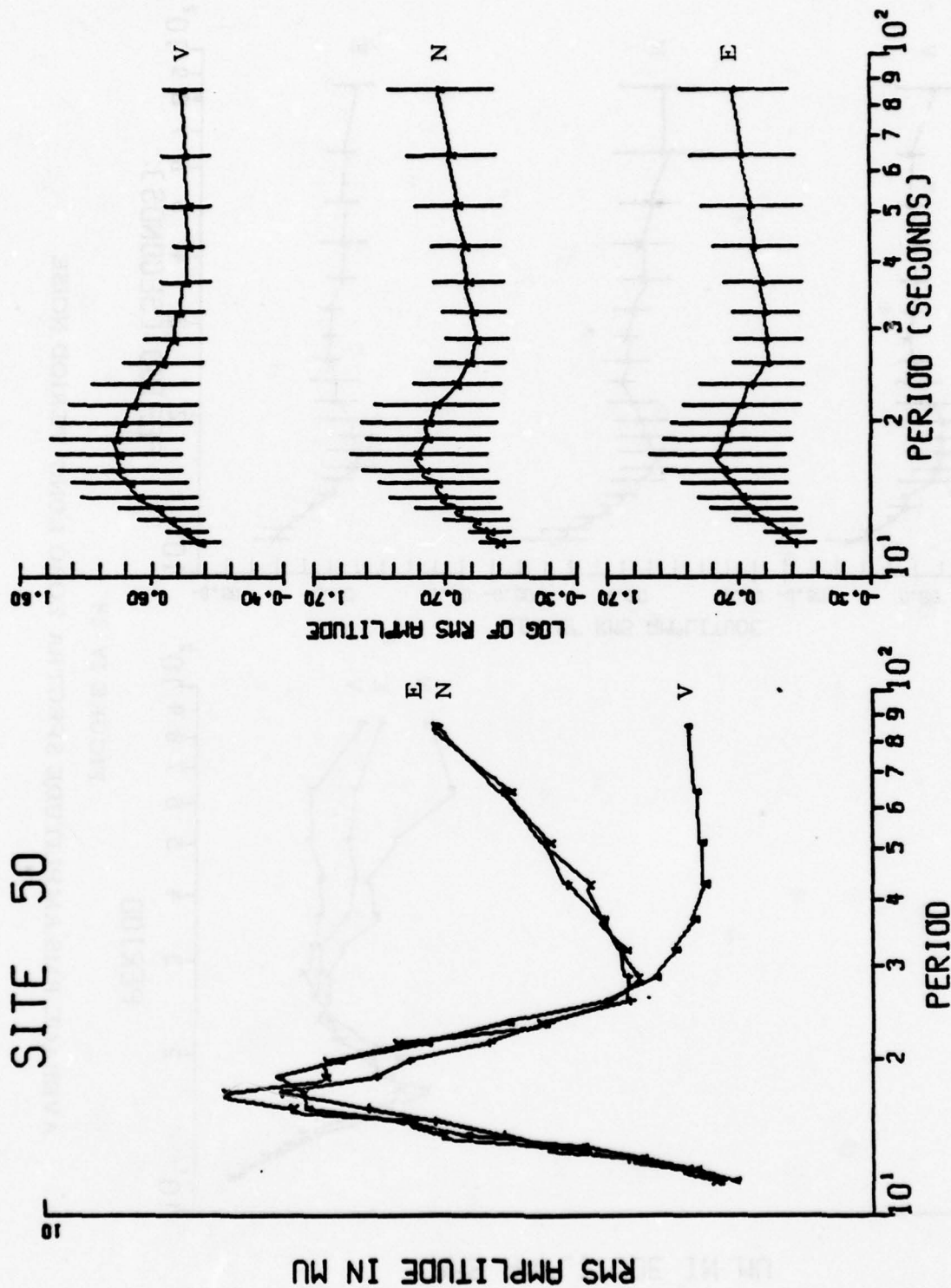
FIGURE IV-27

AVERAGE RMS AMPLITUDE SPECTRA CTAO LONG-PERIOD NOISE

SITE 51
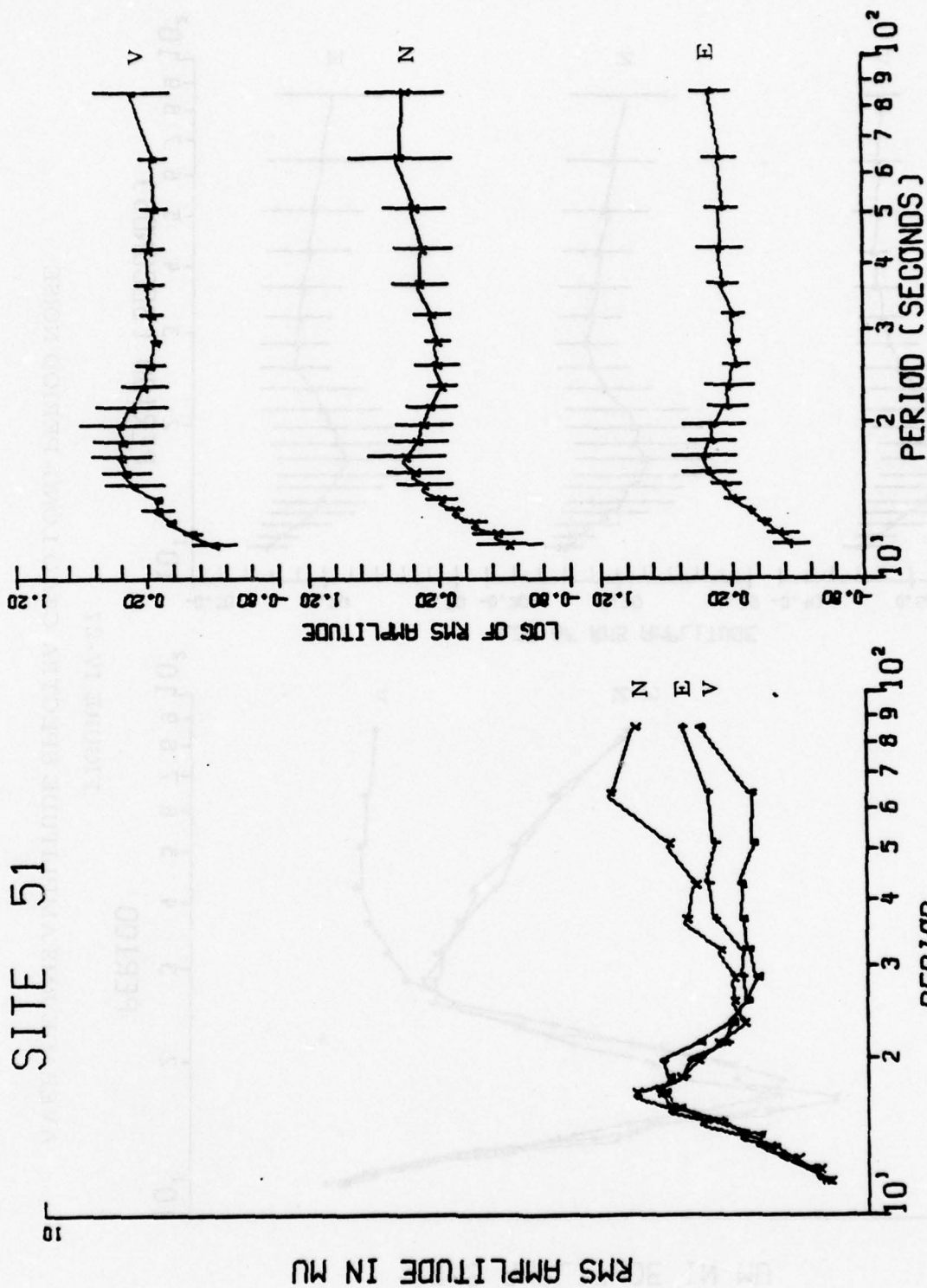
FIGURE IV-28

AVERAGE RMS AMPLITUDE SPECTRA ZOBO LONG-PERIOD NOISE

IV-66
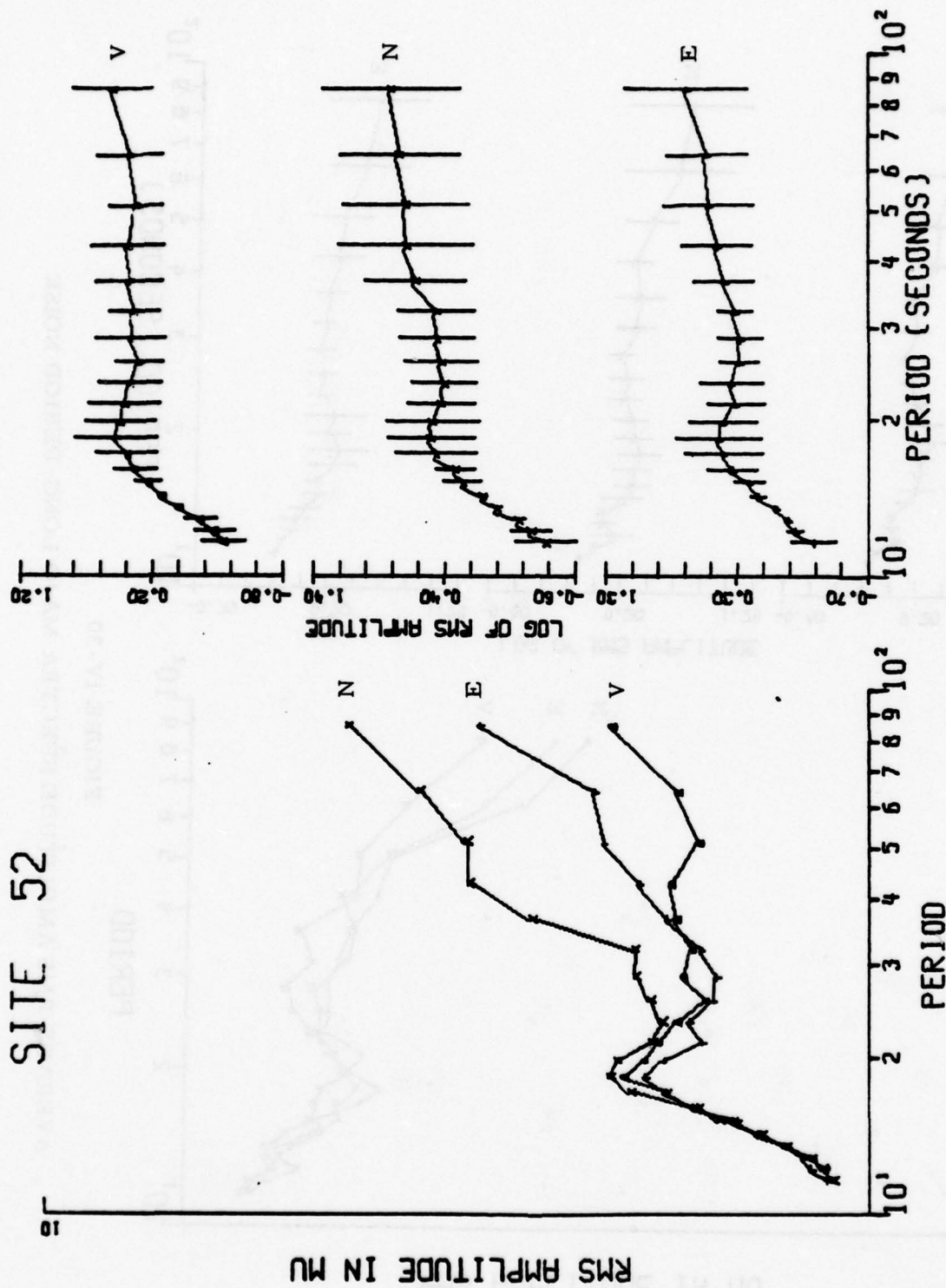
SITE 52

FIGURE IV-29

AVERAGE RMS AMPLITUDE SPECTRA KAAO LONG-PERIOD NOISE

SITE 53

RMS AMPLITUDE IN MU

LOG OF RMS AMPLITUDE

PERIOD (SECONDS)
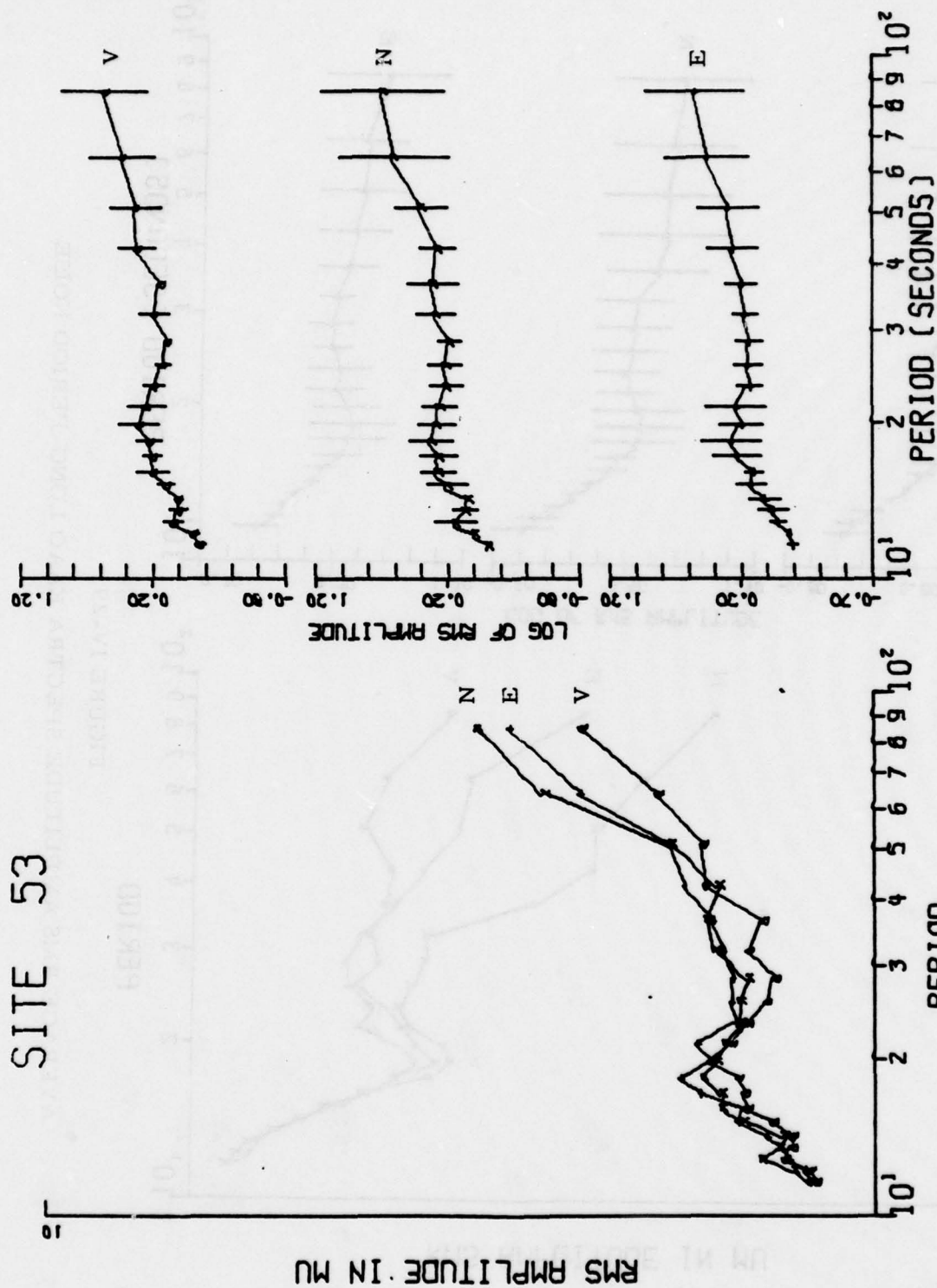
PERIOD

FIGURE IV-30

AVERAGE RMS AMPLITUDE SPECTRA MAJO LONG-PERIOD NOISE

IV-68

● Figures IV-24 and IV-25 - ANMO and CHTO noise: The three components show nearly identical spectral content and level of the local noise field. At each station the noise field has its greatest day-to-day variability between 14 and 25 seconds.

● Figure IV-26 - MAIO noise: The relative height of the 17-second microseismic peaks are small compared to the rest of the MAIO spectra. At periods below 30 seconds, the three components show nearly identical spectral content and level of the local noise field. The horizontal components show a secondary peak at 37 seconds nearly as large as the microseismic peak. The noise field has its greatest variability between 14 and 23 seconds period for all components and at 37 seconds period for the horizontal components.

● Figure IV-27 - CTAO noise: At periods below 30-seconds the three components show very similar spectral content and level of the local noise field. The vertical component 17-second microseismic peak seems to be truncated. At periods above 30 seconds the horizontal components show a strong rise in noise level while vertical component noise level increases only slightly.

● Figure IV-28 - ZOBO noise: At periods below 30 seconds the three components show nearly identical spectral content and level of the local noise field. At periods above 30 seconds, the components separate as horizontal component noise levels rise slightly above vertical component noise, which remains at low levels.

● Figure IV-29 - KAAO noise: At periods below 25 seconds the three components show similar spectral content and level of

the noise field. At periods above 25 seconds the horizontal
components show increasing noise levels, while vertical com-
ponent noise shows little increase below periods of about 70
seconds.

- Figure IV-30 - MAJO noise: The three components show simi-
  lar spectral content and noise level over their entire length.
  Horizontal component noise levels rise slightly above the ver-
  tical component noise level at periods above 50 seconds. The
  17-second microseismic peaks appears rather stunted in ampli-
  tude when compared with the rest of the MAJO spectra.

In general, spectral standard deviations seem to increase with increasing
spectral means. Also, no evidence was found from these spectra supporting
the hypothesis (Strauss and Weltman, 1977) which links oceanic wave energy
with spectral content and noise level.

Peak 20, 25, and 30 second noise amplitudes were measured
on all noise samples as part of the noise analysis. Each value measured
represents the absolute value of the largest zero-to-peak excursion of a wave-
form of given period plus-or-minus two seconds. Tables IV-7, IV-8, and
IV-9 list the means and standard deviations of peak and log peak 20, 25, and
30 second measured amplitudes.

TABLE IV-7a

MEAN PEAK 20 SECOND NOISE AMPLITUDES IN $m\mu$

Station	Vertical		North		East	
	Mean	S. D.	Mean	S. D.	Mean	S. D.
ANMO	25.59	10.90	23.52	10.44	26.04	10.04
CHTO	22.17	8.16	25.42	12.19	23.95	10.60
MAIO	18.13	8.55	15.79	7.43	15.98	9.17
CTAO	26.27	9.97	25.74	9.01	22.13	9.09
ZOBO	18.00	7.35	17.99	7.51	17.57	8.04
KAAO	21.33	10.34	21.86	12.17	20.11	10.45
MAJO	14.71	4.59	15.64	4.62	19.35	7.87

S. D. = Standard Deviation

TABLE IV-7b

MEAN LOG_{10} PEAK 20 SECOND NOISE AMPLITUDES IN $m\mu$

Station	Vertical		North		East	
	Mean	S. D.	Mean	S. D.	Mean	S. D.
ANMO	1.37	0.17	1.33	0.19	1.38	0.17
CHTO	1.31	0.18	1.36	0.19	1.33	0.19
MAIO	1.21	0.20	1.15	0.20	1.14	0.22
CTAO	1.39	0.16	1.38	0.16	1.31	0.18
ZOBO	1.22	0.17	1.21	0.19	1.20	0.18
KAAO	1.27	0.22	1.27	0.23	1.24	0.22
MAJO	1.14	0.13	1.17	0.13	1.25	0.19

S. D. = Standard Deviation

TABLE IV-8a

MEAN PEAK 25 SECOND NOISE AMPLITUDES IN $m\mu$

Station	Vertical		North		East	
	Mean	S. D.	Mean	S. D.	Mean	S. D.
ANMO	22.85	10.05	20.91	10.24	23.78	9.11
CHTO	19.06	7.54	22.28	8.42	24.96	9.52
MAIO	20.06	7.45	20.25	7.76	20.80	8.39
CTAO	24.65	58.98	21.82	6.79	24.26	35.08
ZOBO	17.53	6.85	21.46	8.30	19.84	5.67
KAAO	23.17	9.43	29.16	13.55	24.32	9.28
MAJO	17.44	5.14	19.50	6.08	21.21	5.50

S. D. = Standard Deviation

TABLE IV-8b

MEAN LOG_{10} PEAK 25 SECOND NOISE AMPLITUDES IN $m\mu$

Station	Vertical		North		East	
	Mean	S. D.	Mean	S. D.	Mean	S. D.
ANMO	1.33	0.16	1.28	0.17	1.35	0.16
CHTO	1.25	0.17	1.32	0.16	1.37	0.16
MAIO	1.28	0.15	1.28	0.16	1.29	0.16
CTAO	1.26	0.22	1.32	0.13	1.30	0.20
ZOBO	1.22	0.14	1.30	0.15	1.28	0.11
KAAO	1.33	0.17	1.42	0.20	1.36	0.16
MAJO	1.22	0.12	1.27	0.12	1.31	0.11

S. D. = Standard Deviation

TABLE IV-9a

MEAN PEAK 30 SECOND NOISE AMPLITUDES IN $m\mu$

Station	Vertical		North		East	
	Mean	S. D.	Mean	S. D.	Mean	S. D.
ANMO	12.30	6.26	12.04	6.94	14.66	6.85
CHTO	9.87	4.92	14.05	8.28	13.00	5.77
MAIO	13.78	6.86	17.18	8.38	18.45	8.31
CTAO	11.97	18.77	12.53	6.23	13.30	7.47
ZOBO	11.21	5.14	14.42	5.75	12.99	4.97
KAAO	16.05	8.36	29.64	24.16	21.61	23.30
MAJO	10.52	4.36	15.99	6.17	14.22	5.05

S. D. = Standard Deviation

TABLE IV-9b

MEAN LOG$_{10}$ PEAK 30 SECOND NOISE AMPLITUDES IN mμ

Station	Vertical		North		East	
	Mean	S. D.	Mean	S. D.	Mean	S. D.
ANMO	1.03	0.22	1.02	0.24	1.11	0.21
CHTO	0.94	0.22	1.09	0.21	1.07	0.19
MAIO	1.09	0.20	1.09	0.21	1.07	0.19
CTAO	0.93	0.32	1.05	0.21	1.06	0.24
ZOBO	1.00	0.22	1.13	0.16	1.07	0.22
KAAO	1.15	0.21	1.39	0.25	1.24	0.24
MAJO	0.96	0.28	1.17	0.16	1.10	0.25

S. D. = Standard Deviation

SECTION V

SRO DETECTION CAPABILITY

A.   DISCUSSION

The Seismic Research Observatory detection capability statistics for the five new stations are presented in this section. For any given event, only one of seven conditions, corresponding to seven detection codes, can exist. The conditions are the following:

- Event is detected.

- Event is not detected.

- Event is mixed.

- No data are recorded for the time period.

- Equipment is malfunctioning.

- Event is detected on microfiche only. } Short-Period Only

- Event epicenter is located $> 103^{\circ}$ from station. } Short-Period Only

A mixed event is one that is partially or completely masked by a second signal. This happens when two events arrive at a station at essentially the same time or, when a larger signal arrives before the event of interest, burying the event in its coda. The cause of no data being recorded is the shutting down of the station. Malfunctions refer to the partial failure of the system, from the sensor unit to the reception of data at the Seismic Data Analysis Center, which causes degradation of the seismic data. A microfiche detection only refers to short-period detection capability, and will be discussed in Subsection V-B. Since epicentral distances greater than 103°

constitute the P wave shadow zone, events located farther than 103° from the station of interest were deleted from the short-period data base for that station.

In its simplest form, a station's detection capability would be determined by whether the analyst saw either the event of interest or seismic noise. However, the true detection capability depends greatly on how mixed events, malfunctions, periods of no recorded data, etc., are treated. For this reason, the Seismic Research Observatory detection capability estimates are calculated in two ways.

The first of these is labeled the 'ideal detection capability'. When calculating this estimate, mixed events, events for which no data was recorded, and events containing malfunctions were dropped from the data base. The value of this ideal estimate is that it shows the detection capability improvement possible if the reliability of the instrumentation could be improved and if methods of separating mixed events could be found.

The second estimate is labeled 'actual detection capability', and it considers mixed events, events for which no data was recorded, and events containing malfunctions as non-detections. This approach gives a real-world detection capability estimate.

The quantity used to represent detection capability is the 50 percent detection threshold, denoted by 'm_{b50}'. The 50 percent detection threshold is the bodywave magnitude for which the probability of detection is 0.5. It is computed by fitting the Gaussian probability function to the detection statistics by a maximum likelihood method (Ringdal, 1974).

B.   SHORT-PERIOD DETECTION CAPABILITY ESTIMATES

In the previous evaluations, the Seismic Research Observatory short-period detection capability estimate was computed from data recorded

V-2

by the short-period automatic detector. Therefore, the estimate is dependent upon the performance of the detector. In an effort to circumvent this dependence, the daily recordings from each of the new stations were obtained on microfiche for the period 1 September 1977 to 30 November 1977, and detection statistics were generated using the microfiche as data.

The criteria for determining whether an event was detected on the microfiche were as follows:

- The waveform is at least 3.5 dB above the surrounding noise waveform.
- The waveform begins within ± 20 seconds of the predicted arrival time.

The requirement that the maximum amplitude of the waveform be at least 3.5 dB above the noise seems low, but this is an advantage gained by using microfiche as compared to Calcomp plots. Rather than inferring the noise level from a small segment of data; noise trends could be seen, and identification of an event could be made with more confidence.

Using the microfiche also enabled the analyst to pick emergent waveforms; however, this was done only when the observed start time satisfied the second requirement. It should be noted that although these emergent start times were chosen at the most obvious break from the noise level, they are not necessarily the actual P wave arrival times, but could be as much as several seconds past it.

The second detection criterion is not absolute. It is possible that errors in computation of origin time and location, and choice of start time may all combine to place the first point of detection outside the ± 20 second gate. Also, the expected arrival times were calculated assuming a normal (33 km) depth of focus. In cases where a P wave was observed outside the gate, and no other events could be found in the National Earthquake

Information Service (NEIS) event list, a detection was declared. These cases were, however, very rare.

In order to provide detection codes corresponding to the conditions mentioned at the beginning of this subsection, the microfiche detection statistics were then compared to the automatic detector logs (see Section III). This generated two sets of detection statistics, one for the analyst detections and one for the automatic detections. Each of these two sets were further divided in the manner mentioned in the first part of this section, or, into 'ideal' and 'actual' detection statistics. The four resultant detection capability estimates, calculated from these four sets, are shown for four of the new stations in Figures V-1 to V-16. Station ZOBO (Zongo, Bolivia) is not shown because only two events were detected. The reason for this was too large an epicentral distance to this station for most Eurasian events.

The figures labeled 'Ideal Detection Capability' are composed of non-mixed events detected both by the automatic detector and on the microfiche and those events not detected by either one. All other events were dropped from the detection statistics, i.e., mixed events, events for which no data were recorded, events containing malfunctions, and events detected only on the microfiche. This is the ideal detection capability as 'seen' by the automatic detector.

The figures labeled 'Actual Detection Capability' are composed of all the events in the data base whose epicenters are less than 103° from the station of interest. However, all mixed events, events for which no data were recorded, events containing malfunctions, and events detected only on the microfiche were considered to be non-detections. This is the real-world detection capability as 'seen' by the automatic detector.

The figures labeled 'Ideal Detection Capability - Detector Disabled' are identical to the 'Ideal Detection Capability' except that the former accept

V-4
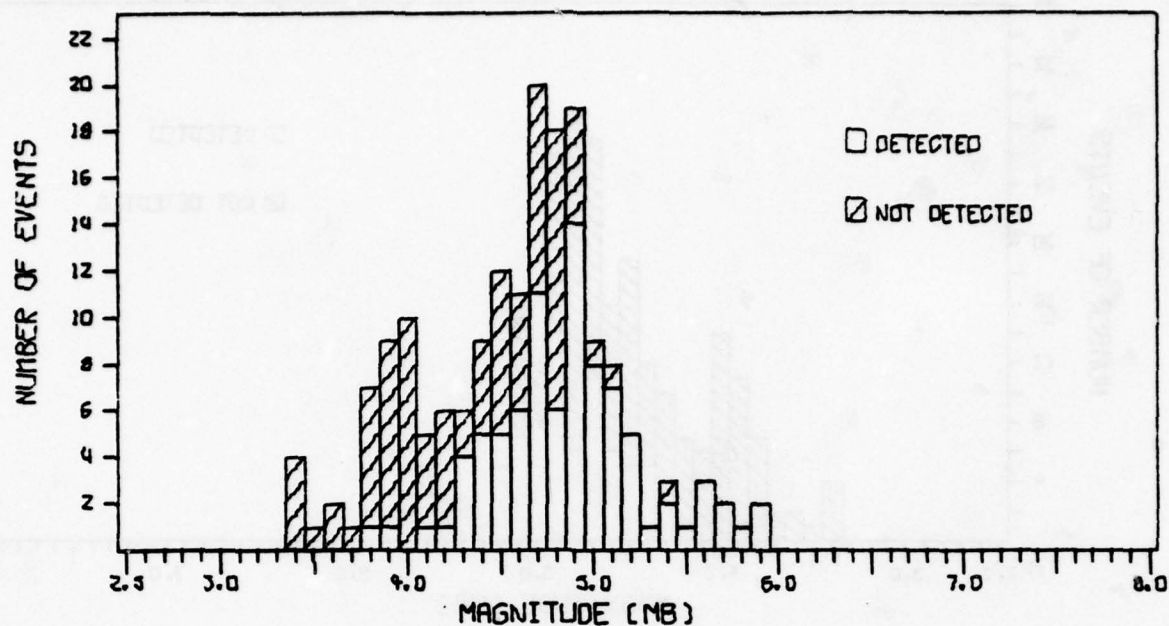
IDEAL CHTO SP DETECTION CAPABILITY
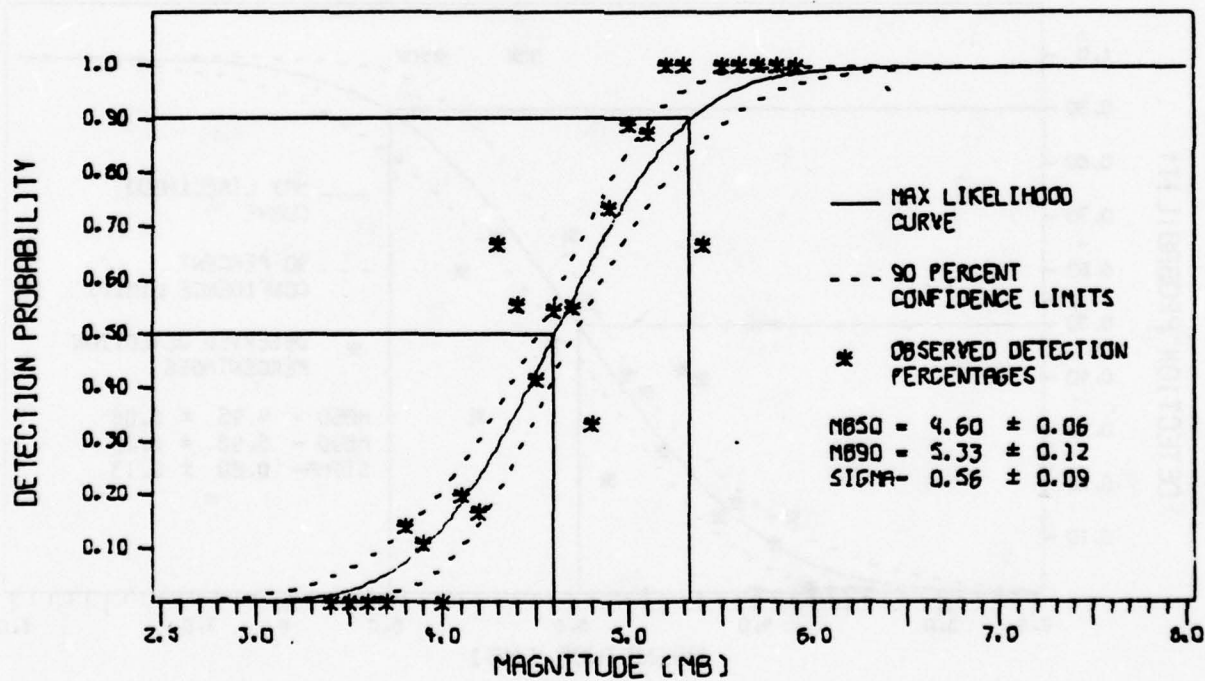
FIGURE V-1

IDEAL CHTO SP DETECTION CAPABILITY

V-5

ACTUAL CHTO SP DETECTION CAPABILITY

FIGURE V-2

ACTUAL CHTO SP DETECTION CAPABILITY

V-6

IDEAL CHTO SP DETECTION CAPABILITY--DETECTOR DISABLED

FIGURE V-3

IDEAL CHTO SP DETECTION CAPABILITY - DETECTOR DISABLED

V-7
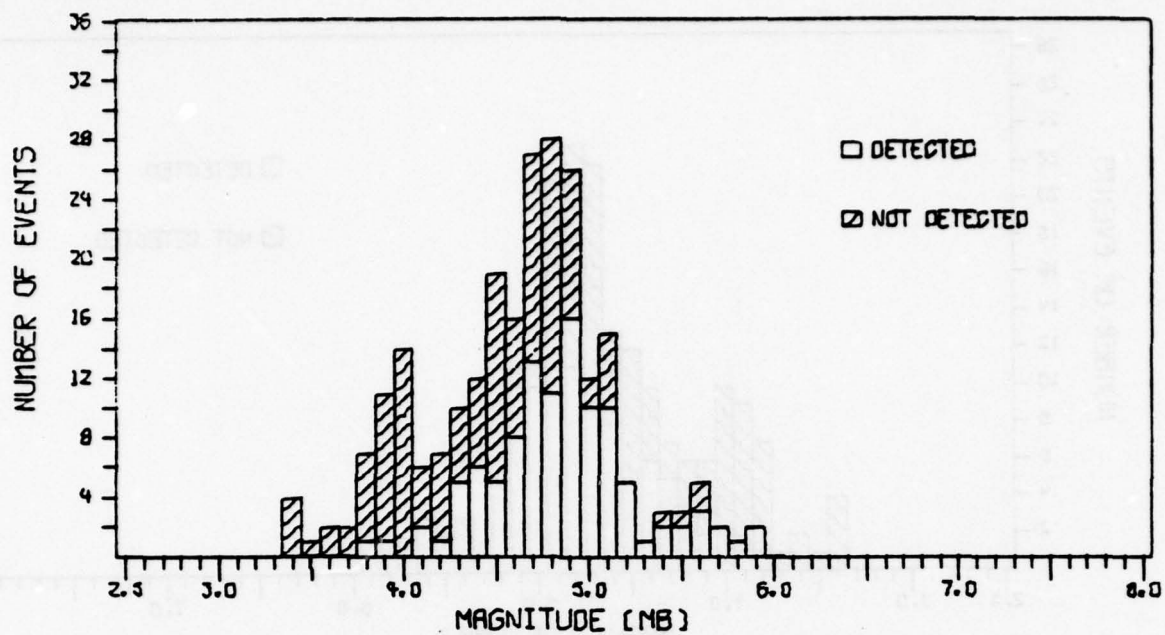
PREDICTED CHTO SP DETECTION CAPABILTY--DETECTOR DISABLED
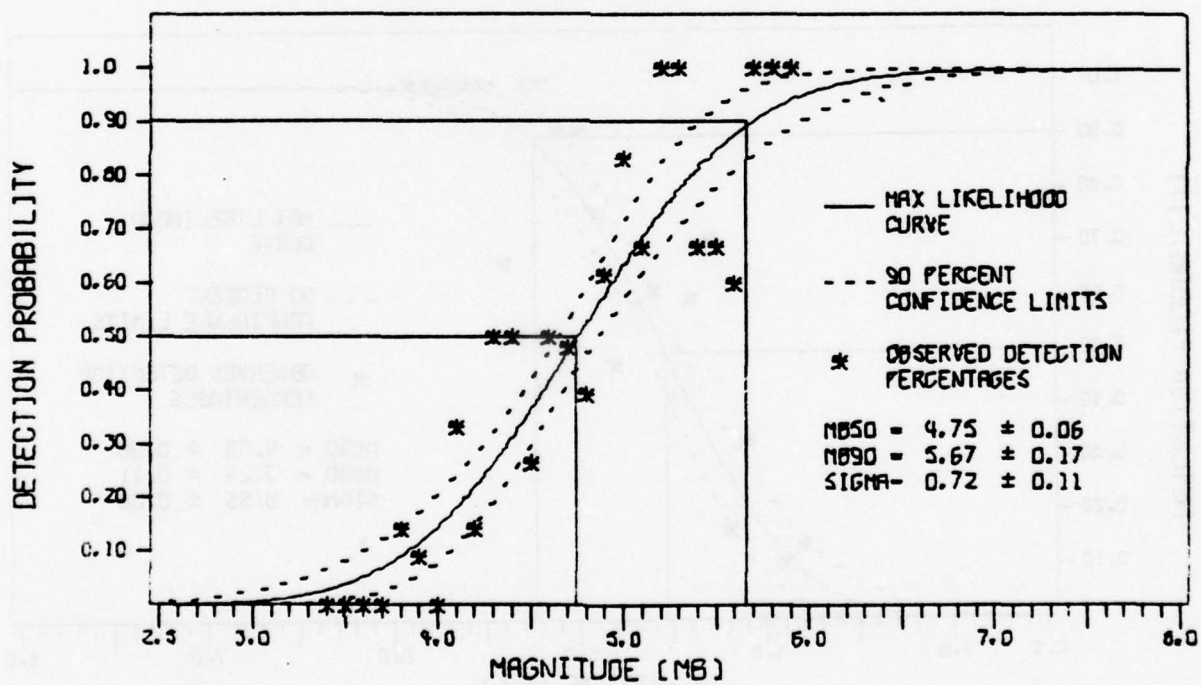
FIGURE V-4

PREDICTED CHTO SP DETECTION CAPABILITY - DETECTOR DISABLED
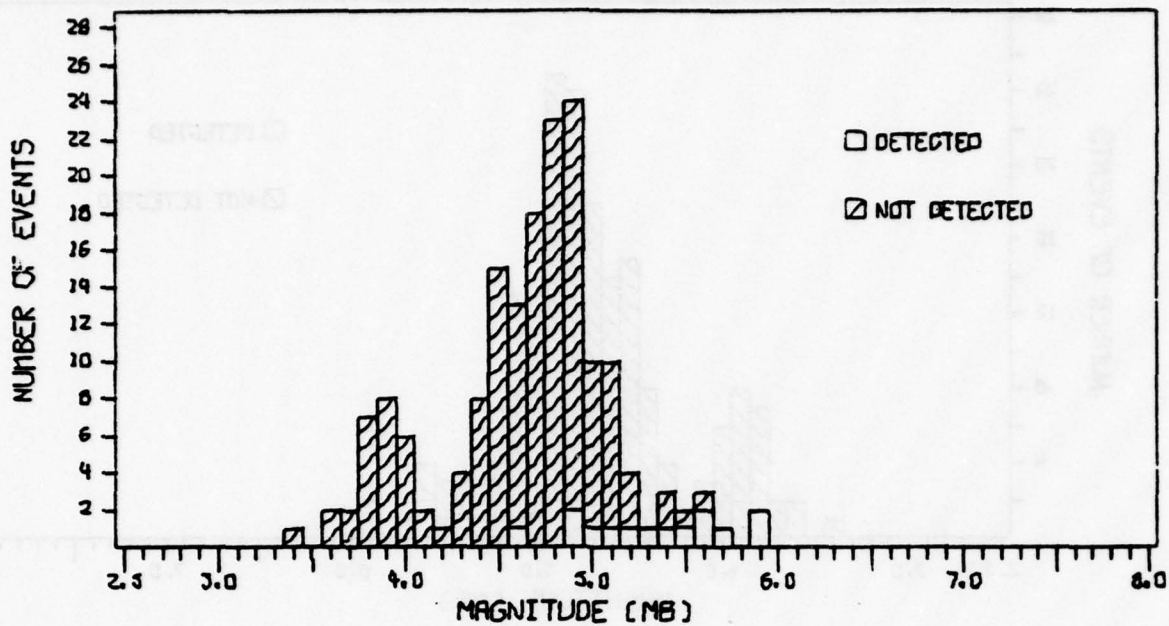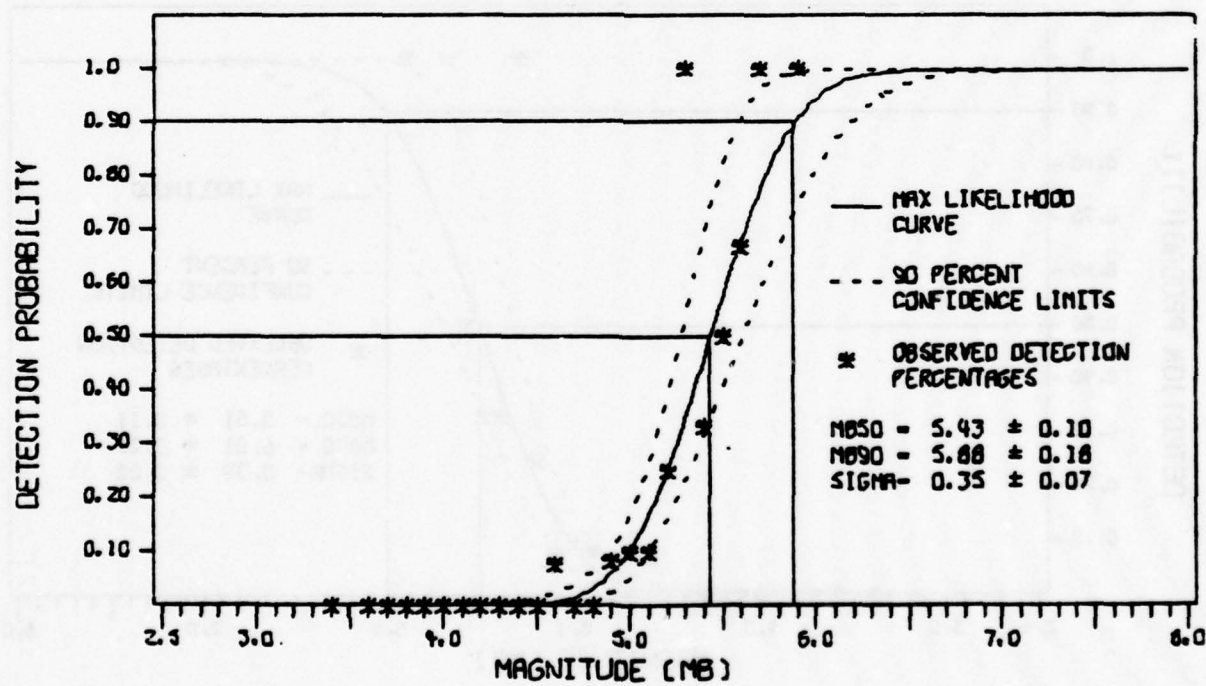
FIGURE V-5

IDEAL CTAO SP DETECTION CAPABILITY

V-9
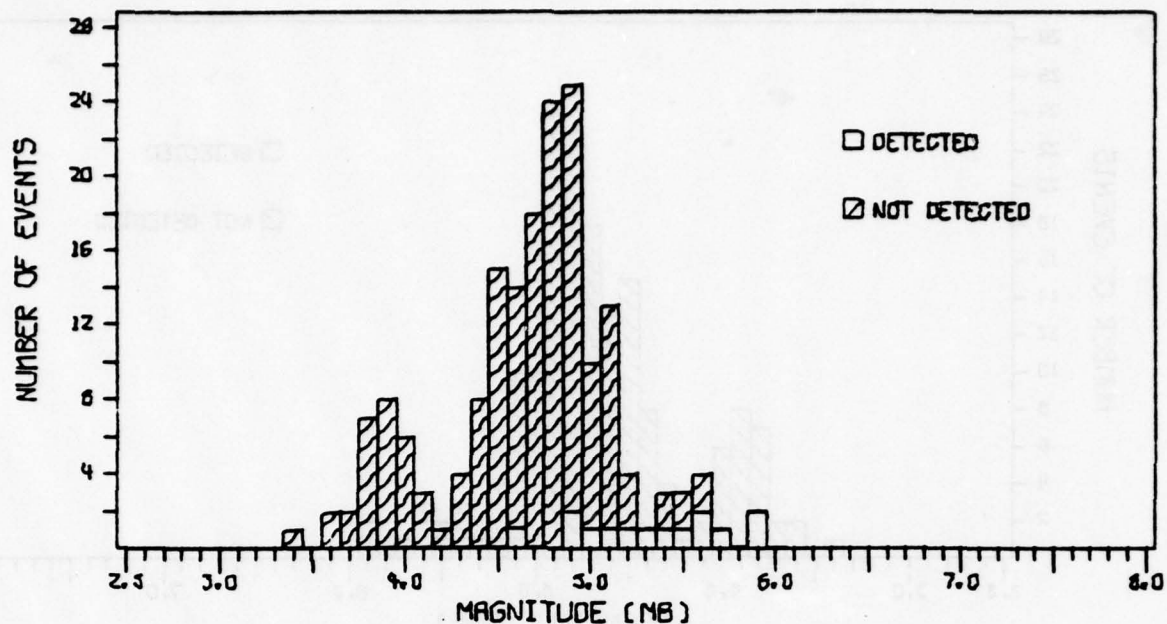
ACTUAL CTAO SP DETECTION CAPABILITY
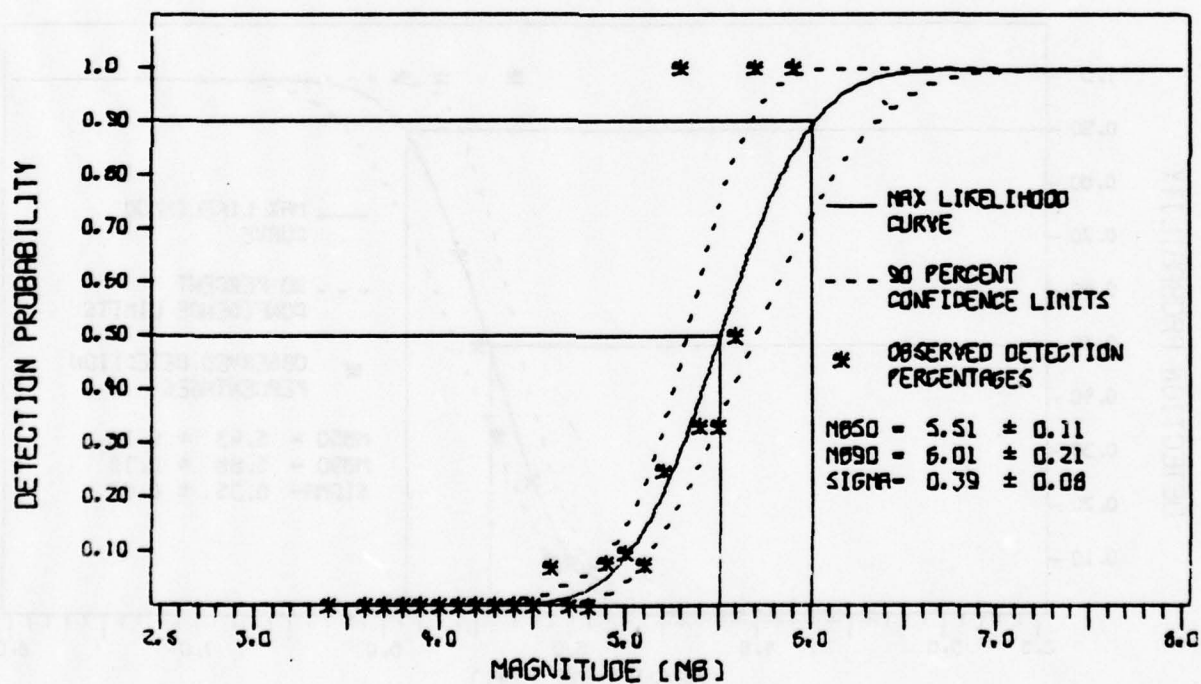
FIGURE V-6

ACTUAL CTAO SP DETECTION CAPABILITY
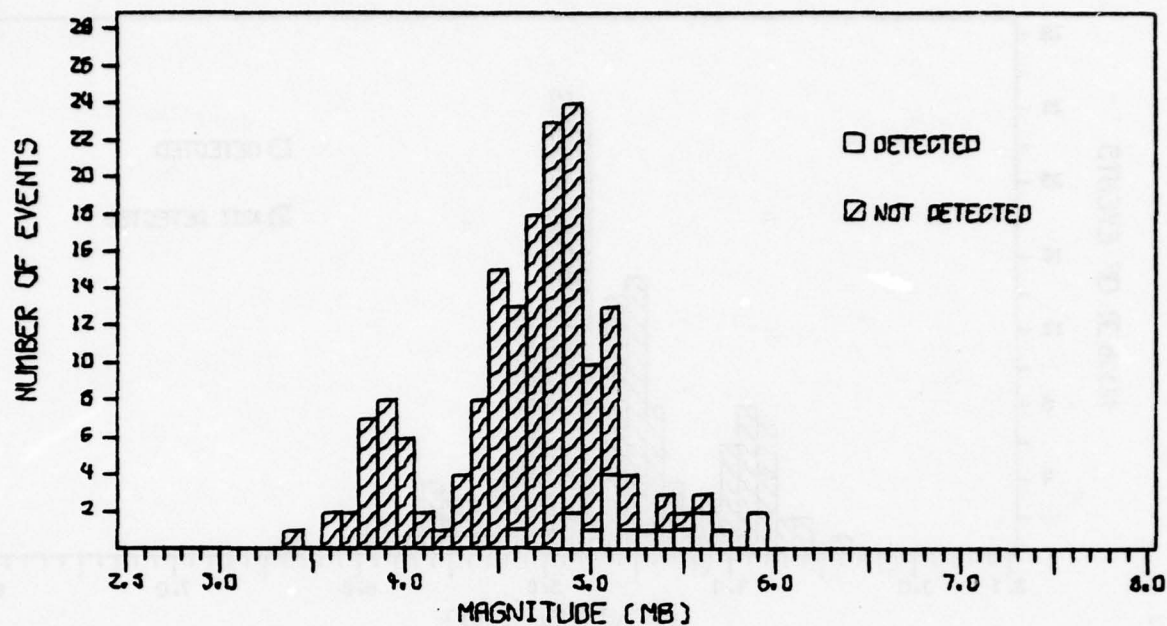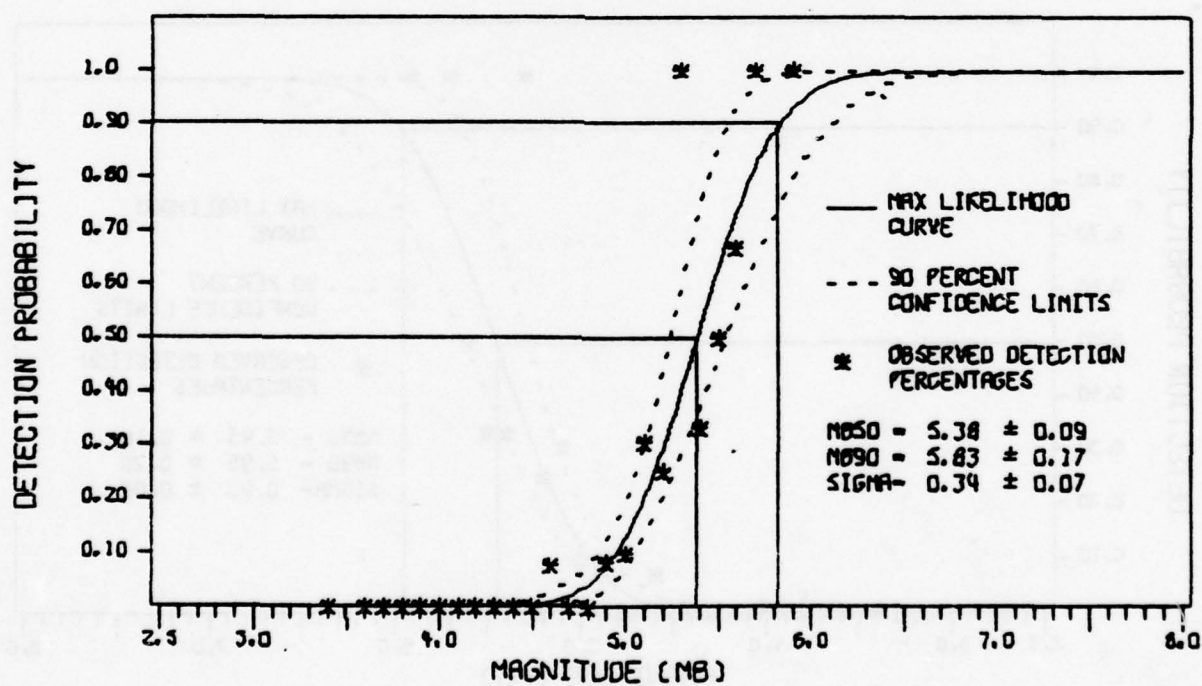
FIGURE V-7

IDEAL CTAO SP DETECTION CAPABILITY - DETECTOR DISABLED

V-11
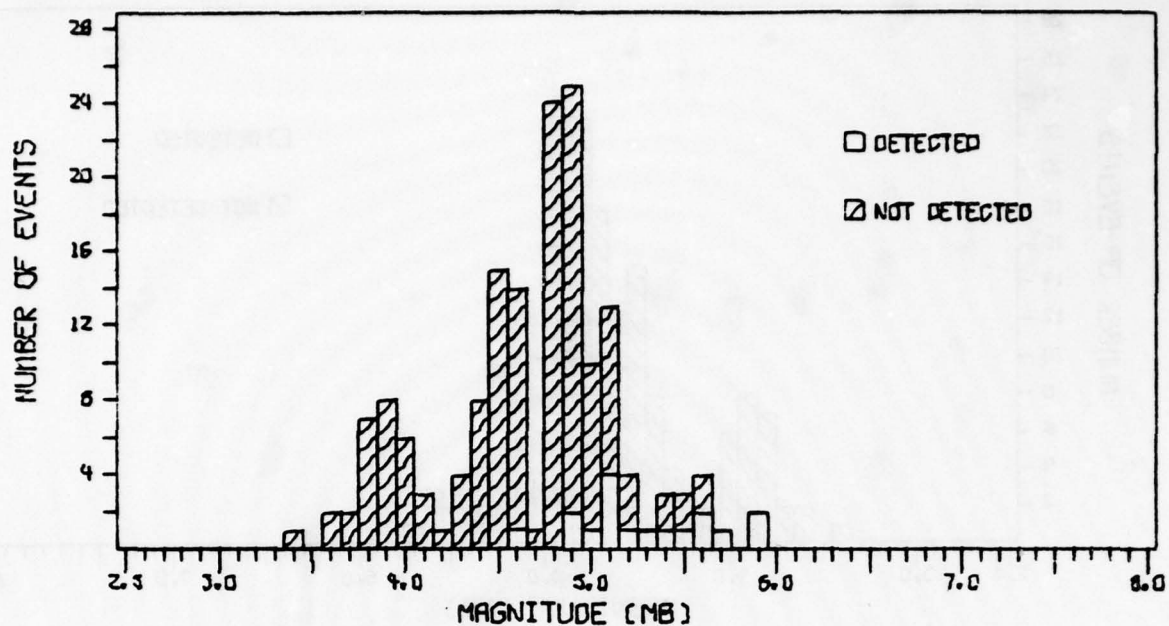
PREDICTED CTAO SP DETECTION CAPABILTY--DETECTOR DISABLED   OO
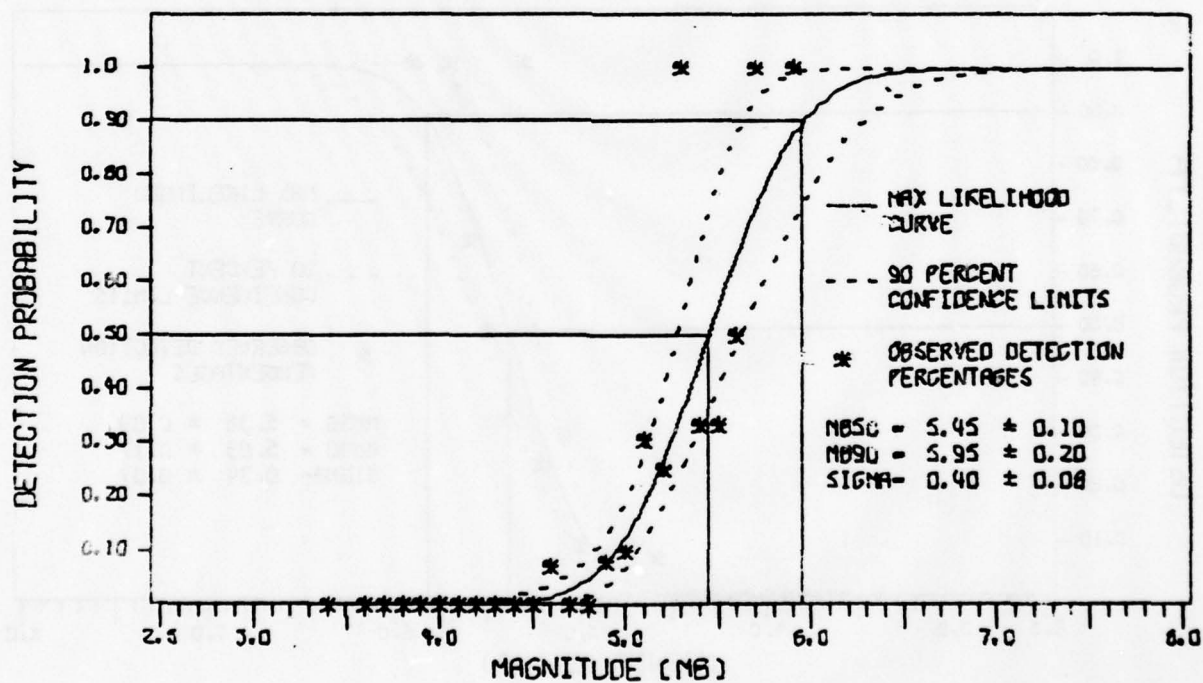
FIGURE V-8

PREDICTED CTAO SP DETECTION CAPABILITY - DETECTOR DISABLED
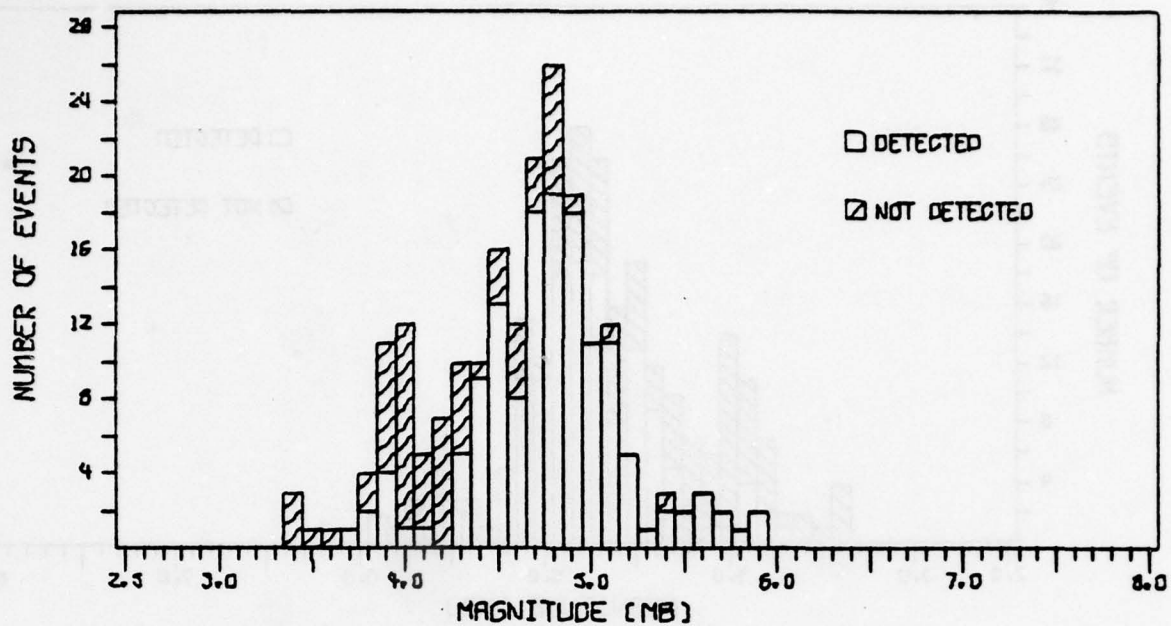
IDEAL KAAO SP DETECTION CAPABILITY
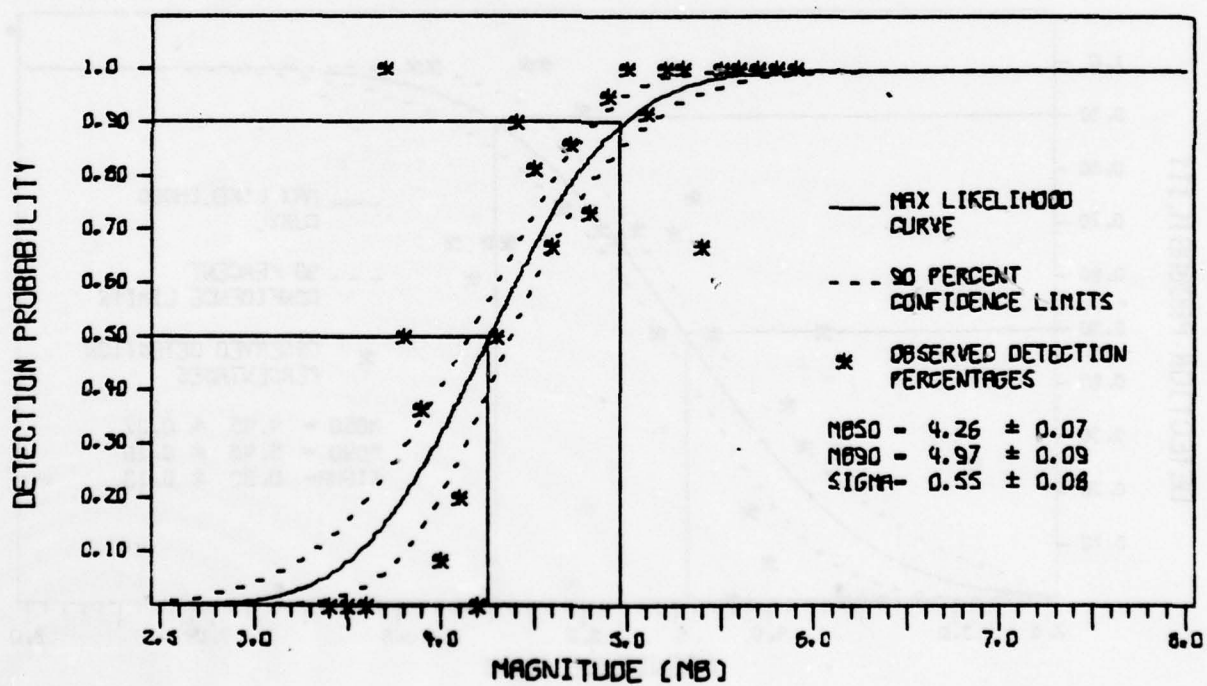
FIGURE V-9

IDEAL KAAO SP DETECTION CAPABILITY
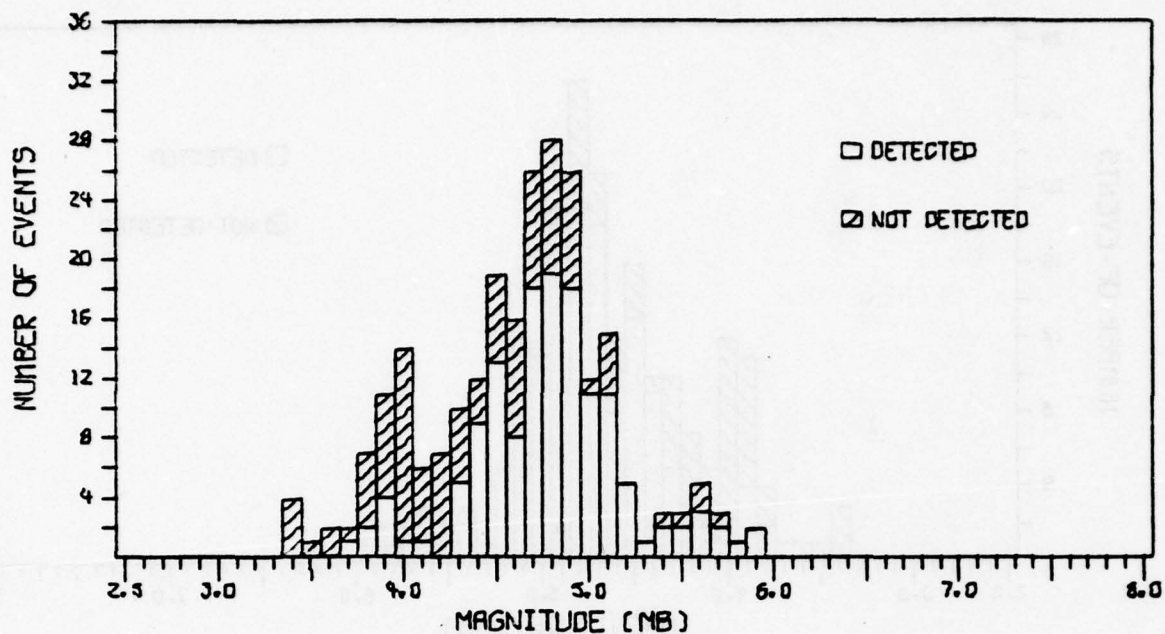
ACTUAL KAAO SP DETECTION CAPABILITY
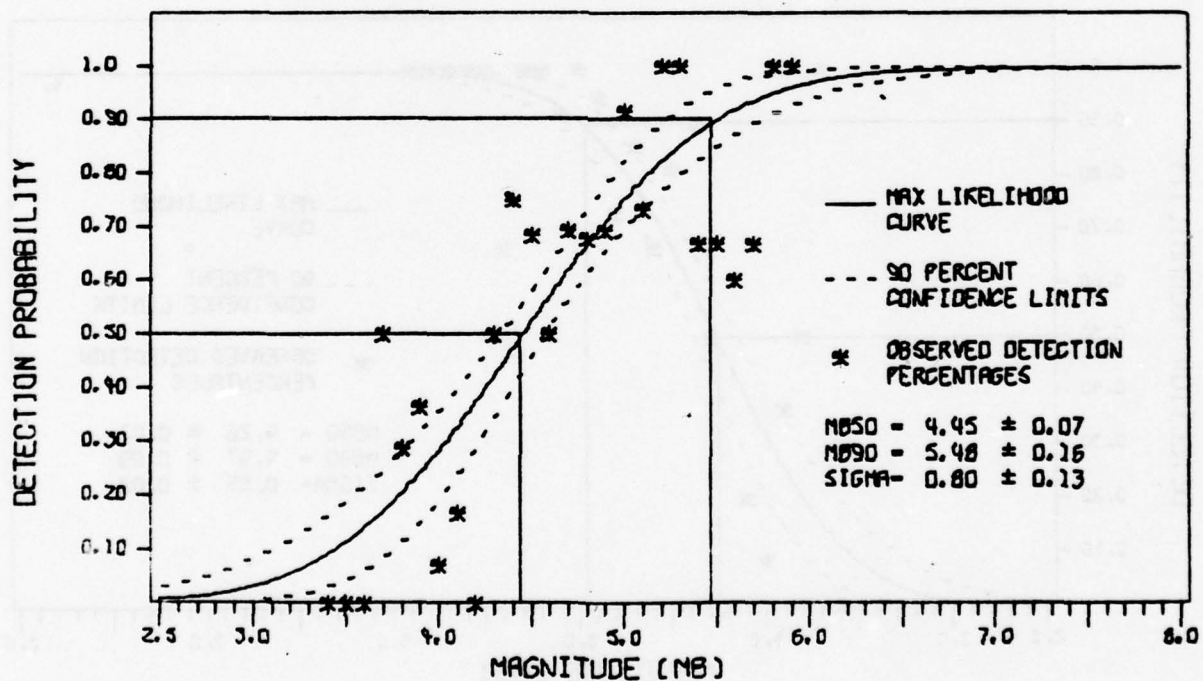
FIGURE V-10

ACTUAL KAAO SP DETECTION CAPABILITY

V-14

IDEAL KAAO SP DETECTION CAPABILITY--DETECTOR DISABLED

FIGURE V-11

IDEAL KAAO SP DETECTION CAPABILITY - DETECTOR DISABLED
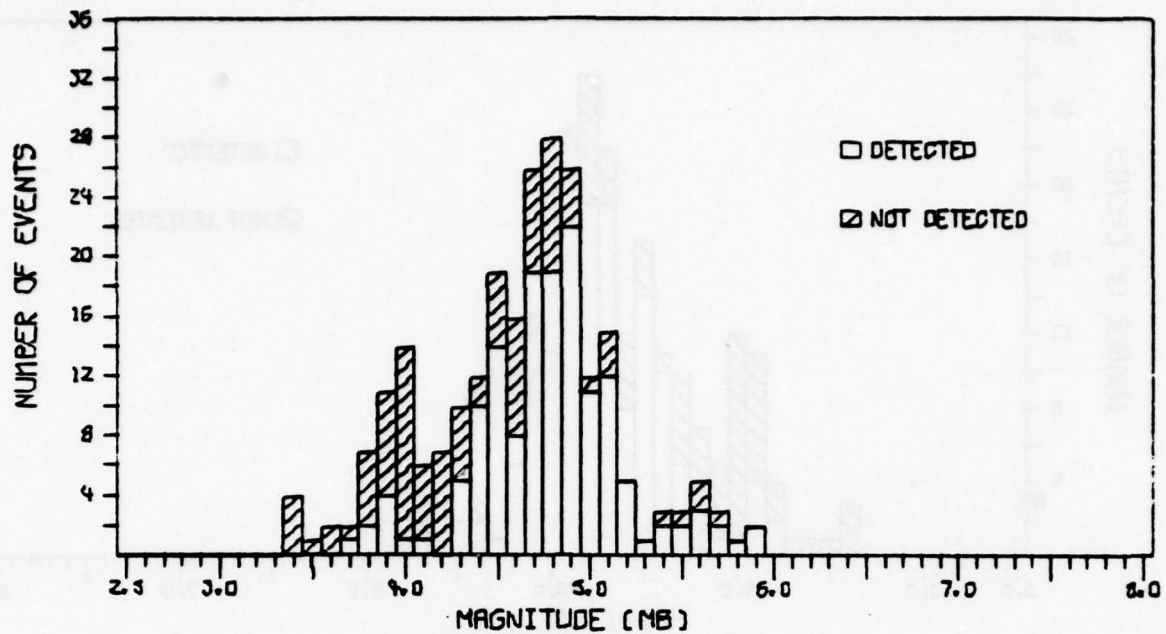
PREDICTED KAAO SP DETECTION CAPABILTY--DETECTOR DISABLEC
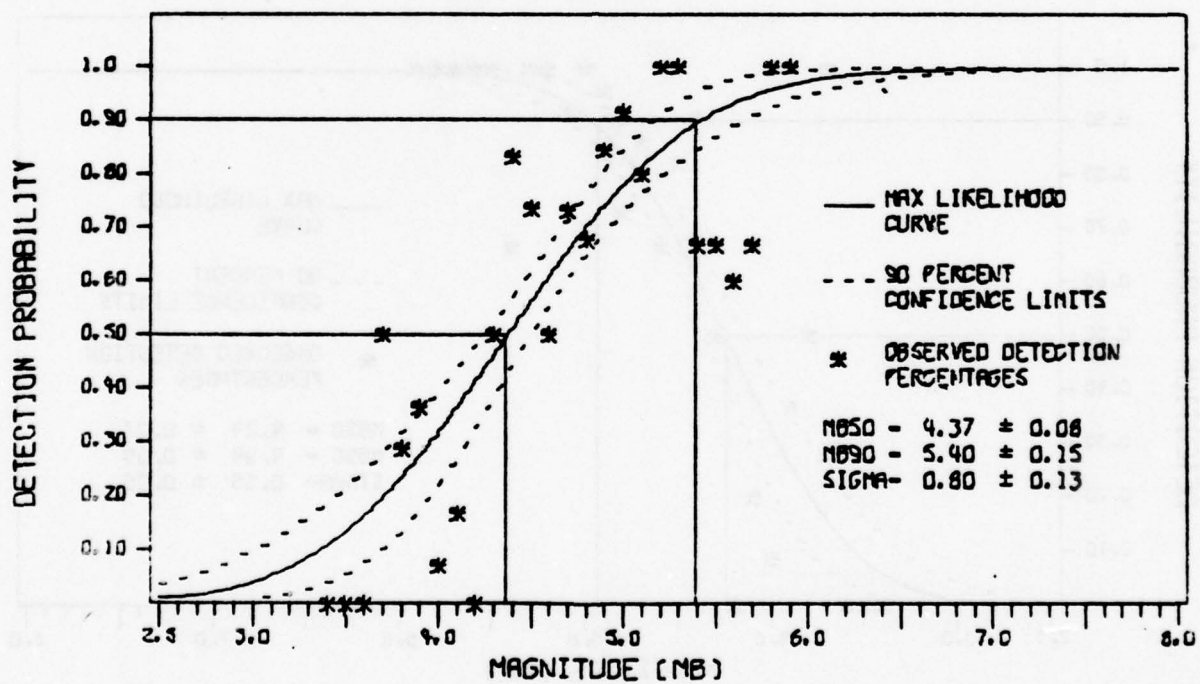
FIGURE V-12

PREDICTED KAAO SP DETECTION CAPABILITY - DETECTOR DISABLED
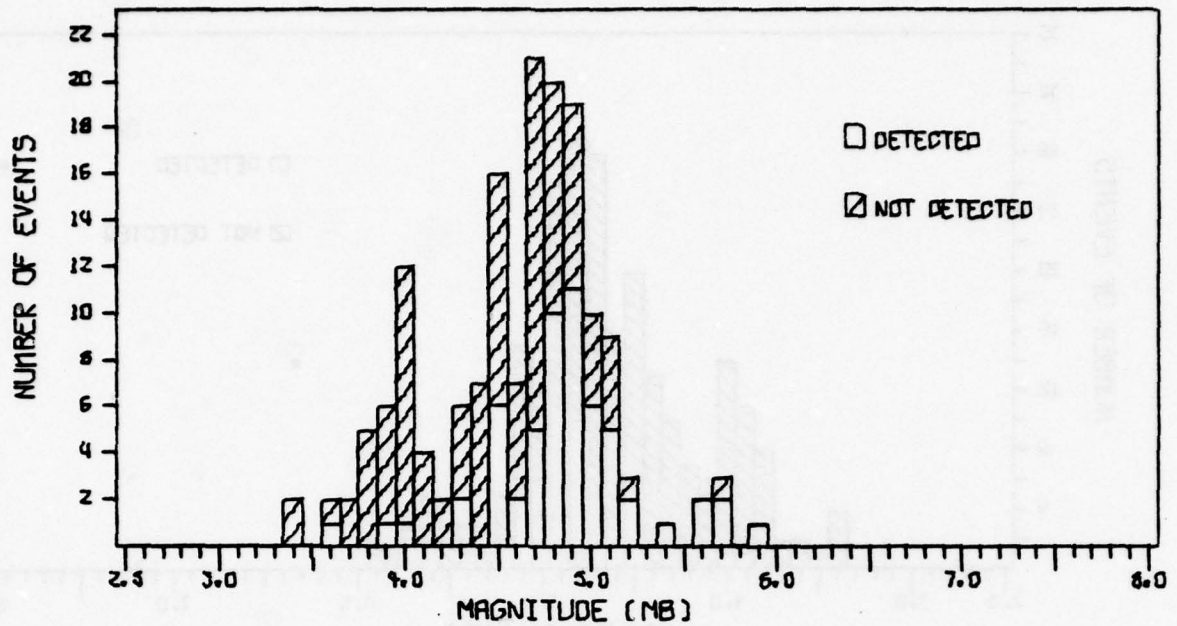
IDEAL MAJO SP DETECTION CAPABILITY

FIGURE V-13

IDEAL MAJO SP DETECTION CAPABILITY

FIGURE V-14

ACTUAL MAJO SP DETECTION CAPABILITY
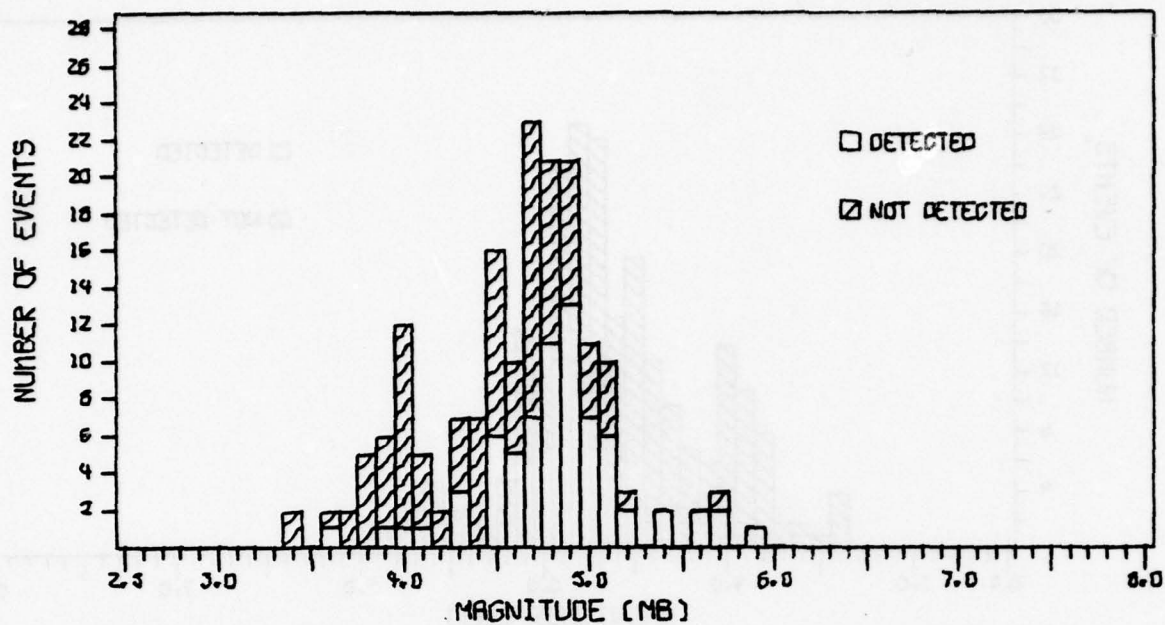
IDEAL MAJO SP DETECTION CAPABILITY--DETECTOR DISABLED
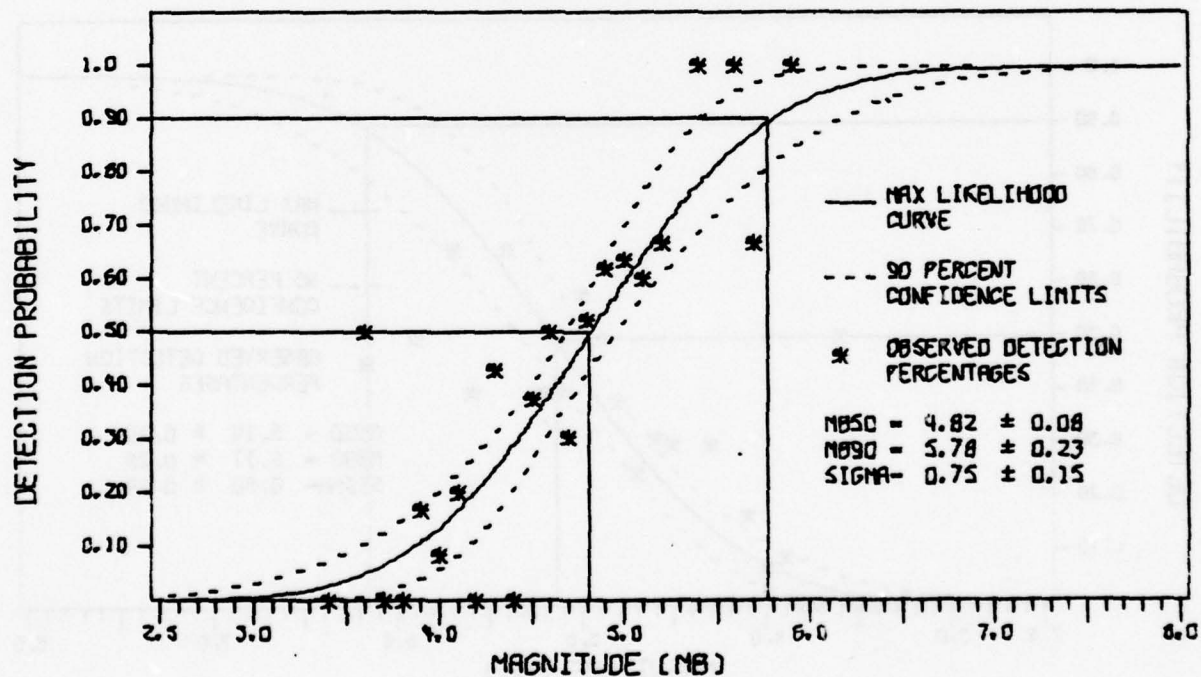
FIGURE V-15

IDEAL MAJO SP DETECTION CAPABILITY - DETECTOR DISABLED
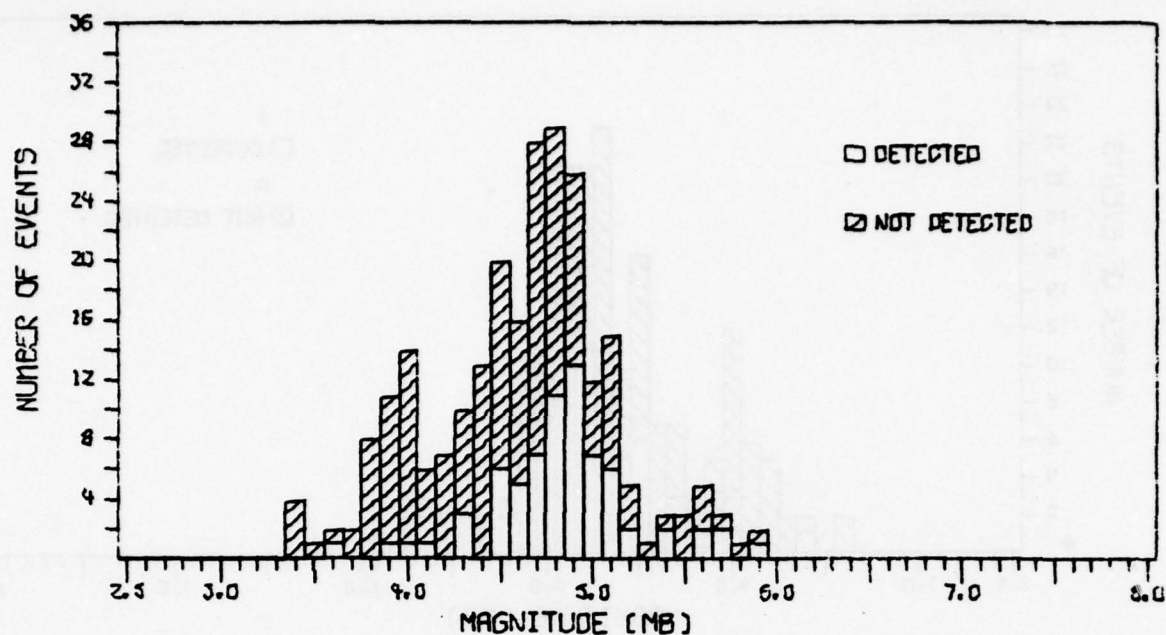
PREDICTED MAJO SP DETECTION CAPABILTY--DETECTOR DISABLED
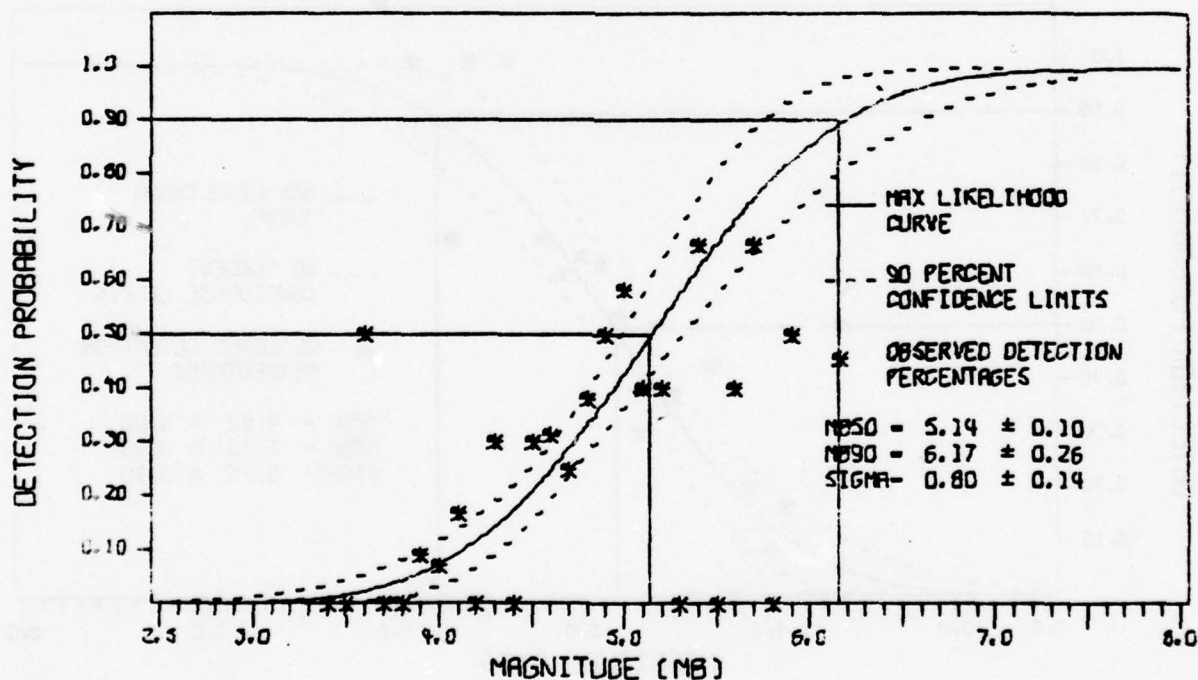
FIGURE V-16

PREDICTED MAJO SP DETECTION CAPABILITY - DETECTOR DISABLED

V-20

events detected only on the microfiche as detections. This is the ideal detection capability that would be computed by an analyst viewing continuous data.

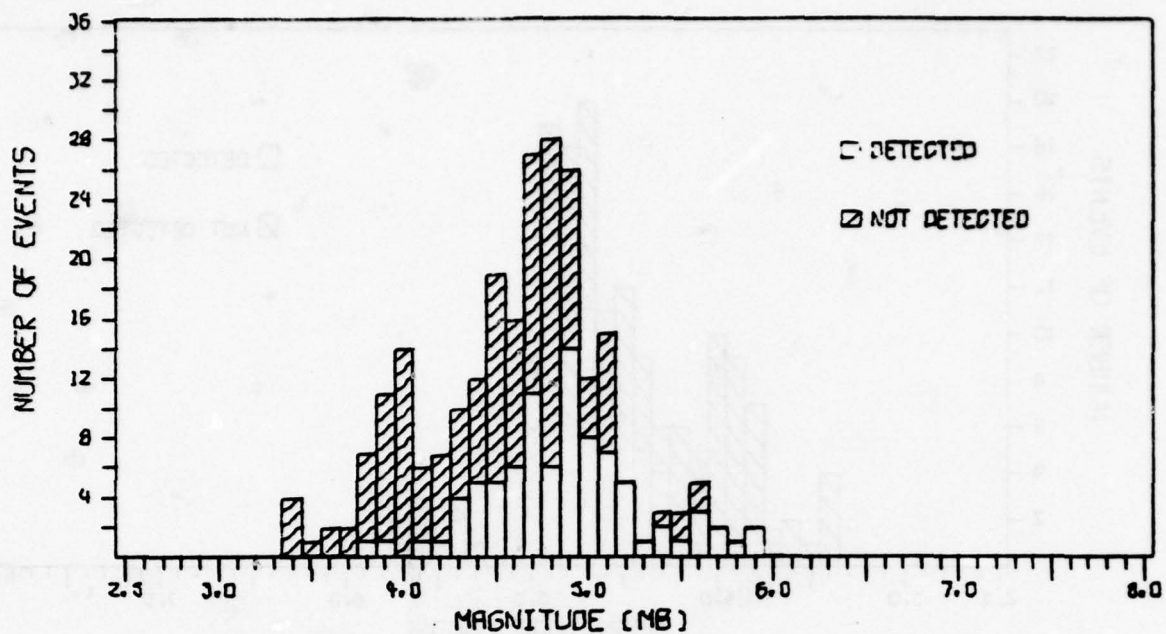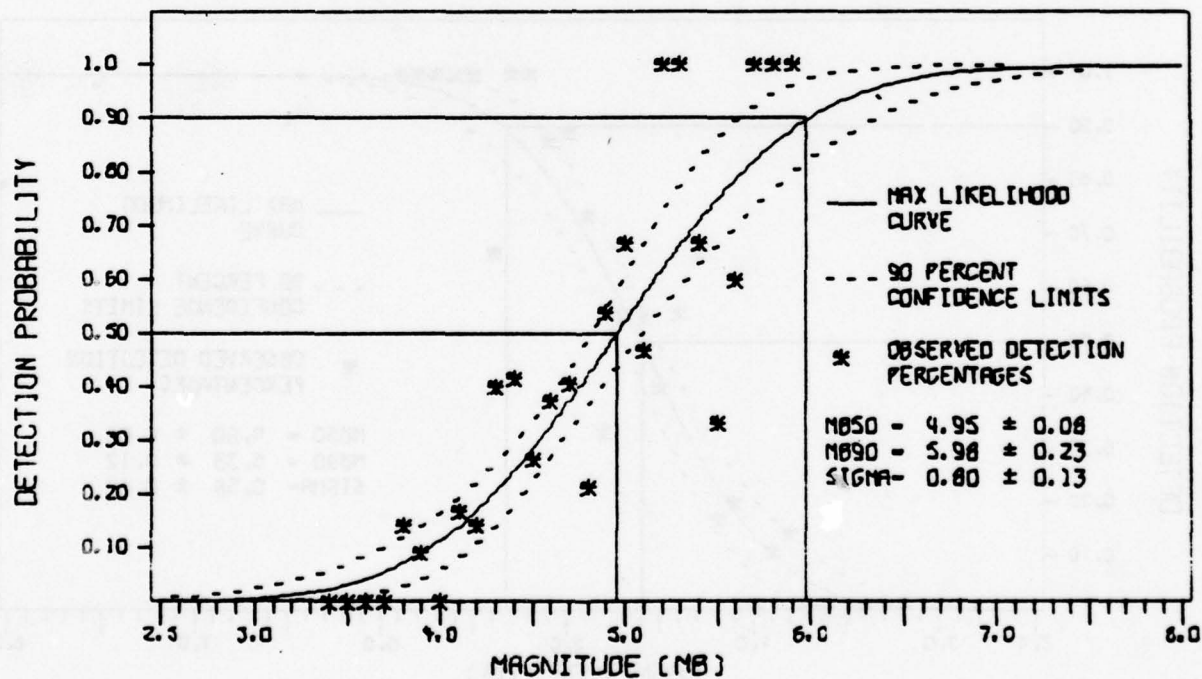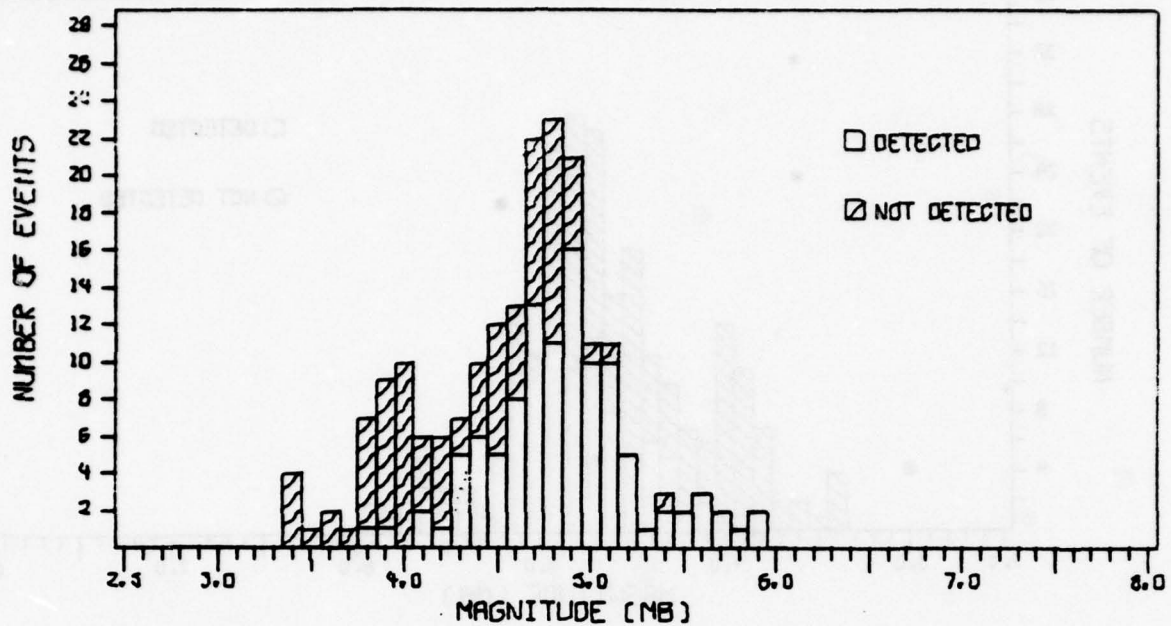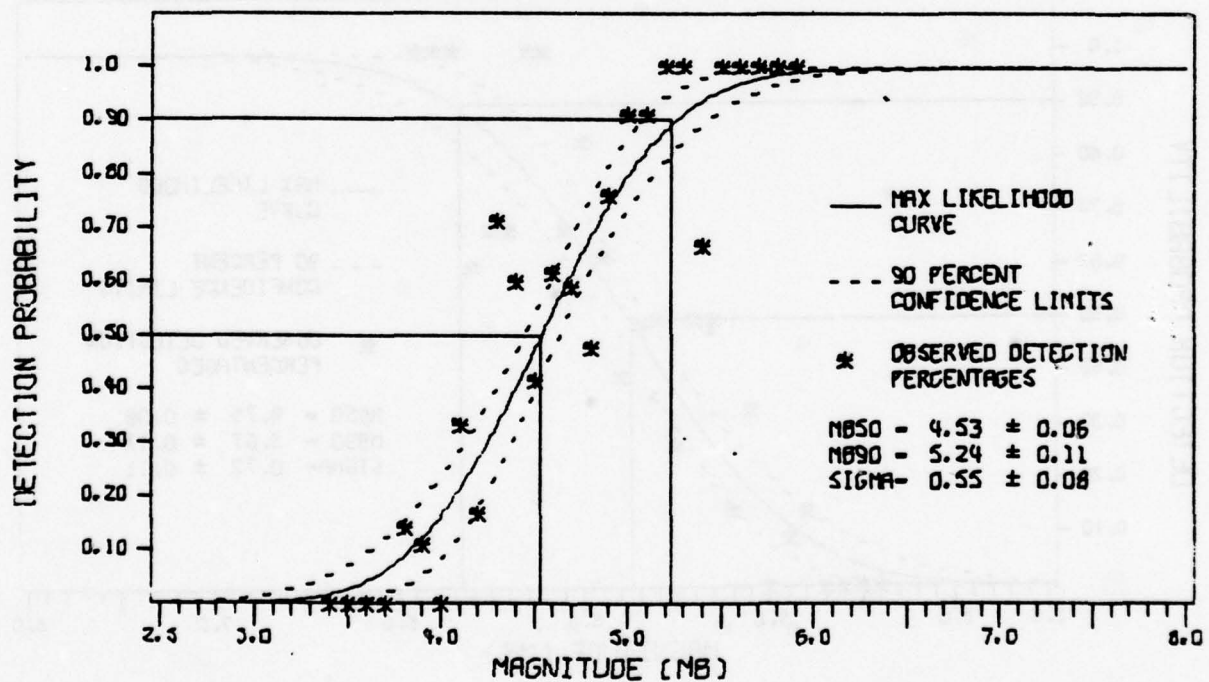The figures labeled 'Predicted Detection Capability - Detector Disabled' are identical to the 'Actual Detection Capability' except that the former accept events detected only on the microfiche as detections. This is a prediction of the actual detection capability that would have been calculated by an analyst viewing continuous data. The difference between the 'Actual Detection Capability' and the 'Predicted Detection Capability - Detector Disabled' is the loss in detection capability caused by use of the automatic detector.

The upper portion of each figure is a histogram giving the detection statistics as a function of bodywave magnitude for that particular case. The lower portion shows the percentage of events detected at each bodywave magnitude (represented by asterisks), the fitted maximum likelihood curve (represented by a solid line), and the 90 percent confidence limits for this curve (represented by dashed lines). The values for 'MB50' and 'MB90' shown on the figures are the 50 and 90 percent detection thresholds as picked from the maximum likelihood curve. The value shown for 'SIGMA' is the standard deviation of the Gaussian probability function obtained by the maximum likelihood method.

The titles for each figure define the station under evaluation and the type of estimation, as defined previously, from which the detection statistics were derived. The short-period detection capability estimates derived from Figures V-1 to V-16 are summarized in Table V-1.

The MAJO and CHTO ideal and actual detection capability estimates differ the most among the four stations, while the CTAO estimates differ the least. The automatic detector, on the average, cost the stations $0.12\ m_b$ units of detection capability. However, the detection loss for CHTO is 0.20 m_b units and for MAJO $0.15\ m_b$ units, two to three times the loss observed for both CTAO and KAAO.

V-21

TABLE V-1
SRO SP DETECTION CAPABILITY

Calculation Type	50 Percent Detection Threshold							
	CHTO		CTAO		KAAO		MAJO	
	m_b	S. D.	m_b	S. D.	m_b	S. D.	m_b	S. D.
Ideal	4.60	0.06	5.43	0.10	4.26	0.07	4.91	0.09
Actual	4.95	0.08	5.51	0.11	4.45	0.07	5.29	0.12
Ideal (Detector Disabled)	4.53	0.06	5.38	0.09	4.24	0.07	4.82	0.08
Predicted (Detector Disabled)	4.75	0.06	5.45	0.10	4.37	0.08	5.14	0.10

S. D. = Standard Deviation

V-22

C. LONG-PERIOD DETECTION CAPABILITY ESTIMATES

Estimates of long-period Seismic Research Observatory detection capability are presented for each of the five stations evaluated in this report. The criteria for determining whether a detection has been achieved for a given event are:

- The presence of dispersion in the signal gate.

- The presence of a peak in the dispersed wave train 3 dB or more above any peak outside the dispersed wave train and inside a time gate starting 600 seconds before the predicted Love wave arrival time and ending 600 seconds after the estimated Rayleigh wave end time.

- The occurrence of the signal onset within ± 180 seconds of the predicted signal onset time.

- Detection of the event on at least two components.

Occasionally, an event is considered to be detected when not all criteria are satisfied. Signal peaks are occasionally less than 3 dB above the noise peaks and still recognized as signals from their dispersion characteristics. Also, at a given station it is sometimes possible to find specific features of a seismic waveform from a given region, which enables the analyst to detect the event even though not all detection criteria have been satisfied. An interesting example of this is discussed in the preliminary Seismic Research Observatory report (Strauss, 1976). The last criterion is intended to reduce the number of false alarms, i.e., declaring an event detected when it is not.

The problem of mixed events is often difficult for the analyst to resolve and may be a source of false alarms. (The term 'false alarm' in this case means declaring a detection when in fact the observed signal is from an event other than that under analysis.) When a signal is observed in the

time gate of the event under analysis, the analyst first checks the waveforms on the three components of motion to see that their inter-relationships are correct. If still in doubt, the analyst checks available event lists to see whether any other reported event could have arrived in the signal gate. In general, the analyst declares a detection if a dispersed signal is observed having the correct inter-relationships between the Love and Rayleigh waves and if no other event has been reported which could be mistaken for the event under analysis.

The long-period detection statistics and derived maximum likelihood curves are presented in Figures V-17 to V-26. The detection capability estimates were calculated in the manner described in the first portion of this section, i.e., an 'ideal detection capability' and an 'actual detection capability'.

Figures V-17 to V-26 are displayed in the same manner as Figures V-1 to V-16 for the short-period detection capability estimates, except that microfiche were not used for the long-period detection statistics. Since no detector is involved, there are only two long-period detection capability estimates for each station rather than four, as for short-period. Each of the figures represents one long-period detection capability estimate, where the upper portion shows a histogram of the detection statistics and the lower portion shows the maximum likelihood curve fitted to these statistics.

The long-period detection capability estimates derived from these figures are summarized in Table V-2. There is considerable difference between the ideal and actual estimates for all the stations except CTAO. One possible reason for the over-all higher difference, as compared to the short-period detection capabilities, is the greater possibility for long-period events to be mixed. ZOBO and MAJO have especially large differences; ZOBO because of the greater distance and thus greater chance for a mixed event, and MAJO because of the large amount of system failure (resulting in no data being recorded).

V-24
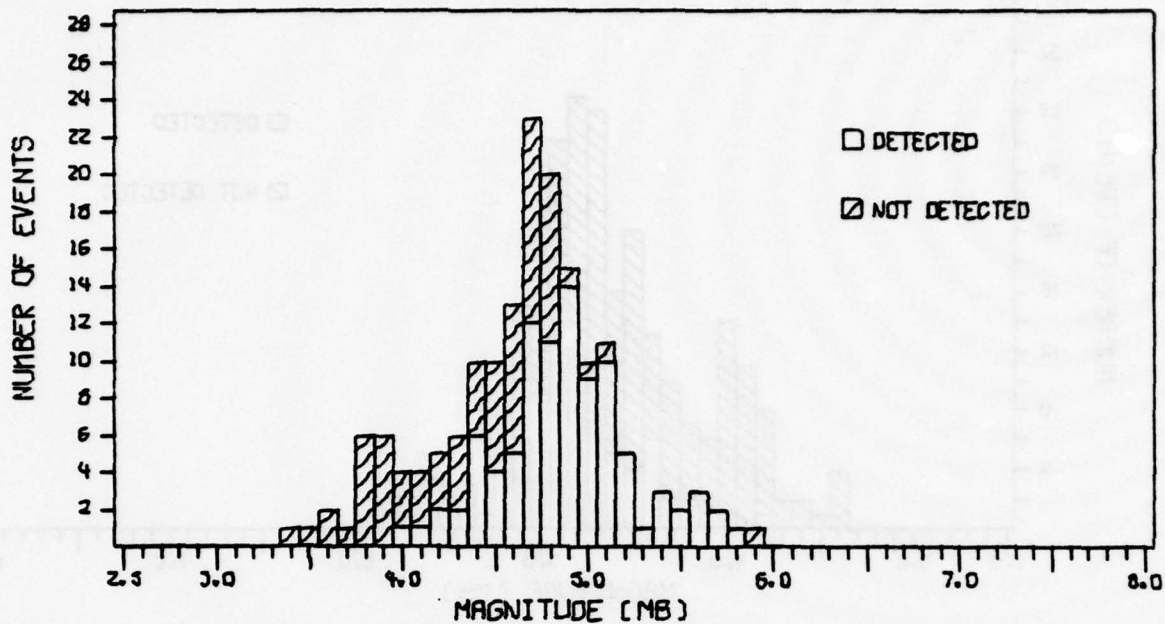
IDEAL CHTO LP DETECTION CAPABILITY
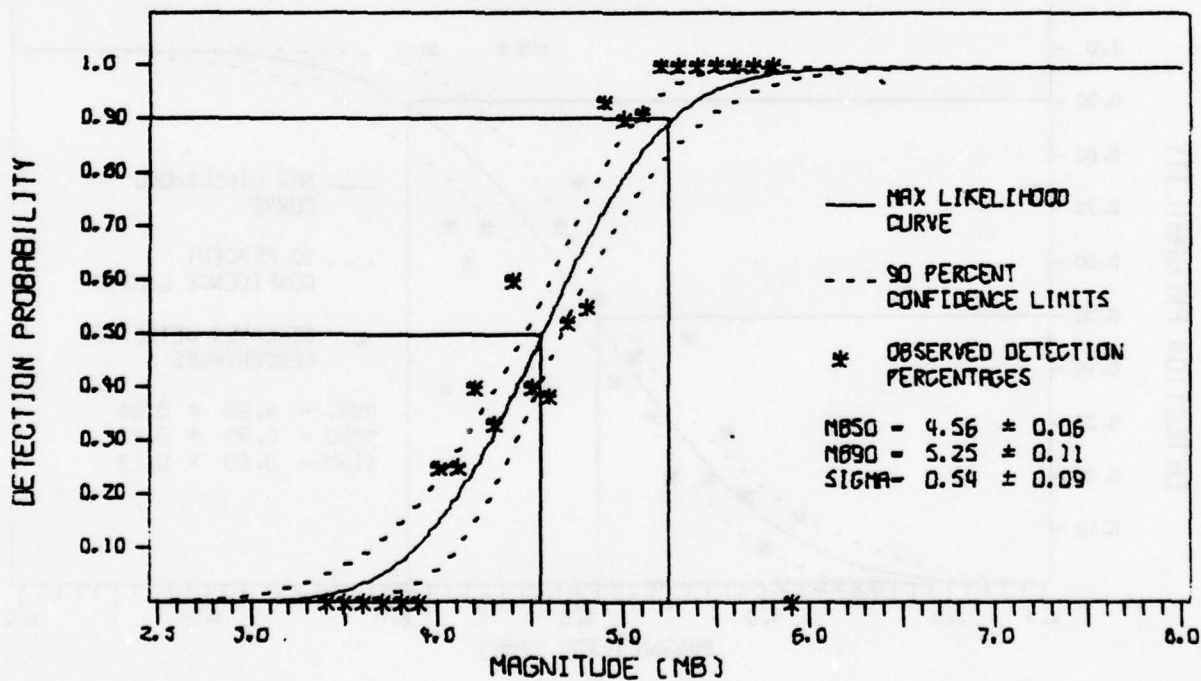
FIGURE V-17

IDEAL CHTO LP DETECTION CAPABILITY

V-25
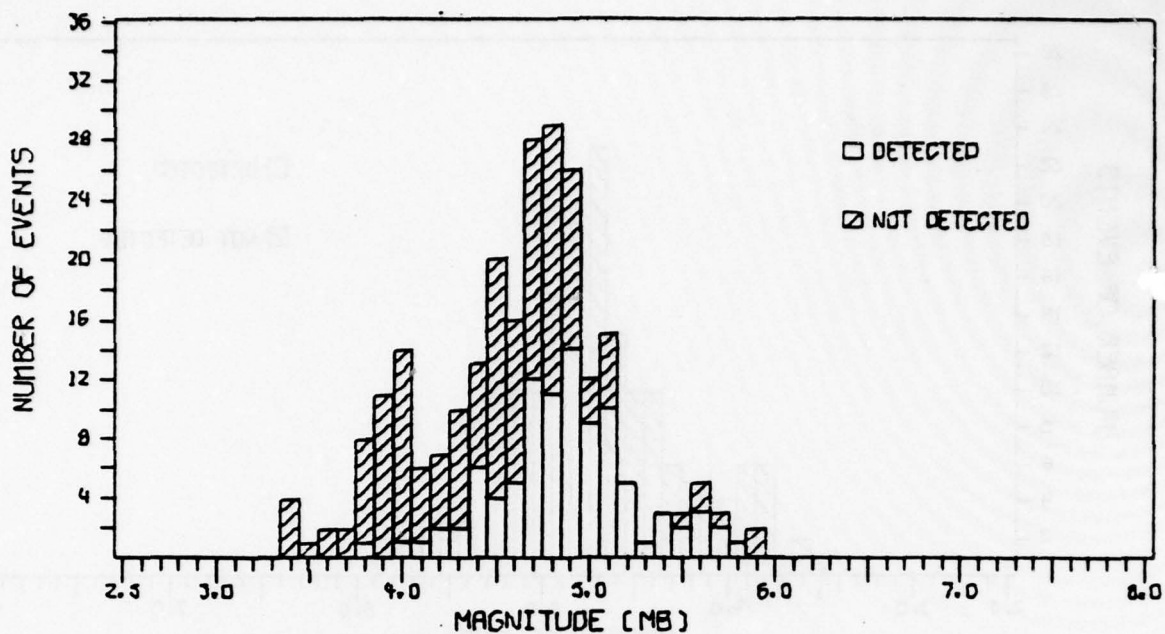
FIGURE V-18

ACTUAL CHTO LP DETECTION CAPABILITY
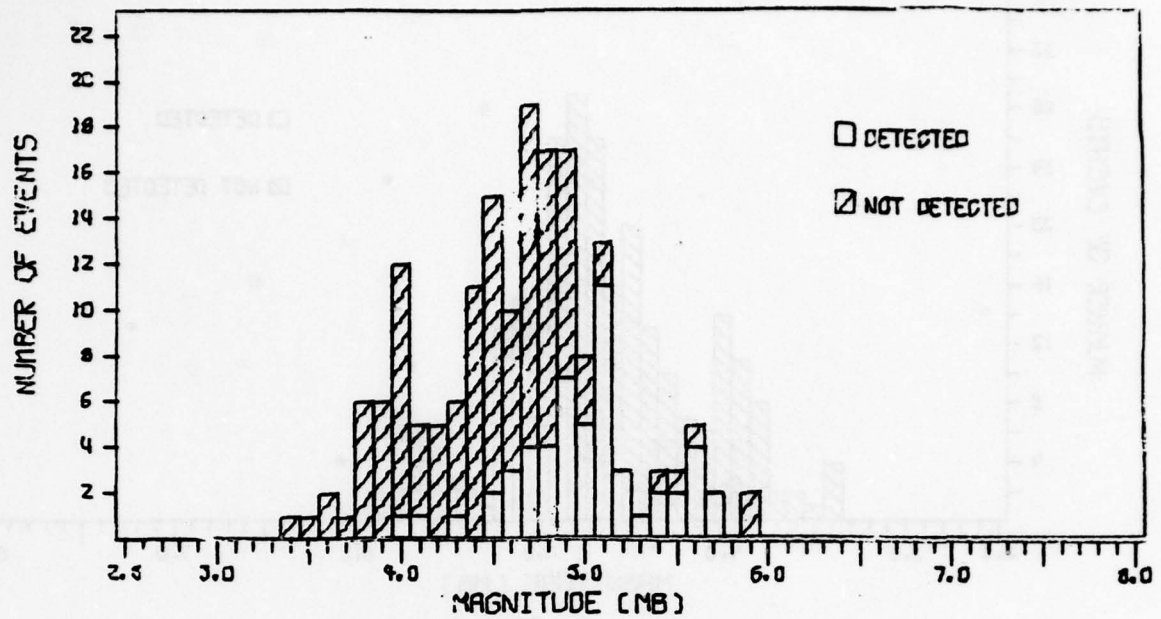
IDEAL CTAO LP DETECTION CAPABILITY
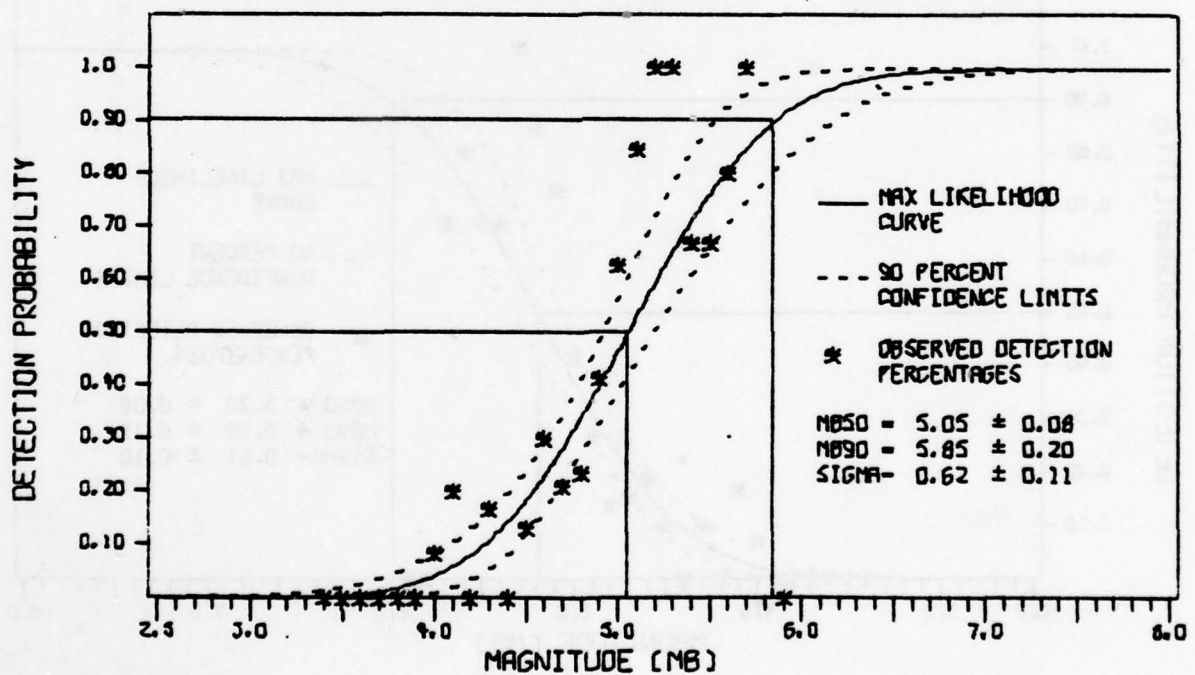
FIGURE V-19

IDEAL CTAO LP DETECTION CAPABILITY
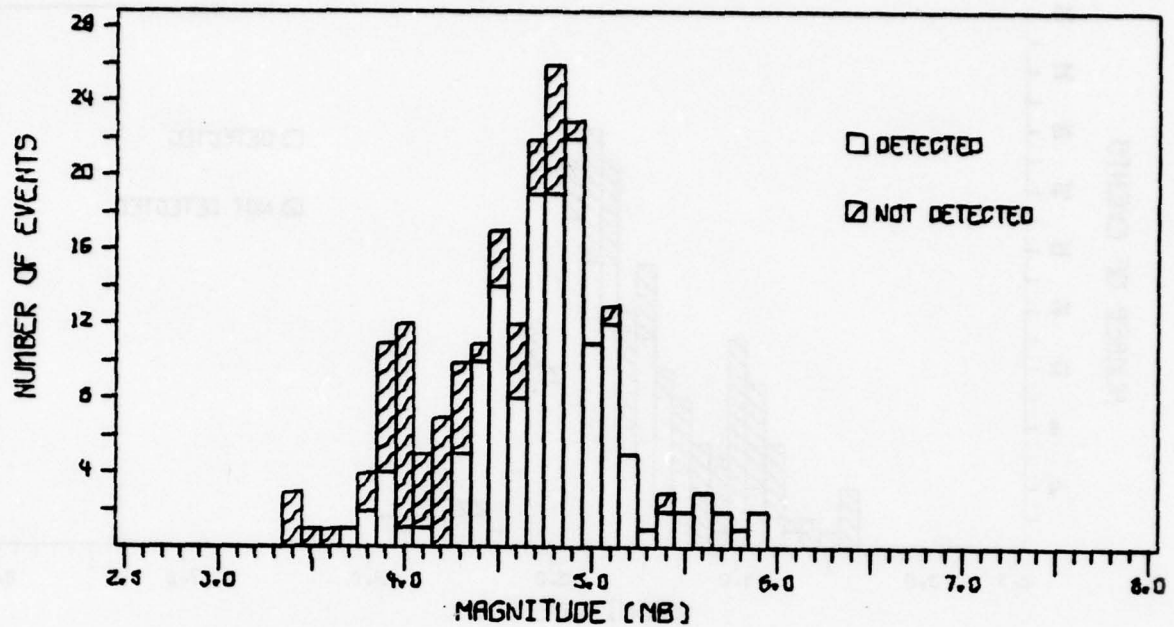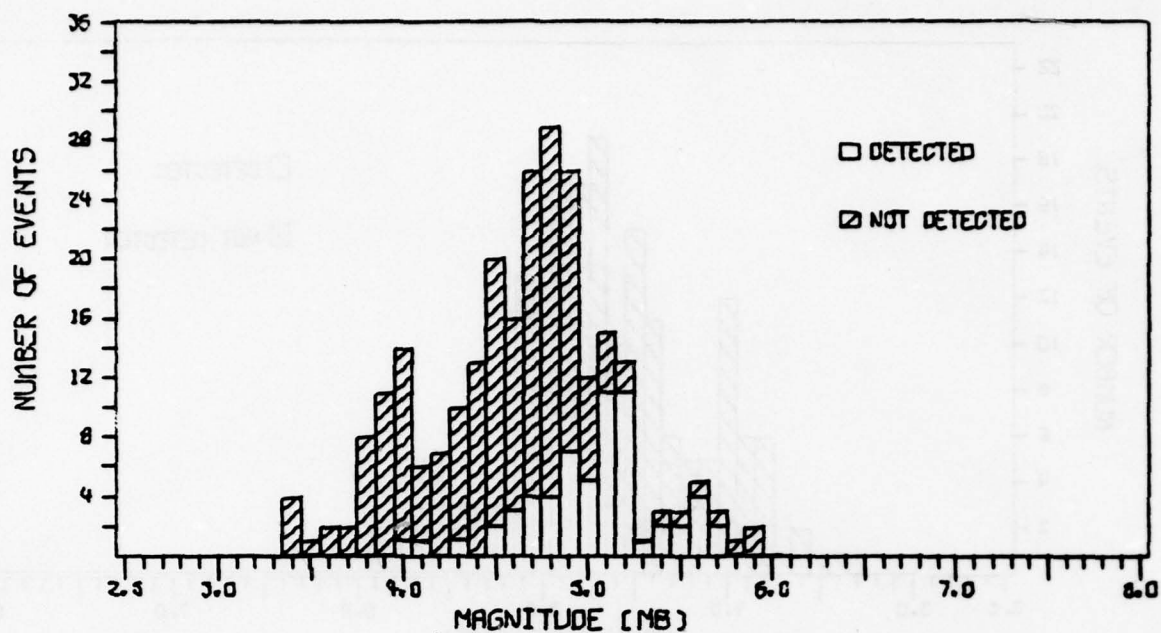
ACTUAL CTAO LP DETECTION CAPABILITY
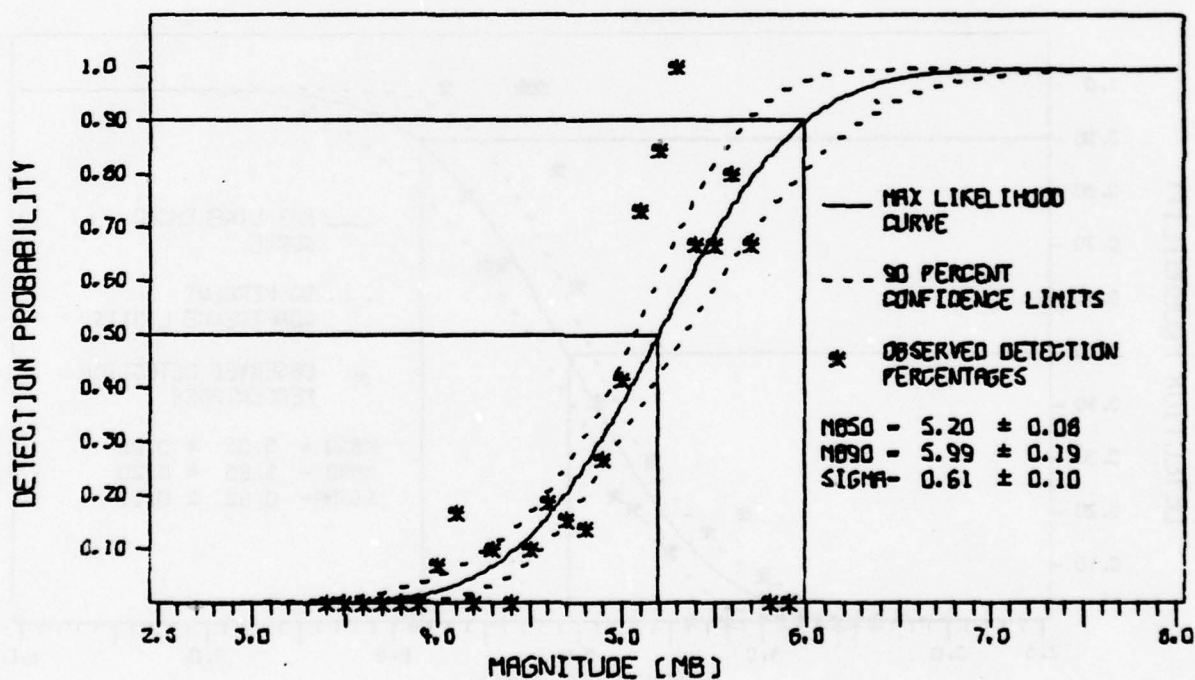
FIGURE V-20

ACTUAL CTAO LP DETECTION CAPABILITY
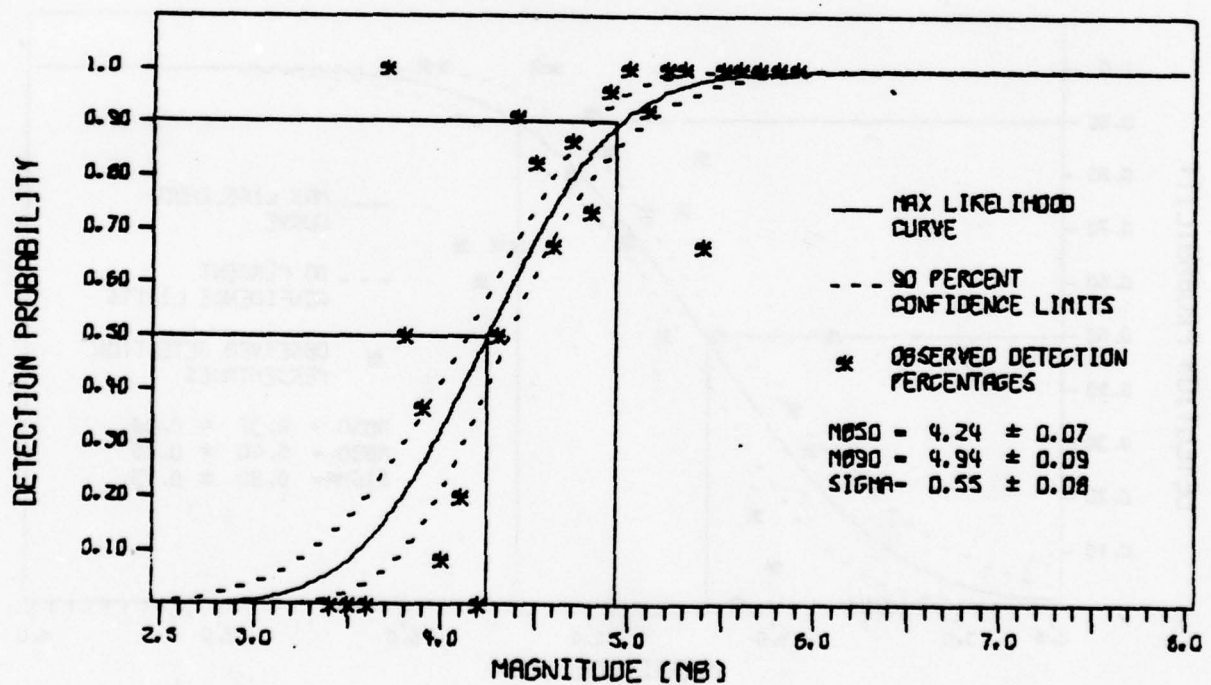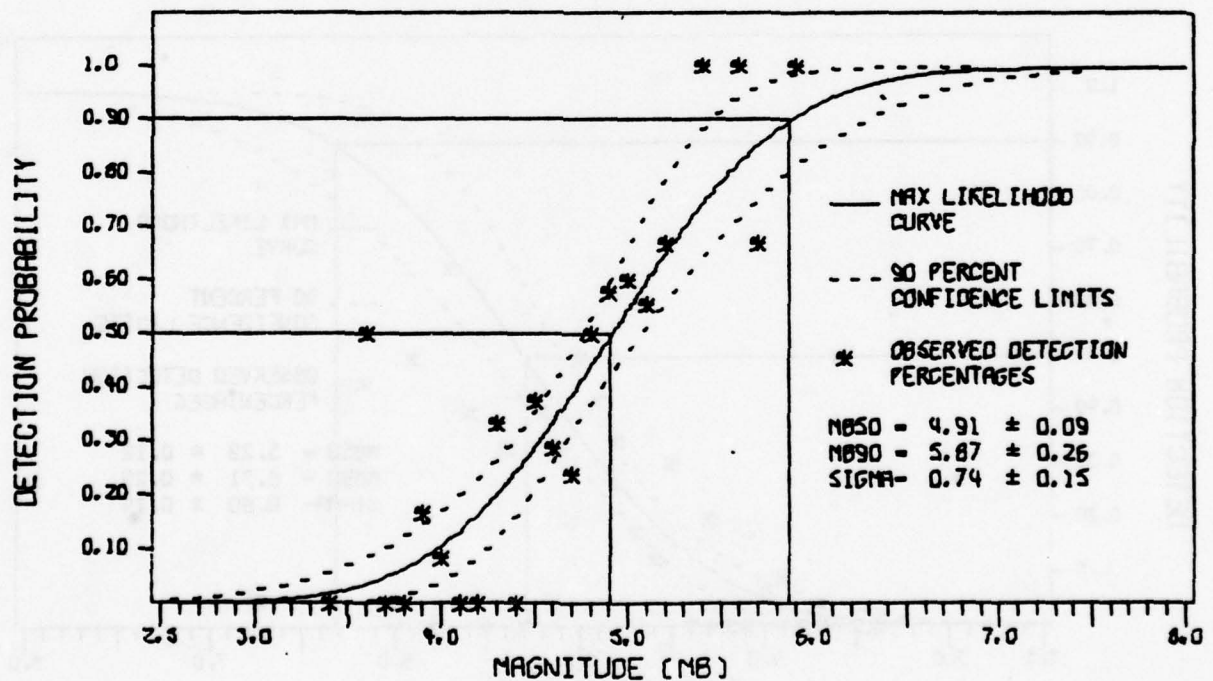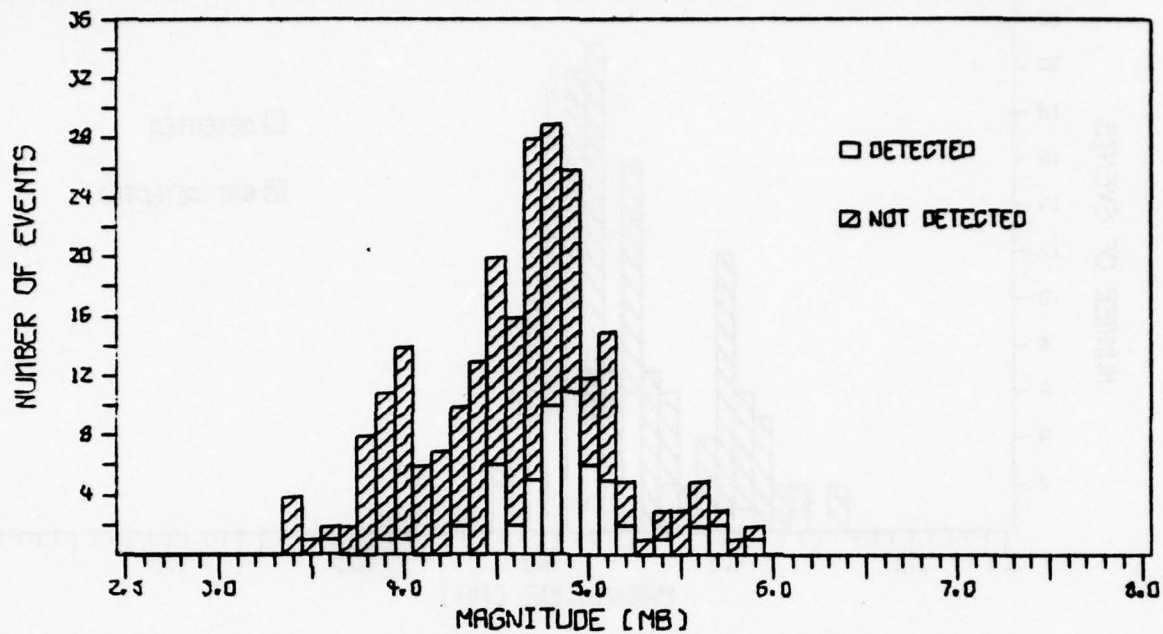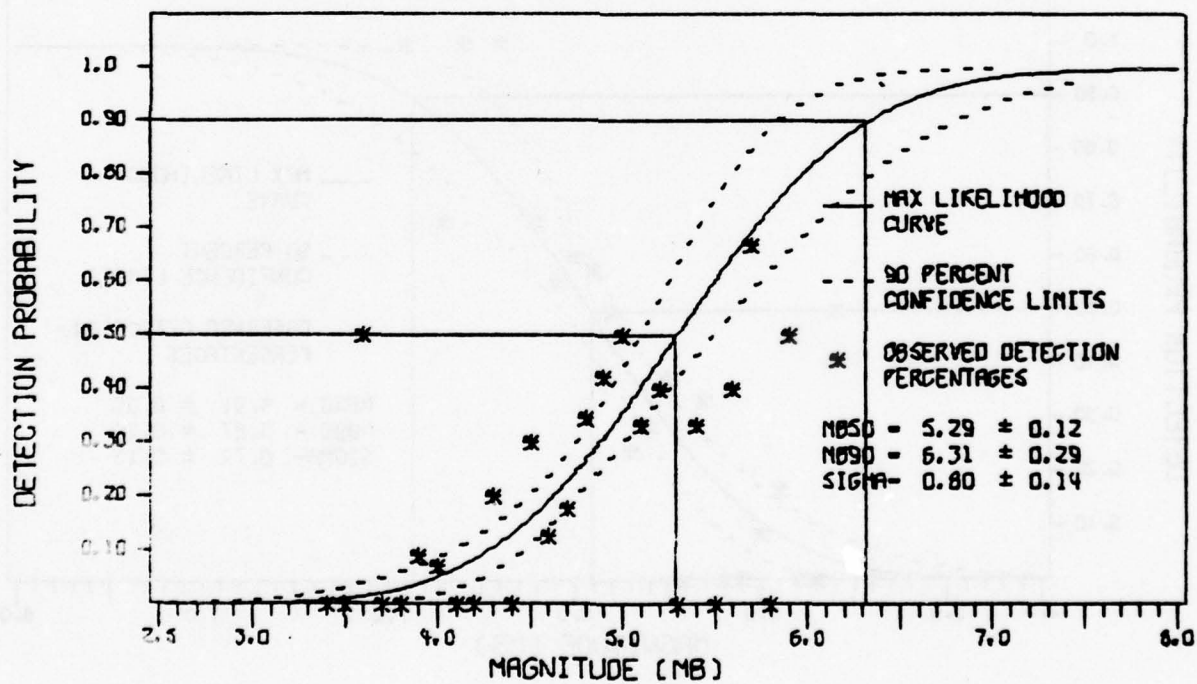
V-28
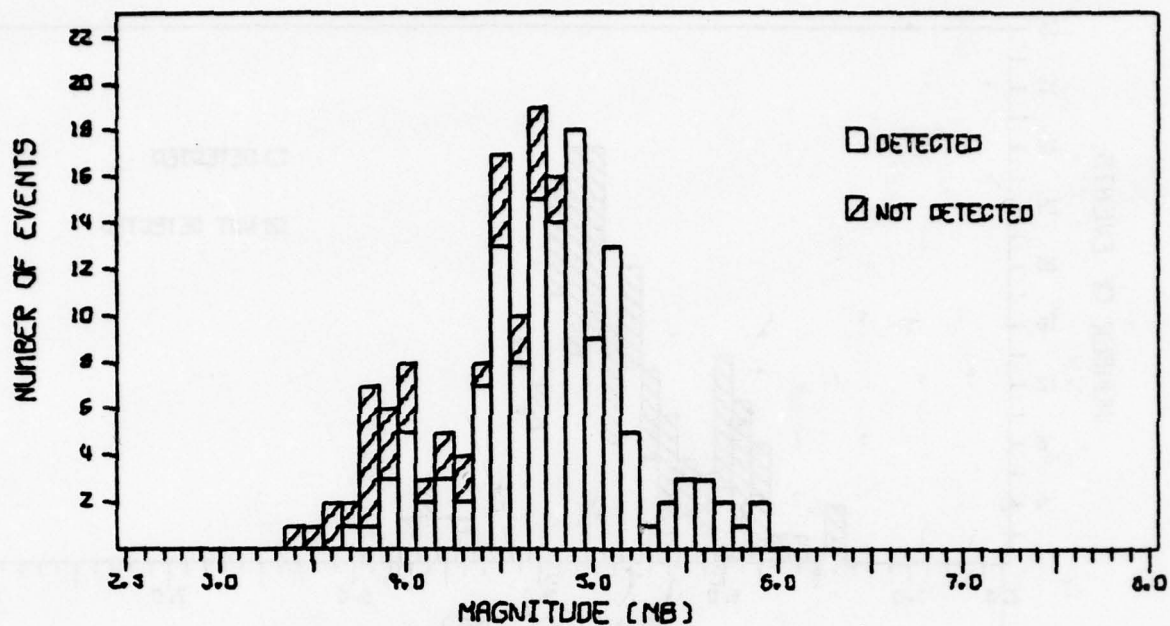
IDEAL KAAO LP DETECTION CAPABILITY
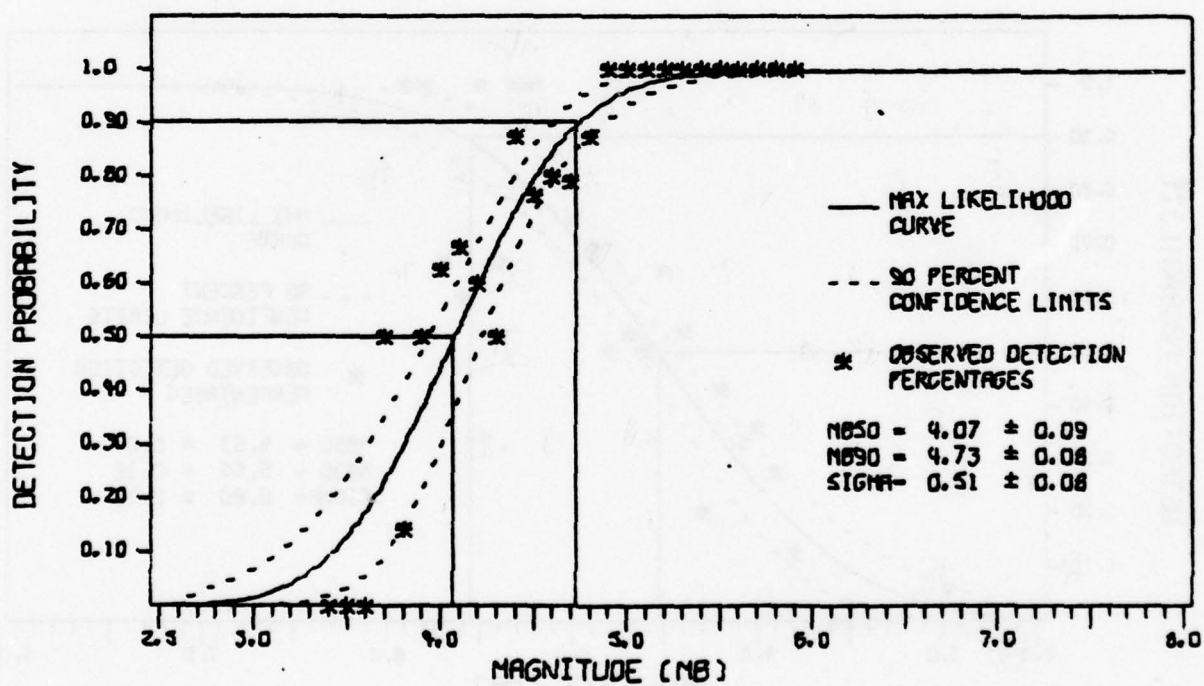
FIGURE V-21
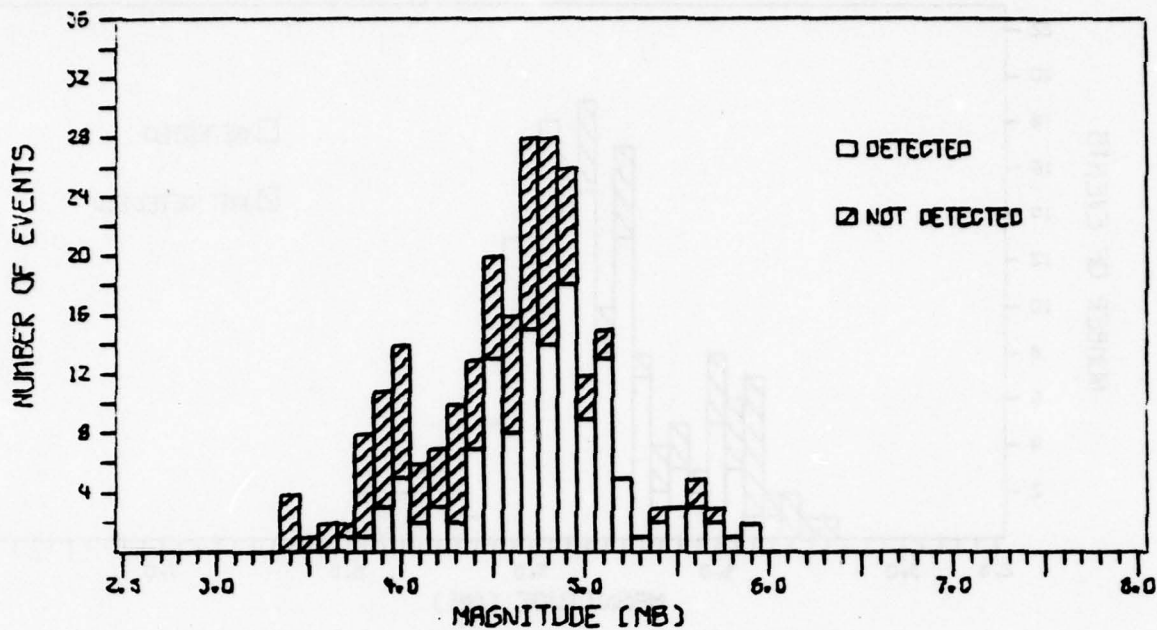
IDEAL KAAO LP DETECTION CAPABILITY

FIGURE V-22

ACTUAL KAAO LP DETECTION CAPABILITY
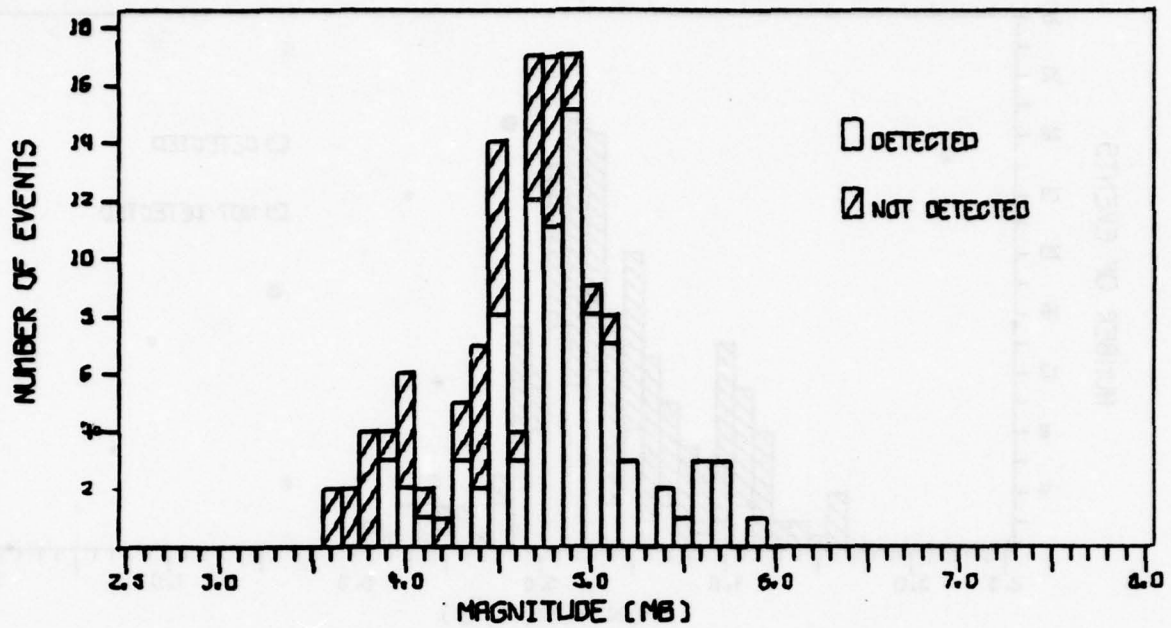
IDEAL MAJO LP DETECTION CAPABILITY
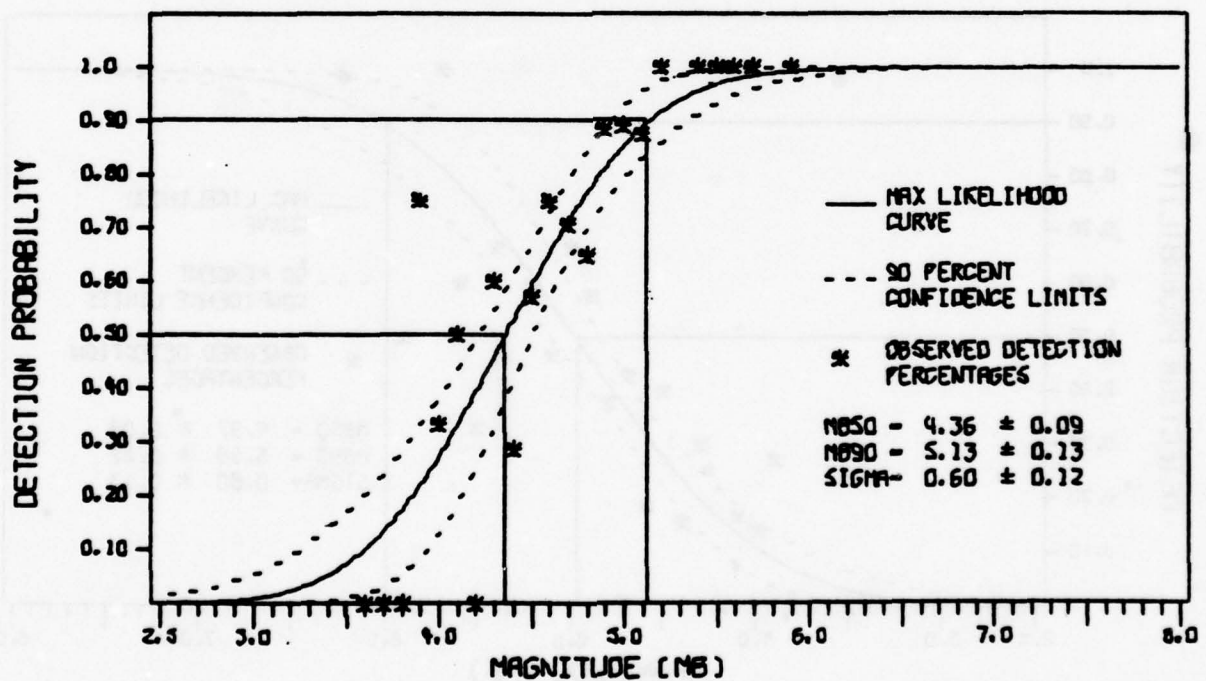
FIGURE V-23

IDEAL MAJO LP DETECTION CAPABILITY
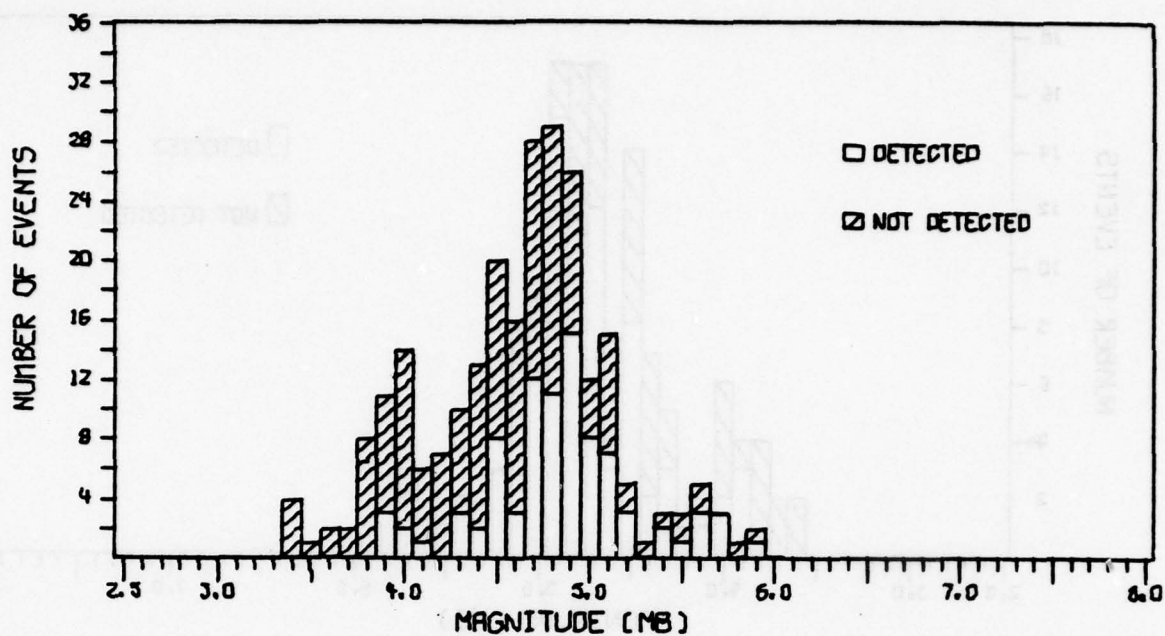
ACTUAL MAJO LP DETECTION CAPABILITY
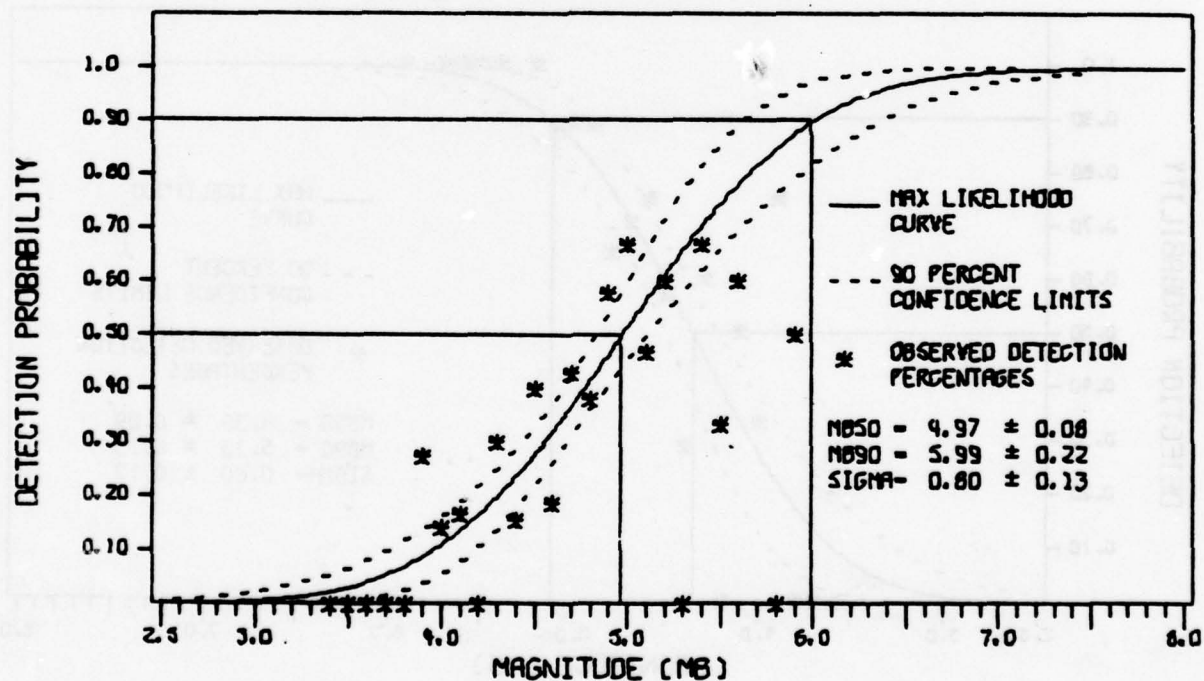
FIGURE V-24

ACTUAL MAJO LP DETECTION CAPABILITY

V-32
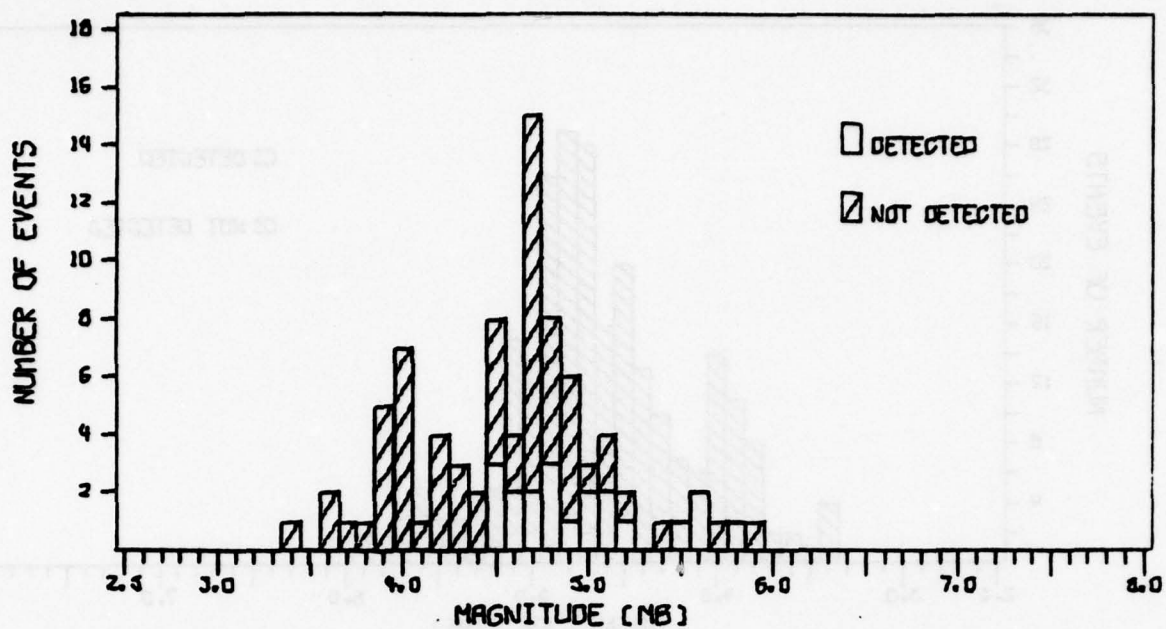
IDEAL ZOBO LP DETECTION CAPABILITY
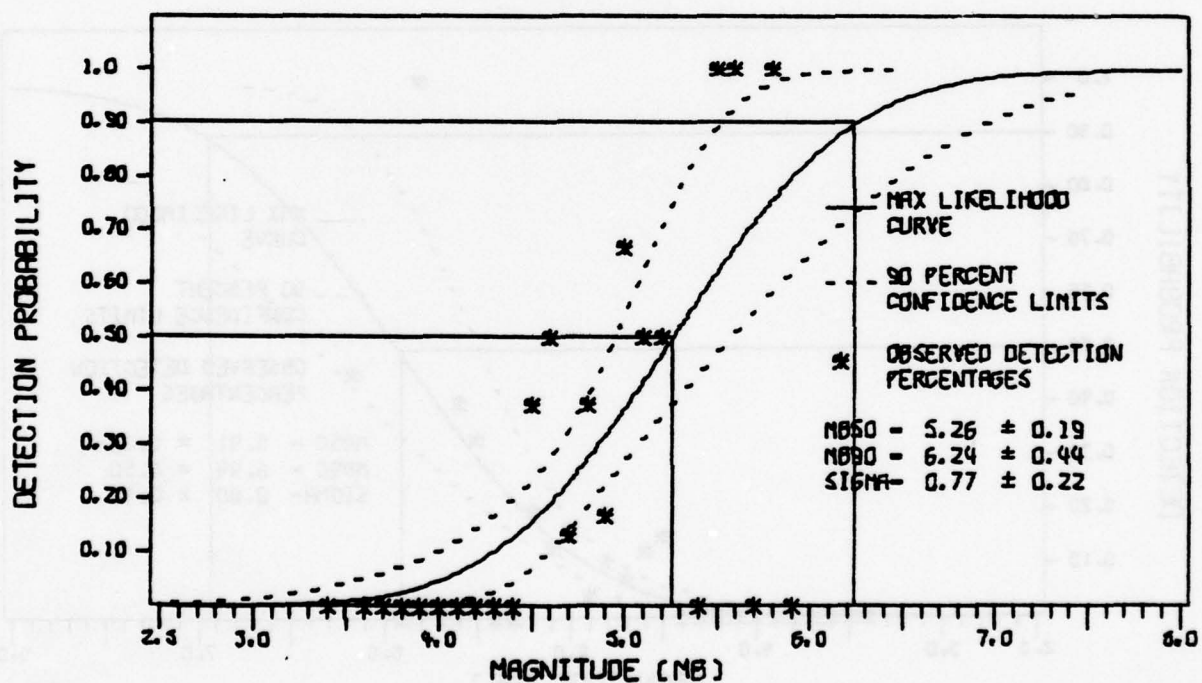
FIGURE V-25
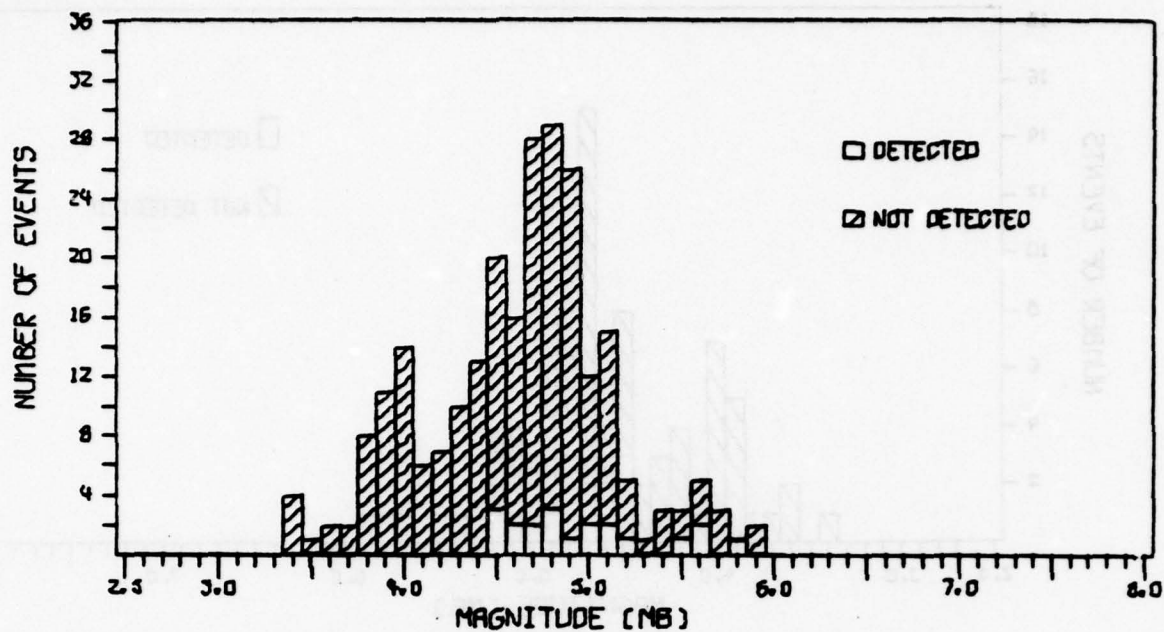
IDEAL ZOBO LP DETECTION CAPABILITY

FIGURE V-26

ACTUAL ZOBO LP DETECTION CAPABILITY

TABLE V-2

SRO LP DETECTION CAPABILITY

Calculation Type	50 Percent Detection Threshold									
	CHTO		CTAO		KAAO		MAJO		ZOBO	
	m_b	S. D.	m_b	S. D.	m_b	S. D.	m_b	S. D.	m_b	S. D.
Ideal	4.56	0.06	5.05	0.08	4.07	0.09	4.36	0.09	5.26	0.19
Actual	4.90	0.08	5.20	0.08	4.53	0.07	4.97	0.08	5.91	0.26

S. D. = Standard Deviation

SECTION VI
EARTHQUAKE-PRESUMED EXPLOSION DISCRIMINATION

A. DISCUSSION

This section considers the question of discriminating between earthquakes and presumed nuclear explosions using long-period data. The discrimination method used is the surface wave magnitude (M_s) versus body-wave magnitude (m_b) plot. This plot of M_s versus m_b is expected to function as an earthquake-presumed nuclear explosion discriminant, since for a given m_b, an explosion produces much weaker Rayleigh waves than does an earthquake. Weichert and Basham (1973) assign the M_s - m_b criterion a 30 percent probability of correctly identifying an explosion, accompanied by a false alarm probability of about 0.1 percent.

B. COMPUTATION OF SURFACE WAVE MAGNITUDES

The equations used in M_s computation are adapted by Strauss (Personal Communication, 1978) from data presented by Nutley and Kim (1975). Mr. Strauss and the authors feel that the M_s - m_b curve is best resolved into three segments, based on epicentral distance:

for
$$\Delta \leq 10^{\circ} \quad M_s = \text{Log}_{10} A/T + 0.89 \, \text{Log}_{10} \Delta + 1.34$$
$$10^{\circ} \leq \Delta \leq 25^{\circ} \quad M_s = \text{Log}_{10} A/T + 1.07 \, \text{Log}_{10} \Delta + 1.16$$
$$\Delta \geq 25^{\circ} \quad M_s = \text{Log}_{10} A/T + 1.66 \, \text{Log}_{10} \Delta + 0.34$$

where

Δ = epicentral distance in degrees

A = peak-to-peak amplitude in millimicrons

T = period in seconds of the measured amplitude.

VI-1

M_s values were calculated automatically from identified detected events stored on event tapes (Section II). The M_s computation routine chooses an edit gate based on expected surface wave arrival times and durations stored in each event header. The times of zero crossings within the edit gate are calculated, and the maximum absolute amplitudes in millimicrons between adjacent zero crossings are found. The associated waveform periods are calculated as two times the time between these adjacent zero crossings. Epicentral distances and sample rates are read from the event header. Quantization factors and instrument response corrections are built into the program. (Instrument response corrections are derived from values supplied by Albuquerque Seismological Laboratory via AFTAC.) M_s values are calculated and printed out. The largest M_s value at each specified period of interest is displayed separately. The analyst may now check these largest M_s values against the plot of the data. If he does not like an M_s value at a particular period (for example, the M_s value appears to be associated with a noise pulse in the signal gate) he can select another value from the M_s list generated by the program.

C.   DISCRIMINATION RESULTS

Table VI-1 lists those events of the data base which may be termed presumed nuclear explosions. They were selected on the basis of their epicentral locations, bodywave magnitudes, and shallow depths. Thus, the events from Flinn and Engdahl Region 41 (Flinn and Engdahl, 1965) were selected because their epicenters are at the Nevada Test Site and their bodywave magnitudes are much larger than known earthquakes in the area. The events from Region 329 were selected because their epicenters are at the eastern Kazakh test site and their bodywave magnitudes are larger than most earthquakes from that area.

TABLE VI-1
PRESUMED NUCLEAR EXPLOSION EVENT LIST
WITH DETECTION STATUS

Event	Region	m_b	Detection Status*				
			CHTO	CTAO	ZOBO	KAAO	MAJO
1630	648	5.7	3	3	2	1	1
1640	329	5.9	2	2	3	3	2
1665	41	4.5	2	2	3	3	1
1689	41	4.8	5	3	3	1	3
1693	336	5.1	4	2	5	2	4
1709	648	4.5	5	2	4	2	2
1759	41	4.4	5	2	4	1	1
1772	329	5.5	5	2	4	3	1
1773	329	5.6	5	2	4	3	1
1781	41	4.7	5	2	4	3	1
1805	41	5.7	1	1	5	4	1
1827	41	4.7	2	2	2	3	3
1828	41	3.8	2	2	5	2	2
1874	329	5.9	1	2	1	2	4

*Detection Status Codes

1 - Event detected according to detection criteria of Section V

2 - Event not detected

3 - Mixed event

4 - System failure, no data recorded

5 - Malfunction (glitch, spike, or the like) in signal gate.

The numbers in the columns under the station headings in Table VI-1 refer to the detection status of the events as recorded at each station. The number 1 indicates that the event was detected, 2 indicates that it was not detected, 3 indicates that it was mixed with another event, 4 indicates no data were recorded for that event, and 5 indicates that a system malfunction obscured the data. These codes indicate that six of the fourteen events cannot be used in the discrimination study, since they were not detected at any of the stations.

Table VI-2 presents M_s values from the various stations which detected presumed nuclear explosions. The average difference between M_s and m_b is 1.6 units. Hudson and Douglas (1975) estimated that for a given m_b, an explosion should yield surface wave magnitudes about 0.5 M_s units lower.

Figures VI-1 through VI-3 show vertical component 25-second surface wave magnitudes for stations CHTO, CTAO, ZOBO, KAAO, and MAJO. Symbols used are: o - earthquake; • - presumed explosion. All presumed nuclear explosions are also labeled by their event numbers. The straight line in each plot represents the M_s - m_b relationship for that data set computed using all earthquake data points.

Referring to Figures VI-1 through VI-3 the following comments can be made:

- Event 1805 shows no separation from either the CHTO, CTAO, or MAJO earthquake M_s population (Figure VI-1 and Figure VI-3) although the M_s values for that event lie on the lower bound of each concerned station's earthquake population. According to the M_s - m_b discriminant this event may have been an explosion or an earthquake.

VI-4

TABLE VI-2

25-SECOND M_s VALUES FOR PRESUMED NUCLEAR EXPLOSIONS - VERTICAL COMPONENT

Event	m_b	M_s				
		CHTO	CTAO	ZOBO	KAAO	MAJO
1630	5.7	---	---	---	3.6	4.3
1640	5.9	---	---	---	3.9	3.9
1693	5.1	---	---	---	3.2	---
1772	5.5	---	---	---	4.0	3.8
1773	5.6	---	---	---	---	3.7
1781	4.7	---	---	---	---	4.7
1805	5.7	4.4	4.6	---	---	4.3
1874	5.9	3.1	---	4.4	---	---
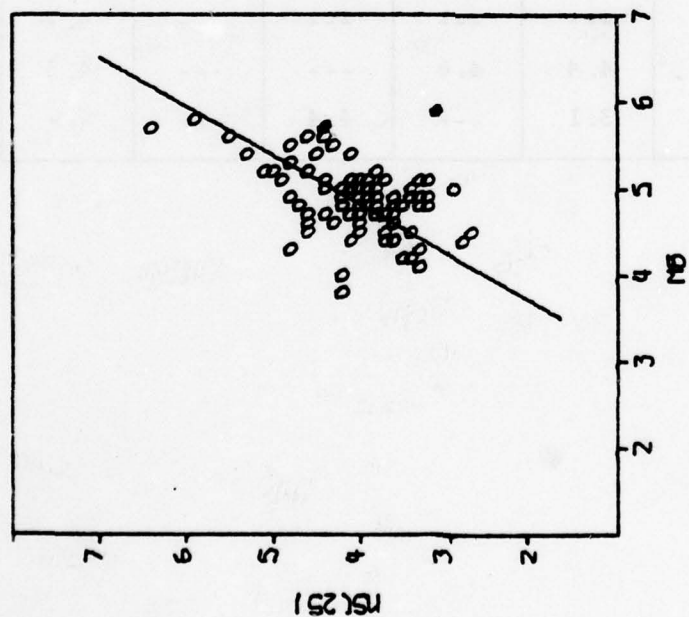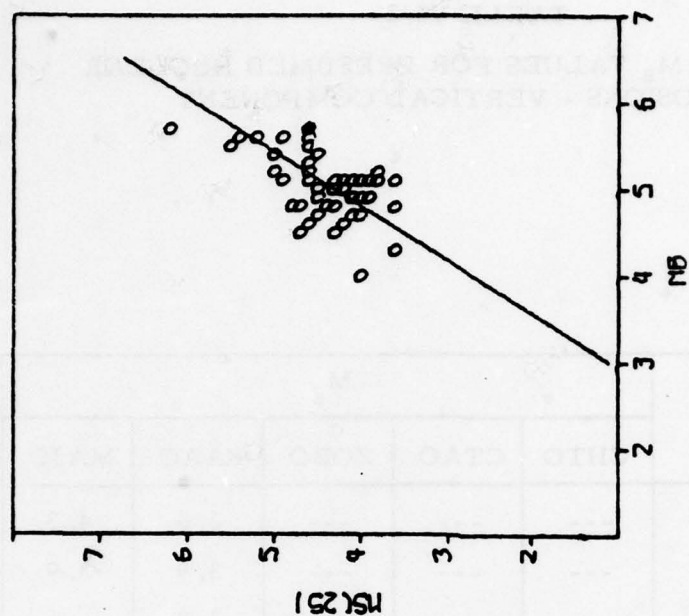
FIGURE VI-1

CHTO AND CTAO VERTICAL COMPONENT 25-SECOND M_s - m_b DATA
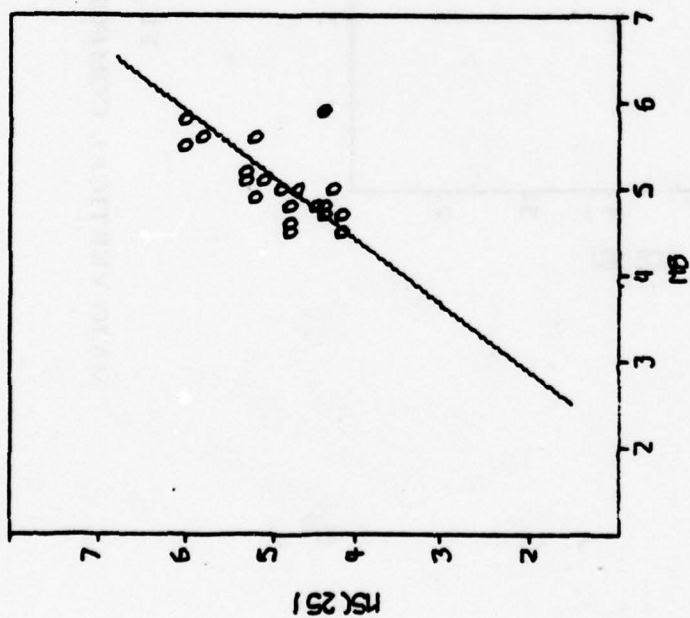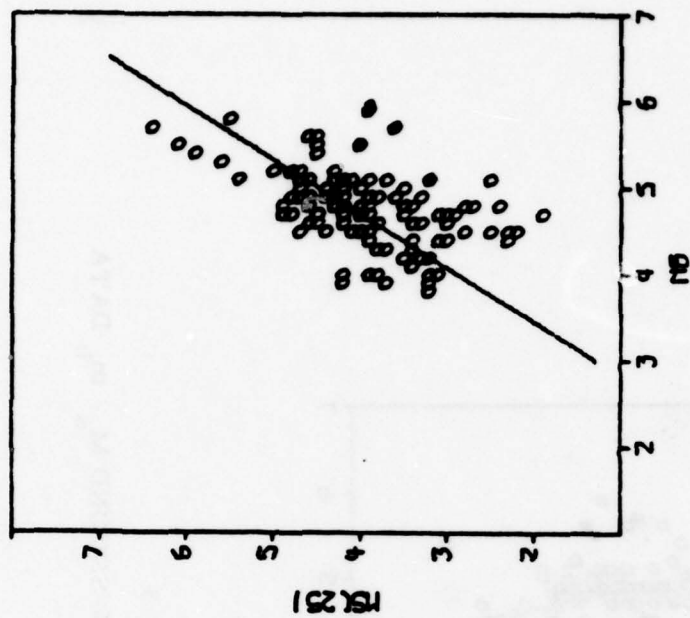
FIGURE VI-2

ZOBO AND KAAO VERTICAL COMPONENT 25-SECOND M_s - m_b DATA
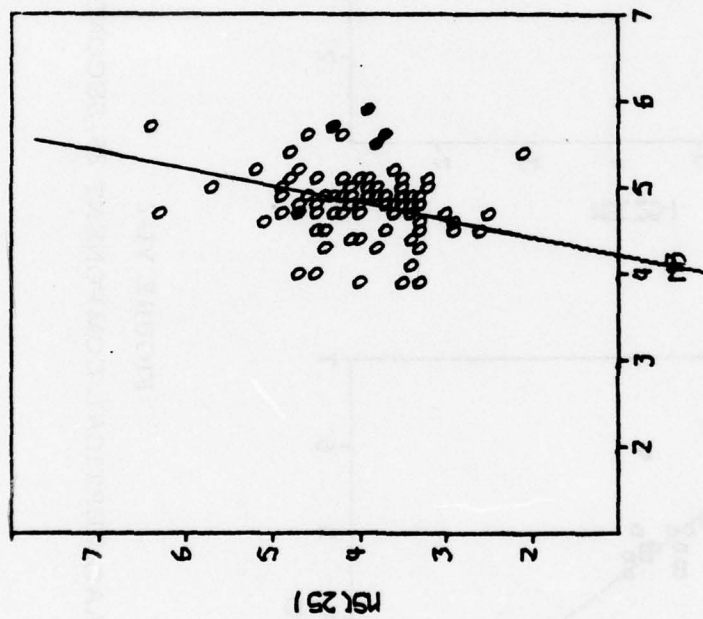
FIGURE VI-3

MAJO VERTICAL COMPONENT 25-SECOND M_s - m_b DATA

- Event 1874's M_s value is well separated from CHTO's and ZOBO's earthquake M_s populations (Figure VI-1). This discriminant would classify it as an explosion.

- Events 1630 and 1640 yielded M_s values which are well separated from the KAAO earthquake population (Figure VI-2) but only marginally separated from the earthquake population of MAJO (Figure VI-3). These events also appear to have been explosions.

- Events 1772 and 1773 yielded M_s values which separate marginally from earthquake M_s populations at MAJO (Figure VI-3). The M_s value recorded at station KAAO for event 1772 also shows marginal separation from earthquakes recorded at that station (Figure VI-2). These events are also probably explosions but more uncertainty exists here than in the classification of the three previously discussed events.

- Event 1693's M_s value lies on the periphery of the KAAO earthquake population (Figure VI-2). Classification of this event is inconclusive.

- Event 1781's M_s value lies well within MAJO's earthquake population (Figure VI-3). This event classifies as an earthquake.

In summary, while no station is infallible when considered alone, CHTO, CTAO, ZOBO, KAAO, and MAJO show potential as contributors to an M_s - m_b discrimination network.

D. M_s - m_b RELATIONSHIPS

Table VI-3 presents the results of fitting a straight line to the M_s - m_b points. The M_s - m_b relationships are presented only for the case of

TABLE VI-3

SRO STATIONS M_s - m_b RELATIONSHIPS FOR VERTICAL COMPONENT 25-SECOND ENERGY

Station	a	b	σ^2	Center of Mass		n
				m_b	M_s	
CHTO	1.86	-4.92	0.08	4.87	4.12	83
CTAO	1.73	-4.31	0.07	4.99	4.33	50
ZOBO	1.52	-2.66	0.04	4.89	4.78	19
KAAO	1.66	-3.71	0.08	4.81	4.25	93
MAJO	5.31	-21.30	0.12	4.79	4.11	66

where: M_s = $am_b + b$

σ^2 = variance normal to the M_s-m_b estimate, and

n = number of M_s-m_b points used in computation.

VI-10

all data points measured at each station.   Note the relatively steep slope and large negative intercept of the MAJO M_s - m_b line.   No explanation has been found.

The reader is referred to Figures VI-1, VI-2, and VI-3 for pictorial representations of both the M_s - m_b relationships presented here and the data points with which these relationships were established.

SECTION VII
CONCLUSIONS

This section summarizes the results of this continued evaluation of the Seismic Research Observatories. The major results are:

A.   DATA QUALITY

- In general, the data quality was good. At all stations except ZOBO, data were degraded by malfunctions less than 4% of the time. Most ZOBO malfunctions were caused by a defective field tape. Other malfunctions were mostly glitches in the signal gate.

- Estimates of station reliability were based on the frequency of occurrence of malfunctions and on estimates of station down-time. ZOBO and MAJO both showed low reliabilities of approximately 0.7 due to relatively large amounts of station down-time. The other stations had reliability figures above 0.8.

- The frequency of mixed event occurrence for long-period waveforms ranged from a low of 0.19 for CHTO and MAJO to a high of 0.46 for station ZOBO. The frequency of mixed event occurrence is high for ZOBO Eurasian events because of the long distance between that station and Eurasia as compared to other stations.

B.   SHORT-PERIOD AUTOMATIC DETECTOR

• During the time period that the detector was studied, detection
probability, P_D, ranged from 50% to 80% while the false alarm
rate (FAR) varied between 0.2 and 2.1 false alarms per hour.
P_D seemed rather independent of FAR; this may reflect FAR
instability inherent in straight STA/LTA-type detectors.

• Detector parameter setting and freezing practices have im-
proved from 1976 to 1977 as evidenced by a more stable rela-
tionship between percent time recorded and number of detec-
tions.

C.   NOISE ANALYSIS

• In order of increasing magnitude, the mean short-period RMS
noise values in the 0.5-4.0 Hz passband (uncorrected for in-
strument response) are: 1.02 mμ at ZOBO, 1.67 mμ at CHTO,
1.94 mμ at KAAO, 3.53 mμ at MAJO, and 5.55 mμ at CTAO.
These values show a strong correlation with station-nearest
coastline separation, indicating that a majority of short-period
noise is derived from ocean wave energy injected at the coast-
line.

• Long-period RMS noise level and trends were investigated in
the passbands: 10-25, 17-41, and 40-64 seconds. A year's
worth of noise data were available for three stations, ANMO,
MAIO, and CTAO. Noise levels for these stations seemed to
change seasonally in the 10-25 and 17-41 second passbands.
However, trends in the 40-64 second passband noise levels
are not easily explained.

- In general, no correlation was suggested by the data between long-period noise level or spectral content and station-coastline separation.

- A comparison between VLPE and SRO/ASRO instrument response corrected spectra for the same sites show significant improvements in noise levels after the installation of borehole seismometers. ASRO instruments showed strong correlation between noise amplitude and noise variance in contrast to their VLPE counterparts.

D. DETECTION CAPABILITY

- Actual 50% m_b short-period Eurasian detection capabilities are: 4.95 at CHTO, 5.43 at CTAO, 4.26 at KAAO, and 4.91 at MAJO.

- Only two short-period events were detected by ZOBO, proving this station a poor detector of Eurasian events.

- Actual 50% m_b long-period Eurasian detection capabilities are: 4.56 at CHTO, 5.05 at CTAO, 4.07 at KAAO, 4.36 at MAJO, and 5.26 at ZOBO.

- Mixed events had very little effect on short-period detection capabilities. Their effect was significant on long-period detection capability, especially at ZOBO.

- The automatic short-period detector as compared to analyst microfiche detection, showed an average loss of 0.12 m_b units in detection capability.

- Station down-time cost MAJO about 0.5 m_b units in detection capability. Down-time for ZOBO also significantly affected

its detection capability. Actual detection capabilities for both stations should improve since all apparent hardware problems have been solved.

E.   DISCRIMINATION

- Stations CHTO, CTAO, ZOBO, KAAO, and MAJO classified four out of fourteen presumed nuclear explosions with some confidence on the basis of an M_s-m_b criterion. Some indication of classification was noted for all but one of the events which were detected, suggesting that these stations would function best as part of a discrimination network.

- The following M_s - m_b relationships were established.

  CHTO : M_s = 1.86 m_b - 4.92

  CTAO : M_s = 1.73 m_b - 4.31

  ZOBO : M_s = 1.52 m_b - 2.66

  KAAO : M_s = 1.66 m_b - 3.71, and

  MAJO : M_s = 5.33 m_b - 21.30

  The anomalous relationship for MAJO could not be explained.

Future work on the evaluation of the Seismic Research Observatory stations should be directed toward the following points:

- Evaluate all stations as they become operational.

- Expand the short-period and long-period noise data bases so that at least one year of data is available at each station for the study of noise level trends.

- Data bases should be individually tailored for at least those stations which are far from Eurasia. In this respect, ZOBO should be re-evaluated in such a way that its detection capability is measured more relevantly.

SECTION VIII
REFERENCES

Chiburis, E. F., 1967; Long-Period L-Array Noise Coherence, Report No. 199, AFTAC Contract Number F33657-67-C-1313, Teledyne Incorporated, Garland, TX.

Eterno, J. S., D. S. Burns, L. J. Freier, and S. W. Buck, 1974; Special Event Detection for an Unattended Seismic Observatory, Report No. R-765, ARPA Contract Number F44620-73-C-0057, The Charles Stark Draper Laboratory, Incorporated, Cambridge, MA.

Fix, James E., 1972; Ambient Earth Motion in the Period Range from 0.1 to 2560 Seconds, Bulletin of the Seismological Society of America, 62, p. 1753-1760.

Flinn, E. A., and E. R. Engdahl, 1965; A Proposed Basis for Geographical and Seismic Regionalization, Reviews of Geophysics, Vol. 3, No. 1, p. 123-149.

Hudson, J. A., and A. Douglas, 1975; On the Amplitudes of Seismic Waves, Geophys. J. R. Astron. Society, 42, p. 1039-1044.

Lacoss, R. T., 1972; Variation of False Alarm Rates of NORSAR, Semi-annual Technical Summary, Seismic Discrimination, Massachusetts Institute of Technology, Cambridge, MA.

Nuttli, O. W., and S. G. Kim, 1975; Surface-Wave Magnitudes of Eurasian Earthquakes and Explosions, Bulletin of the Seismological Society of America, 65, No. 3, p. 693-709.

Prahl, S. R., 1974; Earth Noise at Very Long Period Experiment Stations, Technical Report No. 3, Texas Instruments Report No. ALEX(01)-TR-74-03, AFTAC Contract Number F08606-74-C-0033, Texas Instruments Incorporated, Dallas, TX.

Ringdal, F., 1974; VLPE Network Evaluation and Automatic Processing Research, Technical Report No. 2, Texas Instruments Report No. ALEX(01)-TR-74-02, AFTAC Contract Number F08606-74-C-0033, Texas Instruments Incorporated, Dallas, TX.

Robinson, E. A., 1967; Statistical Communication and Detection with Special Reference to Digital Data Processing of Radar and Seismic Signals, Charles Griffin and Company Limited, London, England.

Schmidt, A. W., and K. S. Wilson, 1978; Seismic Data Preparation Procedures, Technical Report No. 22, Texas Instruments Report No. ALEX(01)-TR-78-10, AFTAC Contract Number F08606-77-C-0004, Texas Instruments Incorporated, Dallas, TX.

Snell, N. S., 1976; Network Capability Estimation, Technical Report No. 4, Texas Instruments Report No. ALEX(01)-TR-76-04, AFTAC Contract Number F08606-76-C-0011, Texas Instruments Incorporated, Dallas, TX.

Strauss, A. C., 1976; Preliminary Evaluation of the Seismic Research Observatories, Technical Report No. 2, Texas Instruments Report No. ALEX(01)-TR-76-02, AFTAC Contract Number F08606-76-C-0011, Texas Instruments Incorporated, Dallas, TX.

Strauss, A. C., and L. C. Weltman, 1977; Continuation of the Seismic Research Observatories Evaluation, Technical Report No. 2, Texas Instruments Report No. ALEX(01)-TR-77-02, AFTAC Contract Number F08606-77-C-0004, Texas Instruments Incorporated, Dallas, TX.

Swindell, W. H., and N. S. Snell, 1977; Station Processor Automatic Signal Detection System, Phase I: Final Report, Texas Instruments Report No. ALEX(01)-FR-77-01, AFTAC Contract Number F08606-76-C-0025, Texas Instruments Incorporated, Dallas, TX.

Unger, R., 1978; Short-Period Noise Envelope Statistics: A Basis for Envelope Detector Design, Technical Report No. 17, Texas Instruments Report No. ALEX(01)-TR-78-05, AFTAC Contract Number F08606-77-C-0004, Texas Instruments Incorporated, Dallas, TX.

Von Seggern, D. H., 1970; A Long-Period Noise Study at Murphy Dome Alaska Seismic Data Laboratory, Report No. 247, AFTAC Contract Number F33657-69-C-0913-PZ01, Teledyne Industries Incorporated, Garland, TX.

Weichert, D. H., and P. W. Basham, 1973; Defference and False Alarms in Seismic Discrimination, Bulletin of the Seismological Society of America, 63, No. 3, p. 1119-1133.

APPENDIX A
THE DATA BASE

The 247 events used for this evaluation of the Seismic Research Observatory stations are listed on the following pages. Short-period detection capability data bases included only those events with station-epicenter distances of less than 103°.

In the data base list, the column headed 'EVNO' gives the identifying number assigned to each event. The columns headed 'DATE' and 'TIME' give the date and origin time of each event. The epicentral coordinates are listed under 'LAT.' and 'LONG.' for latitude in degrees north and longitude in degrees east. The bodywave magnitude is listed under the heading 'MB'. The column headed 'Q' gives the NORSAR quality rating for the parameters of each event where

> 1 = good to excellent quality
>
> 2 = fair to good quality
>
> 3 = poor to fair quality.

The seismic source area is listed in the column headed 'LOCATION'. Finally, the geographic region as defined by Flinn and Engdahl (Flinn and Engdahl, 1965) for each event is listed under the heading 'SUBREG'.

A-1

TABLE A-1
EVENT DATA BASE
(PAGE 1 OF 7)

EVNO	DATE	TIME	LAT.	LONG.	MB	Q	LOCATION	SUBRGG
1630	9/1/77	2.59.57	73.4	54.6	5.7	0	NOVAYA ZEMLYA	648
1631	9/1/77	5.41.46	26.2	126.8	5.6	0	RYUKYU ISLANDS	238
1632	9/2/77	9.13.45	27.5	130.8	4.4	0	RYUKYU ISLANDS	238
1633	9/2/77	9.54.45	23.2	124.9	4.4	0	SW RYUKYU ISLANDS	246
1634	9/2/77	17.16.35	52.5	158.9	4.3	0	NEAR E C KAMCHATKA	218
1635	9/3/77	22.17.25	39.5	69.2	4.6	0	TADZHIK SSR	715
1636	9/3/77	22.27.66	37.0	55.1	4.9	0	IRAN	370
1637	9/3/77	22.45.36	25.7	143.0	4.9	0	OFF E COAST HONSHU	238
1638	9/4/77	16.39.48	23.3	126.1	4.6	0	RYUKYU ISLANDS	211
1639	9/4/77		25.3	141.0	5.2	0	SOUTH OF HONSHU	327
1640	9/5/77	3.22.58	50.7	79.0	5.8	0	EAST KAZAKH SSR	370
1641	9/5/77	16.22.17	36.3	71.7	4.5	0	AFGHANISTAN SSR BOR	221
1642	9/6/77	12.11.40	50.3	157.2	4.9	0	KURILE ISLANDS	707
1643	9/6/77	4.34.10	36.4	69.2	4.9	0	AFGHANISTAN	327
1644	9/7/77		52.2	106.1	3.3	0	LAKE BAIKAL	
1645	9/9/77	2.35.08	43.0	131.0	4.0	0	USSR-NE CHINA BOR	657
1646	9/9/77	2.59.03	34.4	23.1	4.1	0	CRETE	370
1647	9/9/77	12.56.11	36.4	71.2	4.6	0	AFGHANISTAN-USSR BOR	770
1648	9/9/77	6.31.02	34.4	26.1	4.6	0	CRETE	370
1649	9/10/77		34.4	23.1	3.0	0	CRETE	370
1650	9/10/77	16.00.03	57.1	106.2	5.0	0	LAKE BAIKAL	327
1651	9/11/77	23.19.24	35.1	23.3	4.9	0	CRETE	370
1652	9/11/77	20.30.44	35.2	22.2	3.9	0	MEDITERRANEAN SEA	400
1653	9/12/77	2.30.14	34.4	23.1	4.4	0	CRETE	370
1654	9/12/77		35.1	23.3	4.5	0	CRETE	370
1655	9/12/77	2.57.34	35.1	23.3	4.4	0	CRETE	370
1656	9/12/77	9.33.28	37.2	67.2	4.7	0	AFGHANISTAN-USSR BOR	770
1657	9/12/77	10.52.46	35.1	25.5	4.5	0	CRETE	370
1658	9/12/77		45.9	155.8	4.4	0	KURILE ISLAND	221
1659	9/13/77	0.16.09	27.7	56.9	4.7	0	SOUTH IRAN	353
1660	9/13/77	13.48.12	27.7	55.1	4.7	0	SOUTH IRAN	353
1661	9/13/77	20.52.49	35.3	24.6	4.4	0	EASTERN KASHMIR	370
1662	9/14/77	18.56.08	35.1	23.1	4.5	0	CRETE	370
1663	9/15/77	14.36.30	37.0	-116.0	4.5	0	SOUTHERN NEVADA	41
1664	9/15/77	15.19.45	34.4	23.3	4.5	0	CRETE	360
1665	9/15/77	16.38.35	35.3	70.8	4.6	0	HINDU KUSH REGION	370
1666	9/15/77	16.52.33	24.7	125.3	4.1	0	SW RYUKYU IS	246

EVNO	DATE	TIME	LAT.	LONG.	MB	Q	LOCATION	STBERG
1670	9/16/77	7.25. 7	30.1	51.5	4.8	0	IRAN	348
1671	9/17/77	5.25.53	30.9	56.6	4.8	0	IRAN	348
1672	9/17/77	7.57.19	33.9	141.0	4.8	0	OFF E COAST HONSHU	229
1673	9/18/77	5.57.16	34.6	23.0	4.3	0	CRETE	370
1674	9/19/77	0.23. 6	29.6	51.4	4.7	0	SOUTHERN IRAN	353
1675	9/19/77	5.33.38	44.2	149.7	4.0	0	KURILE ISLANDS	221
1676	9/19/77	14.37.52	44.7	149.5	5.0	0	KURILE ISLANDS	221
1677	9/21/77	13.12.43	46.7	141.3	4.8	0	SAKHALIN ISLAND	662
1678	9/21/77	17.38.39	55.7	162.8	5.1	0	NEAR KAMCHATKA	218
1679	9/22/77	17.58.19	30.2	169.8	4.0	0	WEST PAKISTAN	710
1680	9/23/77	20.58. 1	41.5	20.1	4.7	0	ALBANIA	391
1681	9/24/77	20.43.24	35.7	23.2	4.3	0	CRETE	3700
1682	9/25/77	3.12.35	36.3	23.1	4.2	0	CRETE	3707
1683	9/25/77	10.16.36	36.6	137.4	3.6	0	HONSHU JAPAN	227
1684	9/25/77	10.16.36	36.6	71.1	4.7	0	AFGHANISTAN-USSR BOR	717
1685	9/25/77	19.56.57	38.7	31.1	4.3	0	TURKEY	366
1686	9/26/77	1.56.55	52.4	159.7	4.6	0	OFF KAMCHATKA	219
1687	9/26/77	8.21.22	53.1	160.2	4.8	0	NEAR KAMCHATKA	218
1688	9/27/77	19.48. 0	25.1	68.2	4.5	0	WEST PAKISTAN	710
1689	9/27/77	14.	37.2	-116.1	4.8	0	SOUTHERN NEVADA	41
1690	9/28/77	5.24.45	46.5	145.0	4.7	0	SEA OF OKHOTSK	663
1691	9/28/77	22.56.19	36.6	71.6	4.7	0	AFGHANISTAN-USSR BOR	717
1692	9/30/77	7.59.56	52.8	159.0	5.1	0	OFF KAMCHATKA	219
1693	9/30/77	16.50.37	40.1	45.0	4.8	0	WESTERN KAZAKH USSR	336
1694	9/30/77	16.50.37	40.1	45.0	4.8	0	EASTERN CAUCASUS	337
1695	9/30/77	19.17. 8	39.4	73.4	5.5	0	TADZHIK-SINKIANG BOR	717
1696	10/1/77	16.35. 7	36.5	71.0	4.8	0	AFGHANISTAN-USSR BOR	717
1697	10/1/77	15.38.57	35.1	140.2	4.8	0	NEAR HONSHU JAPAN	228
1698	10/1/77	17.38.13	36.1	139.9	5.3	0	HONSHU JAPAN	227
1699	10/1/77	17.38.13	46.8	152.9	5.3	0	KURILE ISLANDS	221
1700	10/1/77	20.15.37	35.9	69.6	4.5	0	HINDU KUSH REGION	718
1701	10/4/77	21.34.51	51.5	156.6	5.2	0	KAMCHATKA	217
1702	10/5/77	16.53.55	26.7	97.0	4.4	0	BURMA	296
1703	10/6/77	10.50.15	36.2	69.2	4.3	0	HINDU KUSH REGION	718
1704	10/6/77	10.50.15	22.2	121.0	4.3	0	TAIWAN REGION	243
1705	10/7/77	12.42.51	38.8	20.6	4.8	0	GREECE	364
1706	10/7/77	18.55. 5	44.9	150.2	4.1	0	KURILE ISLANDS REG	222
1707	10/7/77	23.16. 3	28.1	128.2	5.2	0	RYUKYU ISLANDS	238
1708	10/8/77	10.25.31	35.1	23.3	4.4	0	CRETE	370
1709	10/9/77	11. 0. 0	73.6	53.2	4.5	0	NOVAYA ZEMLYA	648

TABLE A-1

EVENT DATA BASE

(PAGE 3 OF 7)

EVNO	DATE	TIME	LAT.	LONG.	MB	Q	LOCATION	SUBREG
1710	10/10/77		35.65	23.4	4.3	00000	CRETE	370
1711	10/11/77		29.81	27.2	4.0	00000	DODECANESE ISLANDS	369
1712	10/12/77		29.8	128.2	5.6	00000	EAST CHINA SEA	660
1713	10/12/77		41.8	133.7	4.5	00000	SEA OF JAPAN	718
1714	10/		36.1	69.3	4.5	00000	HINDU KUSH REGION	
1715	10/12/77		39.4	21.7	4.7	00000	GREECE	364
1716	10/12/77		42.8	146.6	4.9	00000	OC HOKKAIDO JAPAN	225
1717	10/13/77		35.6	24.1	4.2	00000	CRETE	370
1718	10/		23.6	93.1	5.4	00000	BURMA-INDIA BOR REG	294
1719	10/		23.6	121.7	4.1	00000	TAIWAN	244
1720	10/13/77		37.3	72.1	6.2	00000	TADZHIK USSR	715
1721	10/14/77		37.7	32.2	4.6	00000	TURKEY	366
1722	10/16/77		47.5	153.0	4.7	00000	KURILE ISLANDS	221
1723	10/16/77		36.5	73.0	4.4	00000	AFGHANISTAN-USSR BOR	217
1724	10/		46.9	154.1	4.6	00000	KURILE ISLANDS REG	222
1725	10/16/77		47.9	155.9	5.1	00000	KURILE ISLANDS	221
1726	10/16/77		46.9	154.9	4.7	00000	KURILE ISLANDS	221
1727	10/17/77		25.0	98.3	4.4	00000	BURMA-CHINA BOR REG	297
1728	10/18/77		46.6	154.	5.1	00000	KURILE ISLANDS REG	222
1729	10/18/77		47.0	154.0	5.3	00000	KURILE ISLANDS	221
1730	10/18/77		23.7	107.1	5.2	00000	EASTERN CHINA	667
1731	10/19/77		36.1	71.1	4.5	00000	AFGHANISTAN-USSR BOR	221
1732	10/19/77		39.1	29.2	4.8	00000	KURILE ISLANDS REG	366
1733	10/19/77		39.1	29.2	5.3	00000	TURKEY	
1734	10/19/77		39.4	95.6	5.4	00000	SOUTHERN SINKIANG	321
1735	10/19/77		44.2	152.6	5.2	00000	KURILE ISLANDS	224
1736	10/20/77		22.1	121.6	5.6	00000	TAIWAN	235
1737	10/20/77		31.3	131.6	5.4	00000	KYUSHU, JAPAN	225
1738	10/20/77		47.2	153.0	4.4	00000	KURILE ISLANDS	221
1739	10/20/77		47.3	153.0	4.4	00000	KURILE ISLANDS	221
1740	10/20/77		47.3	154.0	4.9	00000	KURILE ISLANDS	221
1741	10/21/77		47.2	153.0	5.0	00000	KURILE ISLANDS	225
1742	10/21/77		30.8	131.5	5.0	00000	KYUSHU, JAPAN	235
1743	10/21/77			50.8		00000	IRAN	348
1744	10/22/77		35.0	23.2	5.0	00000	CRETE	370

A-4

TABLE A-1
EVENT DATA BASE
(PAGE 4 OF 7)

EVNO	DATE	TIME	LAT.	LONG.	MB	O	LOCATION	STRRNG
1750	10/22/77	11.58.46	36.7	141.3	4.9	00000	NEC HONSHU, JAPAN	228
1751	10/23/77	15.45.28	38.9	121.1	4.1	00000	GREECE	364
1752	10/23/77	15.19.29	43.3	135.5	4.3	00000	NEC EAST RUSSIA	661
1753	10/24/77	18.34.32	34.5	126.8	4.0	00000	KURILE ISLANDS	370
1754	10/24/77	23.40.28	47.2	154.1	5.0	00000		221
1755	10/24/77	23.40.28	40.8	155.6	4.8	00000	KURILE ISLANDS	221
1756	10/25/77	21.55.35	36.5	79.1	5.7	00000	SOUTHERN SINKIANG	328
1757	10/25/77	21.58.00	40.5	141.6	5.1	00000	NEC HONSHU, JAPAN	229
1758	10/26/77	14.15.	37.	-116.0	3.4	00000	OEC HONSHU, JAPAN	241
1759	10/26/77		37.	-116.0		00000	SOUTHERN NEVADA	
1760	10/26/77	17. 2.51	31.5	51.2	4.7	00000	IRAN	348
1761	10/26/77	17.47.51	36.7	139.7	4.7	00000	HONSHU, JAPAN	227
1762	10/27/77	10.22.22	29.7	150.7	4.8	00000	SOUTHERN IRAN	353
1763	10/27/77	5.29.24	40.2	143.2	4.9	00000	OEC HONSHU, JAPAN	229
1764	10/27/77		31.2	93.2	4.8	00000	TIBET	306
1765	10/27/77	6.59.27	35.5	27.6	4.9	00000	DODECANESE ISLANDS	369
1766	10/27/77	9.50.20	39.8	144.8	5.7	00000	OEC HONSHU, JAPAN	226
1767	10/27/77	22.43.12	38.0	27.9	5.0	00000	TURKEY	366
1768	10/28/77	13.16.58	22.4	121.4	5.1	00000	TAIWAN REGION	243
1769	10/28/77					00000		
1770	10/28/77	21.15.21	39.6	73.0	4.5	00000	TADZHIK-SINKIANG BOR.	719
1771	10/28/77	1.53.28	29.9	95.3	4.5	00000	INDIA-CHINA BOR REG	313
1772	10/28/77	10.33.57	49.9	78.9	5.5	00000	EASTERN KAZAKH SSR	329
1773	10/29/77		50.1	78.2	5.1	00000	EASTERN KAZAKH SSR	329
1774	10/29/77		47.1	153.2	4.4	00000	KURILE ISLANDS	221
1775	10/30/77	21.38.39	45.5	146.0	4.4	00000	KURILE ISLANDS	221
1776	10/31/77	9.40.36	56.5	162.3	4.4	00000	NEC KAMCHATKA	218
1777	10/31/77	14.24.46	24.0	122.3	5.0	000C0	TAIWAN REGION	243
1778	11/ 1/77	17.56.27	57.	71.0	5.7	000C0	EASTERN RUSSIA	656
1779	11/ 1/77		57.	71.0	3.7	000C0	AFGHANISTAN-USSR BOR	717
1780	11/ 1/77	17.56.43	36.6	-68.7	4.7	00300	HINDU KUSH REGION	718
1781	11/ 1/77	18.50.28	37.2	-116.2	4.7	00300	SOUTHERN NEVADA	417
1782	11/ 2/77	16.30.40	51.1	138.0	4.9	00300	HONSHU, JAPAN	227
1783	11/ 3/77	2.22.55	42.1	160.1	5.2	00300	OEC KAMCHATKA	219
1784	11/ 3/77			124.0		00300	BULGARIA	359
1785	11/ 3/77	12.28. 1	44.3	149.5	4.6	00320	KURILE ISLANDS	221
1786	11/ 3/77	19.46.15	39.3	143.0	5.1	00320	TURKEY	366
1787	11/ 3/77	19.18. 3	39.2	140.0	4.0	00320	TURKEY	366
1788	11/ 4/77	23.54.45	29.6	81.3	3.9	00320	HONSHU, JAPAN	227
1789	11/ 4/77					00320	NEPAL	310

A-5

EVNO	DATE	TIME	LAT.	LONG.	MB	Q	LOCATION	SUBREG
1790	11/5/77	4. 6.49	37.0	71.0	3.8	2	AFGHANISTAN-USSR BOR	717
1791	11/5/77	6.59	36.6	69.0	3.6	0	HINDU-KUSH REG	718
1792	11/5/77	40.12	47.1	154.0	5.9	2	KURIL ISLANDS	221
1793	11/6/77	39.35	53.1	154.1	5.2	0	NEC KAMCHATKA	218
1794	11/6/77	48.45	42.1	24.1	4.8	0	BULGARIA	359
1795	11/6/77	13.31.41	36.3	71.1	4.5	0	AFGHANISTAN-USSR BOR	717
1796	11/6/77	11.50	46.8	26.2	4.9	0	RUMANIA	358
1797	11/8/77	44.48	48.5	153.6	4.4	0	KURILE ISLANDS	221
1798	11/9/77	21.44.46	34.5	15.4	4.7	0	MEDITERRANEAN SEA	400
1799	11/9/77	20.39.46	44.5	149.4	4.7	0	KURILE ISLANDS	221
1800	11/9/77	1. 0.25	56.0	162.0	4.0	3	NEC KAMCHATKA	218
1801	11/9/77	5.29.44	28.5	55.0	4.6	0	SOUTHERN IRAN	353
1802	11/9/77	8.13.43	47.7	154.3	4.9	0	KURILE ISLANDS	221
1803	11/9/77	11.20.33	36.5	55.0	4.1	0	IRAN	348
1804	11/9/77	21.14.32	47.5	154.3	5.1	0	KURILE ISLANDS	221
1805	11/9/77	22. 0.26	37.0	-116.1	5.7	3	SOUTHERN NEVADA	41
1806	11/00/77	24.12.34	39.4	27.7	4.0	0	TURKEY	366
1807	11/10/77	14.52.39	31.8	56.1	4.7	0	IRAN	348
1808	11/10/77	23.13.57	35.5	27.4	4.8	0	IRAN	348
1809					4.1	0	DODECANESE ISLANDS	369
1810	11/10/77	23.15.41	42.6	24.07	3.4	2	GREECE-BULGARIA BOR	363
1811	11/12/77	3. 49.49	26.6	126.7	3.9	0	RYUKYU ISLANDS	238
1812	11/12/77	16.12.120	44.5	148.3	4.8	0	KURILE ISLANDS	221
1813	11/13/77	42.42.12	41.5	142.0	5.0	0	HOKKAIDO, JAPAN REG	224
1814		21. 2.29	26.5	93.1	5.0	0	EASTERN INDIA	317
1815	11/14/77	4.25.11	52.0	160.0	3.9	2	OFF E COAST KAMCHATK	219
1816	11/15/77	4.43.39	32.0	74.2	3.4	3	SOUTHWESTERN KASHMIR	719
1817	11/15/77	20.20.47	38.0	74.0	3.8	0	TADZHIK-SINKIANG BOR	719
1818	11/15/77	22.58.31	30.0	69.0	3.8	2	PAKISTAN	710
1819			28.1	55.0	3.8	2	SOUTHERN IRAN	353
1820	11/16/77	14.58.39	36.1	140.2	5.1	0	NEC HONSHU JAPAN	228
1821	11/16/77	19.36.18	41.9	142.0	5.2	0	HOKKAIDO JAPAN REG	224
1822	11/16/77	21.11.29	34.1	24.2	3.6	3	AEGEAN SEA	365
1823	11/16/77	21.11.48	42.1	140.7	5.1	2	HOKKAIDO, JAPAN REG	224
1824						0	HOKKAIDO, JAPAN REG	224
1825	11/17/77	6.28.29	42.0	24.1	4.7	0	BULGARIA	359
1826	11/17/77	14.11.20	23.0	94.0	3.7	3	BURMA-INDIA BOR REG	241
1827	11/17/77	19.30.12	37.0	-116.0	3.8	0	SOUTHERN NEVADA	41
1828	11/17/77	20.39.25	37.1	-116.0	3.8	0	SOUTHERN NEVADA	41
1829	11/18/77	24.25.6	41.3	142.2	4.7	0	HOKKAIDO, JAPAN REG	224

TABLE A-1
EVENT DATA BASE
(PAGE 6 OF 7)

EVNO	DATE	TIME	LAT.	LONG.	MB	C	LOCATION	SUBRGS
1830	11/18/77	5.20.11	32.7	88.4	5.7	0	TIBET	306
1831	11/18/77	6.33.22	32.6	88.4	5.6	0	TIBET	306
1832	11/18/77	14.57.242	36.6	66.3	4.4	0	WEST PAKISTAN	710
1833	11/18/77	15.10.42	36.6	137.1	5.4	0	HONSHU, JAPAN	227
1834	11/18/77		32.7	88.3		0	TIBET	306
1835	11/18/77	17.23.24	32.6	88.3	4.9	0	TIBET	306
1836	11/18/77	21.18.330	43.9	147.7	5.4	0	KURILE ISLANDS	221
1837	11/18/77	23.12.503	43.7	88.4	4.4	0	TIBET	306
1838	11/19/77	11.51.14	43.6	147.7	4.4	0	KURILE ISLANDS	221
1839	11/19/77		36.5	71.3	4.8	0	AFGHANISTAN-USSR BOR	717
1840	11/20/77	15.57.16	26.8	126.3	4.9	0	RYUKYU ISLANDS	238
1841	11/20/77	23.57.33	37.4	71.8	4.7	0	AFGHANISTAN-USSR BOR	717
1842	11/20/77	23.40.367	32.2	87.8	4.7	0	TIBET	306
1843	11/21/77	12.32.27	41.0	50.1	4.6	0	CASPIAN SEA	338
1844	11/21/77	14.35.1	53.0	160.1	4.9	0	NEG KAMCHATKA	219
1845	11/21/77	19.43.34	36.7	71.2	4.5	0	AFGHANISTAN-USSR BOR	717
1846	11/21/77	21.19.494	42.7	141.8	4.8	2	HOKKAIDO,JAPAN REG	224
1847	11/22/77	00.7.44	37.0	71.7	3.6	0	AFGHANISTAN-USSR BOR	717
1848	11/22/77	6.56.14	36.5	70.7	3.9	0	HINDU KUSH REGION	719
1849	11/22/77		36.5	71.2	3.4	0	AFGHANISTAN-USSR BOR	717
1850	11/22/77	11.34.9	44.3	84.5	5.0	0	NORTHERN SINKIANG	332
1851	11/24/77	21.31.24	39.5	96.4	3.3	3	BURMA	366
1852	11/24/77	22.30.16	40.4	142.6	4.3	0	OFF HONSHU JAPAN	296
1853	11/25/77	17.24.16	34.	46.0	3.	2	WESTERN IRAN	347
1854	11/25/77					0		
1855	11/25/77	19.47.90	23.7	121.8	4.5	0	TAIWAN STR	244
1856	11/26/77	15.58.407	38.5	24.3	4.6	0	AEGEAN SEA	365
1857	11/26/77	13.19.447	39.5	20.9	5.1	0	GREECE	658
1858	11/26/77	22.46.527	28.0	117.0	3.	2	NORTHEASTERN CHINA	306
1859	11/27/77	22.9.		90.0			TIBET	306
1860	11/27/77	3.57.06	50.0	79.0	3.	3	EASTERN KAZAKH SSR	329
1861	11/27/77	8.36.28	47.0	153.0	5.4	0	KURILE ISLANDS	221
1862	11/27/77	8.58.28	46.1	153.1	3.4	0	KURILE ISLANDS	221
1863	11/27/77	10.15.21	21.1	121.6	4.4	0	TAIWAN REGION	243
1864	11/27/77	18.40.1				0		
1865	11/27/77	20.42.43	37.7	32.0	4.2	0	TURKEY	366
1866	11/28/77	2.19.11	47.0	154.8	5.6	2	KURILE ISLANDS	269
1867	11/28/77	2.59.11	36.0	27.8	3.9	0	DODECANESE ISLANDS	218
1868	11/28/77	6.36.53	56.0	162.0	3.	2	NEG KAMCHATKA	224
1869	11/28/77	10.7.24	42.1	143.1	4.8	0	HOKKAIDO,JAPAN REG	224

A-7

TABLE A-1
EVENT DATA BASE
(PAGE 7 OF 7)

EVNO	DATE	TIME	LAT.	LONG.	M3	Q	LOCATION	SUBREG
1870	11/28/77	23-17-27	21.1	120.9	4.6	000	TAIWAN REGION	243
1871	11/28/77	23-57-39	43.8	148.1	4.9	000	KURILE ISLANDS REG	222
1872	11/29/77	1-53-41	22.2	94.7	4.4	000	BURMA	296
1873	11/29/77	20-17-12	38.0	21.8	3.9	000	GREECE	364
1874	11/30/77	4- 6-58	50.0	78.9	5.9	0	EASTERN KAZAKH SSP	329
1875	11/30/77	5-42- 2	44.5	148.7	4.8	00	KURILE ISLANDS	221
1876	11/30/77	7-51-23	35.5	135.8	4.2	00	SOUTHERN HONSHU, JPP	232

A-8

APPENDIX B
INSTRUMENT-RESPONSE CORRECTED NOISE CHARACTERISTICS

In the course of the evaluation of the Seismic Research Observatory stations, instrument-response corrected noise field characteristics were studied at each station under evaluation. In this appendix to the continuation of the Seismic Research Observatories evaluation, the extension to this study is presented.

To correct the data for the effects of the instrument response, the data were first Fourier transformed into the frequency domain. Noise amplitude spectra were then computed and smoothed to 64 frequencies. The smoothing was performed to simplify the task of making the instrument response corrections. In the course of this smoothing, the spectral values were scaled so that Parseval's formula would hold. This formula, which permits the computation of RMS noise from frequency domain data, is expressed as:

$$RMS_a^b = \left[\Delta f \sum_{i=a}^{b} \left| A(f_i) \right|^2 * C(f_i)^2 \right]^{\frac{1}{2}} \quad \text{(frequency-domain estimate)}$$

where

Δf = the elemental frequency interval,

$\left| A(f_i) \right|^2$ = the discrete Fourier transform spectral density estimate at frequency f_i,

$C(f_i)$ = the instrument response correction at frequency f_i,

a = the initial frequency index, and

b = the final frequency index.

B-1

Figures B-1a through B-6c show the instrument-response corrected RMS noise values plotted against Julian day for the passbands of 10-25, 17-41, and 40-64 seconds. Figures B-7a through B-12c show the RMS noise level trends computed from these values. Since these figures differ from those of Section IV, where the instrument response was not corrected for, only in level, no further discussion will be presented.

Tables B-1 through B-3 present means and standard deviations of instrument response corrected noise in the 10-25, 17-41, and 40-64 second passbands. Tables B-4 and B-5 present means and standard deviations of instrument response corrected peak and log peak 20- and 30-second noise amplitudes. Instrument response corrected mean peak and mean log peak amplitudes were derived from their non-instrument response corrected analogues through the implementation of the following statistical formulae:

Given

$$x = x'/c$$

$$\bar{x} = \frac{1}{c}\bar{x}' \; ; \; \sigma_x = \frac{1}{c}\sigma_{x'}$$

$$\overline{\text{Log } x} = \overline{\text{Log } x'} - \text{Log } c \; ; \; \sigma_{\log x} = \sigma_{\log x'}$$

where x' is a peak noise amplitude and c is an instrument response correction factor. Instrument response corrected and non-instrument response corrected 25-second values are equivalent since the SRO long-period response is normalized at that period. The reader is again referred to Section IV for discussion.

Figures B-1b through B-19 present the mean instrument-response-corrected RMS amplitude spectra for each of the seven stations evaluated here. The right half of each figure displays Log_{10} RMS amplitude spectra. The associated vertical bars represent plus-or-minus one standard deviation. These stations, with the sole exception of MAJO (Figure B-19) display a microseismic peak at a period of about 17 seconds followed by a

B-2

SITE 30
Vertical

North

East

RMS AMPLITUDE IN MU

JULIAN DAY
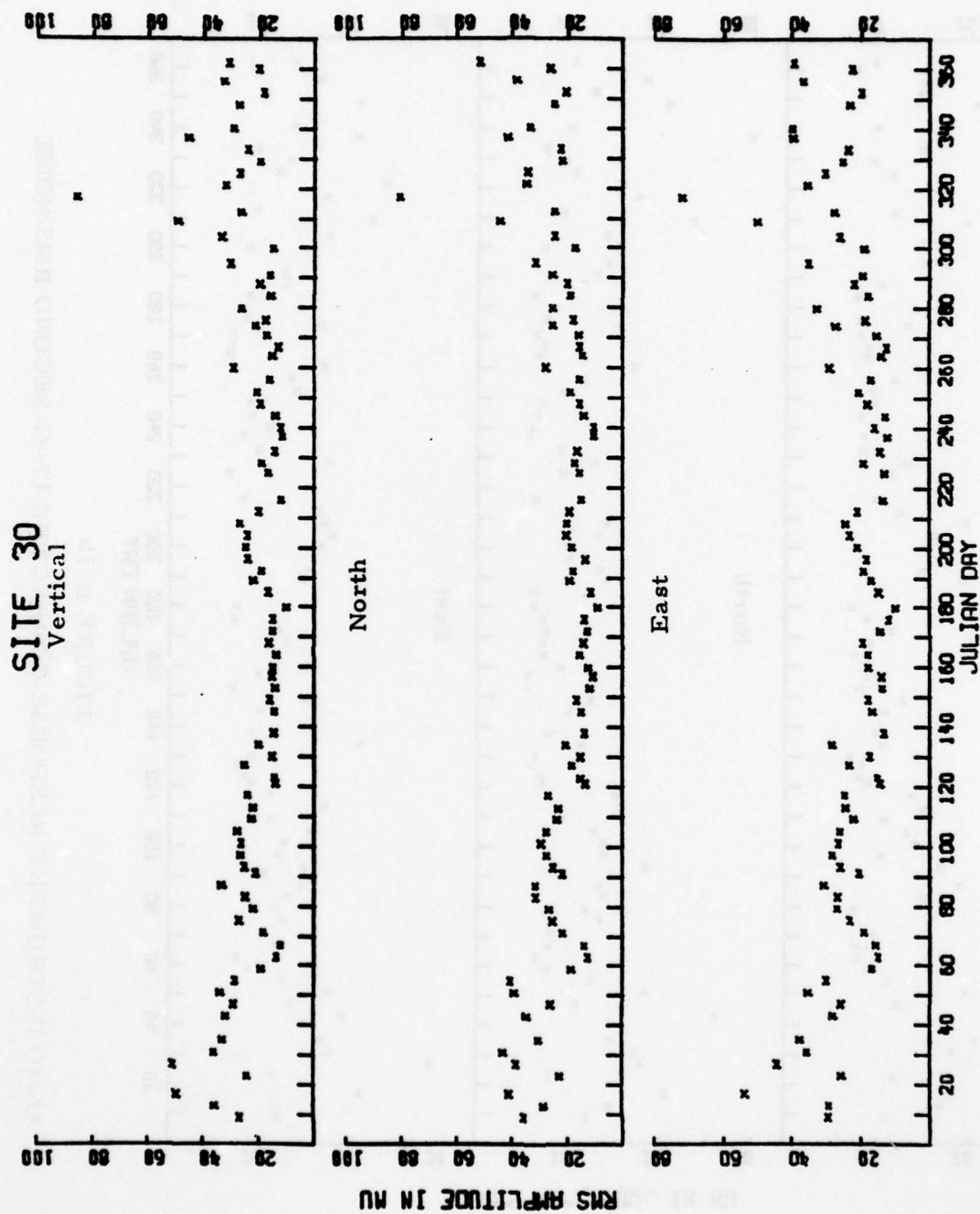
FIGURE B-1a

ANMO INSTRUMENT RESPONSE CORRECTED 10-25 SECOND RMS NOISE

SITE 30
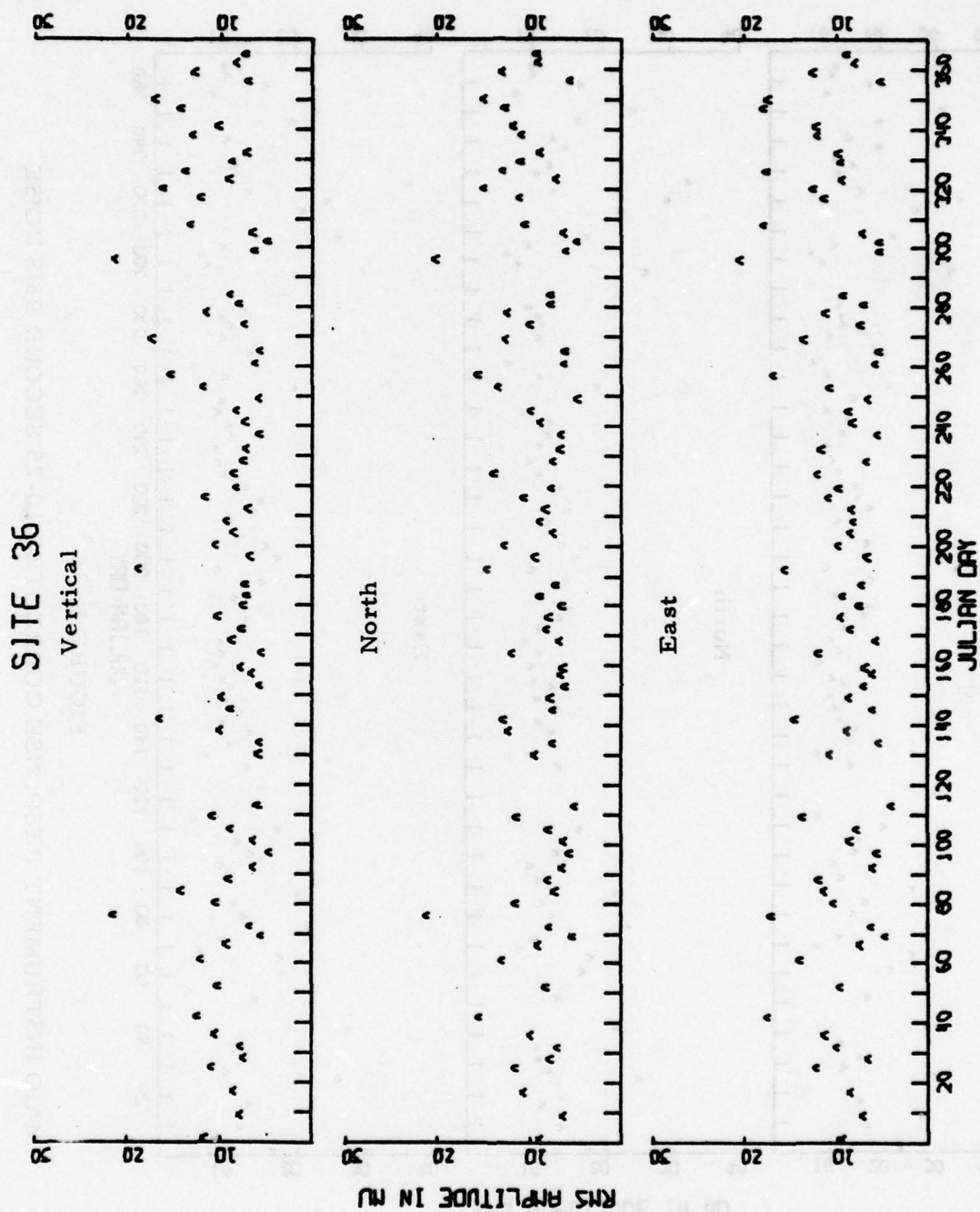Vertical

North

East

RMS AMPLITUDE IN MU

JULIAN DAY
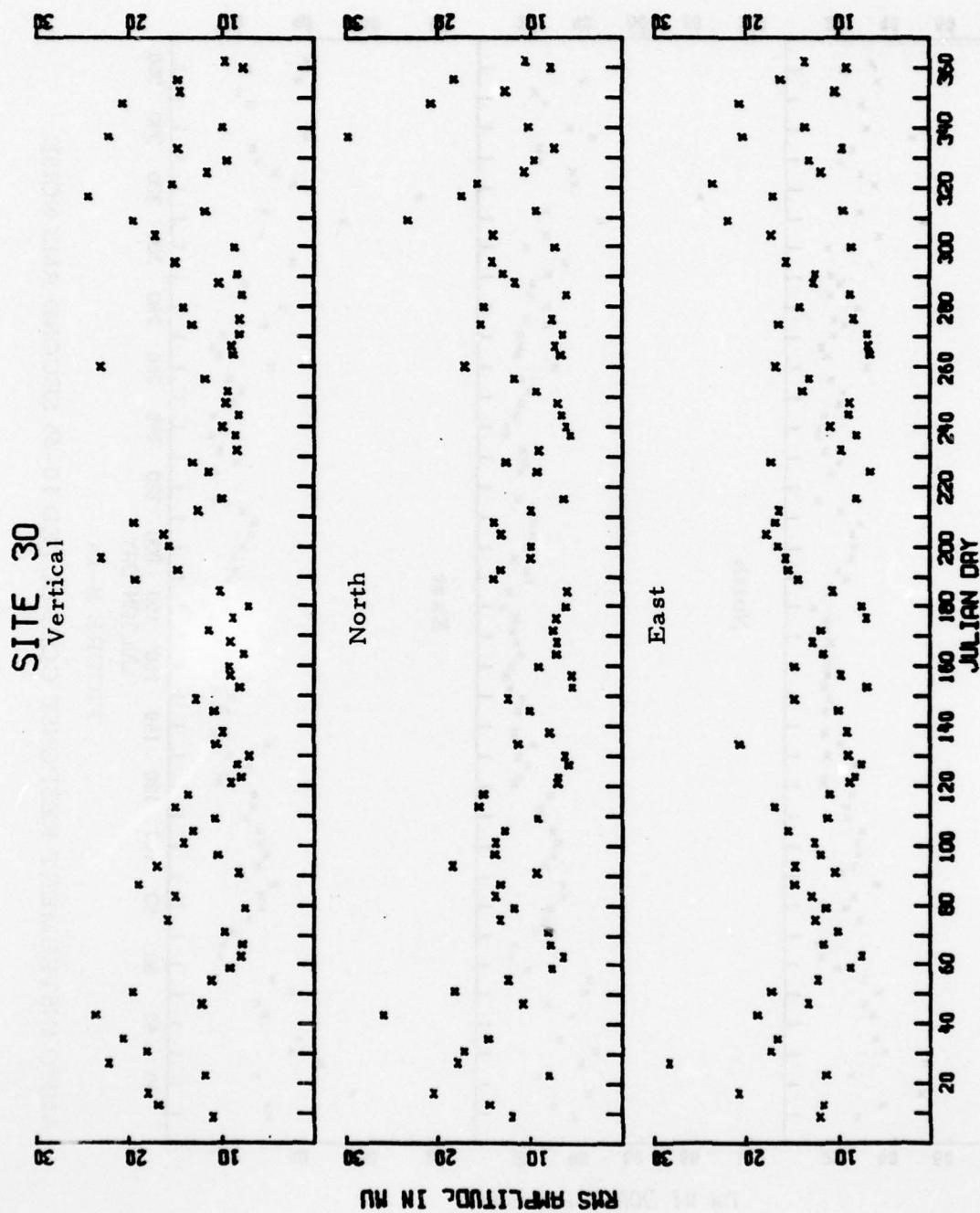
FIGURE B-1b

ANMO INSTRUMENT RESPONSE CORRECTED 17-41 SECOND RMS NOISE
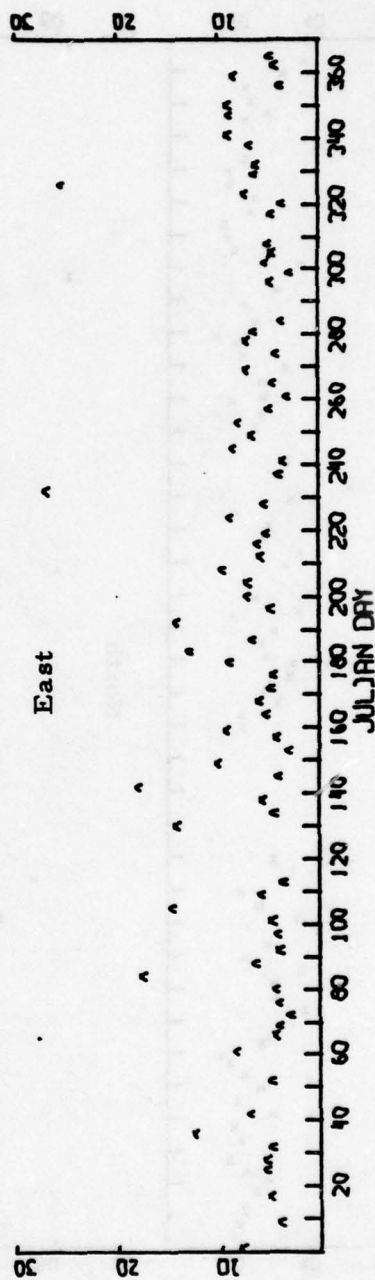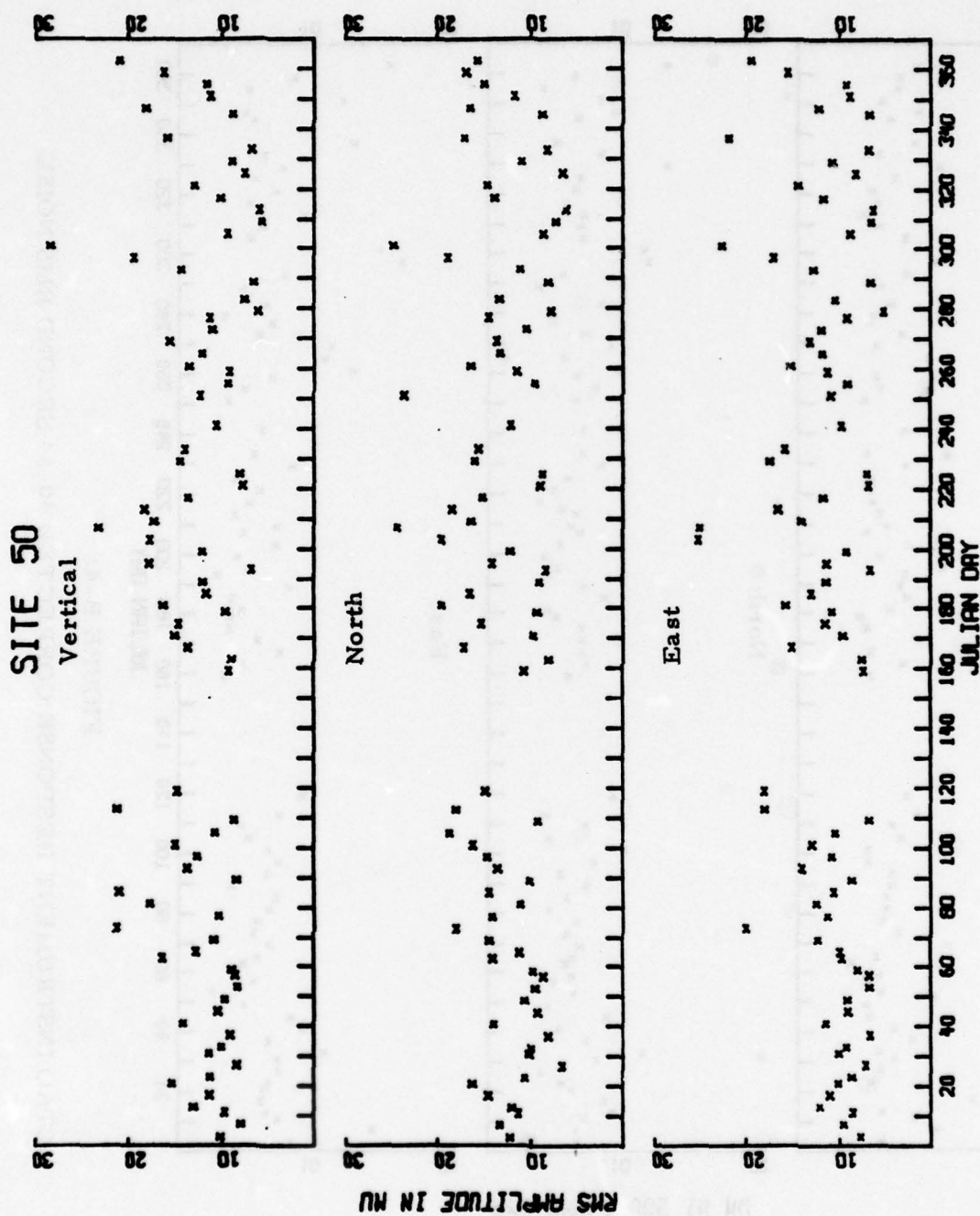
B-4

SITE 30

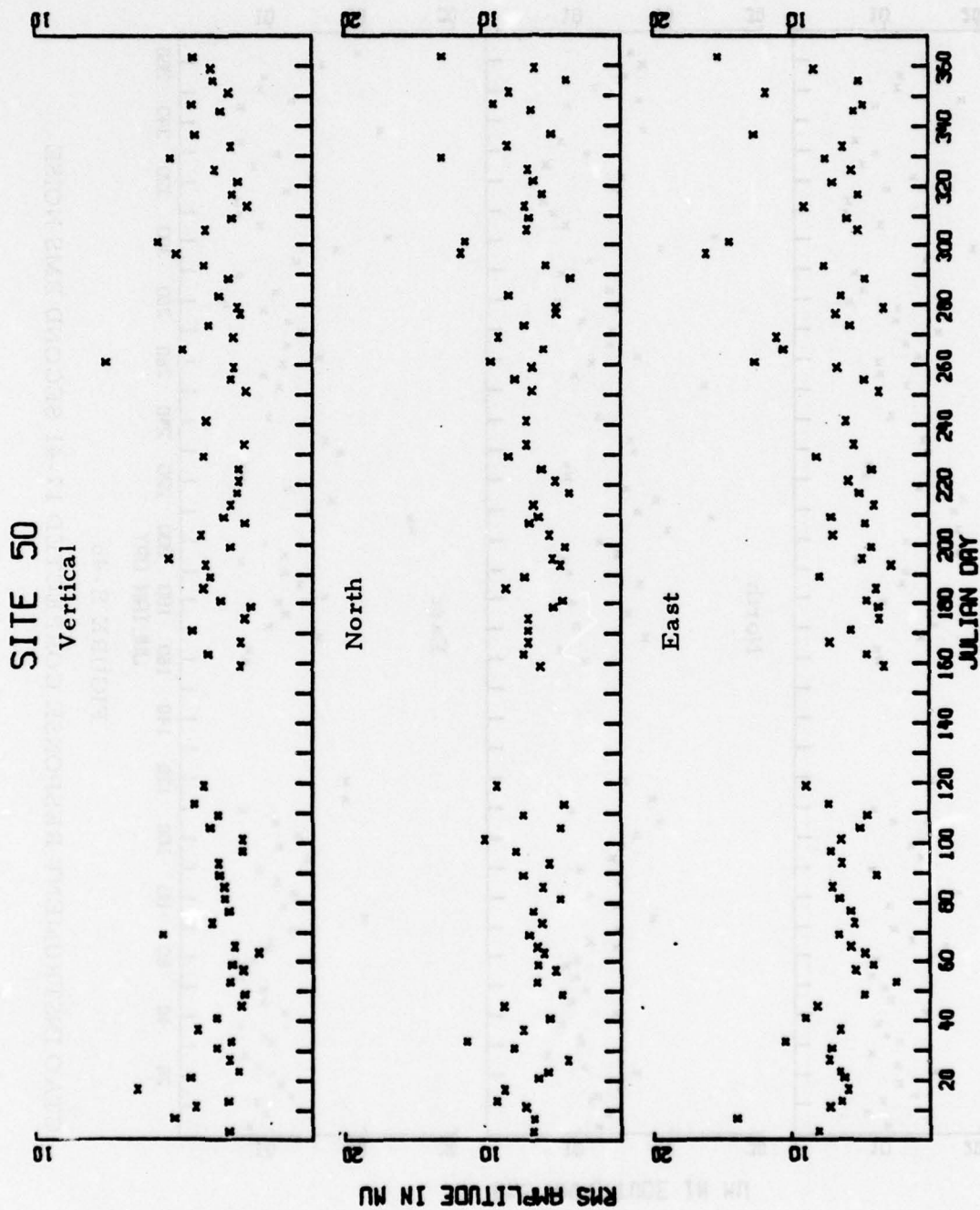× Vertical

North

East

RMS AMPLITUDE IN NU

JULIAN DAY
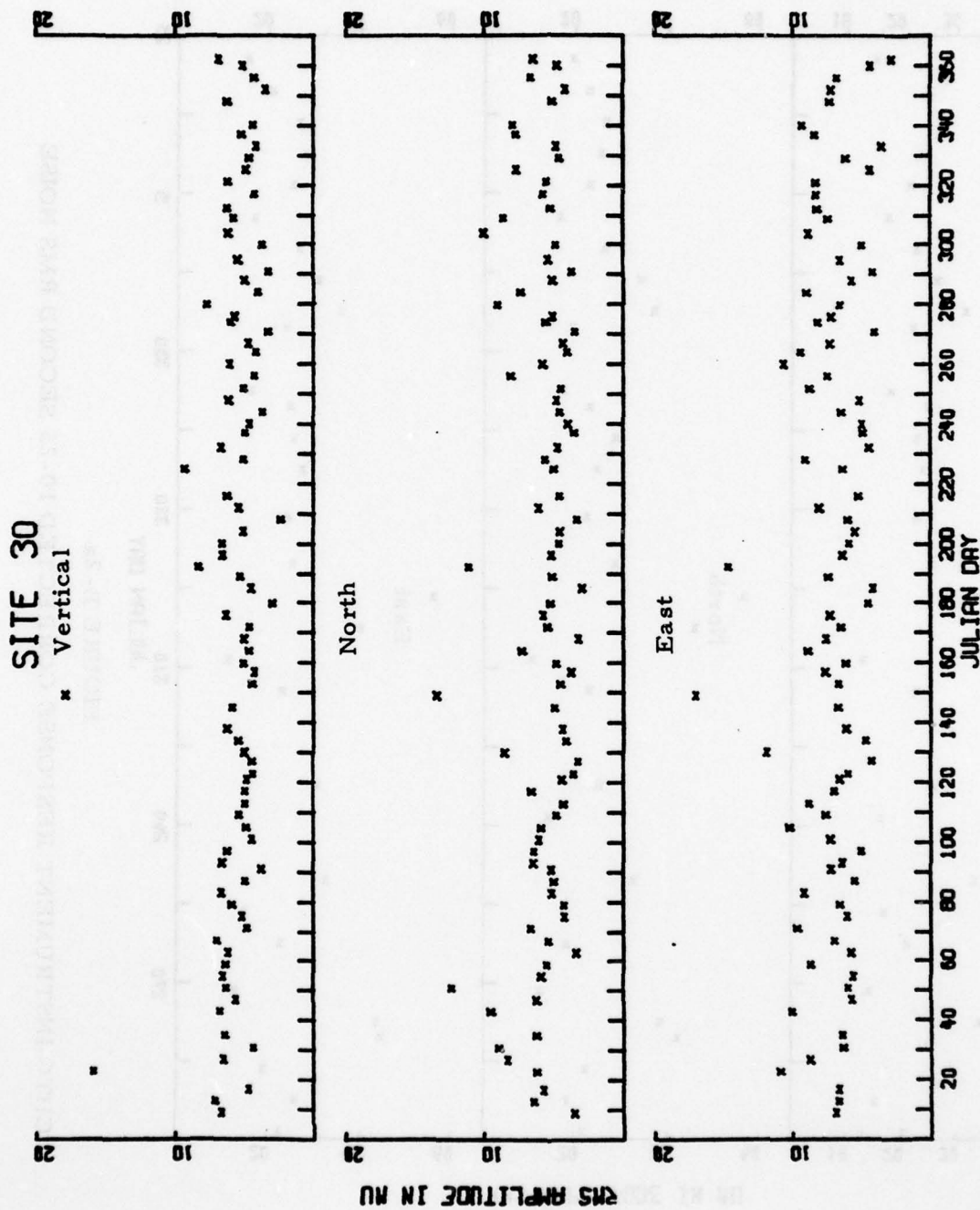
FIGURE B-1c

ANMO INSTRUMENT RESPONSE CORRECTED 40-64 SECOND RMS NOISE

SITE 33

Vertical

North

East

RMS AMPLITUDE IN MU

JULIAN DAY
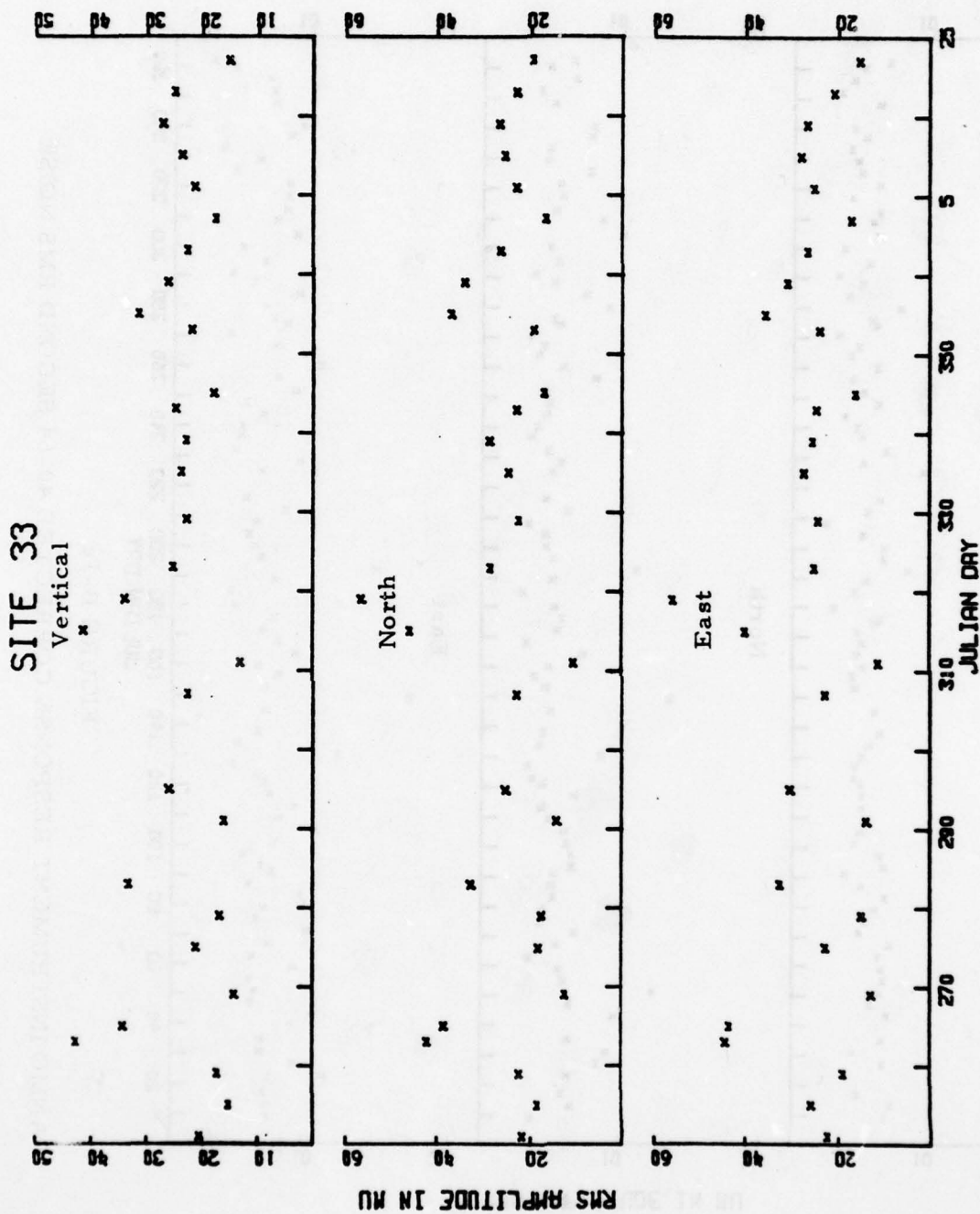
FIGURE B-2a

CHTO INSTRUMENT RESPONSE CORRECTED 10-25 SECOND RMS NOISE

B-6

SITE 33

Vertical

North

East

JULIAN DAY

RMS AMPLITUDE IN MU
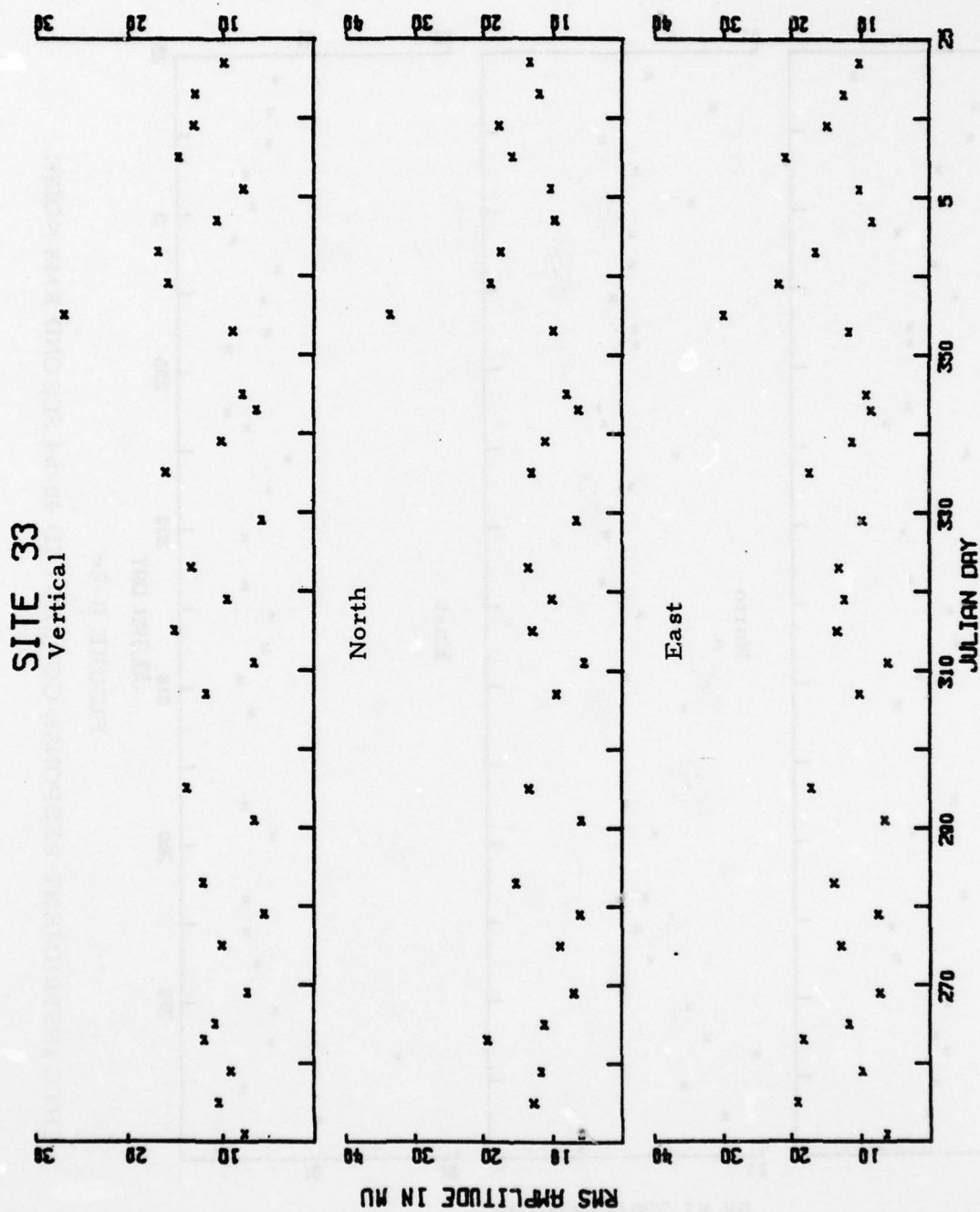
FIGURE B-2b

CHTO INSTRUMENT RESPONSE CORRECTED 17-41 SECOND RMS NOISE

B-7

SITE 33
Vertical

North

East

RMS AMPLITUDE IN MU

JULIAN DAY
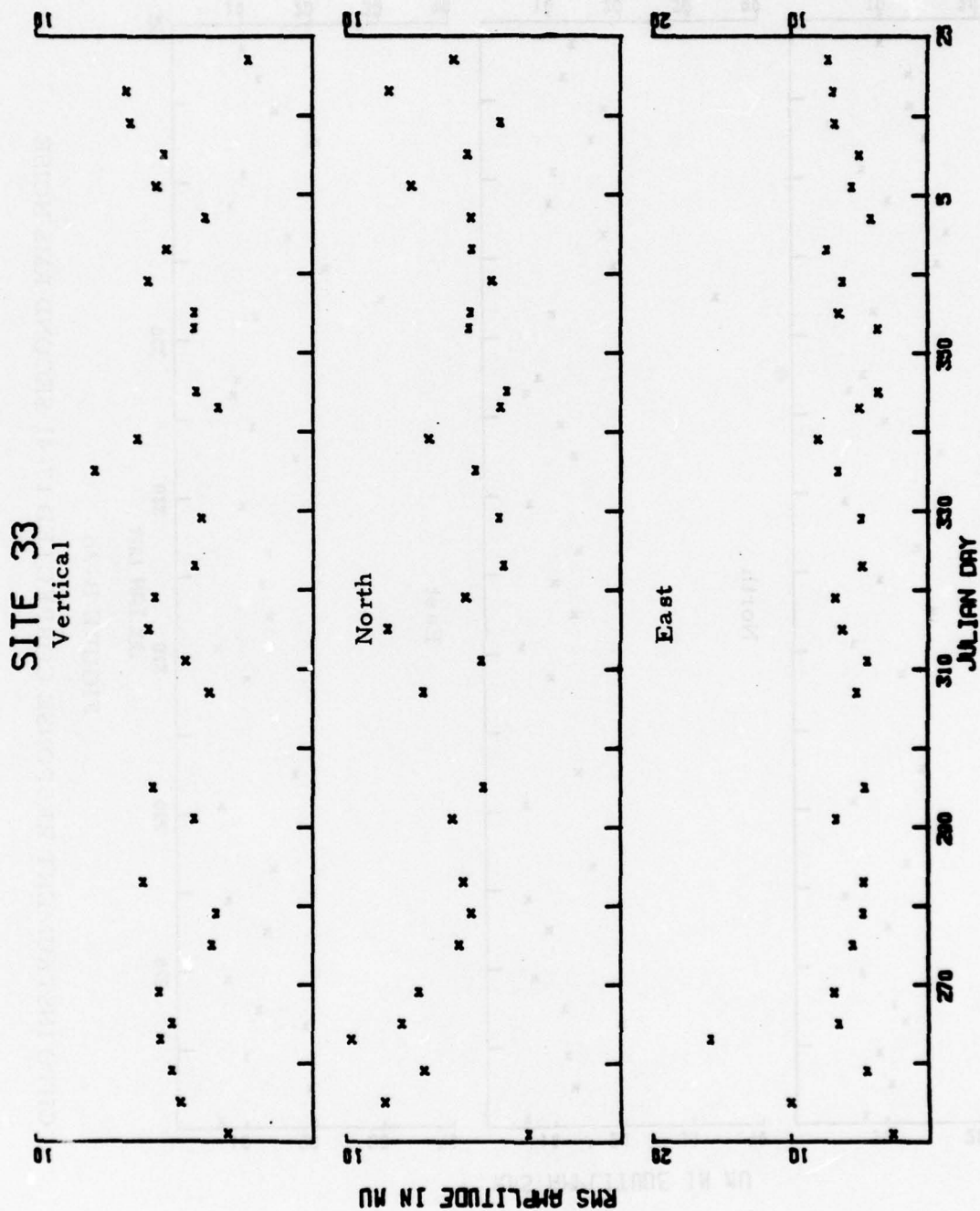
FIGURE B-2c

CHTO INSTRUMENT RESPONSE CORRECTED 40-64 SECOND RMS NOISE

B-8

SITE 36

Vertical

North

East

JULIAN DAY

RMS AMPLITUDE IN MU
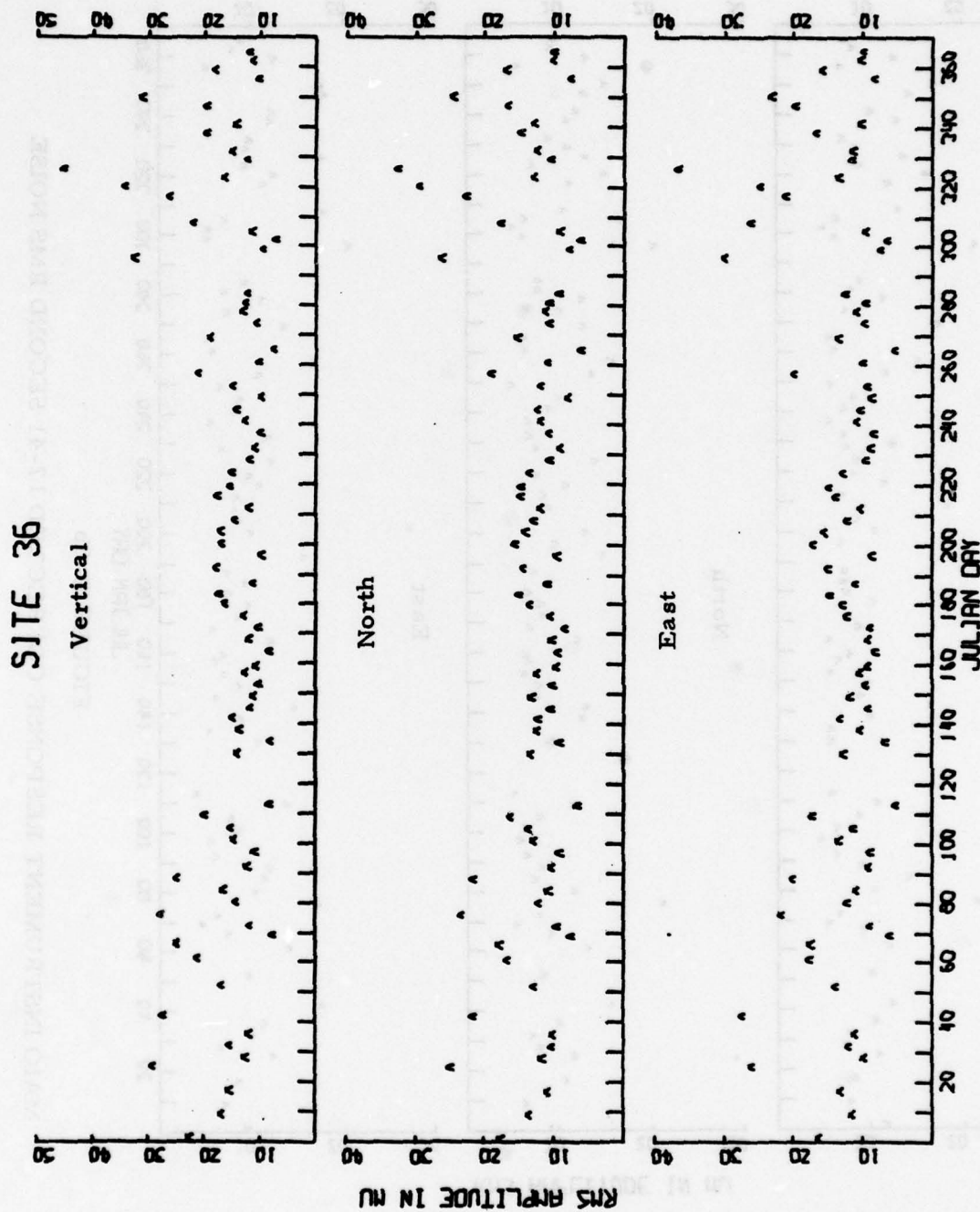
FIGURE B-3a

MAIO INSTRUMENT RESPONSE CORRECTED 10-25 SECOND RMS NOISE

SITE 36

Vertical

North

East

RMS AMPLITUDE IN mμ

JULIAN DAY

FIGURE B-3b

MAIO INSTRUMENT RESPONSE CORRECTED 17-41 SECOND RMS NOISE

SITE 36

Vertical

North

East

RHS AMPLITUDE IN MU

JULIAN DAY
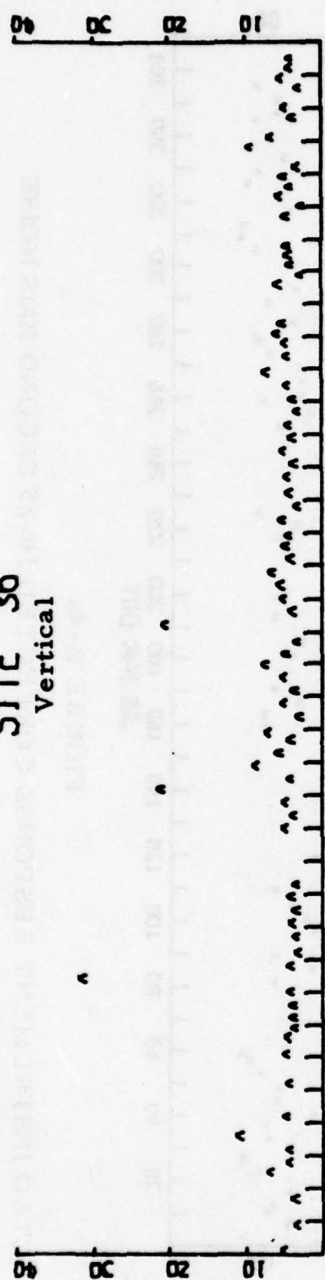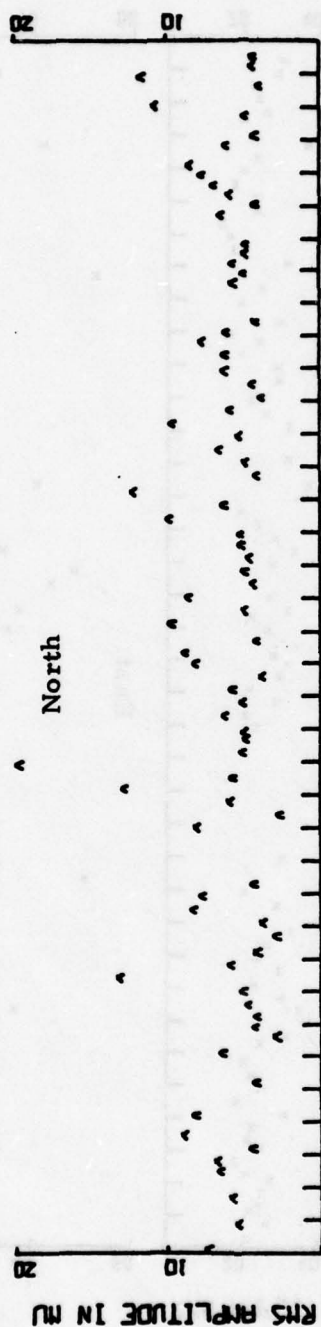
FIGURE B-3c

MAIO INSTRUMENT RESPONSE CORRECTED 40-64 SECOND RMS NOISE

B-11

SITE 50

Vertical

North

East

RMS AMPLITUDE IN MU

JULIAN DAY
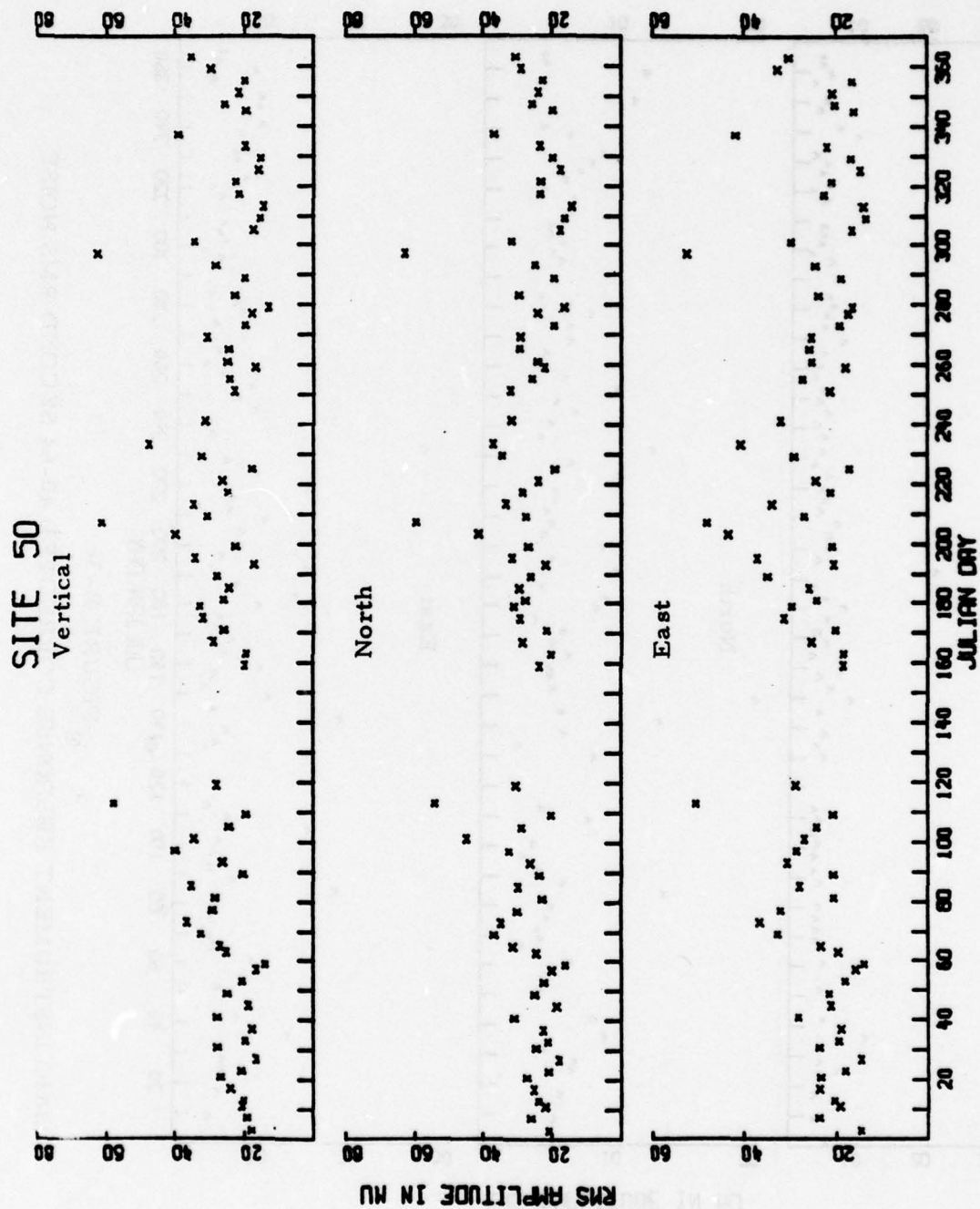
FIGURE B-4a

CTAO INSTRUMENT RESPONSE CORRECTED 10-25 SECOND RMS NOISE

SITE 50

Vertical

North

East

RMS AMPLITUDE IN MU

JULIAN DAY

FIGURE B-4b

CTAO INSTRUMENT RESPONSE CORRECTED 17-41 SECOND RMS NOISE

B-13

SITE 50

Vertical

North

East

RMS AMPLITUDE IN MU

JULIAN DAY

FIGURE B-4c

CTAO INSTRUMENT RESPONSE CORRECTED 40-64 SECOND RMS NOISE

SITE 51

Vertical

North

East

RMS AMPLITUDE IN MU
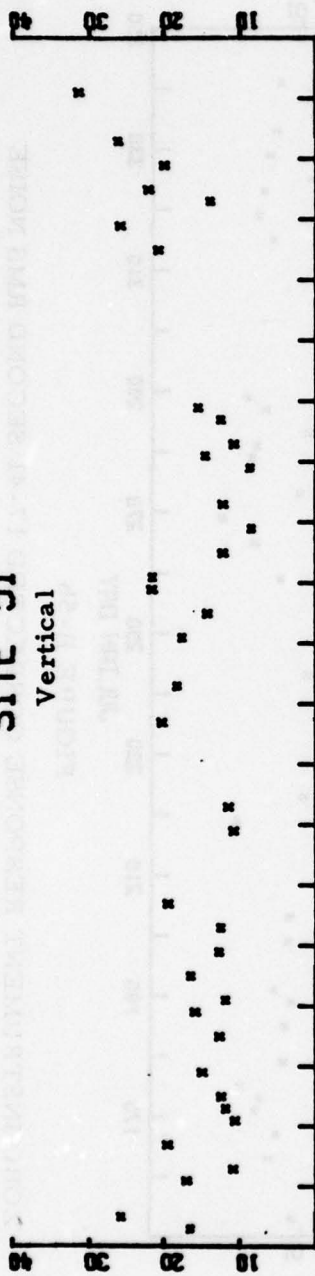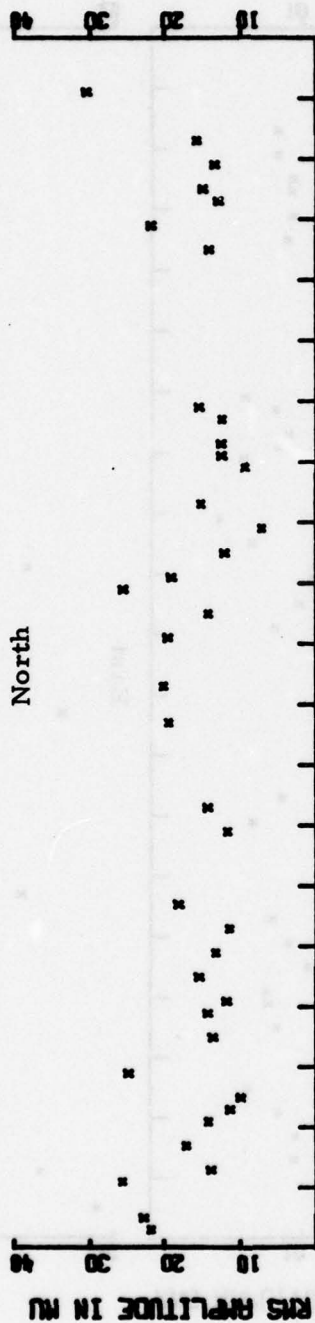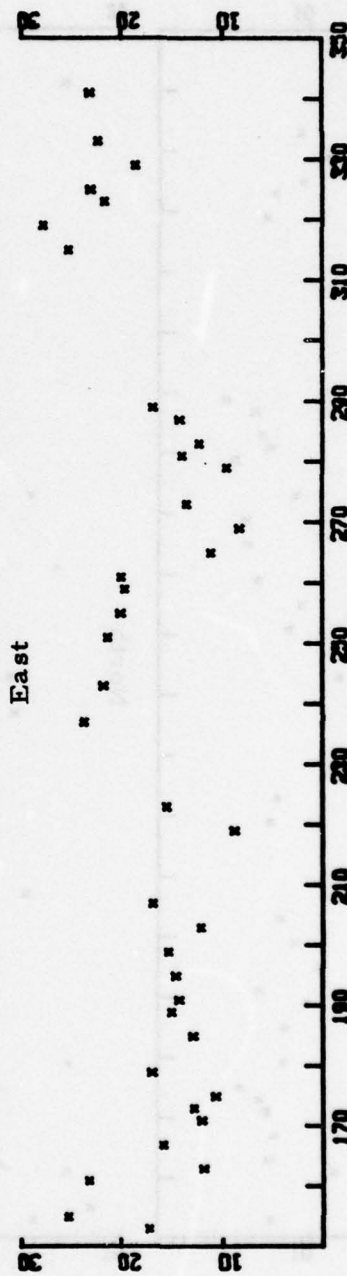
JULIAN DAY

FIGURE B-5a

ZOBO INSTRUMENT RESPONSE CORRECTED 10-25 SECOND RMS NOISE

B-15

SITE 51

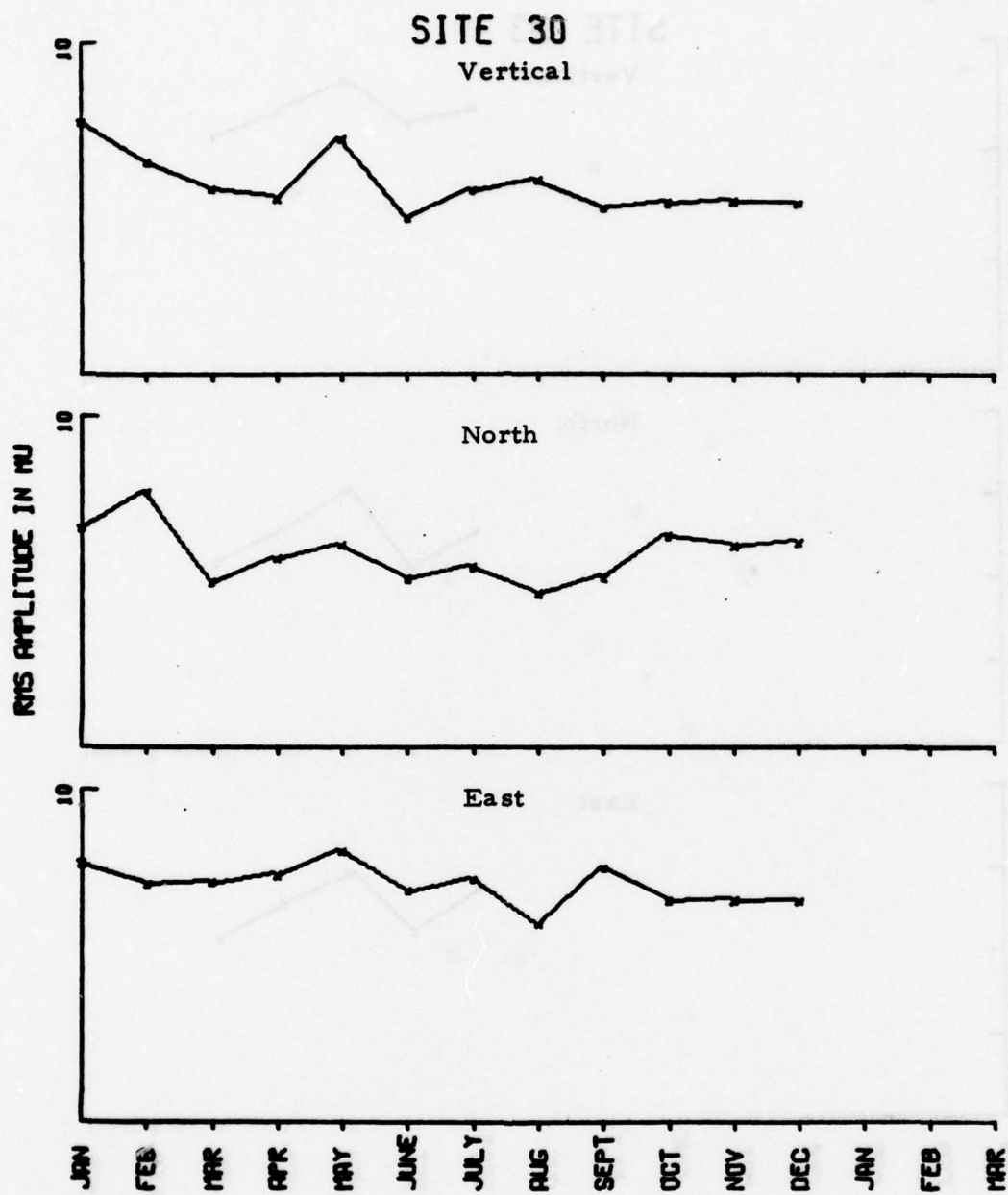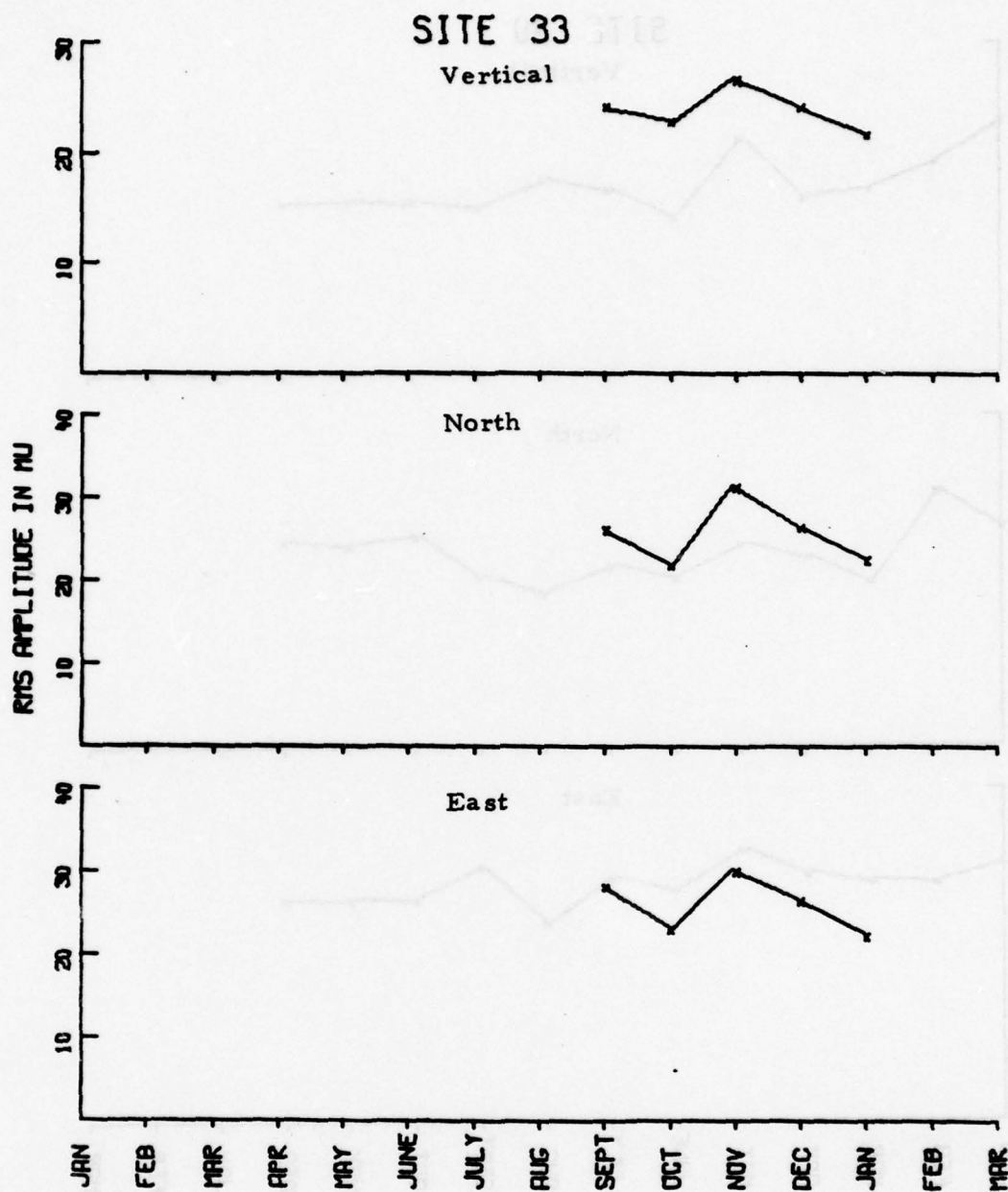ZOBO INSTRUMENT RESPONSE CORRECTED 17-41 SECOND RMS NOISE

FIGURE B-5b

SITE 51

Vertical

North

East

RMS AMPLITUDE IN MU

JULIAN DAY
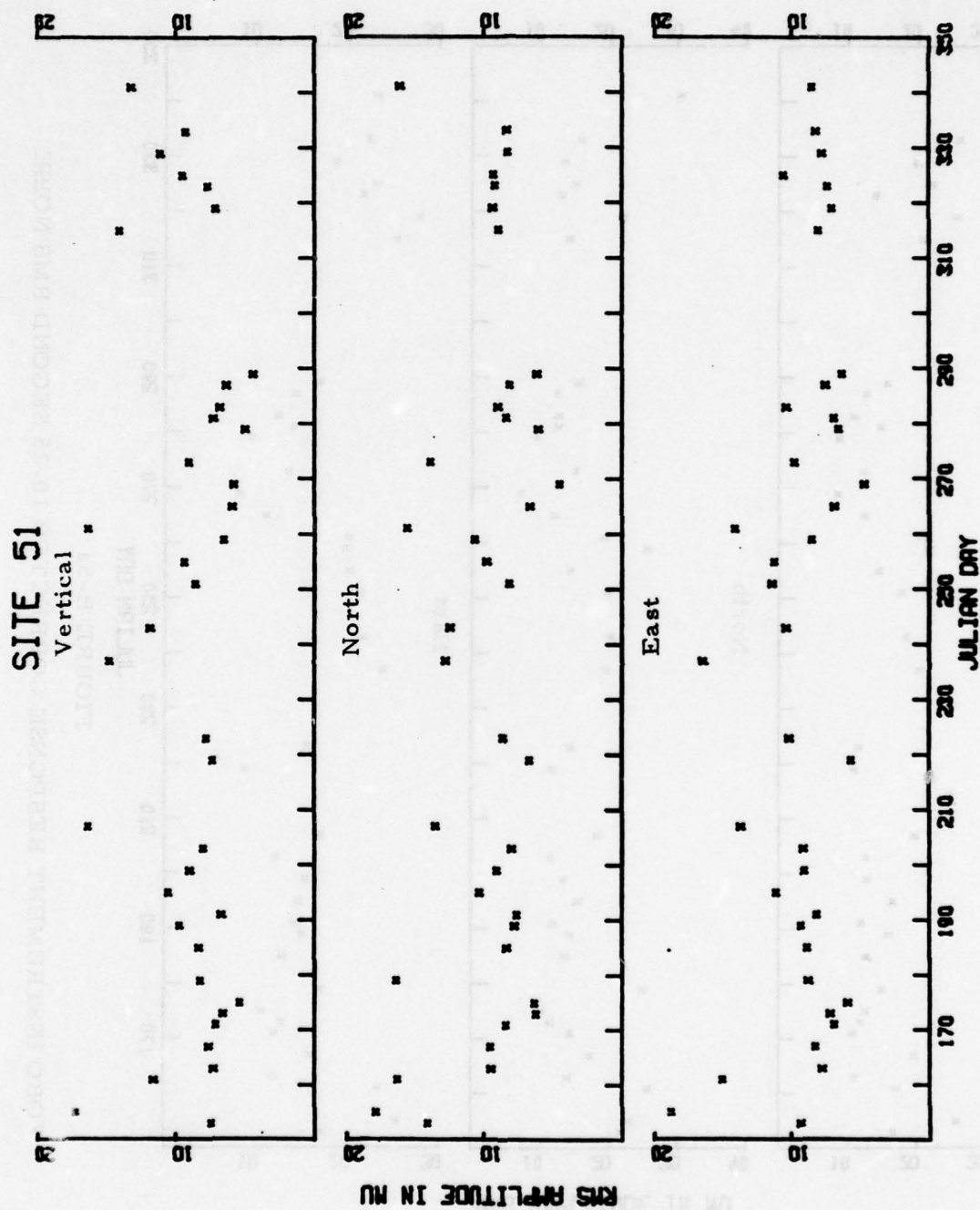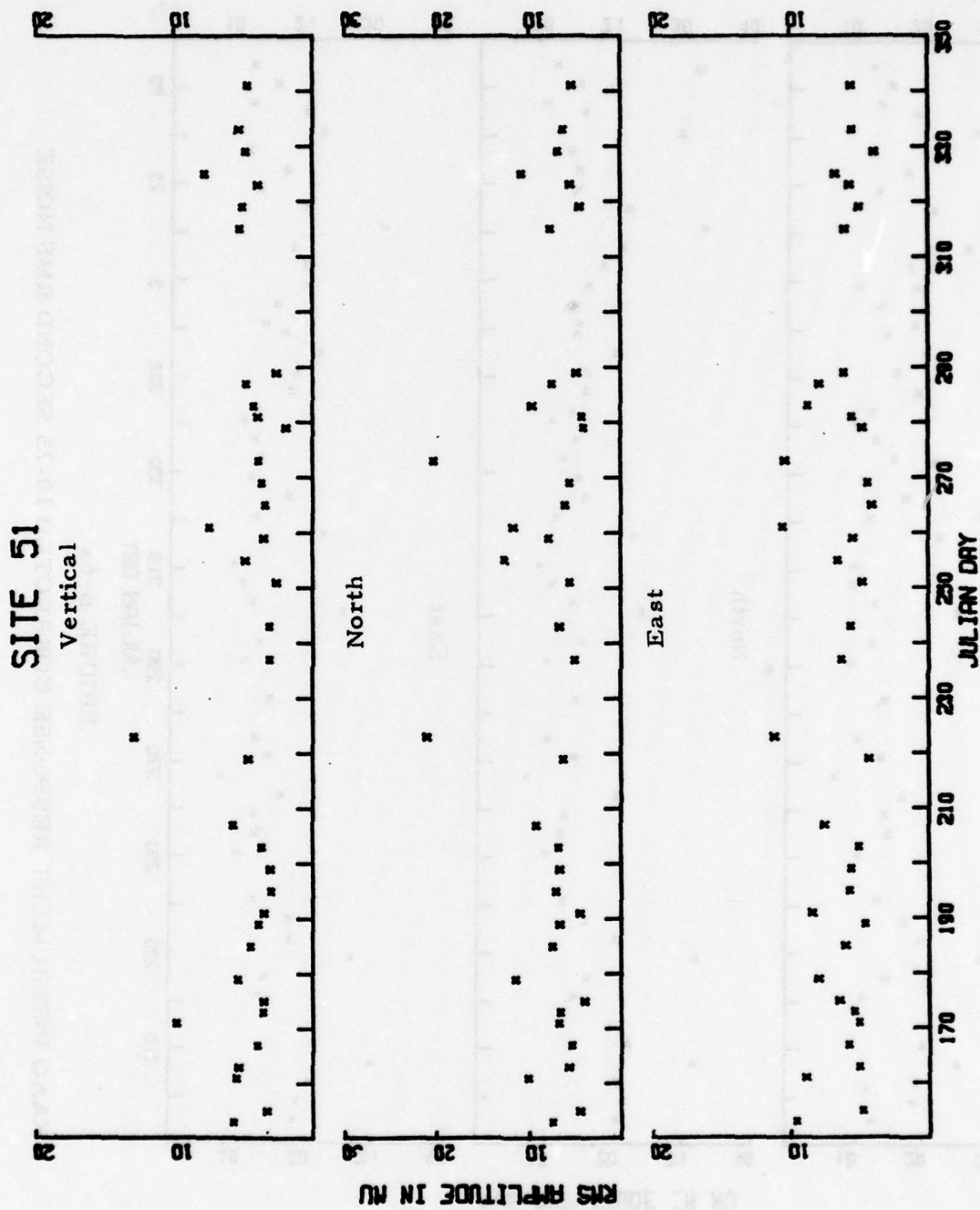
FIGURE B-5c

ZOBO INSTRUMENT RESPONSE CORRECTED 40-64 SECOND RMS NOISE

B-17

SITE 52
Vertical

North

East

RMS AMPLITUDE IN MU

JULIAN DAY
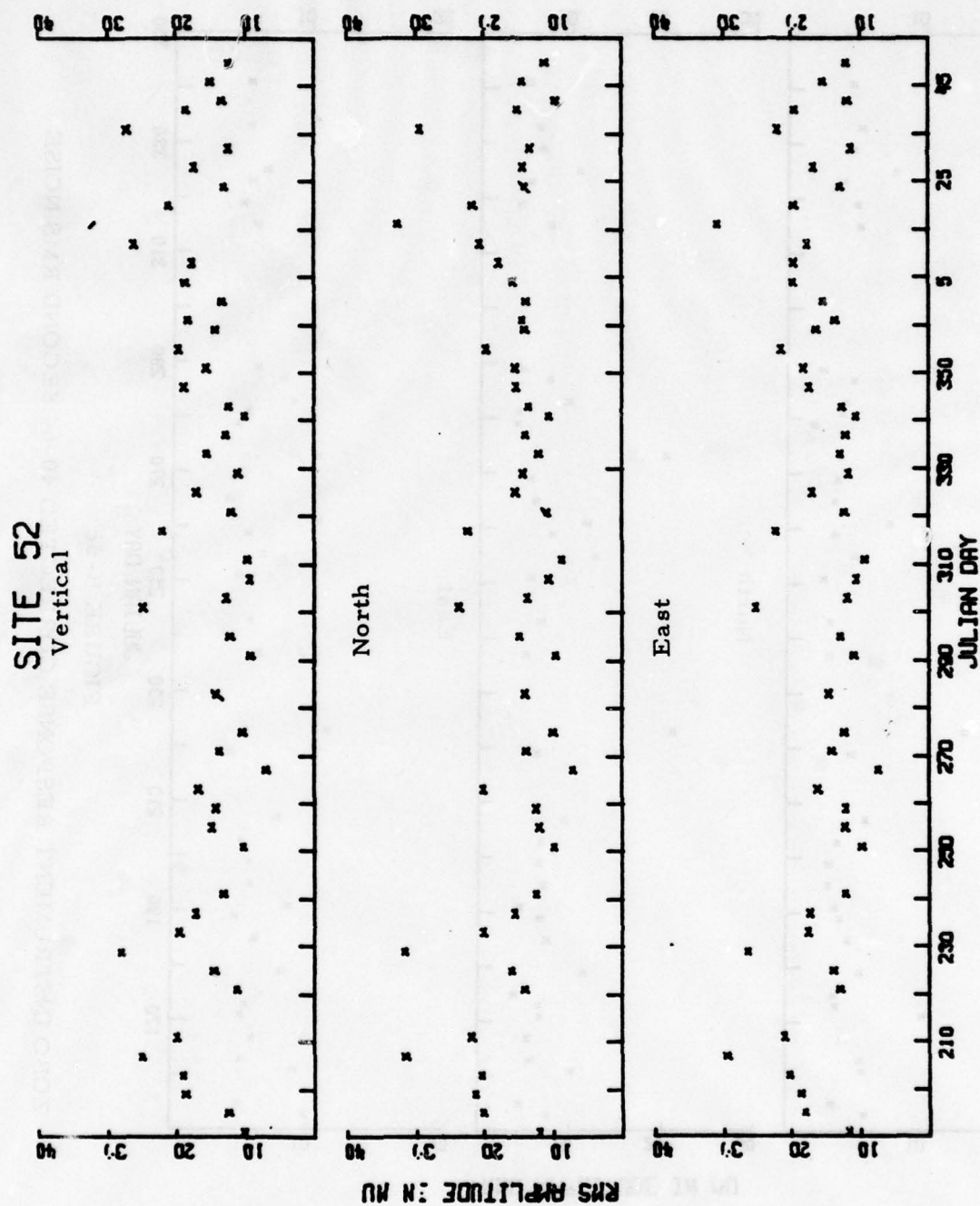
FIGURE B-6a

KAAO INSTRUMENT RESPONSE CORRECTED 10-25 SECOND RMS NOISE

B-18

SITE 52

Vertical

North

East

RMS AMPLITUDE IN MU

JULIAN DAY
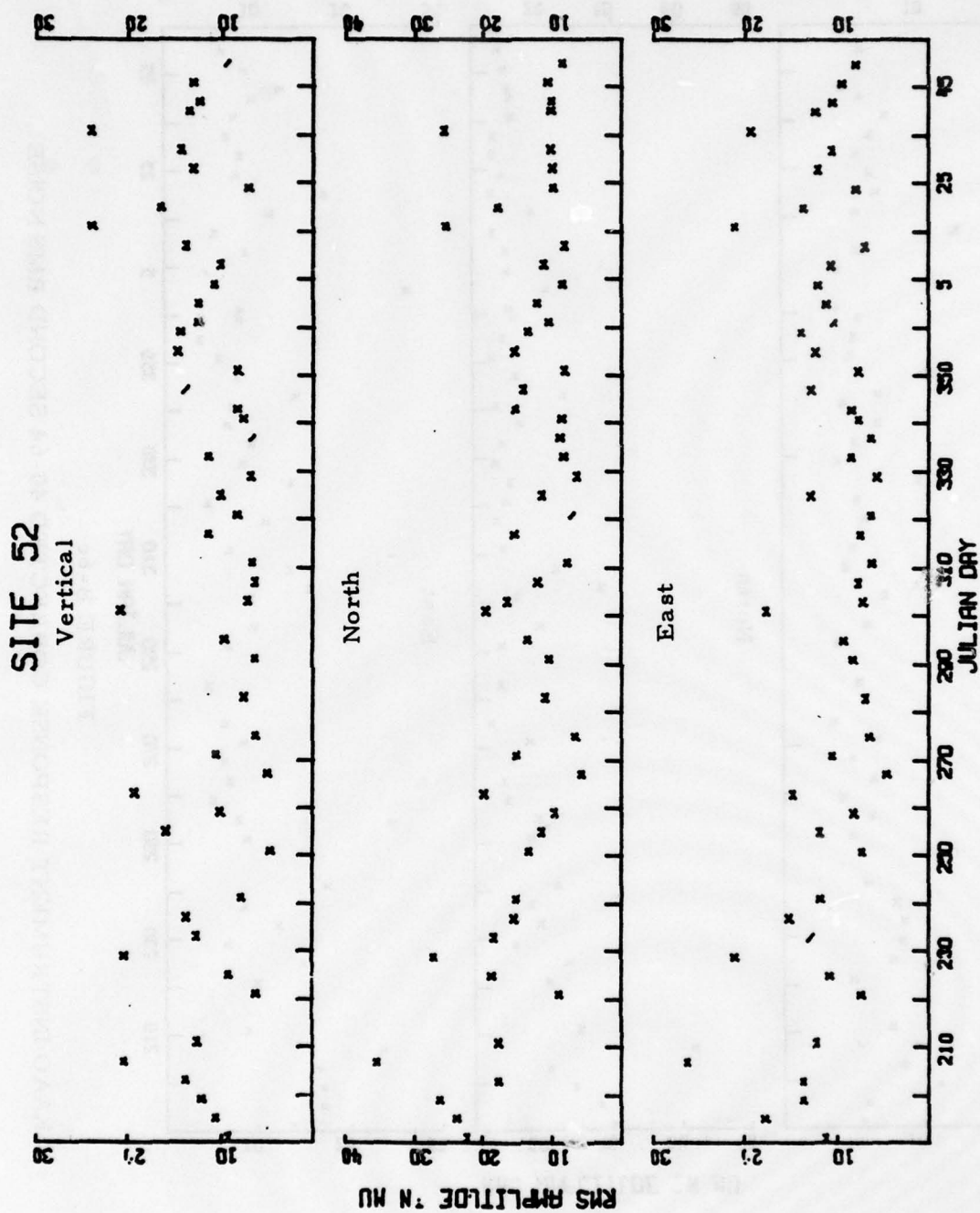
FIGURE B-6b

KAAO INSTRUMENT RESPONSE CORRECTED 17-41 SECOND RMS NOISE

B-19

SITE 52

Vertical

North

East

RMS AMPLITUDE IN MU

JULIAN DAY
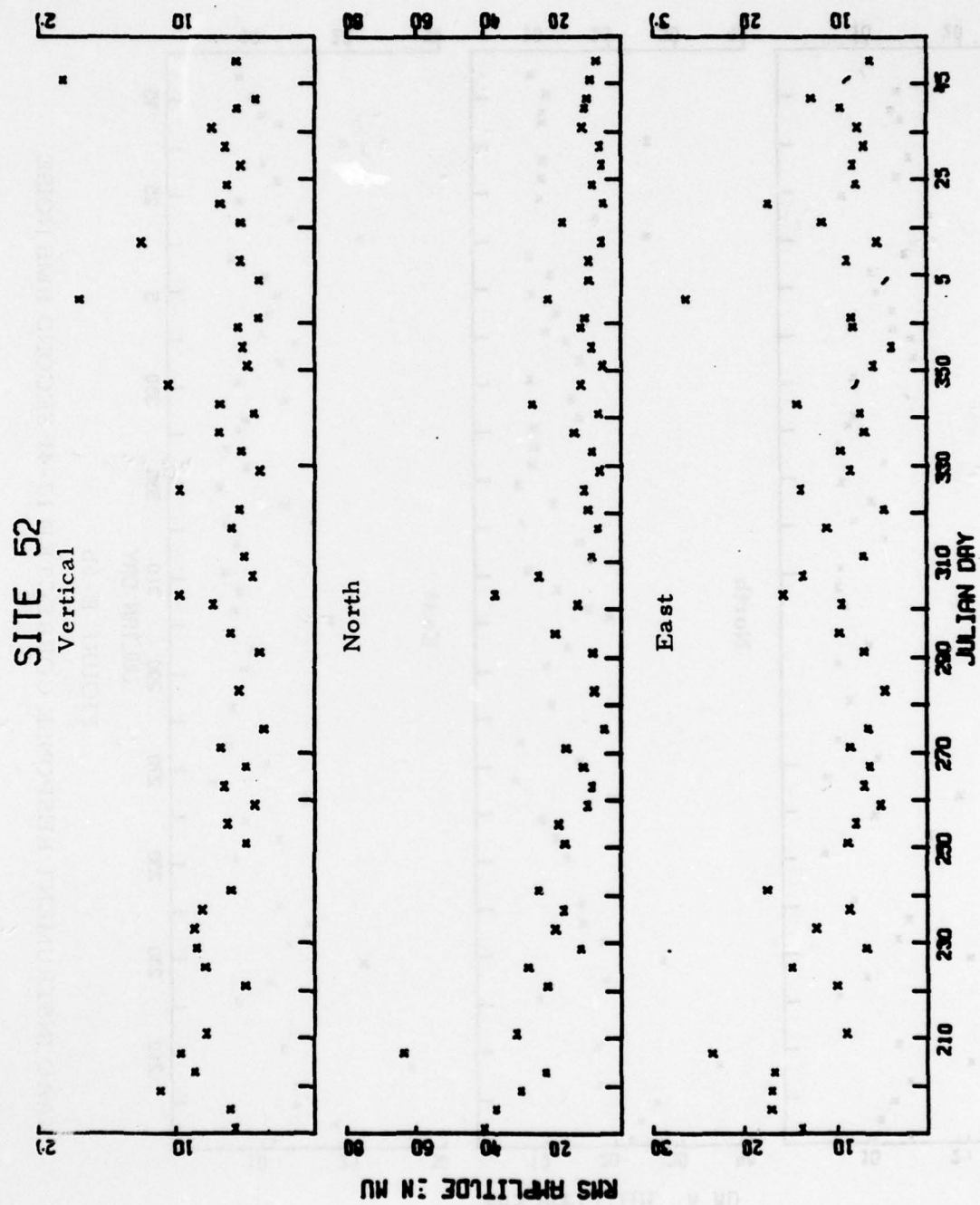
FIGURE B-6c

KAAO INSTRUMENT RESPONSE CORRECTED 40-64 SECOND RMS NOISE

SITE 30

Vertical

North

East
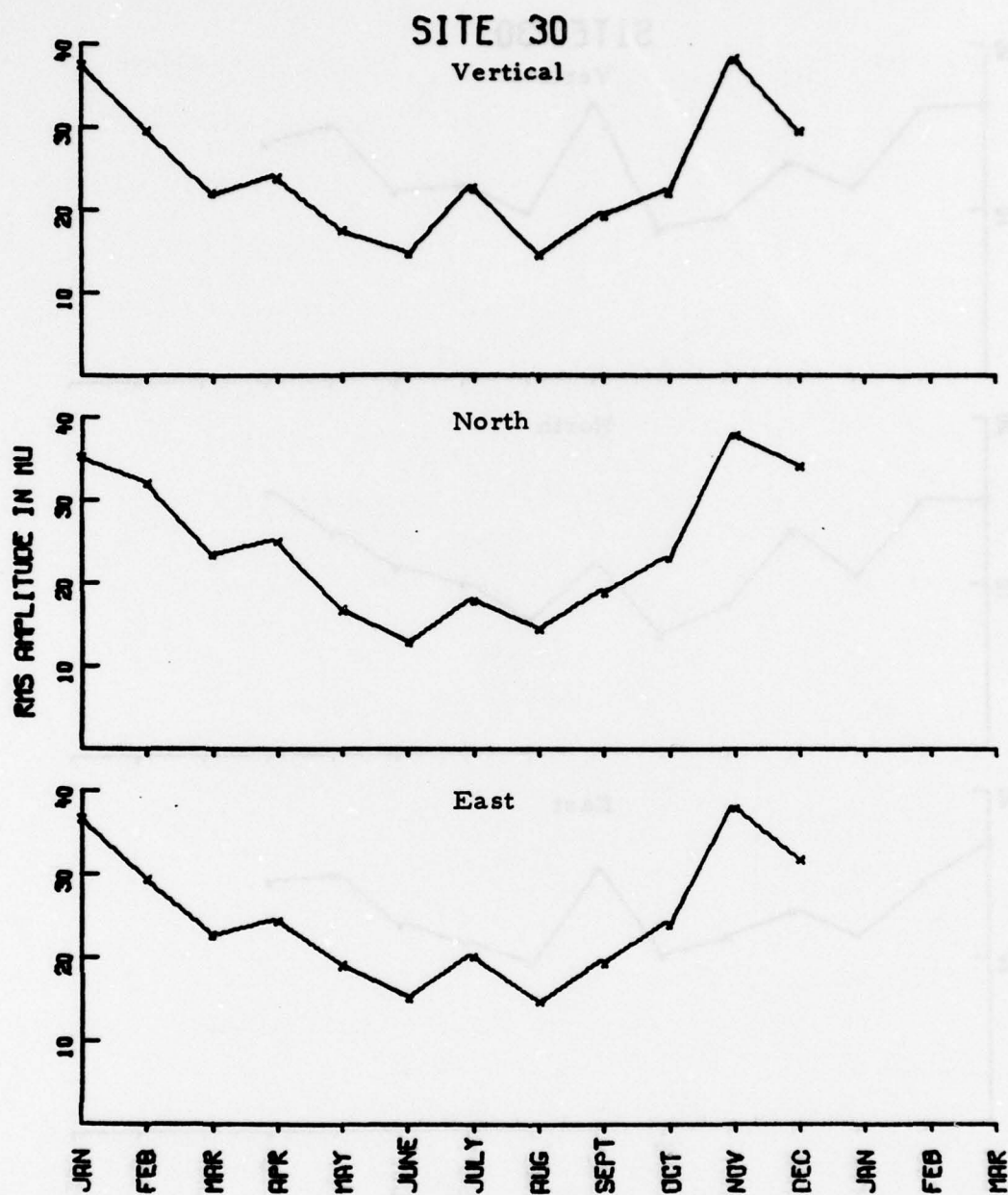
FIGURE B-7a

ANMO INSTRUMENT RESPONSE CORRECTED 10-25 SECOND
RMS NOISE TRENDS

B-21

SITE 30
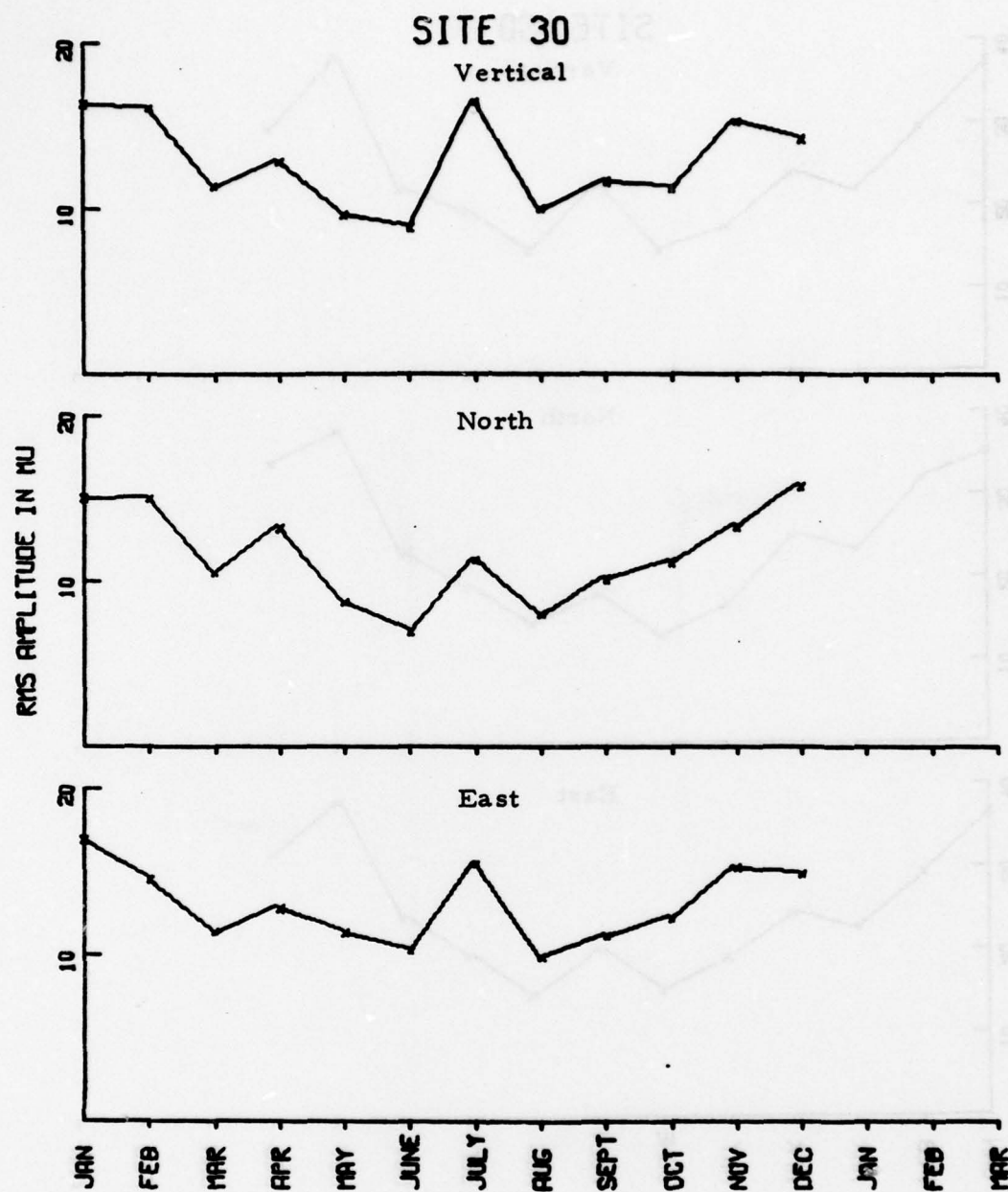
FIGURE B-7b

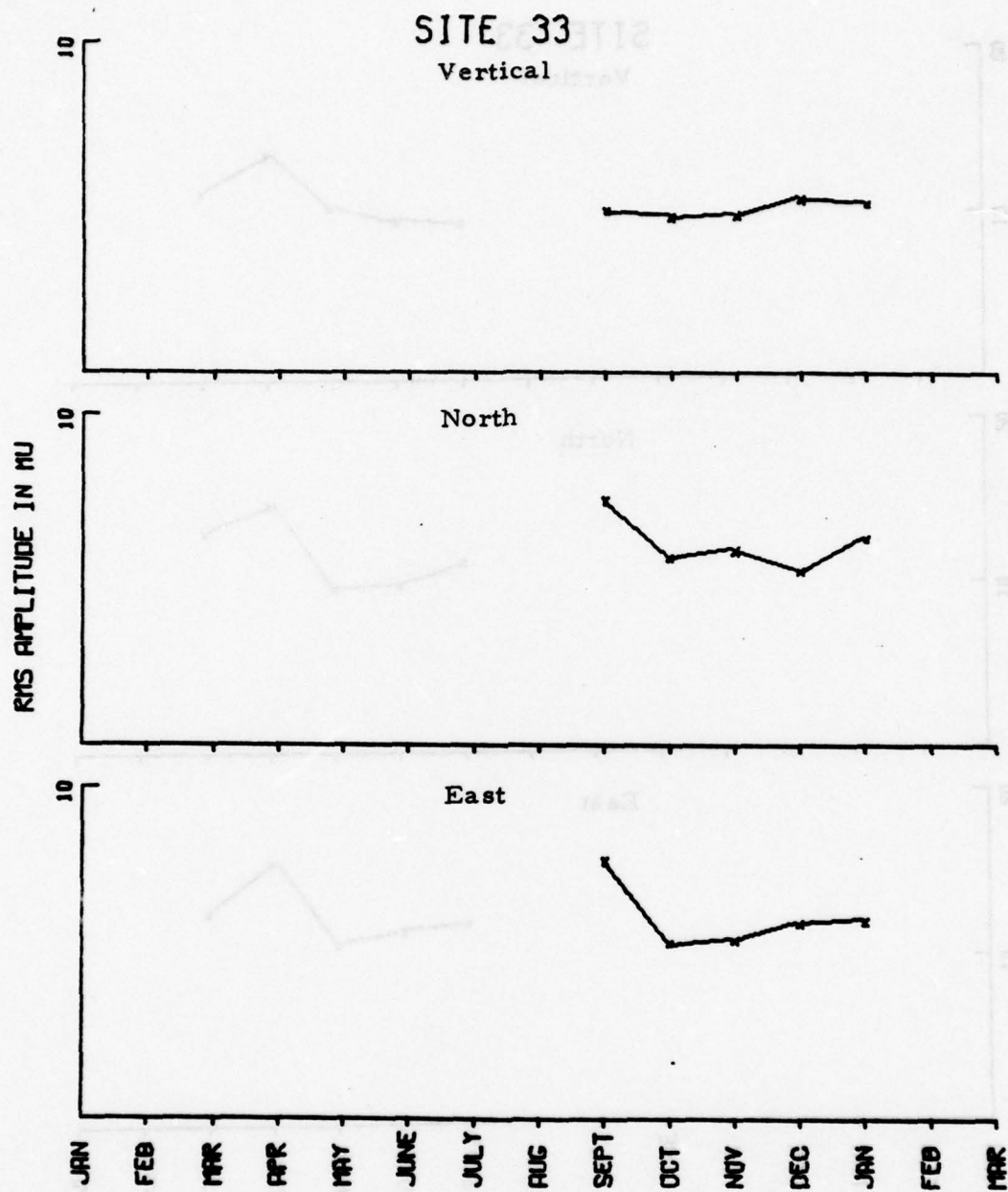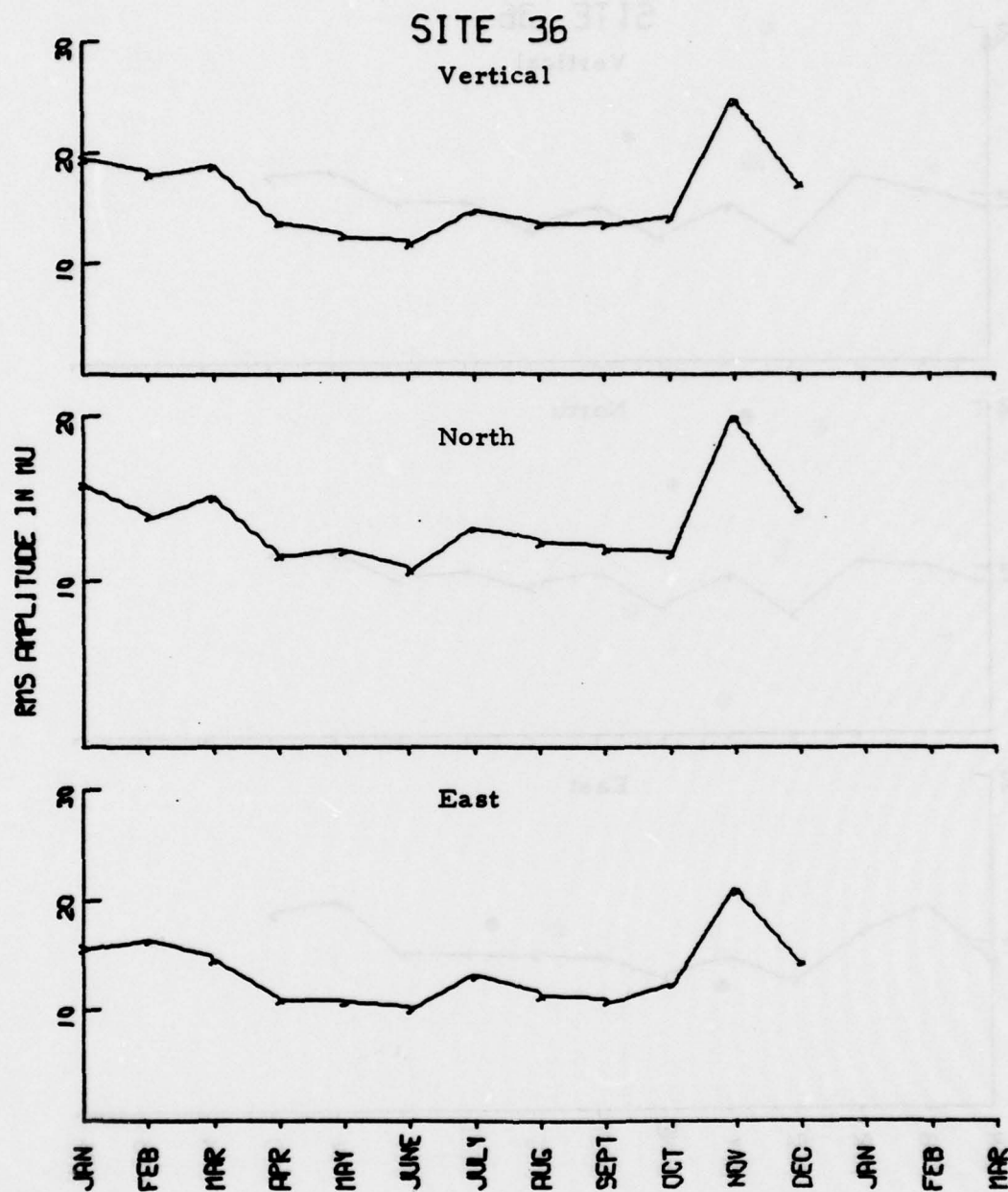ANMO INSTRUMENT RESPONSE CORRECTED 17-41 SECOND
RMS NOISE TRENDS

B-22

SITE 30

Vertical

North

East

FIGURE B-7c

ANMO INSTRUMENT RESPONSE CORRECTED 40-64 SECOND
RMS NOISE TRENDS

B-23

SITE 33

FIGURE B-8a

CHTO INSTRUMENT RESPONSE CORRECTED 10-25 SECOND
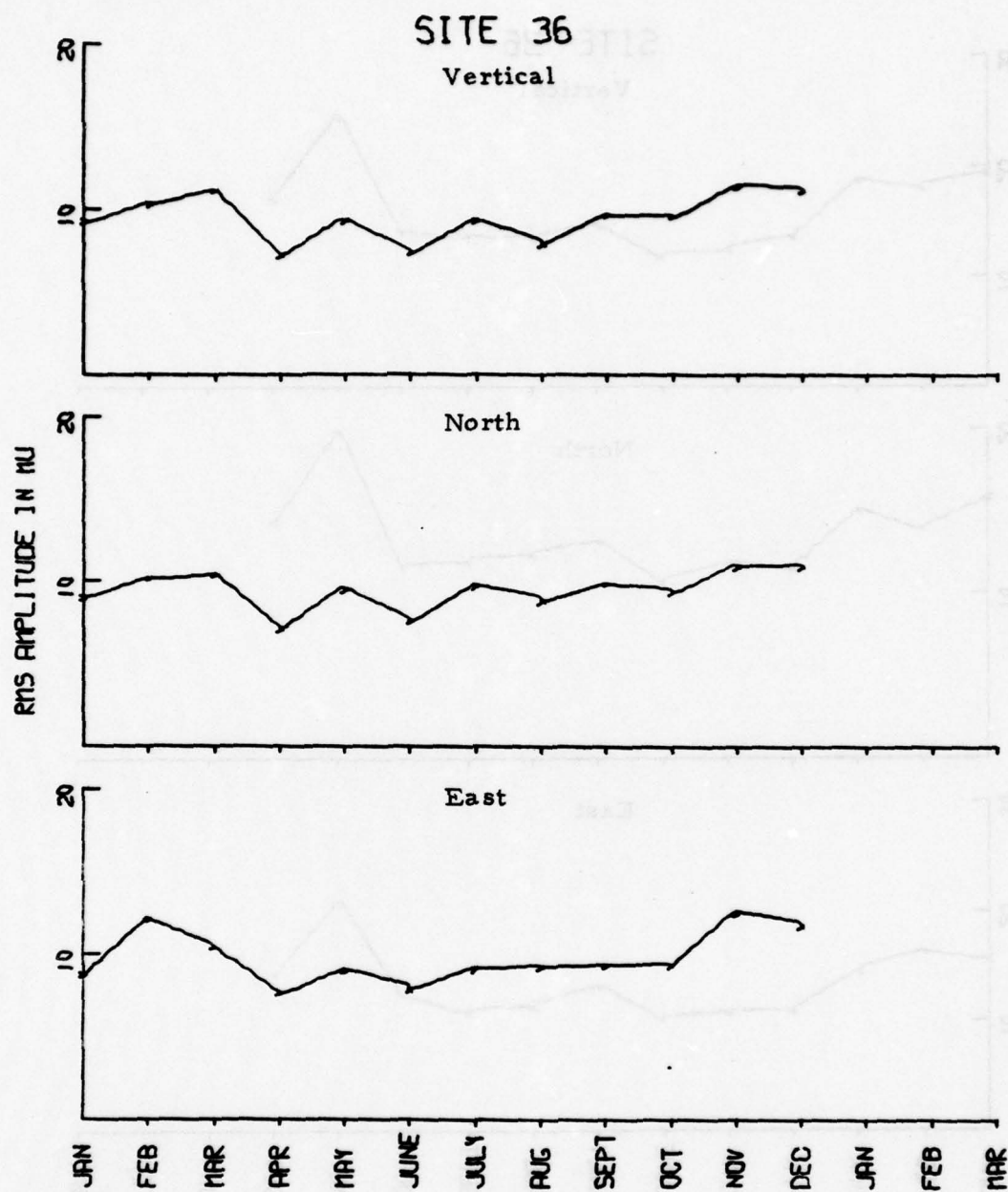RMS NOISE TRENDS

SITE 33
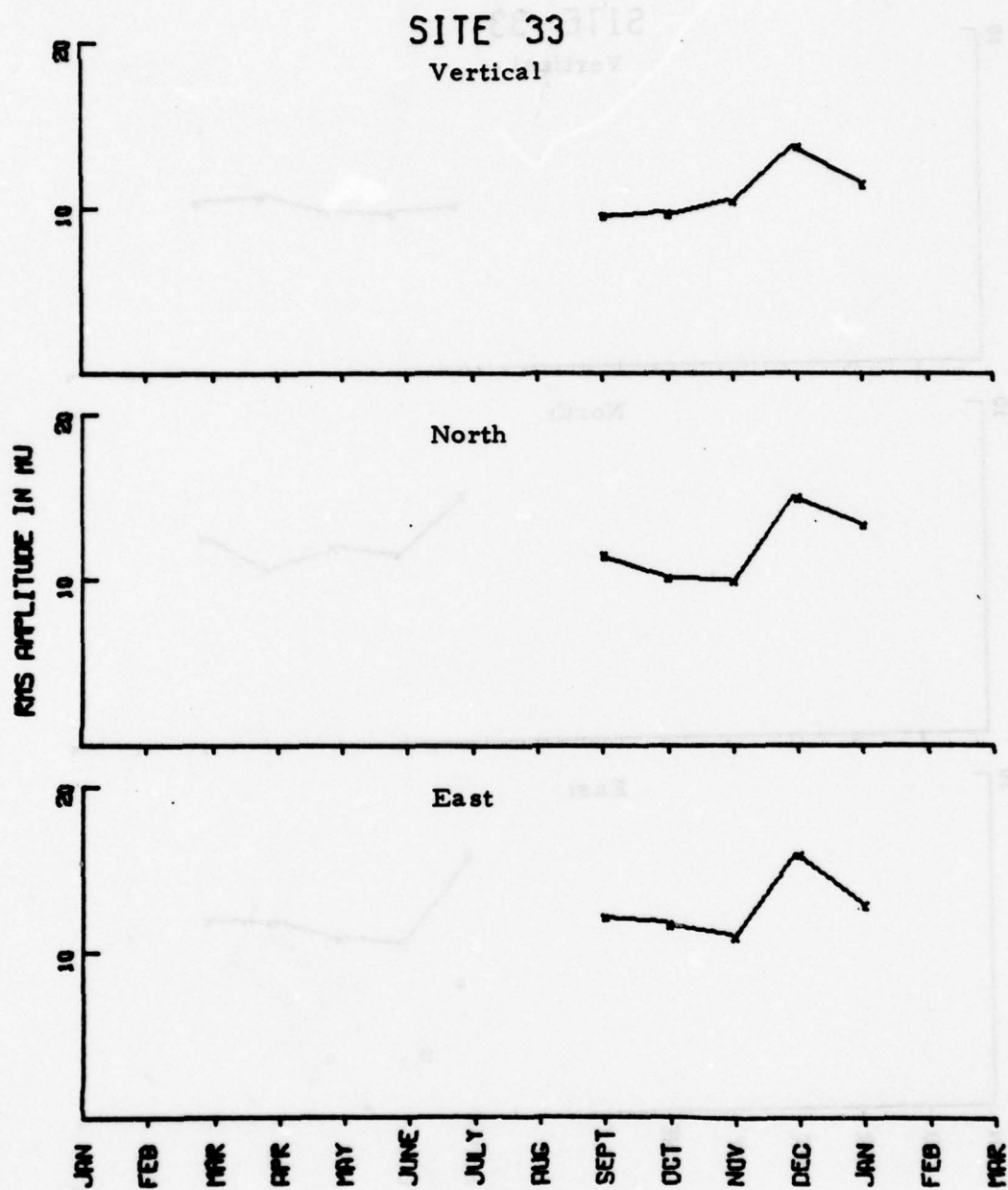
FIGURE B-8b

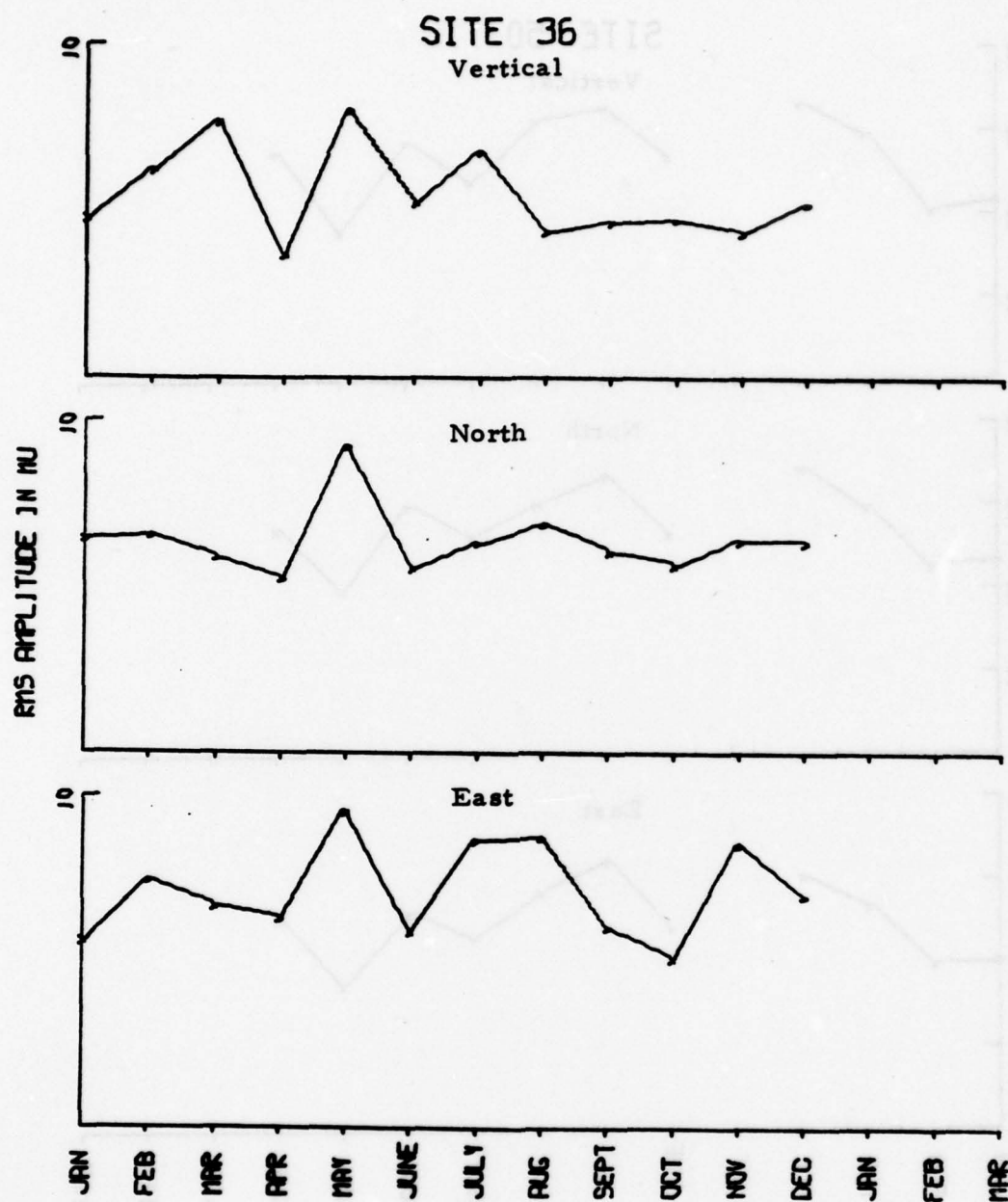CHTO INSTRUMENT RESPONSE CORRECTED 17-41 SECOND
RMS NOISE TRENDS

B-25

SITE 33

Vertical

North

East

RMS AMPLITUDE IN MU

JAN FEB MAR APR MAY JUNE JULY AUG SEPT OCT NOV DEC JAN FEB MAR

FIGURE B-8c

CHTO INSTRUMENT RESPONSE CORRECTED 40-64 SECOND
RMS NOISE TRENDS

B-26

SITE 36

Vertical

North

East

RMS AMPLITUDE IN MU

JAN FEB MAR APR MAY JUNE JULY AUG SEPT OCT NOV DEC JAN FEB MAR

FIGURE B-9a

MAIO INSTRUMENT RESPONSE CORRECTED 10-25 SECOND
RMS NOISE TRENDS

B-27

FIGURE B-9b

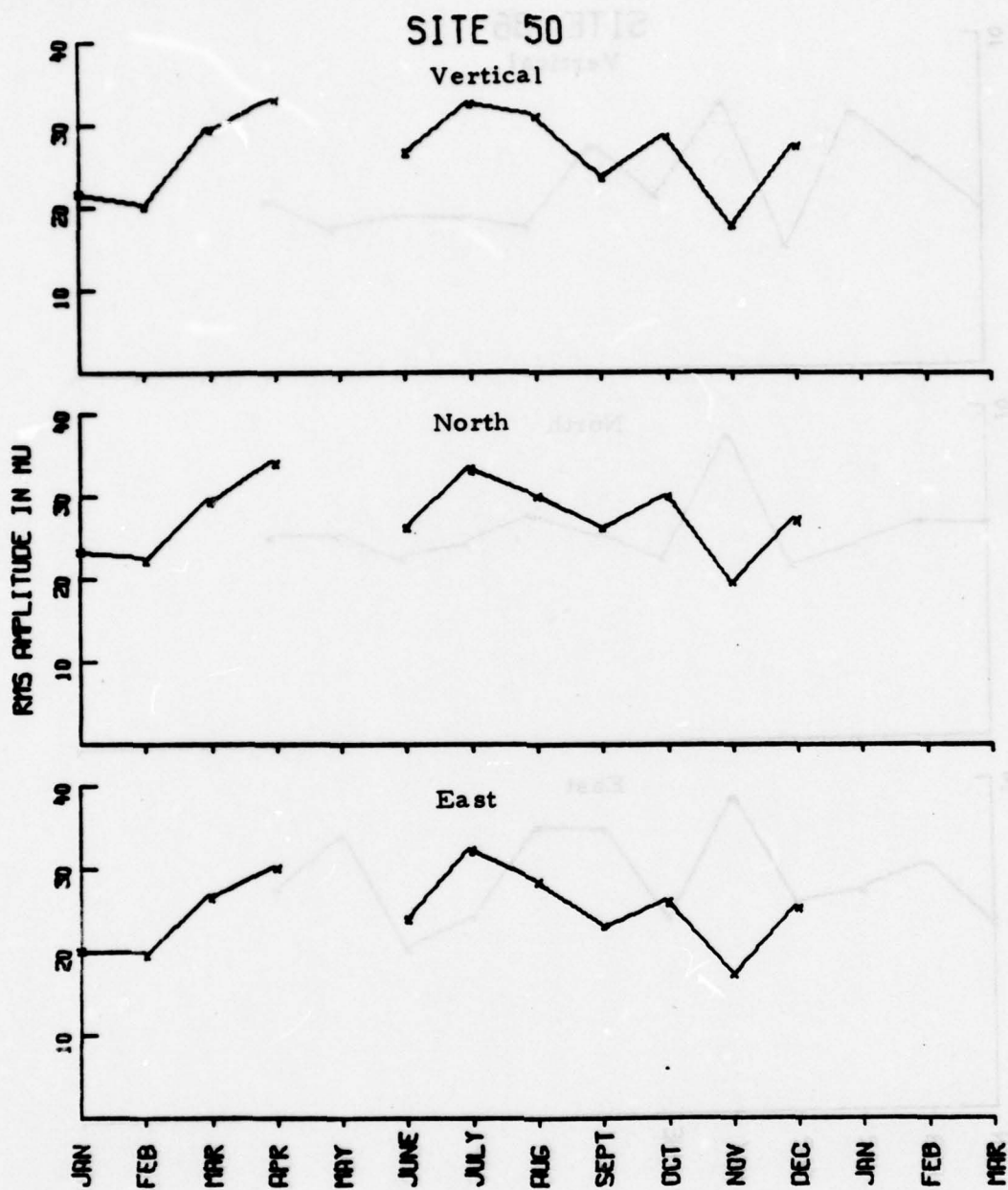MAIO INSTRUMENT RESPONSE CORRECTED 17-41 SECOND
RMS NOISE TRENDS

SITE 36

Vertical

North

East

RMS AMPLITUDE IN MU

JAN FEB MAR APR MAY JUNE JULY AUG SEPT OCT NOV DEC JAN FEB MAR

FIGURE B-9c

MAIO INSTRUMENT RESPONSE CORRECTED 40-64 SECOND
RMS NOISE TRENDS

B-29

FIGURE B-10a

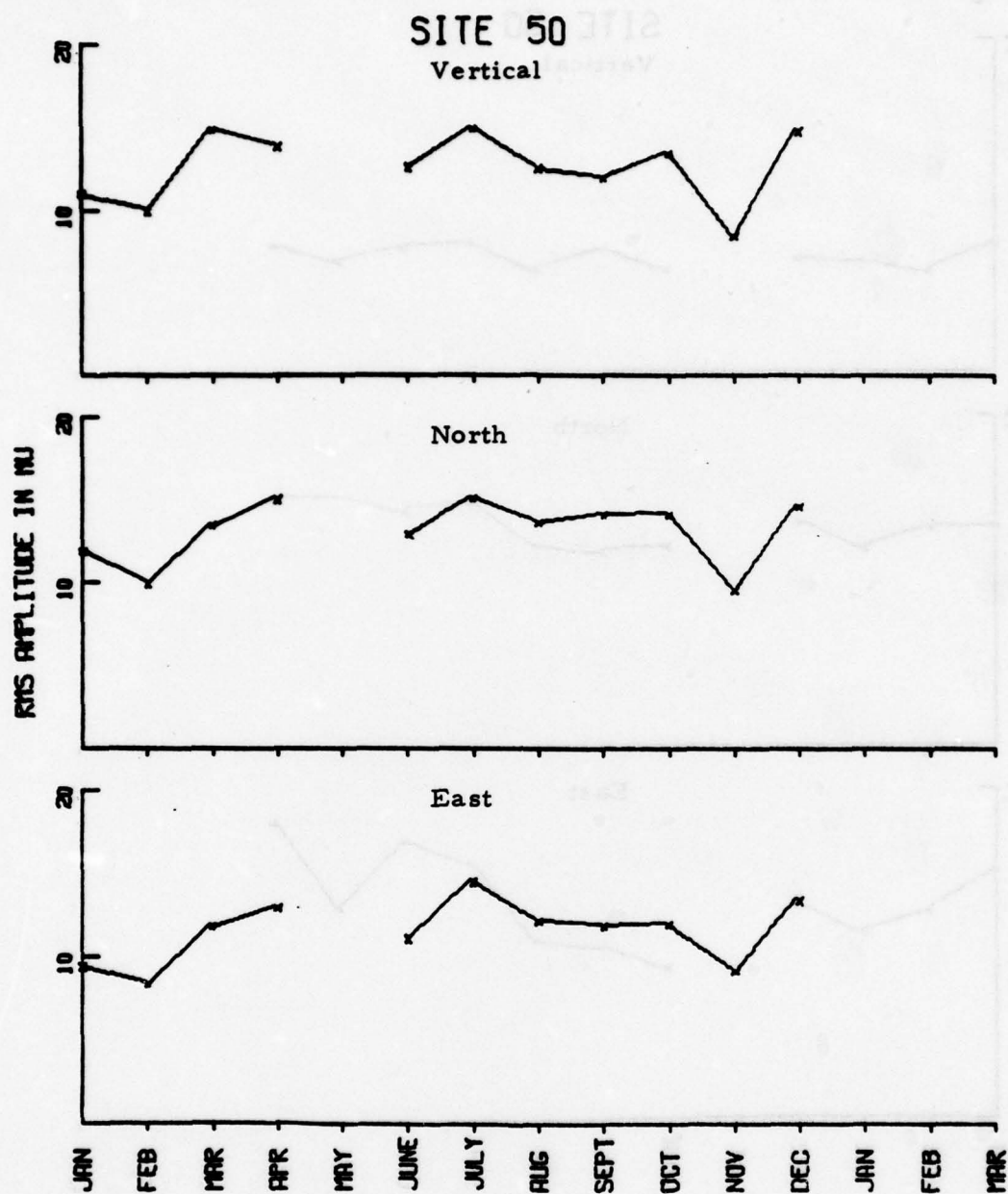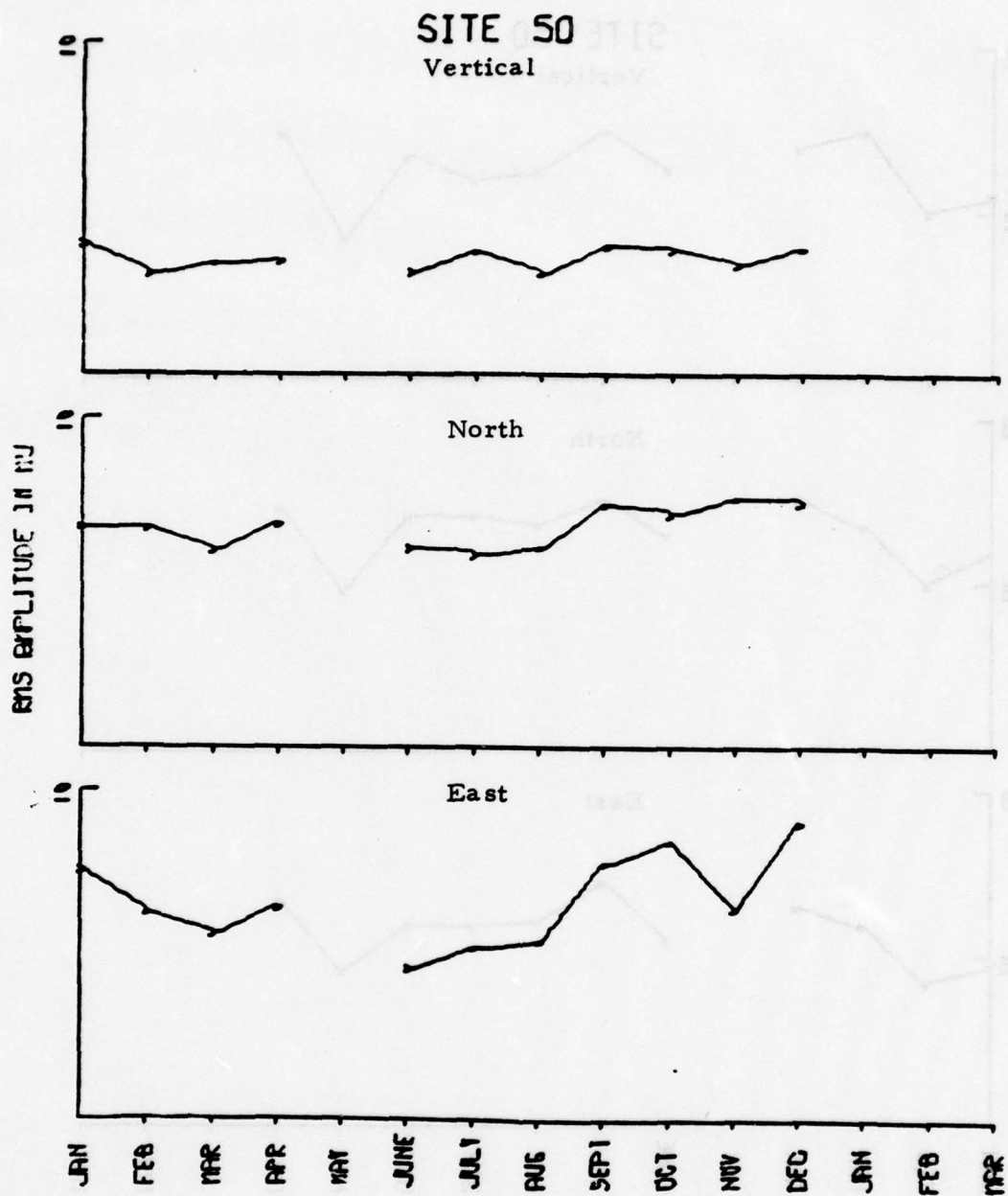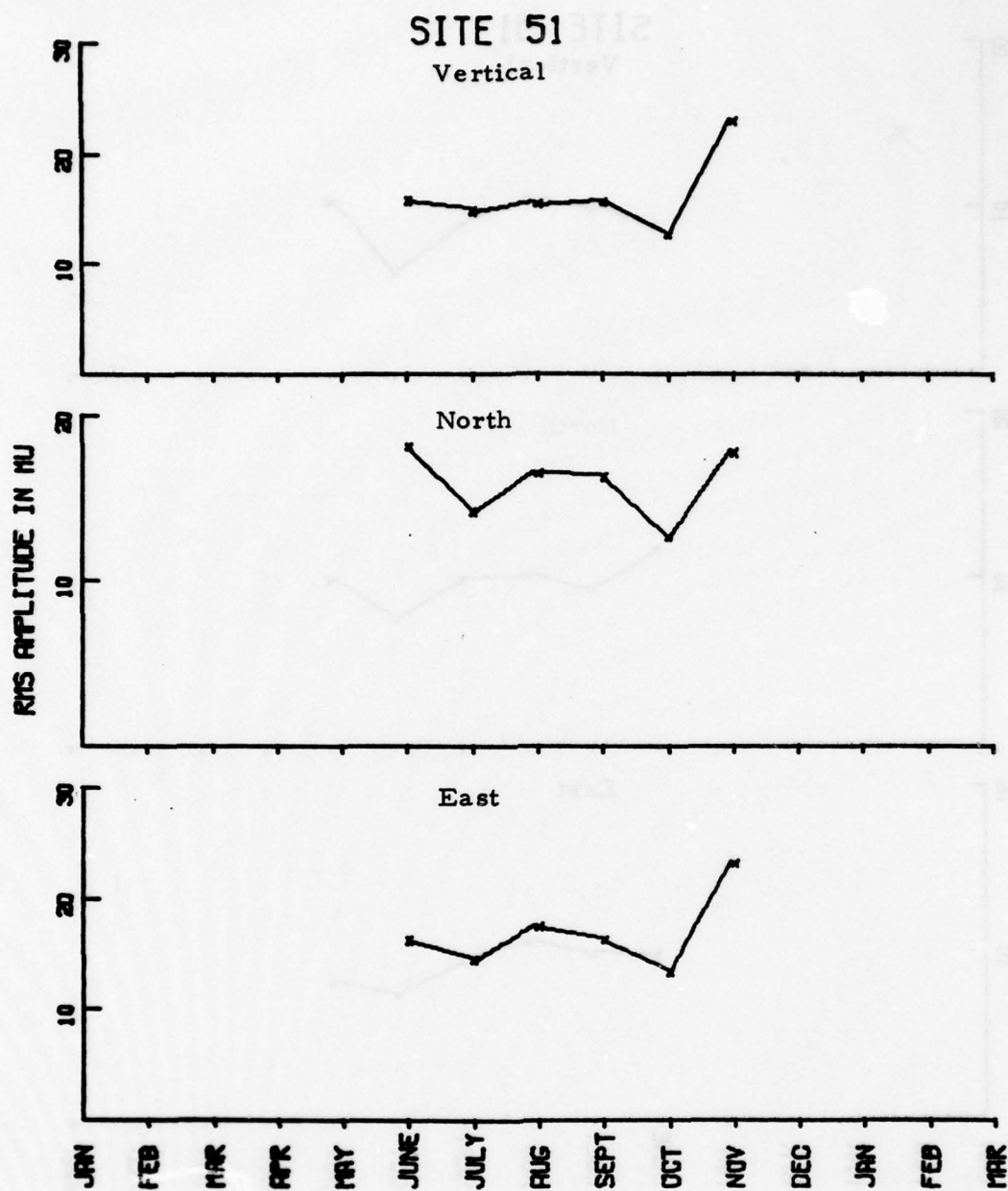CTAO INSTRUMENT RESPONSE CORRECTED 10-25 SECOND
RMS NOISE TRENDS

B-30

SITE 50

Vertical

North

East

RMS AMPLITUDE IN MU

JAN FEB MAR APR MAY JUNE JULY AUG SEPT OCT NOV DEC JAN FEB MAR

FIGURE B-10b

CTAO INSTRUMENT RESPONSE CORRECTED 17-41 SECOND
RMS NOISE TRENDS

B-31

SITE 50

Vertical

North

East

RMS AMPLITUDE IN mμ

JAN FEB MAR APR MAY JUNE JULY AUG SEPT OCT NOV DEC JAN FEB MAR

FIGURE B-10c

CTAO INSTRUMENT RESPONSE CORRECTED 40-64 SECOND
RMS NOISE TRENDS

B-32

FIGURE B-11a

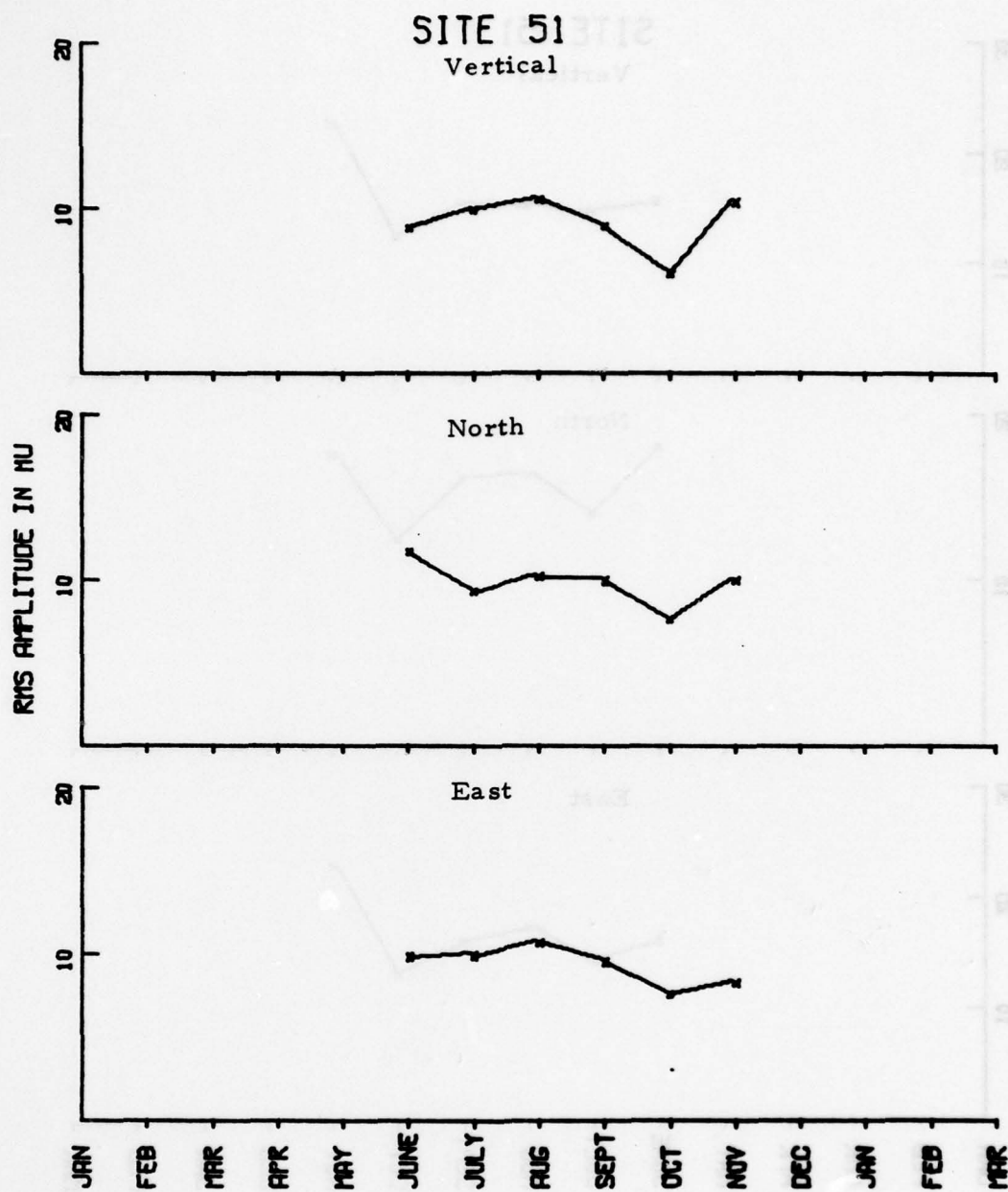ZOBO INSTRUMENT RESPONSE CORRECTED 10-25 SECOND
RMS NOISE TRENDS

B-33

FIGURE B-11b

ZOBO INSTRUMENT RESPONSE CORRECTED 17-41 SECOND
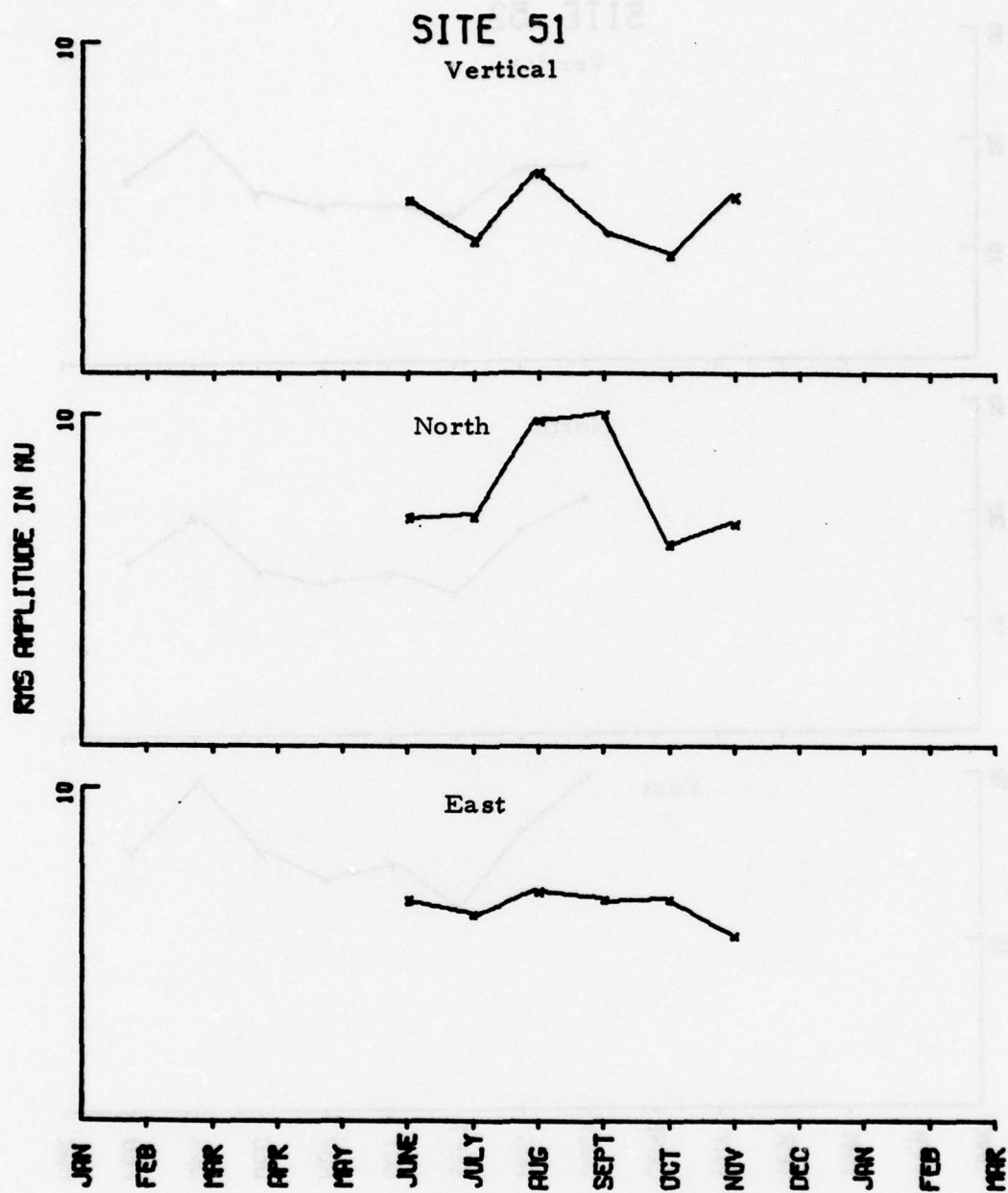RMS NOISE TRENDS

FIGURE B-11c

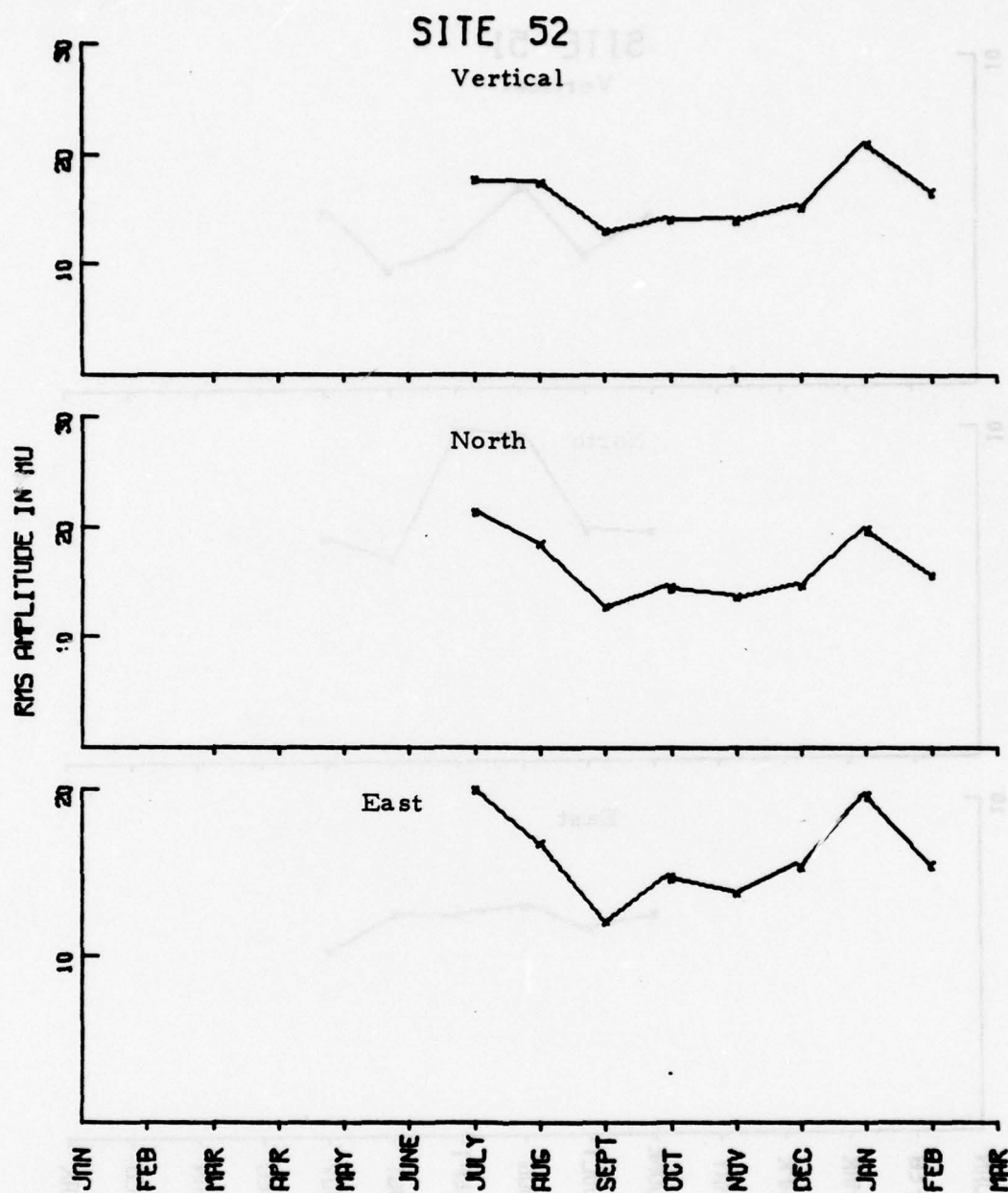ZOBO INSTRUMENT RESPONSE CORRECTED 40-64 SECOND
RMS NOISE TRENDS

FIGURE B-12a

KAAO INSTRUMENT RESPONSE CORRECTED 10-25 SECOND
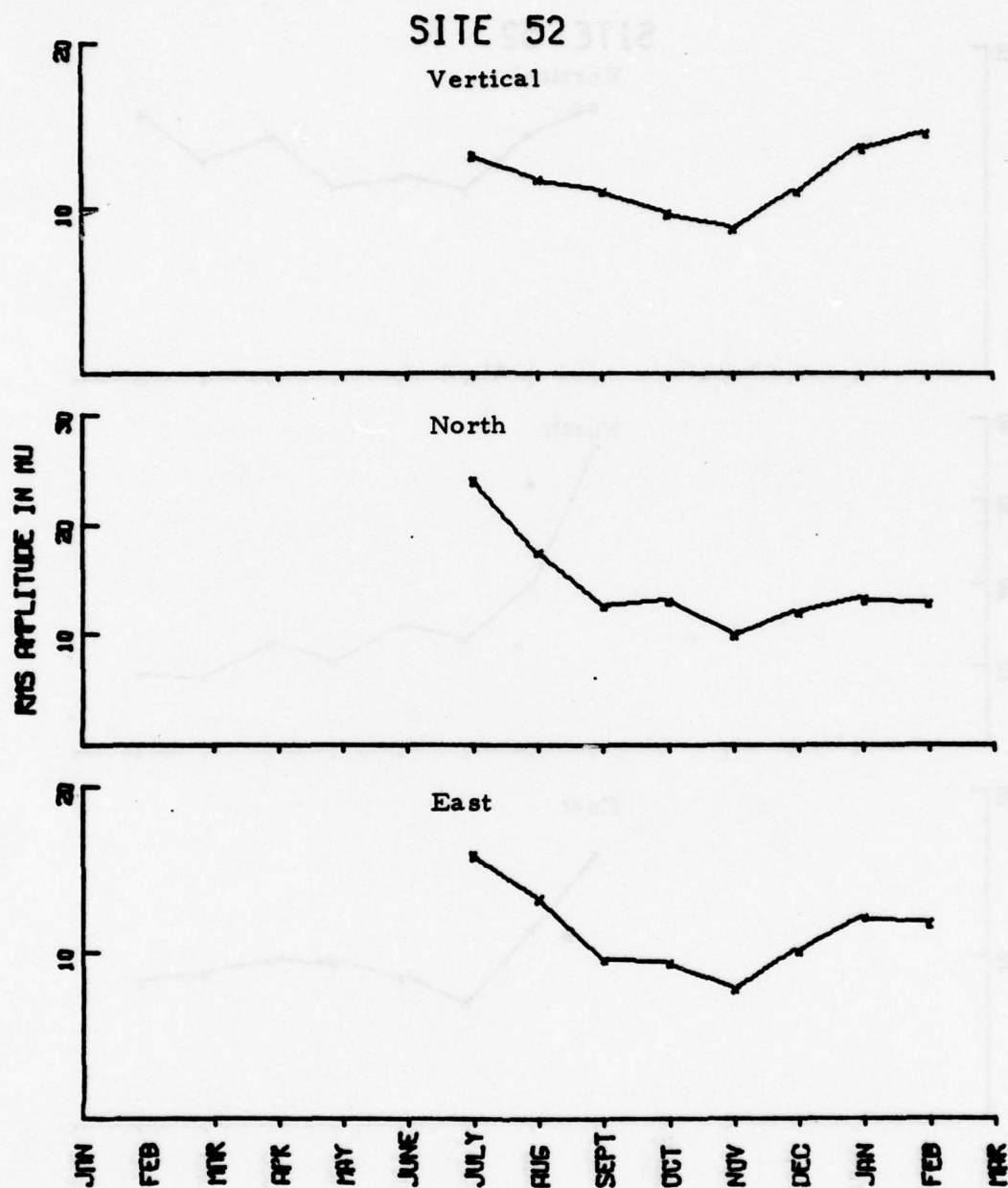RMS NOISE TRENDS

SITE 52

FIGURE B-12b
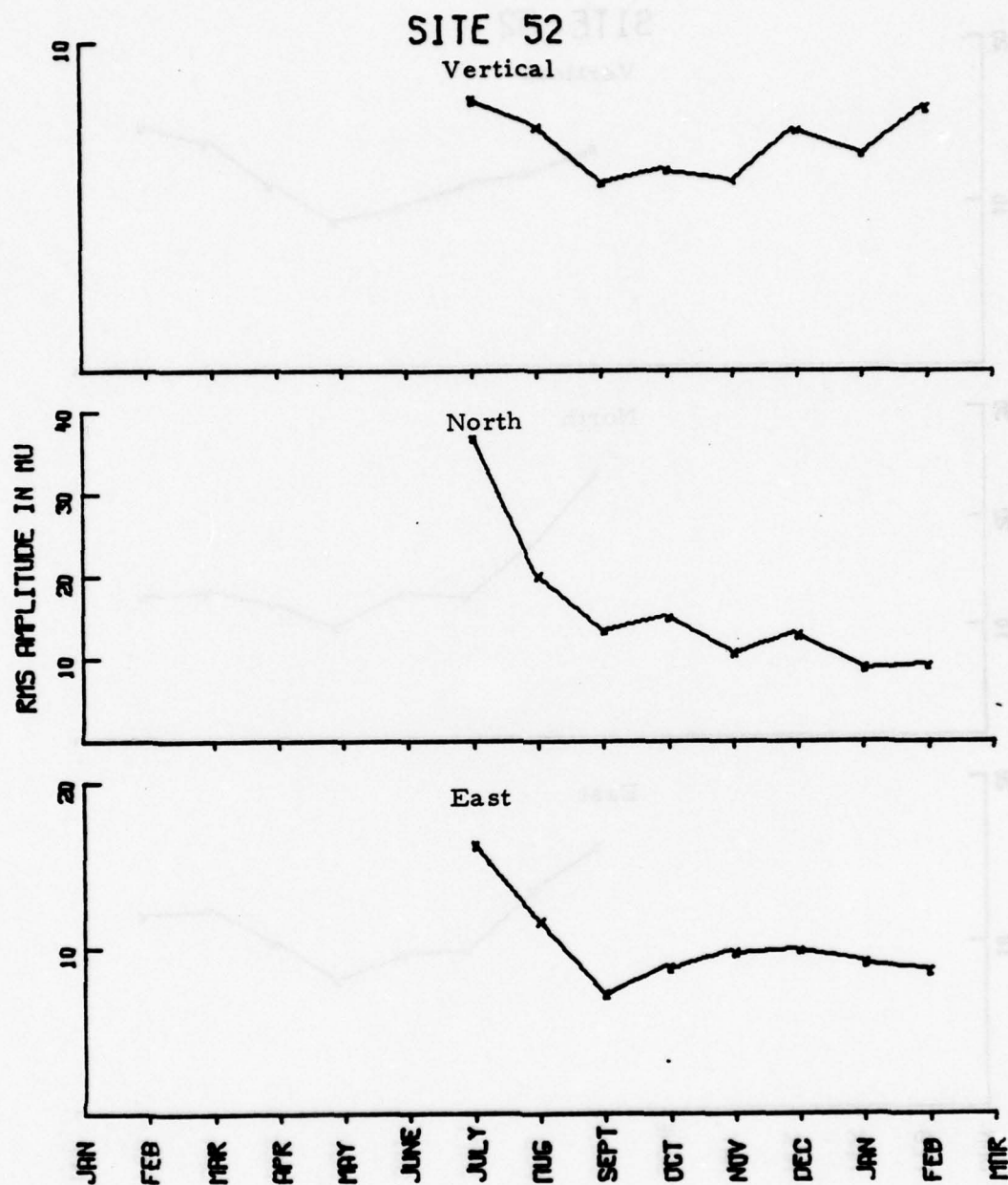
KAAO INSTRUMENT RESPONSE CORRECTED 17-41 SECOND
RMS NOISE TRENDS

FIGURE B-12c

KAAO INSTRUMENT RESPONSE CORRECTED 40-64 SECOND
RMS NOISE TRENDS

TABLE B-1

INSTRUMENT RESPONSE CORRECTED MEAN 10-25 SECOND
RMS NOISE AMPLITUDES IN $m\mu$

Station	Vertical		North		East	
	Mean	S. D.	Mean	S. D.	Mean	S. D.
ANMO	23.69	11.01	23.64	11.09	24.11	10.23
CHTO	23.85	7.44	25.69	10.19	26.09	10.03
MAIO	15.79	6.81	13.40	5.16	13.29	5.84
CTAO	26.31	9.69	27.17	8.58	24.64	8.39
ZOBO	16.32	5.31	16.07	5.08	16.90	5.12
KAAO	16.01	5.34	16.35	5.84	16.00	5.02
MAJO	15.08	6.74	17.62	7.08	17.12	6.66

S. D. = Standard Deviation

TABLE B-2

INSTRUMENT RESPONSE CORRECTED MEAN 17-41 SECOND
RMS NOISE AMPLITUDES IN $m\mu$

Station	Vertical		North		East	
	Mean	S. D.	Mean	S. D.	Mean	S. D.
ANMO	12.67	4.63	11.40	4.83	12.07	4.37
CHTO	11.12	4.39	12.14	5.64	12.93	5.36
MAIO	9.47	3.70	9.45	3.33	9.77	3.70
CTAO	12.44	4.44	13.00	4.11	11.42	4.36
ZOBO	9.07	3.25	9.91	3.33	9.29	3.00
KAAO	11.50	4.72	14.96	8.50	11.65	5.81
MAJO	7.85	1.95	8.76	2.37	9.48	2.68

S. D. = Standard Deviation

TABLE B-3

INSTRUMENT RESPONSE CORRECTED MEAN 40-64 SECOND RMS NOISE AMPLITUDES IN $m\mu$

Station	Vertical		North		East	
	Mean	S. D.	Mean	S. D.	Mean	S. D.
ANMO	5.64	2.10	5.74	1.98	7.10	2.23
CHTO	4.96	1.22	6.02	1.55	6.06	2.36
MAIO	5.46	4.11	6.27	2.71	7.10	4.39
CTAO	3.46	0.96	6.65	2.81	6.63	1.99
ZOBO	4.69	2.04	7.58	3.77	6.36	1.87
KAAO	7.14	3.47	11.49	7.85	11.13	8.88
MAJO	7.06	3.13	8.69	3.79	8.62	3.92

S. D. = Standard Deviation

TABLE B-4a

INSTRUMENT RESPONSE CORRECTED MEAN PEAK 20 SECOND
RMS NOISE AMPLITUDES IN $m\mu$

Station	Vertical		North		East	
	Mean	S. D.	Mean	S. D.	Mean	S. D.
ANMO	31.13	13.26	28.61	12.70	31.68	12.21
CHTO	26.97	10.48	30.92	14.83	29.14	12.89
MAIO	22.06	10.40	19.21	9.04	19.44	11.15
CTAO	31.96	12.13	31.31	10.95	26.92	11.06
ZOBO	21.90	8.94	21.89	9.14	21.37	9.78
KAAO	25.95	12.58	26.59	14.80	24.46	12.71
MAJO	17.89	5.59	19.03	5.62	23.54	9.57

S. D. = Standard Deviation

TABLE B-4b

INSTRUMENT RESPONSE CORRECTED MEAN LOG_{10} PEAK
20 SECOND NOISE AMPLITUDES IN $m\mu$

Station	Vertical		North		East	
	Mean	S. D.	Mean	S. D.	Mean	S. D.
ANMO	1.46	0.17	1.42	0.19	1.47	0.17
CHTO	1.40	0.18	1.45	0.19	1.42	0.19
MAIO	1.30	0.20	1.24	0.20	1.23	0.22
CTAO	1.48	0.16	1.47	0.16	1.40	0.18
ZOBO	1.31	0.17	1.30	0.19	1.29	0.18
KAAO	1.36	0.22	1.36	0.23	1.33	0.22
MAJO	1.23	0.13	1.26	0.13	1.34	0.19

S. D. = Standard Deviation

TABLE B-5a

INSTRUMENT RESPONSE CORRECTED MEAN PEAK 30 SECOND NOISE AMPLITUDES IN $m\mu$

Station	Vertical		North		East	
	Mean	S. D.	Mean	S. D.	Mean	S. D.
ANMO	12.50	6.36	12.24	7.05	14.90	6.96
CHTO	10.03	5.00	14.28	8.41	13.21	5.86
MAIO	14.00	6.97	17.46	8.52	18.75	8.45
CTAO	12.16	19.08	12.73	6.33	13.52	7.59
ZOBO	11.39	5.22	14.65	5.84	13.20	5.05
KAAO	16.31	8.50	30.12	24.55	21.96	23.68
MAJO	10.69	4.43	16.25	6.27	14.45	5.13

S. D. = Standard Deviation

TABLE B-5b

INSTRUMENT RESPONSE CORRECTED MEAN LOG_{10} PEAK
30 SECOND NOISE AMPLITUDES IN $m\mu$

| Station	Vertical		North		East	
	Mean	S. D.	Mean	S. D.	Mean	S. D.
ANMO	1.04	0.22	1.03	0.24	1.12	0.21
CHTO	0.95	0.22	1.10	0.21	1.08	0.19
MAIO	1.10	0.20	1.18	0.24	1.23	0.20
CTAO	0.94	0.32	1.06	0.21	1.07	0.24
ZOBO	1.01	0.22	1.14	0.16	1.08	0.22
KAAO	1.16	0.21	1.40	0.25	1.25	0.24
MAJO	0.97	0.28	1.18	0.16	1.11	0.25

S. D. = Standard Deviation
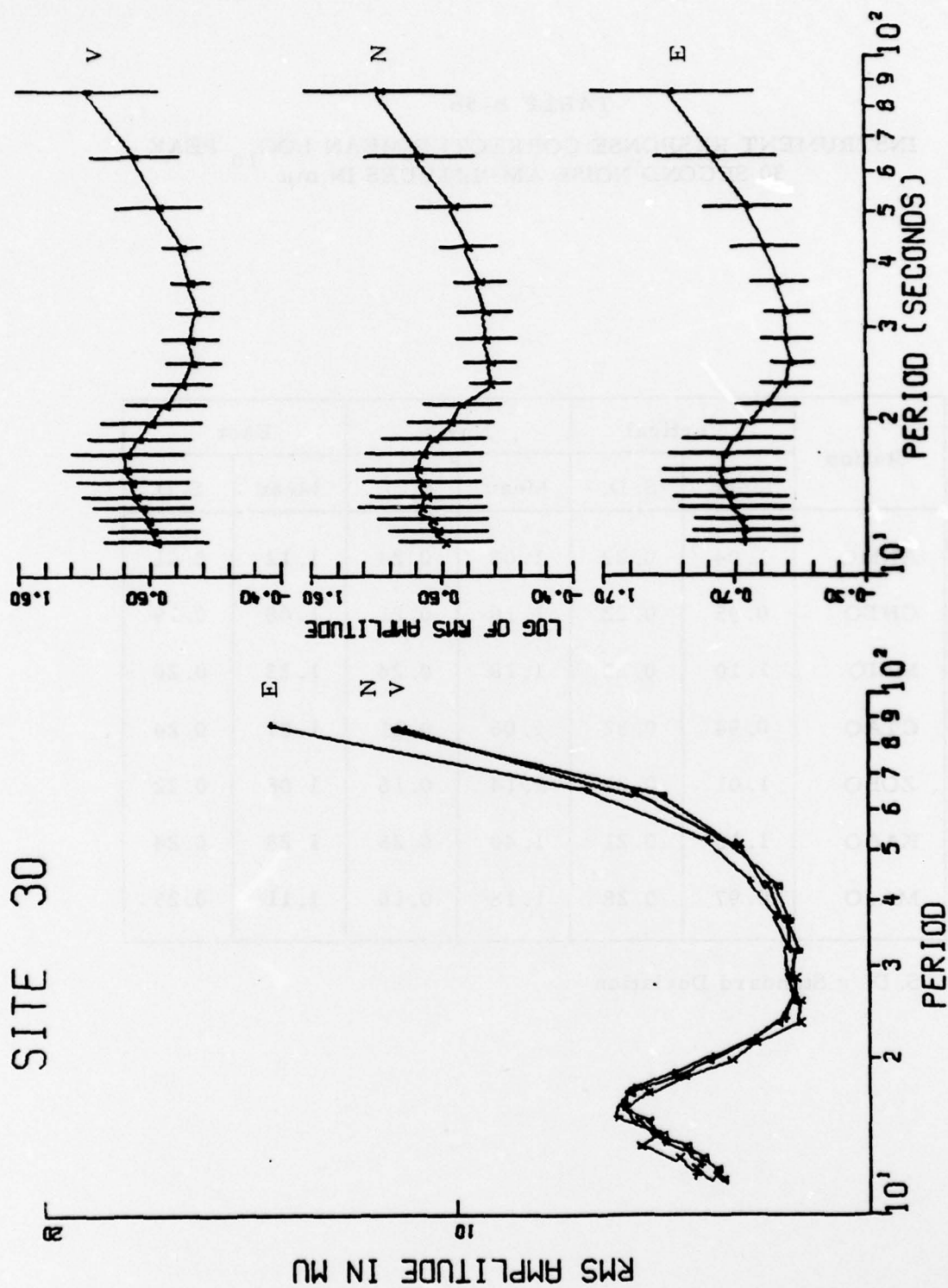
FIGURE B-13

AVERAGE RMS AMPLITUDE SPECTRA - ANMO LONG- PERIOD
NOISE - INSTRUMENT RESPONSE CORRECTED

SITE 33
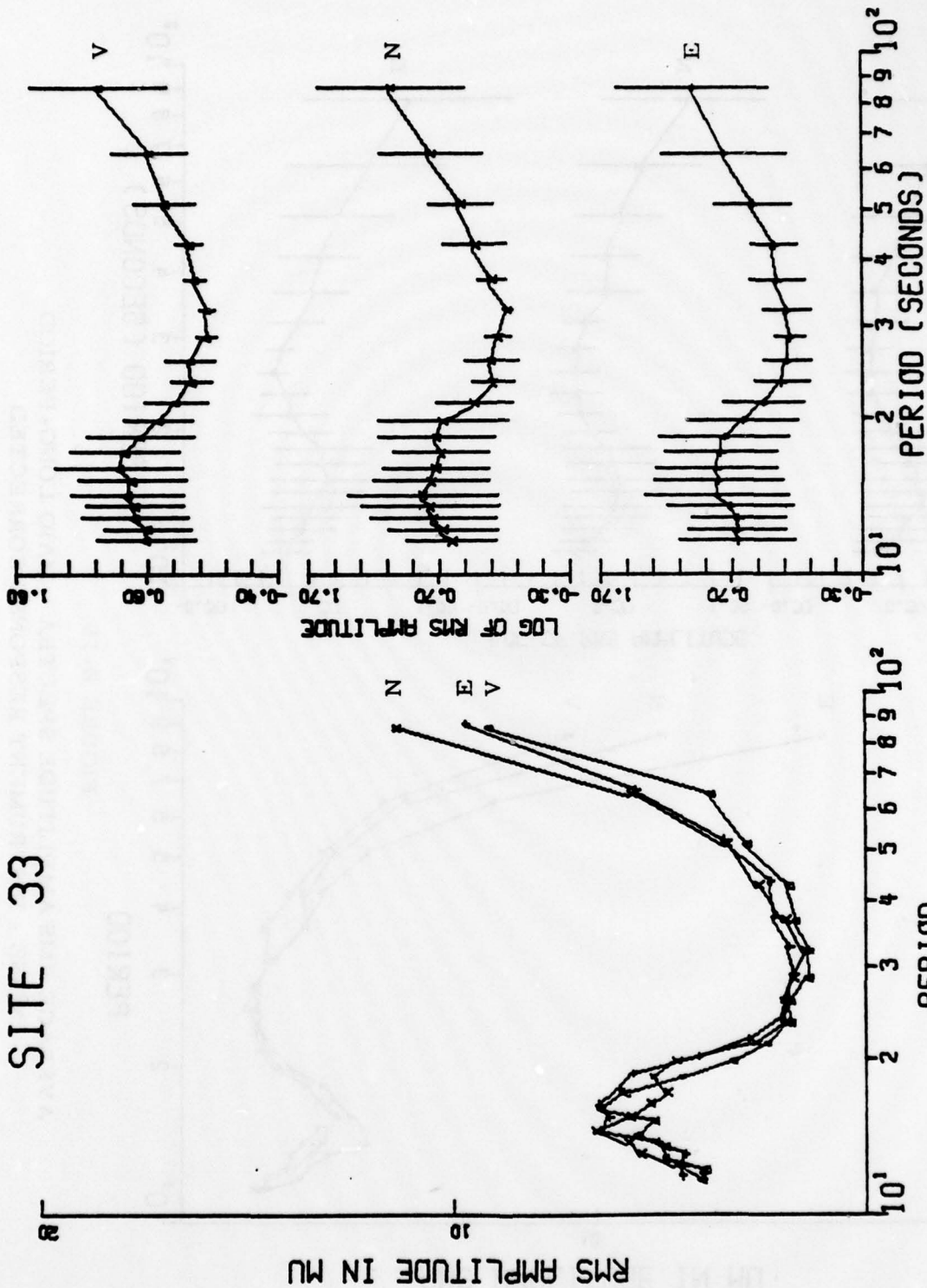
FIGURE B-14

AVERAGE RMS AMPLITUDE SPECTRA - CHTO LONG-PERIOD
NOISE - INSTRUMENT RESPONSE CORRECTED

B-47
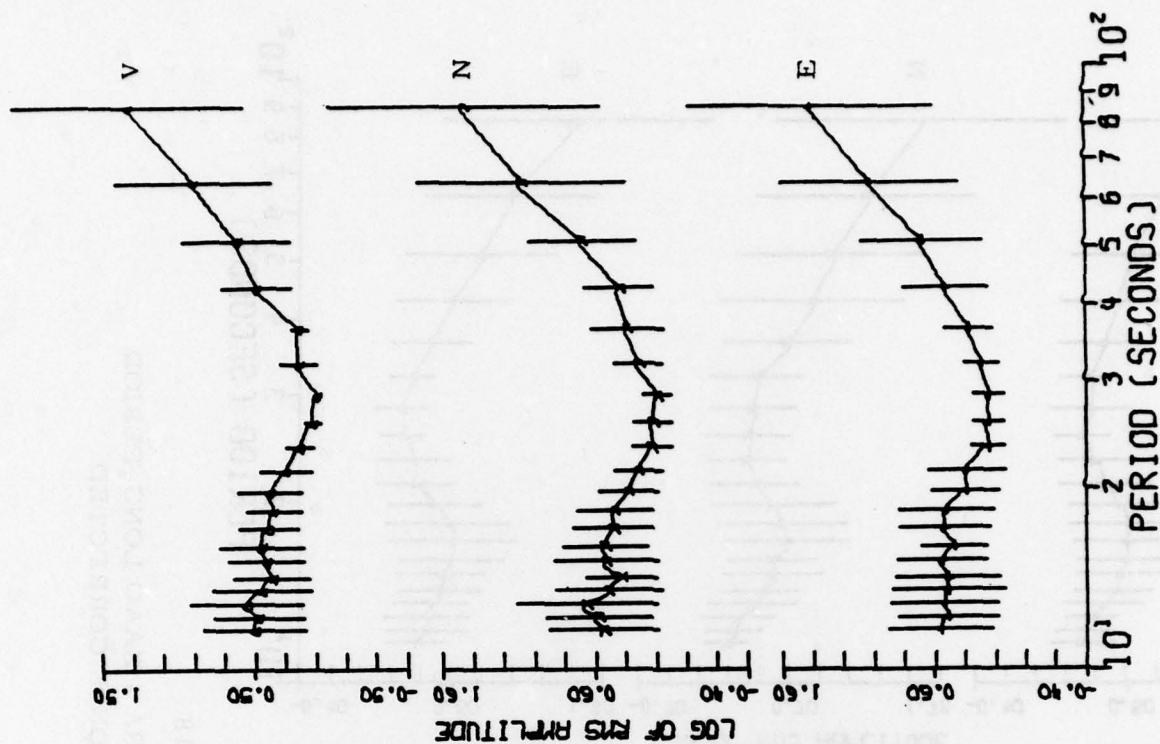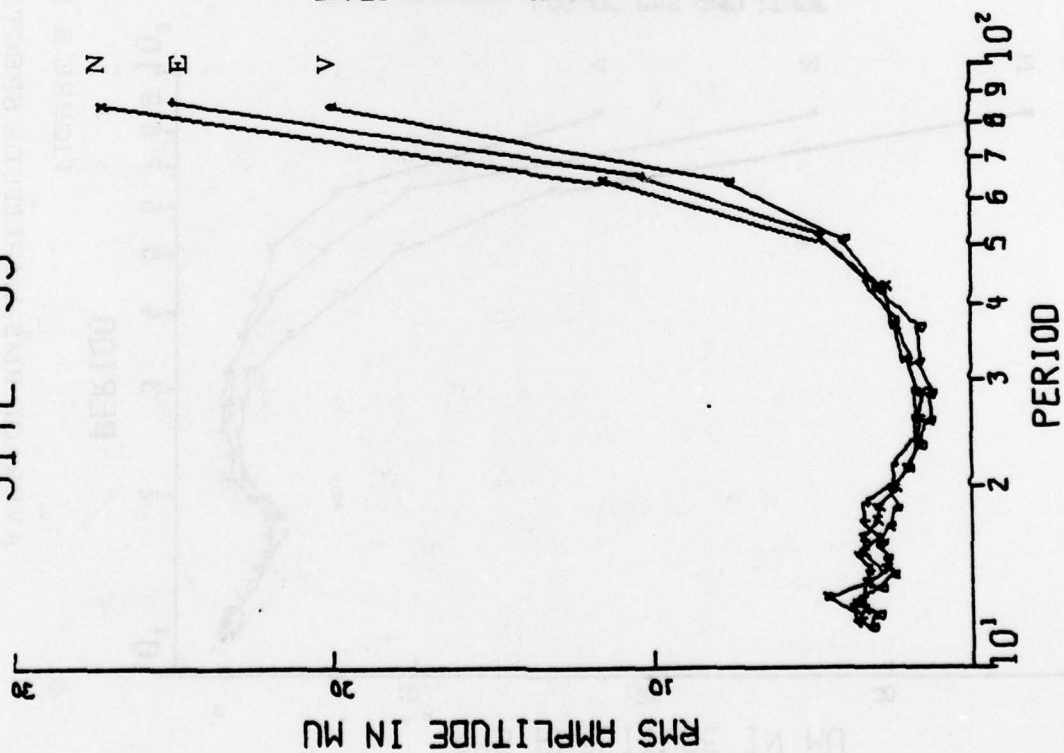
SITE 36
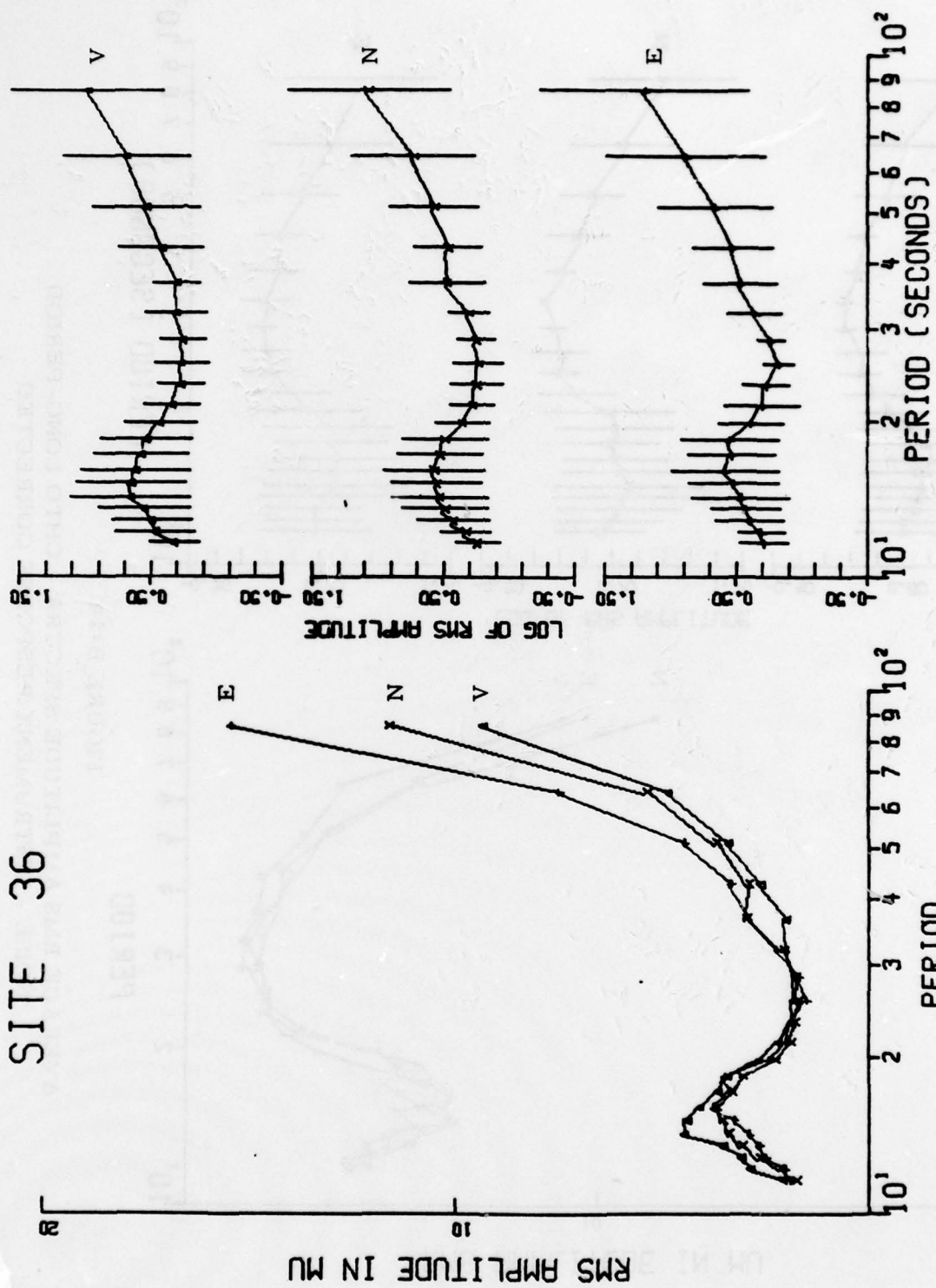
FIGURE B-15

AVERAGE RMS AMPLITUDE SPECTRA - MAIO LONG-PERIOD
NOISE - INSTRUMENT RESPONSE CORRECTED
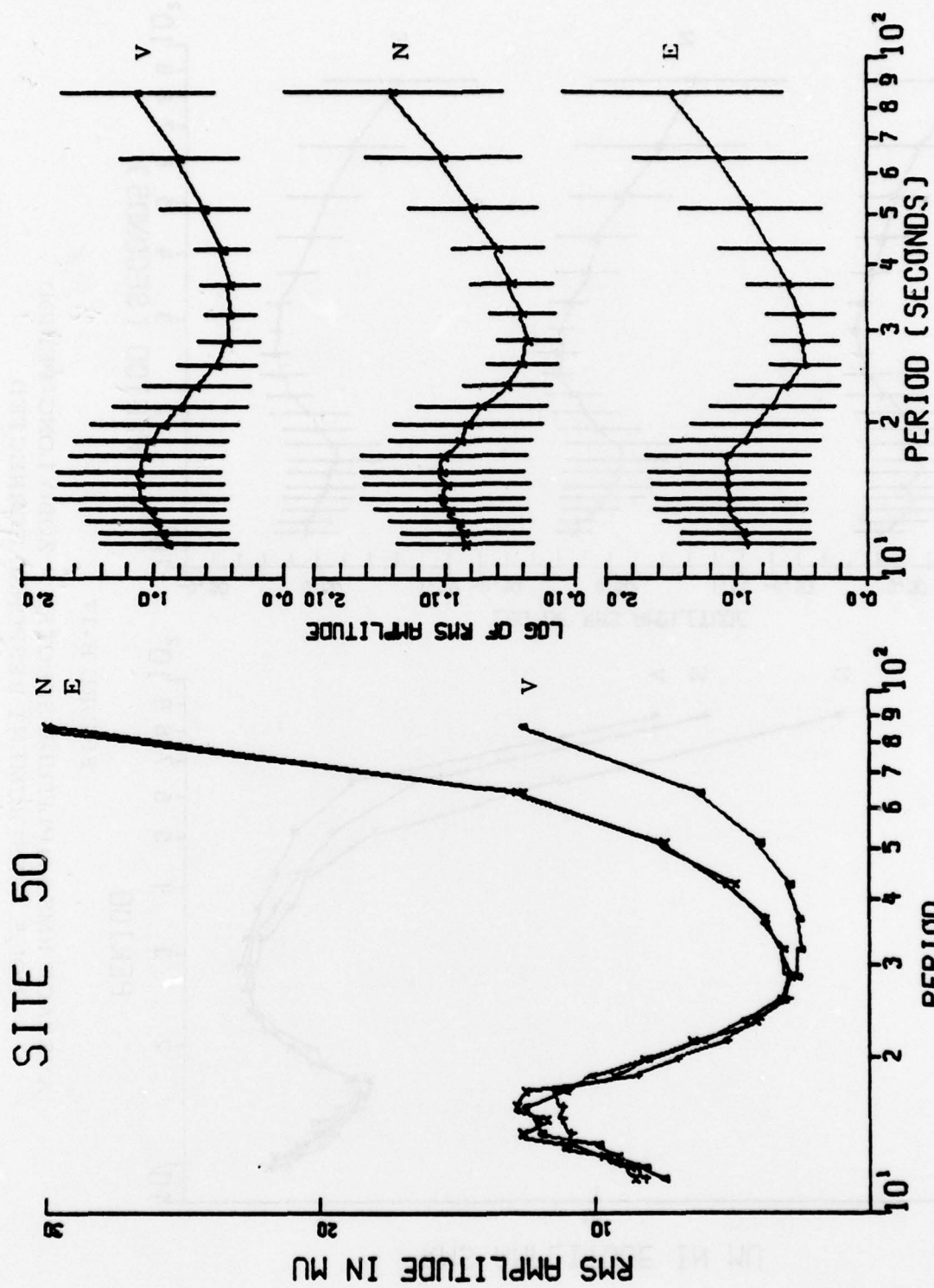
SITE 50

AVERAGE RMS AMPLITUDE SPECTRA - CTAO LONG-PERIOD
NOISE - INSTRUMENT RESPONSE CORRECTED

FIGURE B-16

B-49
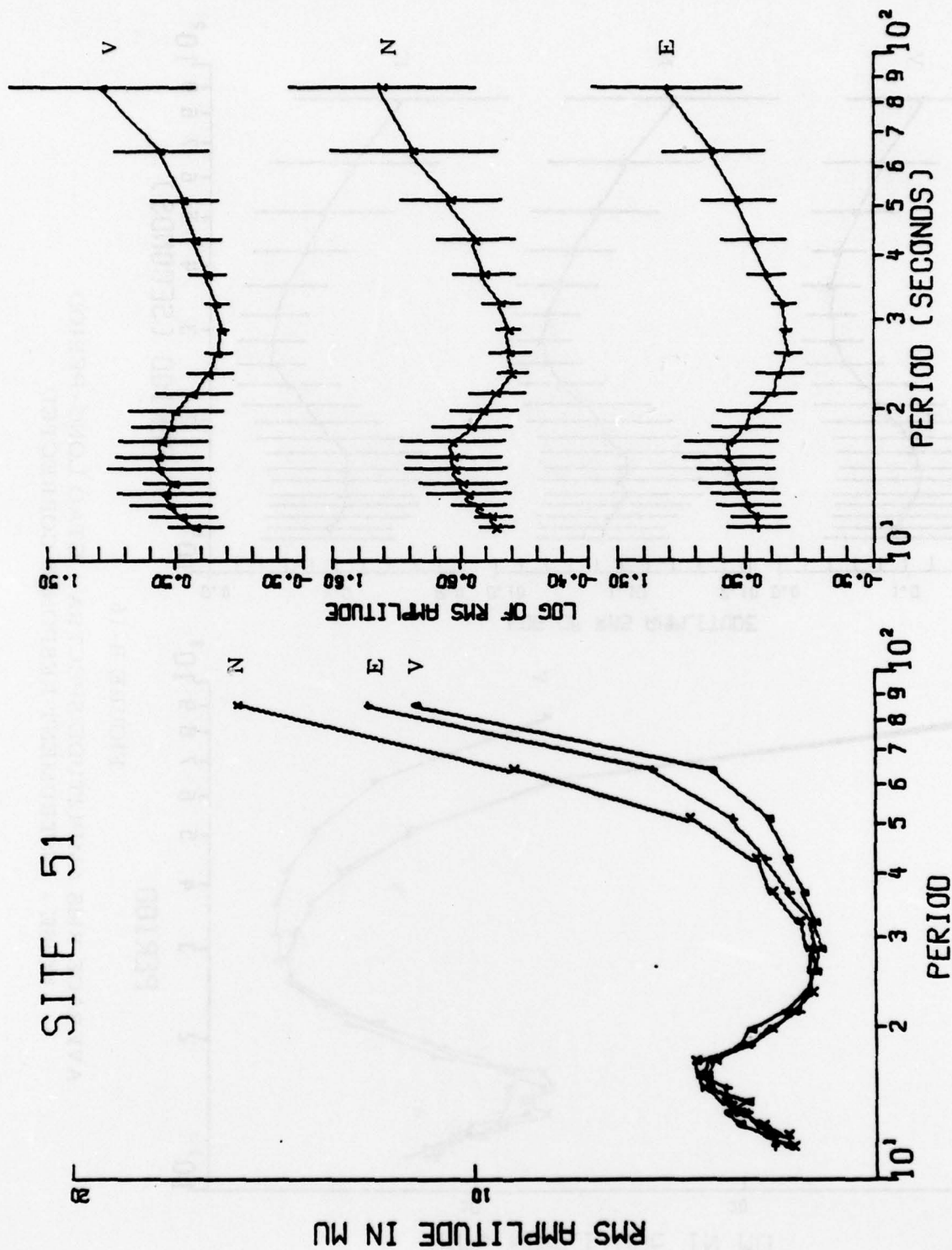
SITE 51

FIGURE B-17

AVERAGE RMS AMPLITUDE SPECTRA - ZOBO LONG-PERIOD
NOISE - INSTRUMENT RESPONSE CORRECTED
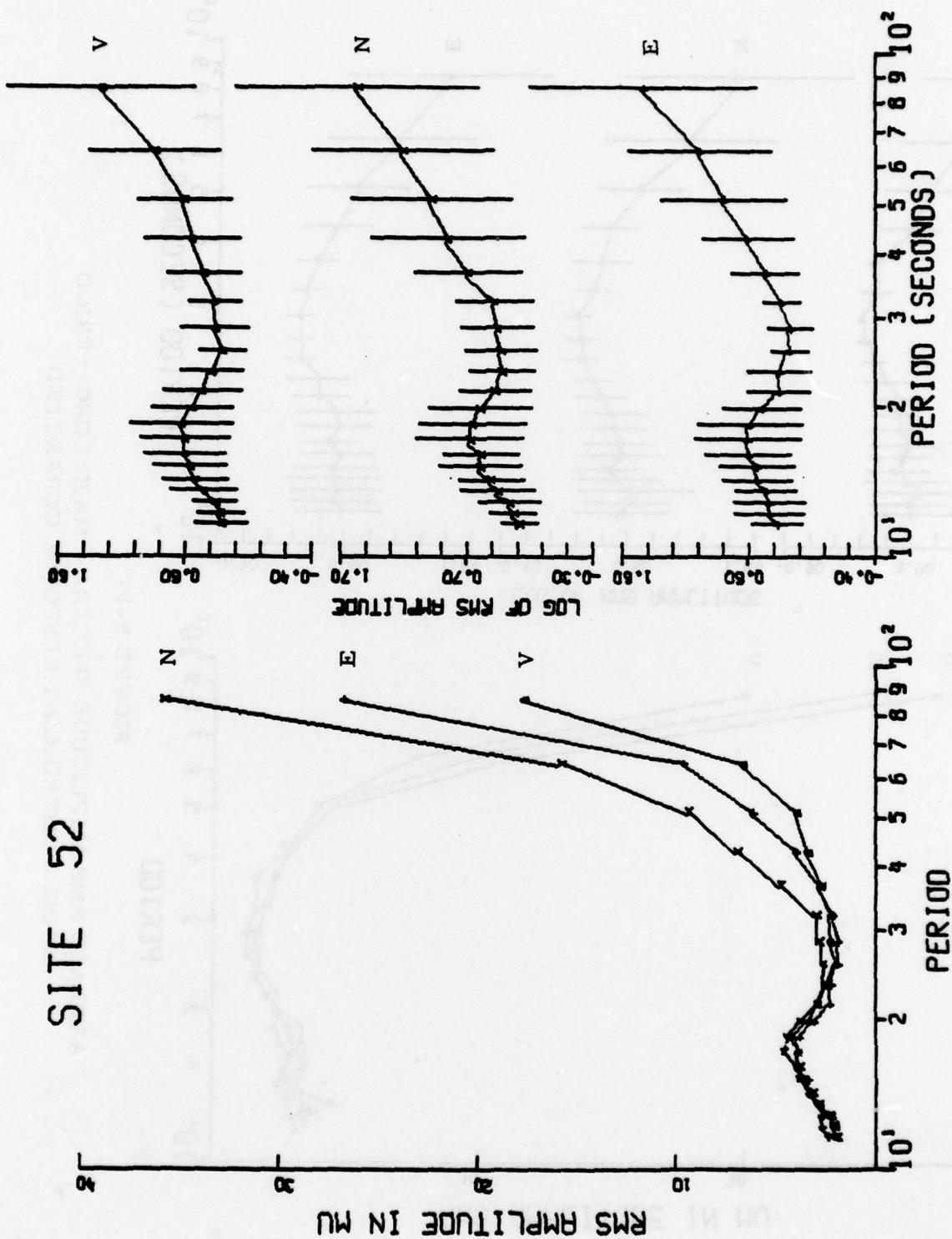
FIGURE B-18

AVERAGE RMS AMPLITUDE SPECTRA - KAAO LONG-PERIOD
NOISE - INSTRUMENT RESPONSE CORRECTED

SITE 53

RMS AMPLITUDE IN MU

PERIOD

LOG OF RMS AMPLITUDE

PERIOD (SECONDS)

FIGURE B-19

AVERAGE RMS AMPLITUDE SPECTRA - MAJO LONG-PERIOD
NOISE - INSTRUMENT RESPONSE CORRECTED

B-52

minimum in the period range 25-28 seconds. Noise amplitudes beyond this minimum appear to rise almost monotonically. This spectral structure is also evident at NWAO and SNZO, and to some extent at GUMO and TATO (Strauss and Weltman, 1977). Similar spectral structures have been published for ambient earth motion measurements at Queens Creek, Arizona; LASA; Las Cruces, New Mexico; and Ogdensburg, New Jersey (Fix, 1972). Spectral analyses at Murphy Dome, Alaska (Von Seggern, 1970); and of the TFSO array (Chiburis, 1967) also indicated strong microseismic noise peaks at 17 seconds. The lack of a spectral peak at station MAJO may be due to the fact that only twenty noise samples are involved in the average.

Reprinted for comparison purposes in Figures B-20 through B-24 are noise spectra generated for the VLPE stations located at or near SRO/ASRO stations, see Table B-6 (Prahl, 1974). The Chiang Mai and Albuquerque VLPE stations were replaced with SRO borehole seismometers. As was expected, noise amplitudes dropped significantly. We furthermore observe that, in contrast to the VLPE station noise, the spectral amplitude variances of SRO/ASRO station noise are strongly correlated with the noise spectral amplitudes. At CTAO,the variances are less strongly correlated than other SRO/ASRO stations (Figure B-16). Also, the spectral amplitudes and amplitude variances are larger at VLPE CTA than at ASRO CTAO. A comparison of SRO ZOBO spectra with those of VLPE ZLP reveal markedly distinct characteristics. ZOBO's three components appear practically identical below 30 seconds and remain similar at higher periods. ZLP's three components show much less similarity to one another. However, these two stations do not share the same location as do the other station pairs, which may account for the spectral differences observed. On the other hand, SRO station MAJO and VLPE station MAT do share locations and these two stations also show distinctly different spectra. While the three component interrelationships seem normal for both sites, the MAJO spectra appear damped between periods of 12 and 20 seconds. It should be remembered, though, that the MAJO spectra are preliminary and based on only 20 noise samples.

B-53

SITE 9.

Albuquerque, New Mexico
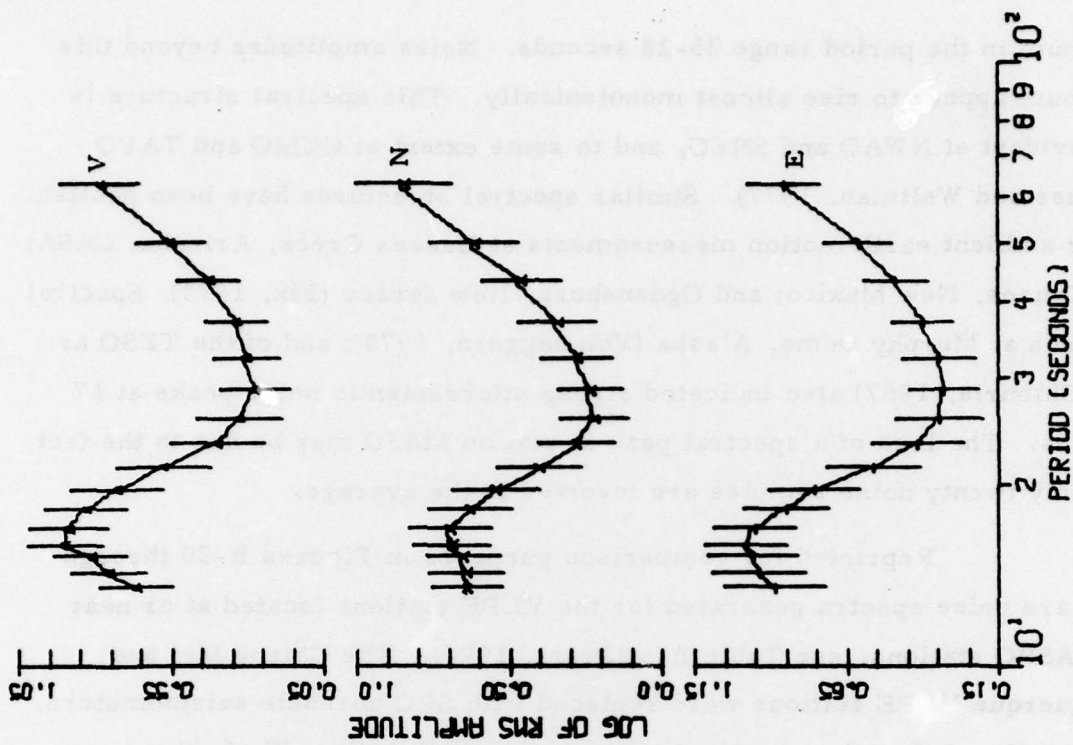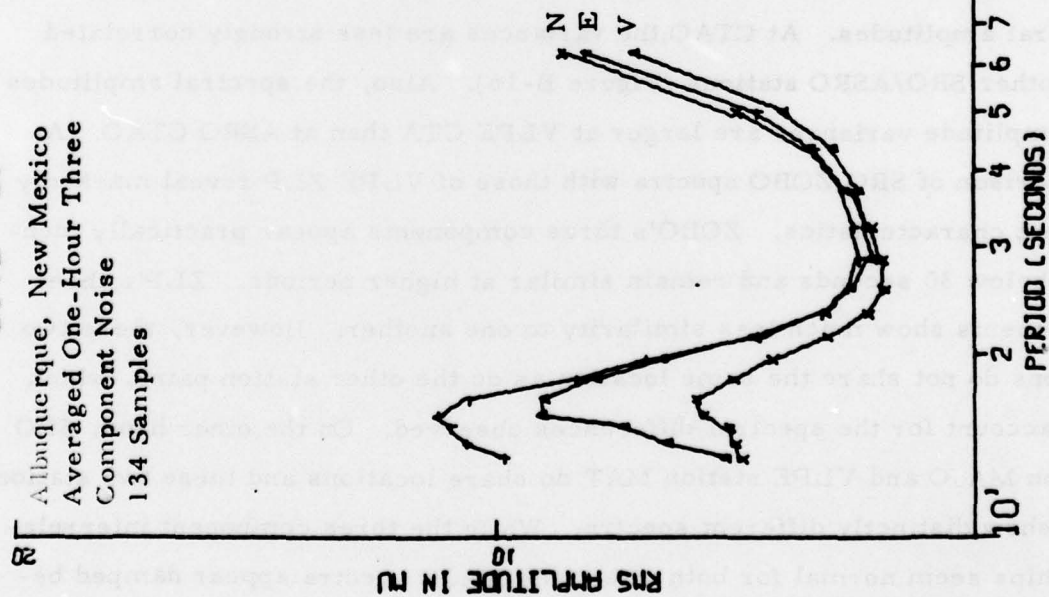Averaged One-Hour Three
Component Noise
134 Samples

THREE COMPONENT RMS NOISE AMPLITUDE SPECTRA
AT VERY LONG PERIOD EXPERIMENT STATION ALQ

FIGURE B-20

SITE 2.

Chiang Mai, Thailand
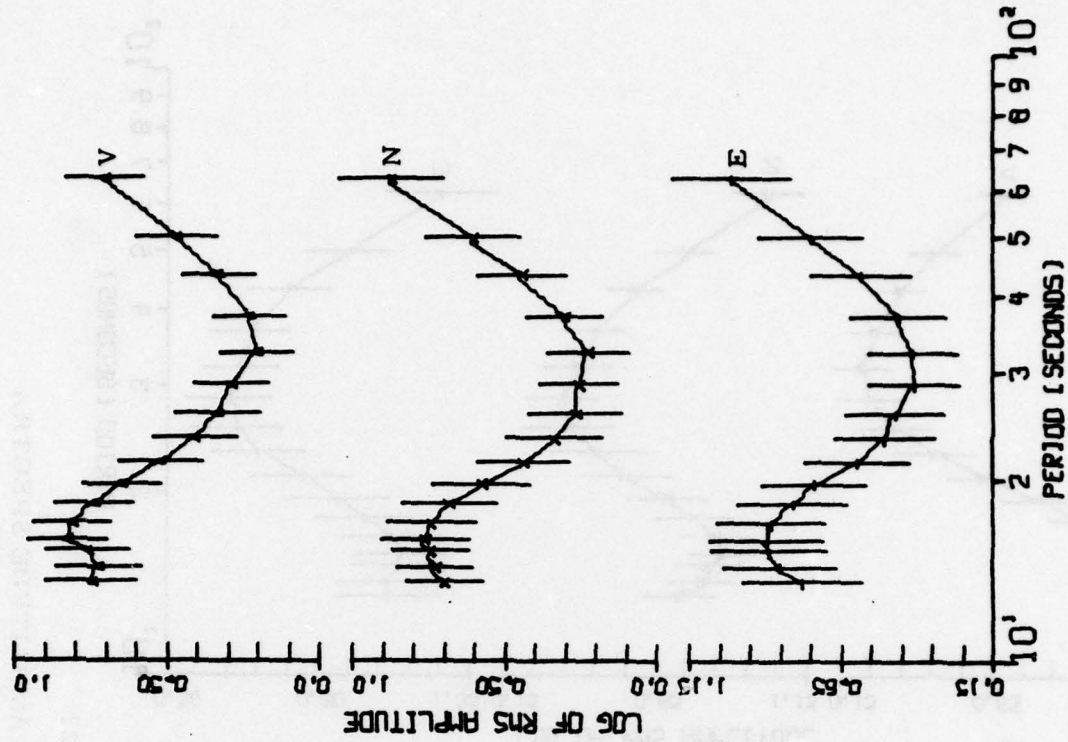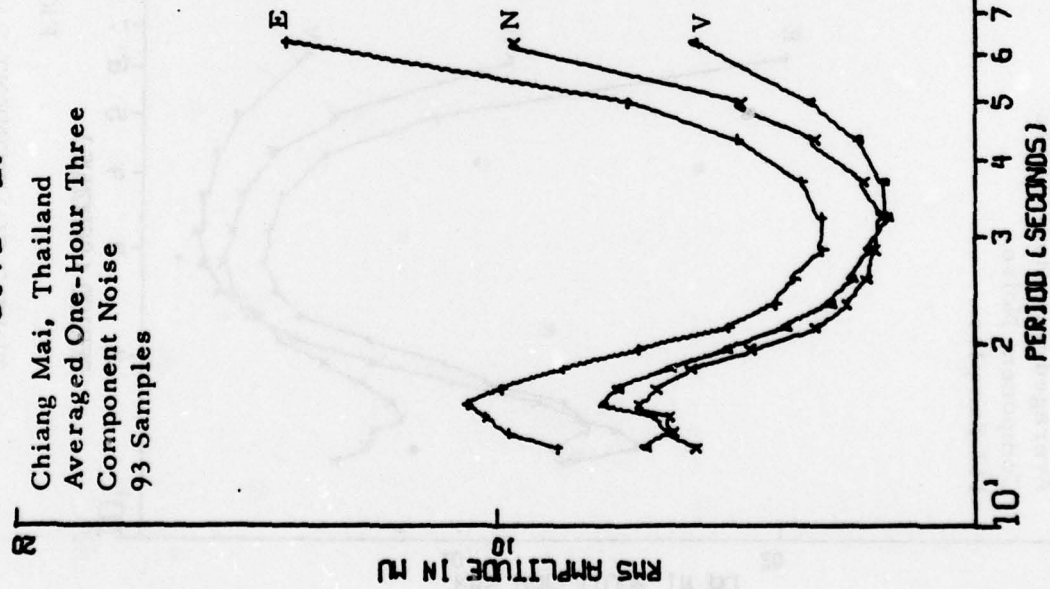Averaged One-Hour Three
Component Noise
93 Samples

THREE COMPONENT RMS NOISE AMPLITUDE SPECTRA
AT VERY LONG PERIOD EXPERIMENT STATION CHG

FIGURE B-21

B-55
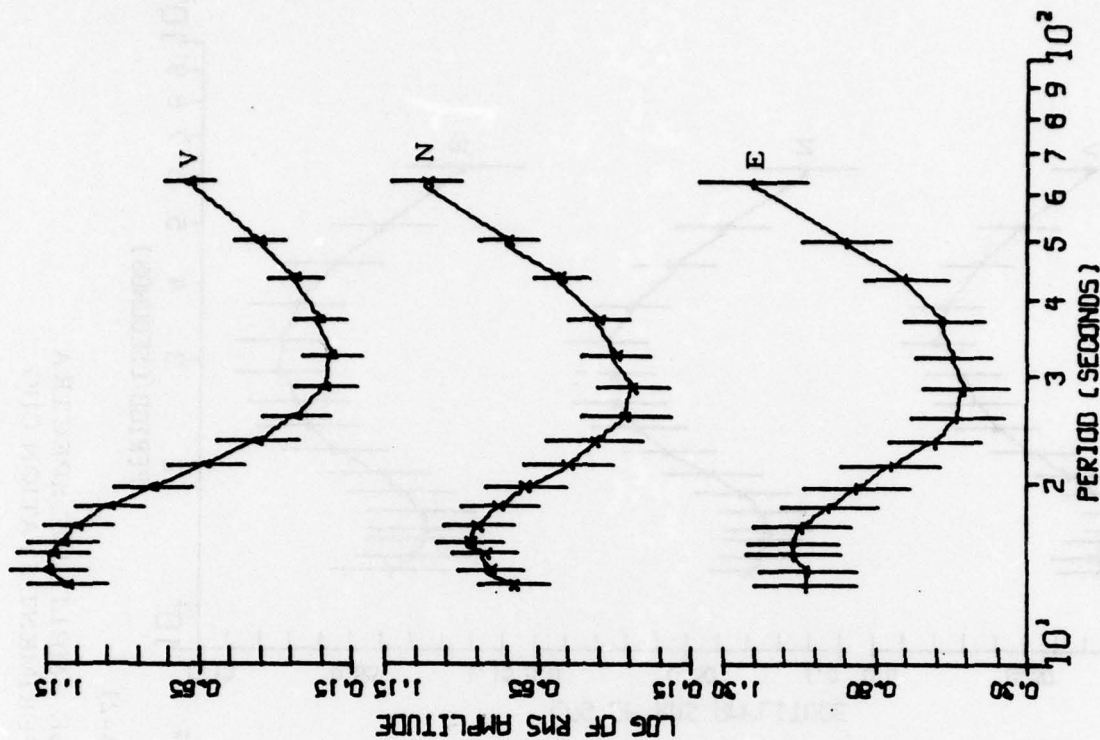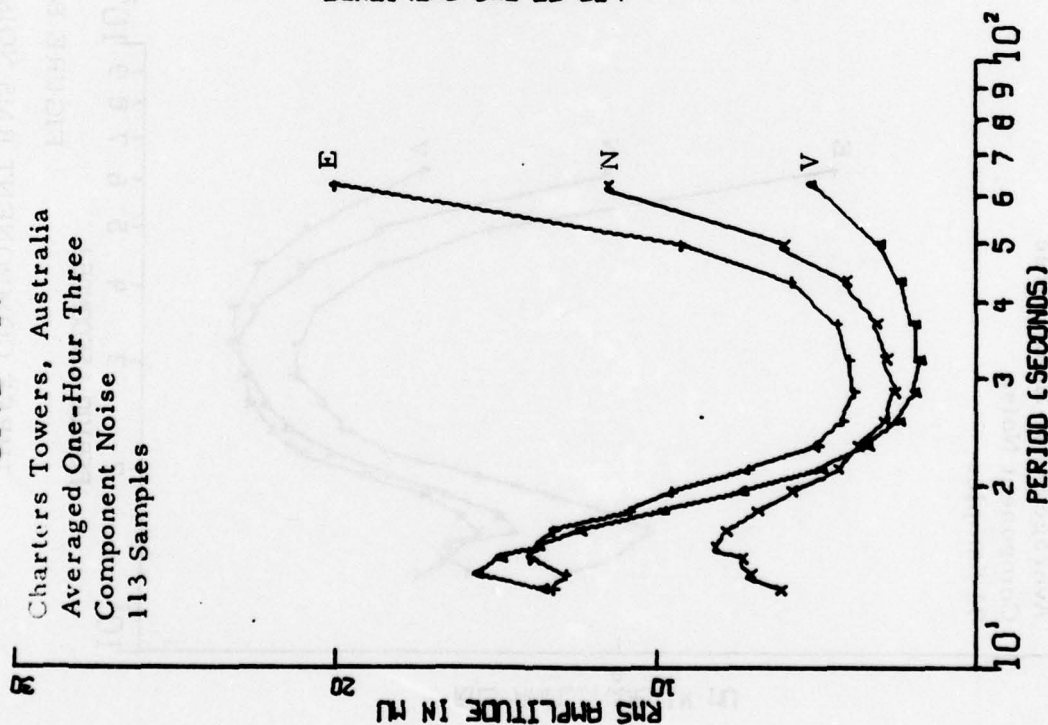
FIGURE B-22

THREE COMPONENT RMS NOISE AMPLITUDE SPECTRA
AT VERY LONG PERIOD EXPERIMENT STATION CTA

SITE 10.

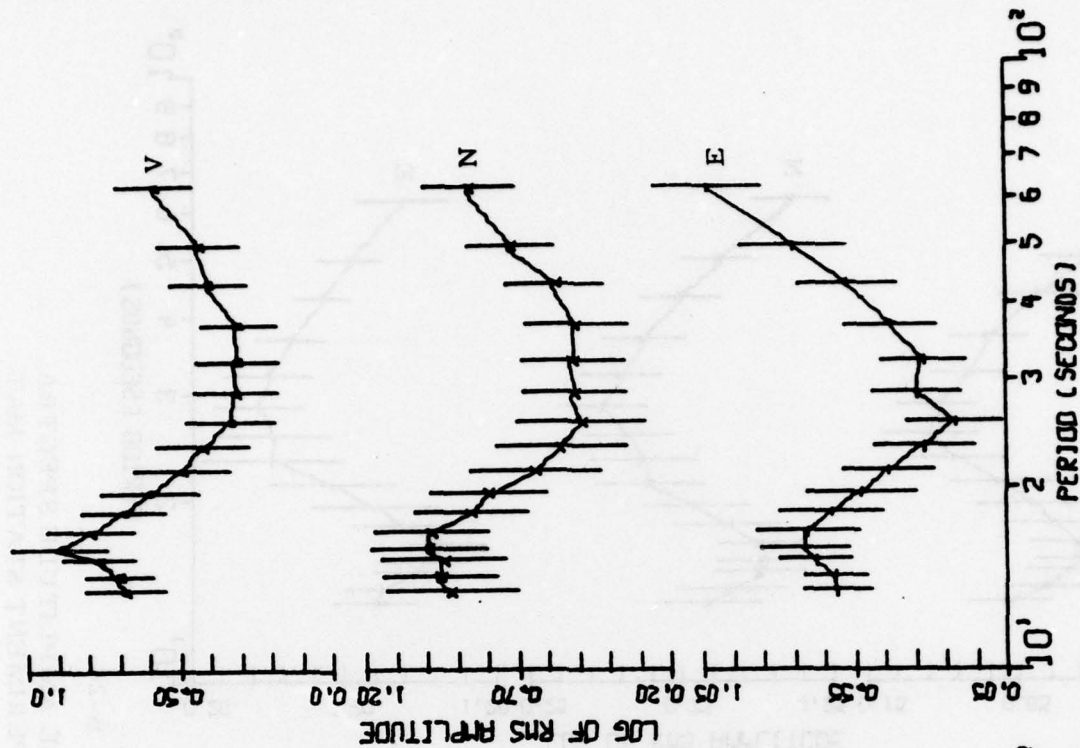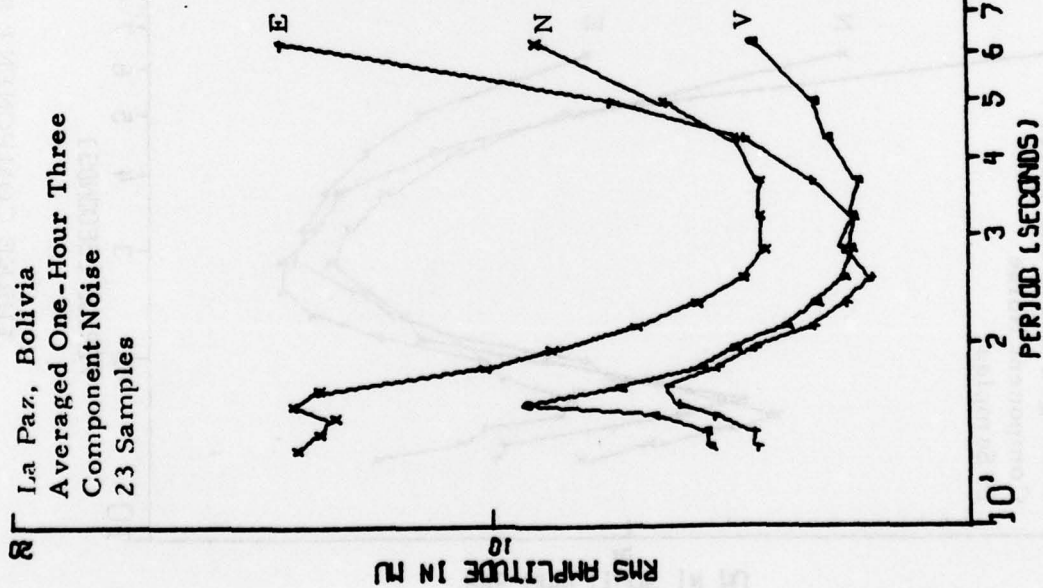La Paz, Bolivia
Averaged One-Hour Three
Component Noise
23 Samples

FIGURE B-23

THREE COMPONENT RMS NOISE AMPLITUDE SPECTRA
AT VERY LONG PERIOD EXPERIMENT STATION ZLP

B-57

SITE 11.

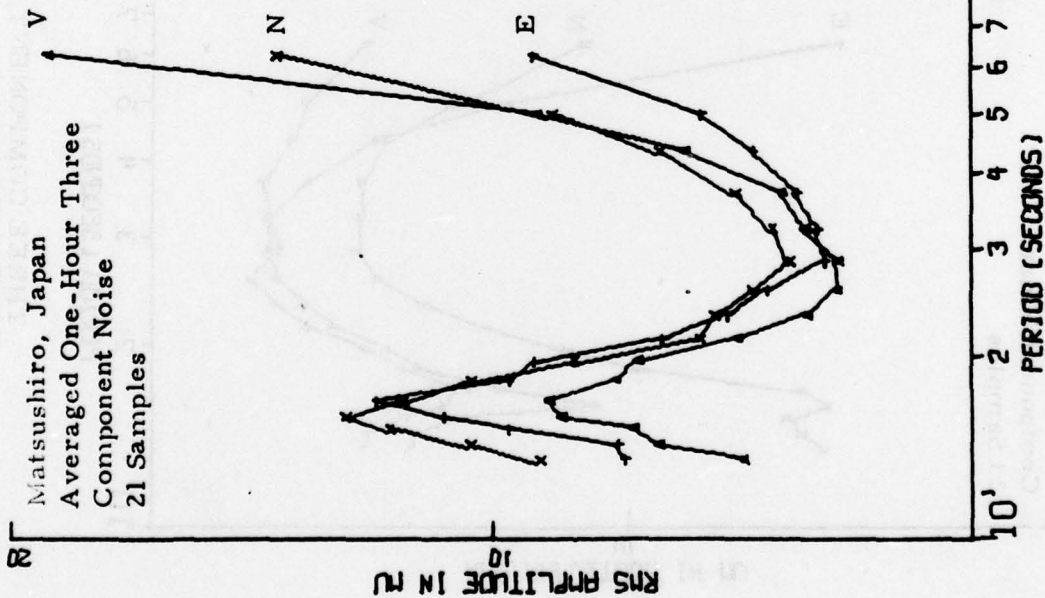Matsushiro, Japan
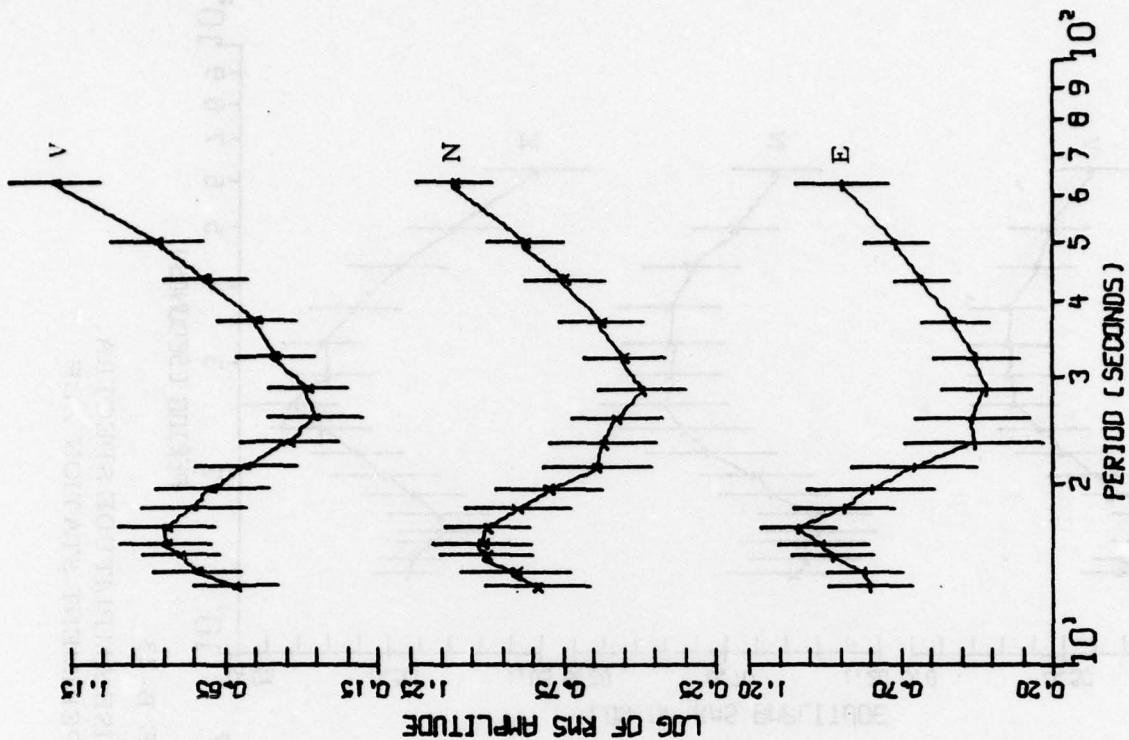Averaged One-Hour Three
Component Noise
21 Samples

THREE COMPONENT RMS NOISE AMPLITUDE SPECTRA
AT VERY LONG PERIOD EXPERIMENT STATION MAT

FIGURE B-24

TABLE B-6

VERY LONG PERIOD EXPERIMENT STATIONS AND LOCATIONS

Station Name	Station Designator	Numeric Designator	Latitude	Longitude
Charters Towers, Australia	CTA	1	20.09S	146.26E
Chiang Mai, Thailand	CHG	2	18.79N	98.98E
Albuquerque, New Mexico	ALQ	9	34.94N	106.46W
La Paz, Bolivia	ZLP	10	16.50S	68.13W
Matsushiro, Japan	MAT	11	36.54N	138.21E